Development of Polycaprolactone Microparticles as a Protein Delivery System for the Treatment of Tendon Disorders.

Grace Walden

This thesis is submitted in partial fulfilment of the requirements for the degree of philosophy.

University of East Anglia, Norwich

Department of Chemistry and Pharmacy

June 2019

Preface

The work described within the 220 pages of this thesis is, to the best of my knowledge, original and my own work, except where due reference has been made.

Grace Walden

January 2019

"Good stuff Grace. Won't be too long now before you will be Dr. Walden. Love Dad x"

20/07/2017

Abstract

This thesis describes the development of a microparticle system, containing bioactive molecules for use in the regeneration of tendon tissue. An introduction is given into the cause of tendon injury and subsequent changes to the tissue post healing, as well as the shortcomings in treatments. The current state of the art in the field is given, including the use of cells and proteins for tissue engineering, polymer candidates for regenerative medicine, click chemistry for protein conjugation, and microparticles as drug delivery systems.

The 3 results and discussion chapters highlight the successful synthesis of a microparticle system template that can conjugate proteins via an azide-alkyne click chemistry dibenzocyclooctyne linking unit. The synthesis of a novel polymer; polycaprolactone azide is described in chapter 2, showing the ability to conjugate to the linking unit in 30 minutes. Chapter 3 describes the subsequent use of the polymer for the formulation of microparticles via membrane emulsion technique. Microparticles from 10-153 μm were produced, with size controlled by altering process parameters such as stir speed and polymer concentration. A live/dead staining assay showed microparticles display no toxicity to tenocytes. The availability of the azide is demonstrated by the conjugation of an alkyne containing fluorescent compound to microparticles. Chapter 4 shows the successful conjugation of 4 proteins; bovine serum albumin, human serum albumin, transforming growth factor βeta 1 and 3 to microparticles. This reaction was efficient, with human serum albumin conjugation occurring in 10 minutes in physiological conditions. Two different linking molecules, with a conserved dibenzocyclooctyne core, were used. Attachment to the microparticles was via azide-alkyne click reaction and to protein via either an N-hydroxysuccinimide ester or thiol-maleimide reaction.

Chapter 5 reviews the translation of academic research to a commercial product, supported by a 3-month studentship with Neotherix Ltd. Chapter 6 is a brief conclusion on the success of the project and future work that could be attempted to progress it further.

Acknowledgements

I would like to thank Dr Aram Saeed and my funding body EPSRC for giving me the opportunity to study for my PhD. Also, sincere thanks go to my other supervisor's Dr Mike Raxworthy, Dr Graham Riley and Professor Simon Donell for their continued support and advice throughout the whole process in their respective areas of expertise. Special thanks go to Dr Mike Raxworthy and Neotherix Ltd for giving me the opportunity to experience the industrial side of research and for allowing me to participate in MedTech Best.

My unending gratitude goes to my family, friends and loved ones without whom I would not be here today. The support you have given me throughout the years has allowed me to continue through my lows when the insurmountable task of completing a PhD threatened to defeat me. You have shown your love with your words of encouragement and belief. You have been shoulders to cry on and soundboards for advice and ideas. You have put a roof over my head and allowed me to take my stress out on you when needed. For all of this I am eternally grateful. My only hope is that I have done you proud and I can repay you all the favour in your times of need.

I would like to thank all my colleagues at UEA for their support, friendship and advice. I would especially like to thank the PhD students and postdocs of Prof Mark Searcy's lab that were around during my time at UEA. You taught me the techniques that I have learnt through the years and have given me invaluable advice when I was certain there was nothing left to try with an experiment. Best of all though, you have been my after-work drinking buddies when the tequila called!

Lastly, I would like to dedicate the work contained within this thesis to my Dad. I really wish you were still here for a celebratory hug and pint. I know you always knew I would, but I made it out the other side Dad.

Thank you for it all,

Grace

List of publications

In refereed journals

1. **Grace Walden**, Xin Liao, Simon Donell, Michael J Raxworthy, Graham P Riley and Aram Saeed. A Clinical, Biological and Biomaterials Perspective into Tendon Injuries and Regeneration. *Tissue Engineering Part B Reviews. 2017. DOI: 10.1089/ten.TEB.2016.0181 (Published)*

2. Xin Liao, **Grace Walden**, Noelia Dominguez-Falcon, Simon Donell, Michael J Raxworthy, Graham P Riley and Aram Saeed. A direct comparison of linear and star-shaped poly(dimethylaminoethyl acrylate) polymers for polyplexation with DNA and cytotoxicity in cultured cell lines. *European Polymer Journal.* 2017. *DOI: 10.1016/j.eurpolymj.2016.08.021 (Published)*

3. **Grace Walden**, Xin Liao, Graham P Riley, Simon Donell, Michael J Raxworthy, and Aram Saeed. Synthesis and fabrication of surface-active microparticles using membrane emulsion technique and rapid conjugation of model protein via strain-promoted azide-alkyne click chemistry in physiological conditions*. Bioconjugate Chemistry. 2019. DOI: 10.1021/acs.bioconjchem.8b00868 (Published)*

Contents

Chapter 1: Introduction

Chapter 2: Synthesis

Chapter 3: Microparticle Production and Optimisation

Chapter 5: Industrial Translation

Chapter 6: Overall Conclusions and Future Work

Appendices

List of Figures

List of Tables

List of Schemes

List of Appendices

List of Abbreviations

Abbreviation	Meaning
ADSCs	Adipose derived stem cells
BCA	Bicinchoninic acid
BFGF	Basic fibroblastic growth factor
BMP	Bone morphogenetic proteins
BMSCs	Bone marrow derived stem cells
BSA	Bovine serum albumin
CAGR	Compound annual growth rate
$CDCl_3$	Deuterated chlorofom
CuAAC	Copper(I) catalysed azide-alkyne cycloaddition
Da	Dalton
DBCO	Dibenzocyclooctyne
DBCO-Mal	Dibenzocyclooctyne-PEG4-maleimide
DBCO-NHS	Dibenzocyclooctyne-PEG4-N-hydroxysuccinimidyl ester
DCM	Dichloromethane
DIPEA	N,N-Diisopropylethylamine
DOSY	Diffusion-ordered spectroscopy
DTNB	5,5’-dithio-bis-(2-nitrobenzoic acid)

Abbreviation	Meaning
ECM	Extracellular matrix
EDC	1-ethyl-3-(3-dimethylaminopropyl)carbodiimide hydrochloride)
EDTA	Ethylenediaminetetraacetic acid
Em	Emission
Ex	Excitation
FDA	Food and drug administration
FGF	Fibroblast growth factor
FITC	Fluorescein isothiocyanate
FMOC	Fluorenylmethyloxycarbonyl protecting group
GAGs	Glycosaminoglycans
GPC	Gel permeation chromatography
GRGDS	Glycine-Arginine-Glycine-Aspartic acid-Serine pentapeptide
h	Hour(s)
HATU	2-(7-Aza-1H-benzotriazole-1-yl)-1,1,3,3-tetramethyluronium hexafluorophosphate
HPLC	High-performance liquid chromatography
HSA	Human serum albumin
IGF	Insulin like growth factor
IR	Infrared

Abbreviation	Meaning
LC-MS	Liquid chromatography mass spec
M	Molar
m	Multiplet
MALDI-TOF	Matrix assisted laser desorption/ionisation-time of flight
min	Minute(s)
Mn	Number average molecular weight
MSCs	Mesenchymal stem cells
MTS	3-(4,5-dimethylthiazol-2-yl)-5-(3-carboxymethoxyphenyl)-2-(4-sulfophenyl)-2H-tetrazolium
mw	Molecular weight
MWCO	Molecular weight cut off
N_3	Azide
NHS	N-hydroxysuccinimide
nm	Nanometre
NMR	Nuclear magnetic resonance
NSAIDs	Non-steroidal anti-inflammatory drugs
O/W	Oil in water emulsion
O/W/O	Oil in water in oil emulsion
PBS	Phosphate-buffered saline

Abbreviation	Meaning
PCL	Poly(caprolactone)
PCL-N_3	Poly(caprolactone)azide
PCLT	Poly(caprolactone)triol
PDGF	Platelet derived growth factor
PDI	Polydispersity index
PEG	Poly(ethylene glycol)
PLA	Poly(lactic acid)
PLGA	Poly(lactic-co-glycolic acid)
PPM	Parts per million
PRP	Platelet rich plasma
PVA	Poly(vinyl alcohol)
R	Ringed
ROP	Ring opening polymerisation
RPM	Revolutions per minute
s	Singlet
SDS	Sodium dodecyl sulfate
SEM	Scanning electron microscopy
SMCC	Succinimidyl-4-(N-maleimidomethyl)cyclohexane-1-carboxylate
SPAAC	Strain-promoted azide-alkyne cycloaddition

Abbreviation	Meaning
t	Triplet
TCEP	Tris(2-carboxyethyl)phosphine hydrochloride
TEOA	Triethanolamine
TFA	Trifluoroacetic acid
TGA	Thermogravimetric analysis
TGF-β	Transforming growth factor β
TIPS	Triisopropylsilane
TEMED	Tetramethylethylenediamine
TNB	5-sulfido-2-nitrobenzoate
TRL	Technology readiness levels
UV/Vis	Ultra violet / visual spectroscopy
v	Volume
VEGF	Vascular endothelial growth factor
w	Weight
W/O	Water in Oil Emulsion
W/O/W	Water in Oil in Water Emulsion
δ	Chemical shift

Chapter 1: Introduction

1. Tissue Engineering and Regenerative Medicine

The body's natural response to injury is an attempt to heal, with the immediate activation of appropriate repair pathways.[1] Some tissues such as skin are able to self-regenerate, however other tissues, including tendons have little or no regenerative capacity. The 'Holy Grail' of tissue engineering and regenerative medicine (TERM) is to be able to repair damage by stimulating self-renewal, so that the regenerated tissue completely recapitulates the pre-existing tissue before disease.[2–4] Ideal TERM therapies aim to either produce functional tissue *in vitro* that can be subsequently implanted, or to stimulate the production of *de novo* tissue *in vivo*. A successful TERM therapy could be useful in the treatment of previously life threatening or incurable diseases.[5] Similarly, TERM therapies can be used to improve patient's quality of life, by application in chronic diseases where tissue abnormalities result in morbidity and decreased mobility, such as tendon disorders. Within the field of orthopaedic surgery, damage to tendons is the most common soft tissue injury.[6] Worldwide, of the 30 million musculoskeletal injuries reported, over half involve tendons and ligaments, and as many as 50% of sports-related injuries involve tendons.[7,8] The prevalence of such injuries is only set to rise with the increase in average life expectancy and popularity of high mechanical load activities such as gymnasium use, football and athletics.[9] Tendon injury is debilitating, associated with pain, and long term suffering for the patient, and the tissue is characterised by low cellularity and limited healing capacity.[2] As a consequence, the treatment of tendon disorders would be aided by the identification of an appropriate TERM strategy.

The most effective strategies incorporate knowledge across a whole range of disciplines including materials science, stem cell research and developmental biology to progress the healing and development of tissues and organs.[10] T.E.R.M strategies usually take a three-pronged combinatorial approach (Figure 1).[11] This includes the use of cells, proteins and scaffolds, each with their own unique role to play in the regeneration of new tissue. Cells are an essential component of the healing potential of tissue and by supplementing these to the site of repair, regeneration may be initiated.[12,13] Without cells and the synthesis of new matrix components there is no healing response seen in tissue.[11]

Signalling molecules, such as growth factors, can aid the recapitulation of the specific spatial and temporal progression of natural tissue healing and can be tailored specifically to the tissue of interest.[14] Scaffolds can be used as a delivery vehicle for these signalling molecules or to support the growth and 3D structure of the newly forming tissue.[15] The scaffold can provide a suitable environment for the attachment, proliferation and migration of cells, therefore providing a foundation for matrix remodelling and tissue regeneration.[11]

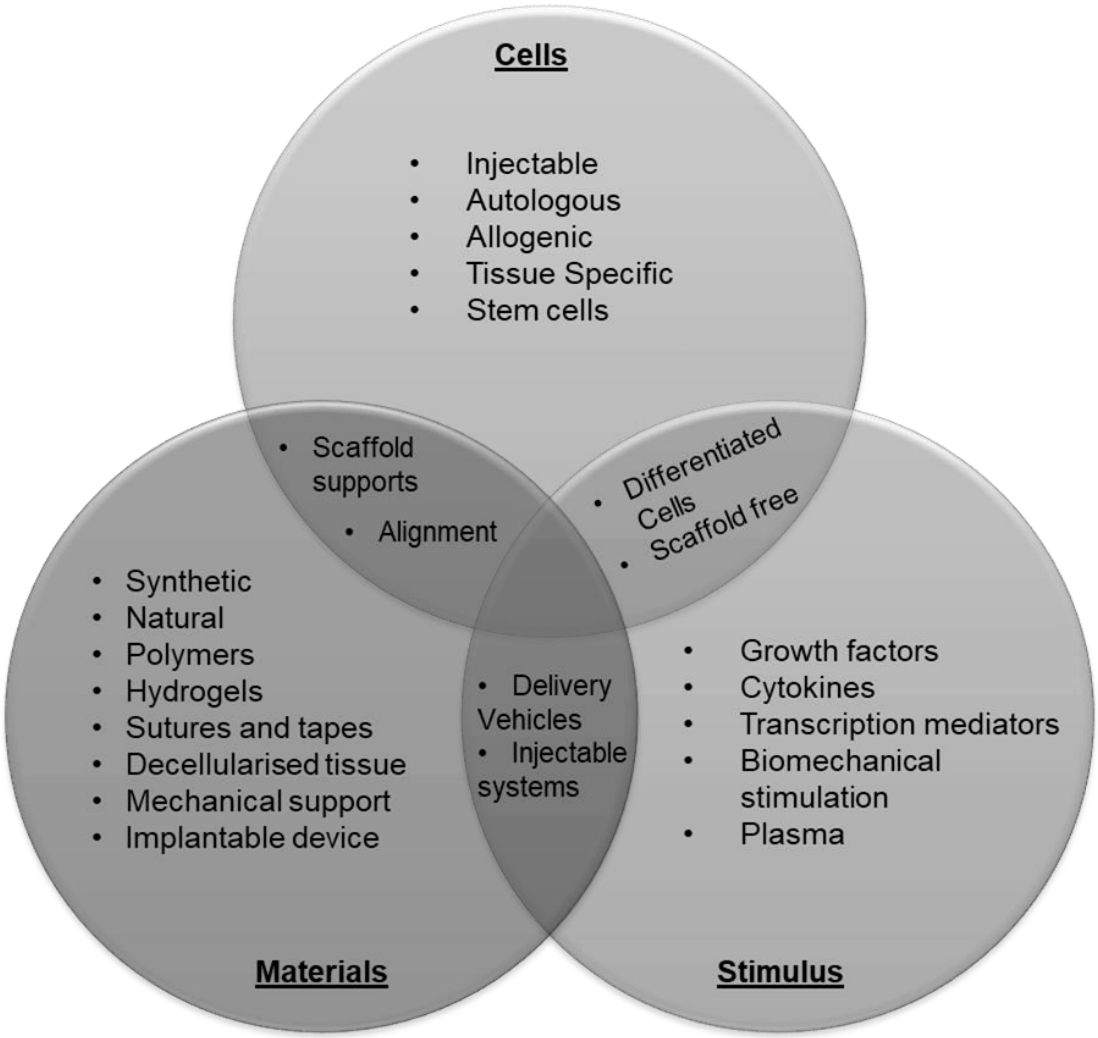

Figure 1: Tissue engineering and regenerative medicine strategies. Cells, stimuli and materials can be used in combination, or alone, for the treatment of diseased tissue.

2. Characteristics of Healthy Tendons

In order to begin the successful development of a TERM therapy for the treatment of disease or injury, it is paramount that there is a fundamental understanding of the normal development of the healthy tissue to be targeted.[2] It is important to understand the cellular composition, and elucidate the key molecular components essential to the development and maintenance of healthy tissue, so that the engineered tissue can fully imitate the native state.[16]

2.1. Structure and Function of Tendons

Tendons are tough bands of fibrous, viscoelastic, connective tissue that connect every muscle of the body to bone.[17] Their primary function is the transmission of forces generated by muscle to the corresponding bone, essential for the conversion of muscle-induced tensile stress to movement.[9,18] It is critical that tendons have the ability to withstand large exerting tensile forces, and are able to provide an effective buffering system, absorbing shock and preventing muscular damage.[18] The location of the tendon within the body, and its function which is decided by the forces acting upon it from surrounding muscle, has an impact on its structure.[19] Tendons bearing large forces are more likely to be short and broad, such as those of the quadriceps, whereas those intended for small and delicate movements, like the flexor tendons of the hands, will be long and thin.[19] The length and breadth of tendons is related to the amount of collagen present.[18] The Achilles tendon bears the greatest tension and is estimated to transmit forces as high as twelve times that of the human body weight.[20] All muscles have both a proximal and a distal tendon, connected to the muscle at the myotendinous junction, and to the bone at the osteotendinous junction.[19] The insertion site of the tendon to bone is known as the enthesis and is formed of four distinct regions of tissue.[21] The enthesis is capable of withstanding forces four times greater than that of the tendons mid-substance, with the myotendinous junction being the weakest point of the tendon.[20]

Tendons are formed from the continual aggregation of the smallest structural unit, collagen, into an increasingly complex architecture.[20] The resident cells of

the tendon; tenocytes, synthesise the collagen precursor molecule tropocollagen.[2] Tropocollagen molecules, catalysed by lysyl oxidase, then crosslink to form a stable molecule of collagen.[22] Spontaneous aggregation of multiple collagen molecules then results in the formation of collagen fibrils.[20] These fibrils then continually agglutinate to form progressive hierarchal structures beginning with a collagen fibre, leading to a primary fibre bundle, also known as a sub fascicle, a secondary fibre bundle, termed a fascicle, a tertiary fibre bundle and ultimately the tendon unit.[2,19,22] Surrounding each fibre and connecting the fascicles together, is a network of connective tissue known as the endotendon (Figure 2).[19] This fine, sheath-like network is responsible for supplying the tissue with blood vessels, nerves and a lymphatic system.[2] Additionally, it provides the lubrication necessary for collagen fibres to easily glide over one another during movement.[19] The entire tendon unit is then encompassed with the epitenon, a dense network of collagen.[2] The tendon can sometimes also be encompassed by a secondary meshwork of double layered areolar connective tissue, known as the paratenon.[23]

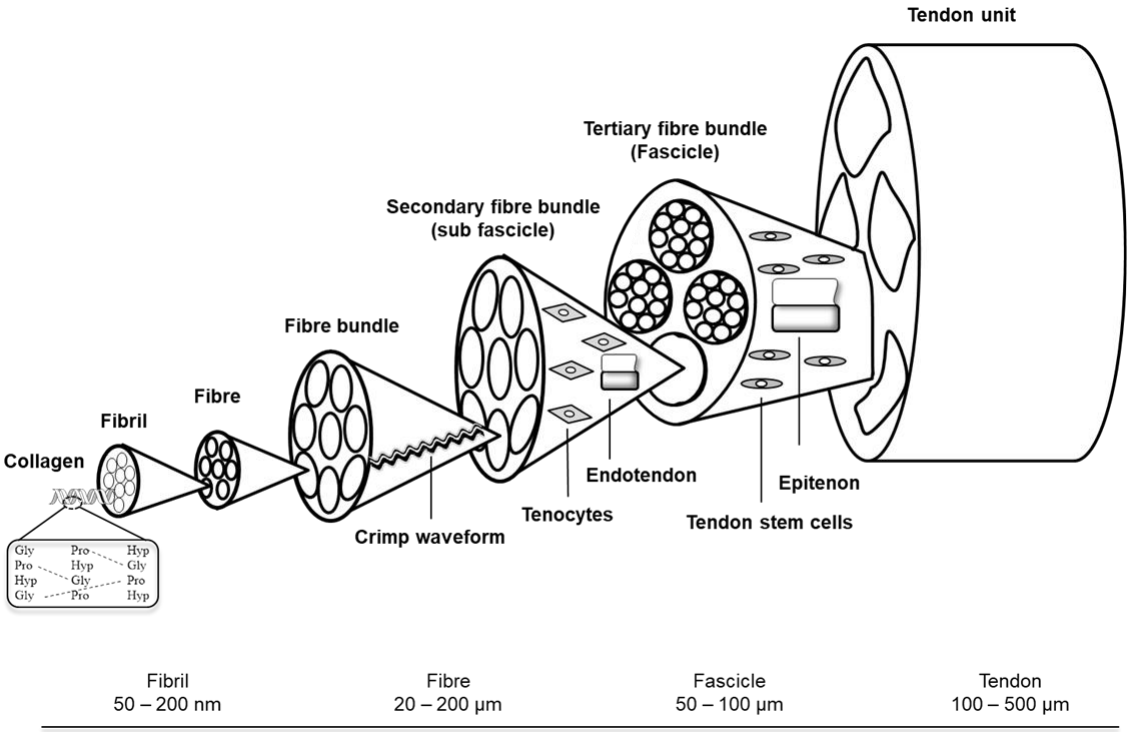

Figure 2: Hierarchical structure of tendon tissue. Collagen is the smallest unit, and with continual accumulations into increasingly large complexes forms the final tendon tissue.

This fatty tissue is present in the interstices of the fascicles and acts as a protective layer against friction and assists in the movement of tendon against adjacent tissue.[19] The epitenon and the paratenon are often considered in combination and termed the peritenon or peritendineum.[2] It is the highly organised and aligned structure of tendon tissues that allows it to carry out its function. It is able to withstand high loading forces by modifying its structure after mechanical stimulation via a process known as mechanical adaptation.[20] At rest, a highly organised crimped configuration can be seen in the tissue.[18] Once under tensile strain the crimped formation enables the tissue to distend, absorbing large forces. This conformational change allows for the tendon tissue to be stretched up to 2%, which is known as the 'toe region'.[20] This stretching is temporary and after the stimulus has receded the tissue is able to revert back, displaying the characteristic crimped formation once again.[19] This is due to the effect of elastin molecules present in the tissue.[20] However, the resistive capability of tendons is not infinite and if the stretching limit is exceeded, this crimp formation is lost and the tissue becomes vulnerable. If stretching of the tendon continues to 4%, the result is microscopic tears, with further stretching up and past 10% causing rupture of the tendon (Figure 3).[20] Continual overuse and excessive mechanical load of the tendon results in repeated macroscopic tears, forming scar tissue, and eventually a weakened tendon, exhibiting the clinical condition known as tendinopathy.[16,17]

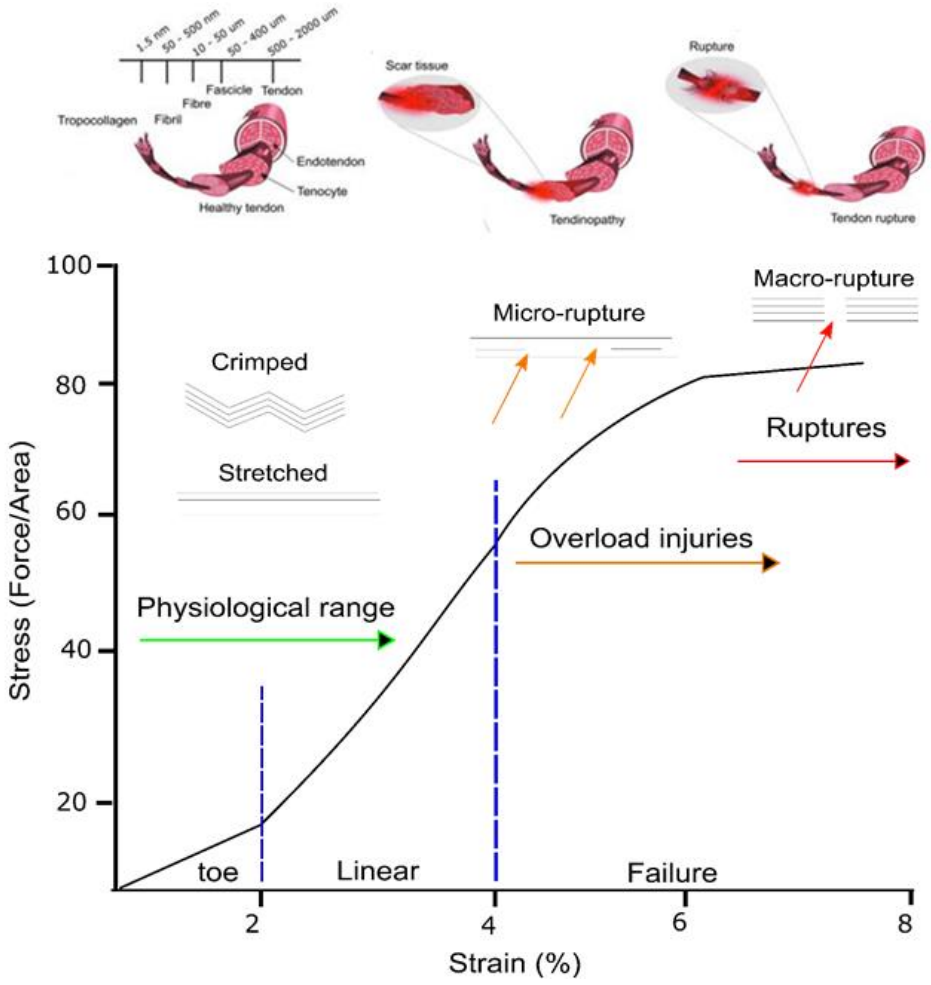

Figure 3: Stress-strain curve of tendon tissue. Tendons ability to resist tensile forces is shown in the toe and linear region where the crimped structure of the tissue allows them to distend and absorb shock. Trauma to the tissue is seen above 4% strain. Adapted from Walden *et al*.[49]

2.2. Cellular and Molecular Composition

Tendon tissue is characterised by low vascularity and hypocellularity.[2] The predominant cell type found in tendon tissue is the elongated fibroblast-like cells known as tenocytes.[24] These account for as much as 95% of the cellular composition of the tissue and are situated within the aligned collagen fibres of the epitenon and endotendon.[18,22,24,25] These cells are responsible for the synthesis of collagen, essential for the hierarchical architecture of the tissue and extracellular matrix components.[2] The additional 5% is comprised of progenitor cells, chondrocytes, synovial cells and vascular cells.[22,24] The extracellular

matrix (ECM) of tendon is responsible for the structural and biomechanical support of the cells and helps to define tissue shape, act as a scaffold, and is composed of the essential biomolecules such as proteoglycans, glycosaminoglycans (GAGs), glycoproteins, and collagens.[20] The extracellular matrix has the ability to respond to stimuli and is able to remodel its microenvironment in response to stresses and traumas. This is mediated by the action of matrix metalloproteinases and is essential for the repair, development and function of the tendon tissue.[24] Proteoglycans and GAGs are necessary for the tissues to withstand compressive forces and allow for the easy gliding of fibres during mechanical deformation.[9,19,26–28] Their functions include; acting as shock absorbers and lubricants through the retention of water, conferring elasticity, maintaining organisation, growth and assembly of collagen fibrils, providing cell adhesion sites and the binding of secreted growth factors.[9,23]

Collagen is the most abundant protein found in tendon, with collagen type I accounting for 95% of the total collagen in the tissue.[7,20] Collagen type I is highly organised and aligned, and is found in the mature collagen fibrils of healthy tendon. [24,29] Structurally it comprises three parallel polypeptide chains, consisting of repeating glycine and proline residues, allowing the formation of a triple helix which facilitates hydrogen bonding and crosslinking, stabilising the molecule.[30] A decrease in collagen type I is indicative of a weakened tendon and results in decreased tensile strength and ability to withstand mechanical load.[31] Collagen type III, and V provide the remaining 5% of collagens in tendon.[20]

Type III collagen is located chiefly in the endotendon and epitenon.[9] It is weaker than collagen type I due do a decrease in crosslinking and visually produces smaller and thinner fibres, which have a decreased resistive capacity.[27,28,31] Collagen type III is much less organised resulting in decreased mechanical strength.[20] In healthy tendon it is synthesised at significantly lower levels in comparison to collagen type I.[27] However, it is upregulated in damaged tendon, and synthesised in abundance, during the repair process.[27,29] Increase in the production of collagen type III, relative to type I, can lead to the formation of adhesion sites between tendon and surrounding tissue, a reduction in

mechanical strength, an increased risk of rupture, and ultimately the formation of scar tissue.[27] Despite these drawbacks, collagen type III is essential for the initiation of the healing process of tendon and to provide a provisional matrix in response to injury, as well as being essential for fibrillogenesis of collagen type I.[31,32]

3. Tendon Injury and Healing

In order to engineer the regeneration of diseased tendon tissue successfully, it is important to understand fully the natural healing process that takes place after injury. Future successful advances will be underpinned by this knowledge.[33] Post injury to the tendon, two pathways of repair occur; the intrinsic and the extrinsic, which work synergistically.[2] Most repair is carried out by the intrinsic pathway where proliferation of fibroblasts present within the epitenon and endotendon occurs, resulting in cellular migration to the site of the lesion and the synthesis of new matrix materials.[2,24,28] The extrinsic pathway is associated with migratory inflammatory cells and fibroblasts from surrounding tissues.[2,28] Fibroblast cells have an important role in the initial closure of the wound after injury by exerting contractile forces on the extracellular matrix. However, excessive fibroblast contraction can result in the formation of scar tissue and increased collagen production.[20] The natural healing of tendon tissue after trauma can be characterised into three overlapping stages; inflammation, repair, and remodelling (Figure 4).[28]

Inflammation predominates in the first week immediately after injury and is associated with swelling of the tissue. After the initial tear a blood clot is formed, beginning the inflammatory process and acting as a scaffold for migratory cells.[23] Platelets in this clot release chemoattractants and cell proliferative growth factors such as insulin like growth factor (IGF), platelet derived growth factor (PDGF), and basic fibroblastic growth factor (BFGF). These growth factors are important for the recruitment of surrounding fibroblasts and tenocytes, and the production of new matrix materials.[20] They also release histamines essential for the vasodilation of blood vessels allowing for increased permeability.[33] Within the first twenty four hours inflammatory cells, such as

macrophages, invade the lesion and are responsible for the phagocytosis and removal of necrotic tendon tissue. [18,28] Transforming growth factor-β (TGF-β) is released from invading macrophages, which is essential for the production of new collagen fibres.[33] Vascular endothelial growth factor (VEGF) stimulates angiogenesis and the re-establishment of vascularisation to the healing tissue.[34]

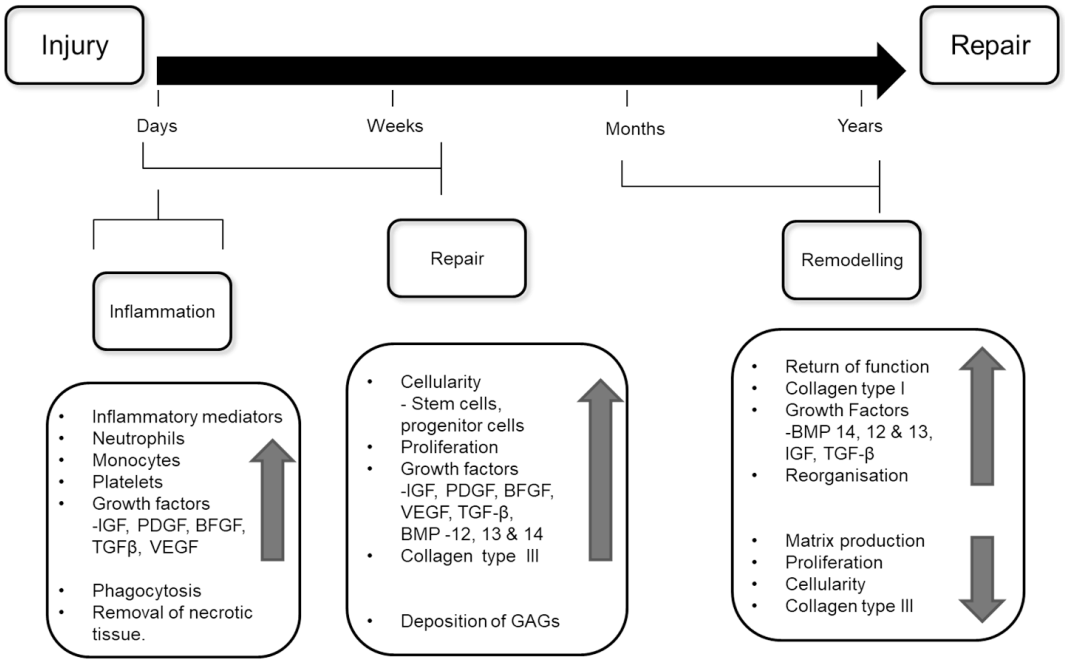

Figure 4: Repair process of tendon injuries. Shown are the cellular and molecular changes in the tissue, where up arrows denote an increase or upregulation and down arrow a decrease or down regulation.

The repair phase of tendon healing is characterised by the synthesis of new matrix materials, collagen, GAGs, and proteoglycans. This process begins two days after tendon injury and can persist for a further six weeks.[23,33] This stage is characterised by hyper-cellularity, upregulation of growth factors, increased protein synthesis, and neovascularisation. It is during this period when growth factors such as IGF, BFGF, PDGF, VEGF, TGF-β and bone morphogenetic proteins (BMPs) have the most activity.[33] GAG and water content is elevated throughout this process.[20] During this repair phase the synthesis of the essential components of tendon tissue, which will allow the wound to heal, occurs. However, this is a reparative process rather than regenerative and therefore the collagen synthesised in the most abundance is type III.[18,23,28,35]

The remodelling process is concerned with reshaping and resizing the tissue.[36] This is a prolonged period which begins six weeks after injury and lasts approximately a year.[23] Cellularity, protein content and vascularity slowly begins to return to normal and the synthesis of new materials decreases.[18] Collagen fibre crosslinking increases and the tissue stabilises with a return of some stiffness and tensile strength.[20] Eventually the tissue begins to develop a scar like phenotype.[28]

The repaired tendon tissue is both structurally and biomechanically inferior to the original uninjured tendon.[18,21,22] The resulting tissue is characterised by a broad range of cellular and molecular deviations from the native tissue (Figure 5).[24] This includes altered protein content and composition, abnormal vascularity, which is associated with the onset of pain, and an increase in collagen type III relative to type I.[24,28] This increase in collagen type III results in disorganised, aberrantly aligned fibrils and the presence of scar tissue.[4,23] This results in the clinical presentation of tendinopathy. This is characterised by a reduction of mobility, an increase in pain and morbidity for the patient and overall a weaker tendon that is prone to rupture and tears.[4,28]

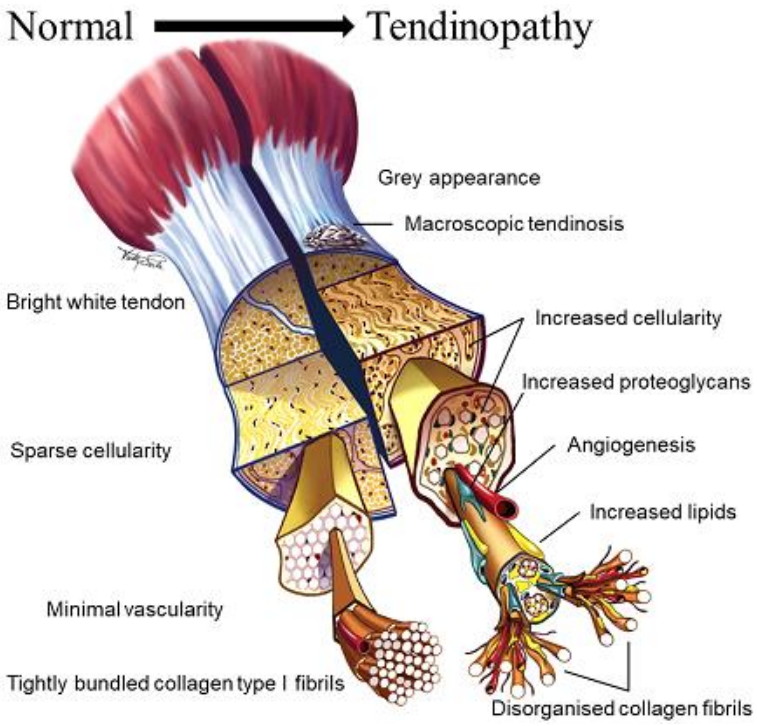

Figure 5: Changes in tendon tissue post injury. Both tissue architecture and molecular composition are altered in tendinopathy. Adapted from Scott et al.[259]

4. Tendinopathies

Tendinopathy is the umbrella term used to describe a broad spectrum of several different tendon pathologies.[37] The term tendinopathy does not suggest anything about the underlying pathology of the tendon and includes; degenerative tendon, inflammatory tendon, failures at enthesis, and paratenon injury.[38,39] Most tendinopathies are not caused by one single factor and there are many contributory elements which can be either intrinsic or extrinsic. These factors can include age, gender, disease, occupation and physical training.[22,39] Tendinopathy can either be classified as acute, resulting from excessive overload, or chronic, due to an underlying degenerative condition. This explains the tendency for tendinopathy to occur in young patients with active lifestyles and the elderly.[16] Degeneration and repeated micro-traumas are considered as the primary causative factor of chronic pain-free tendinopathy and often results in tendon that is likely to 'spontaneously' rupture.[23,39] In fact, studies have found that in 97% of spontaneous ruptures, an underlying degenerative pathology was existent before the incident.[16] Tendinopathy can also be used to describe adhesions that form as a result of scar tissue. These hinder the gliding of the tendon and lubrication with surrounding tissue and result in reduced mobility after injury.[15,40] The most common site for tendon injury is near, or at, the enthesis. This area is highly stressed and subjected to higher strains and forces, combined with the fact that the tissue here is the least vascular of the entire tendon. Tendons most susceptible to tear are the patellar tendon, the Achilles tendon, the medial and lateral extensors of the elbow, the long head of the biceps, and rotator cuff in the shoulder.

5. Current Treatment Options for Tendon Injuries

The current, readily available treatments for tendinopathy are focused upon the management of pain rather than healing of the underlying causative issues.[24] These include the use of non-steroidal anti-inflammatory drugs (NSAIDs), steroidal injections, exercise and mobilisation therapies, and as a last resort, surgery. NSAIDs such as ibuprofen are of the most benefit in tendinitis, in which inflammation is a key component. Here they are able to inhibit the synthesis of

prostaglandins, a chemoattractant implicated in the onset of inflammation and pain. However, this treatment option is not viable when the tendinopathy is no longer accompanied by inflammation, such as degenerative conditions. As a result the use of NSAIDs as a first line response and management of tendinopathy is controversial and is lacking efficacy.[41]

Exercise and mobilisation therapy is another widely used method for the treatment of tendinopathies, with stretching and strengthening activities being the most commonplace.[41] Gradual increase in applied tension has a positive effect on cell proliferation, stimulation of growth factors, and synthesis of collagen. Conversely, immobilisation has been shown to have serious deleterious effects on the tendon. Immobilisation can result in the deposition of uneven collagen fibrils, decreased tissue stiffness and resistive capacity, and decreased cellular metabolic activity.[20] On the other hand, if excessive pressure is applied too soon after injury, this can also result in a detrimental response, resulting in impaired healing.[42] This means that the precise mobilisation strategies employed need to be tightly controlled for improved healing, and quick recovery times. Additionally, the precise therapy, and quality of treatment, can vary between clinics. To date there is no defined procedure that dictates the best mobilisation activities, and so healing times, and results from patient-based evidence, fluctuates widely.[41] Therefore, more work needs to be carried out to produce an evidence-based, exercise regimen, which is able to demonstrate successful tissue remodelling. This would allow for more consistent results demonstrating improved strength and function of damaged tissue.

Surgery is a last resort treatment when other avenues have been exhausted, or rupture of the tendon has occurred. Ruptures resulting in lesions greater than 5 mm do not heal naturally and thus surgery is usually the only option.[9] Surgical treatment aims to remove the frayed and damaged tissue and then reconnect the torn ends by suturing them together.[43] Over the last few decades a multitude of suture techniques and materials have been proposed each with their own benefits.[9] Regardless of the numerous advances in both materials and techniques in search of the ideal treatment method, surgery still has multiple complications associated with it. [15,42] Re-rupture is common, and in

rotator cuffs has been reported to be as high as 94%.[42] Long term outcomes for patients are highly variable, and morbidity remains high even after what is considered successful treatment.[2,28] Additionally, further complications postoperatively are prevalent, such as the increased risk of early onset osteoarthritis, chronic pain, and in the case of allografts, the risk of immune rejection. Furthermore, to date, attempts to regenerate tendon tissue after damage at the enthesis have proven problematic.[2] Currently surgical procedures are often chosen on clinician preference rather than established evidence-based guidelines. This explains the vast multitude of suture materials and techniques available, and the absence of a single 'gold standard' treatment option. Surgical intervention is yet to yield consistently satisfying results without the presence of pain, reduced motility, morbidity or high risk of re-rupture for patients.[21,28]

It is apparent that current treatments in tendinopathy are both unreliable and inefficient.[24] The practiced therapies are not supported by satisfactory clinical trials, are not effective, and fail to address the underlying pathophysiological changes that have occurred to the tissue.[16] When considering the current treatment options available to patients, the need for the development of a successful system that incorporates the knowledge of the native tissue, and aims to address the underlying pathological issue, with the goal of a regenerative outcome is apparent.

6. Tissue Engineering Approaches to Tendon Injuries

T.E.R.M therapies have focused around the delivery of cells and proteins to the repair site of damaged tendon. Natural tendon tissue is characterised with hypo-cellularity and as a result has limited healing capacity. Therefore it is hypothesised that supplementation of essential cells and growth factors can boost the healing potential of the tissue, increasing the synthesis of essential collagens and matrix components resulting in restoration and regeneration.[2,12,13]

6.1. Cell-Based Therapies

Many different cell populations have been used for the regeneration of tendon injuries, each with their own advantages and disadvantages (Table 1). Tenocytes are the primary cell type within healthy tendon tissue and as such have achieved popularity as a cell-based therapy for tendinopathy.[28] They are responsible for the synthesis of collagen and extracellular matrix components and have shown success in small animal models, and clinical trials.[7,13,18,41,44] However, these therapies are limited by the potential for donor site morbidity to occur and the need for cell expansion once harvested, which can lead to the loss of metabolic activity, specific tendon markers, and phenotype.[7,25,45] Tendon-derived stem cells have also been investigated, offering the advantage of being a tendon-specific, multipotent cell line for the treatment of tendon disorders.[7,46] As tendon progenitor cells they have the ability to express tendon specific biomolecules such as collagen type I, decorin, biglycan, tenomodulin, and scleraxis, as well as being self-renewable.[7,13] However they suffer from a slow metabolic rate, and lose their ability to differentiate after multiple passages, resulting in poor proliferation *in vitro*.[46] Additionally, these cells are difficult to harvest because of their limited availability, only accounting for 4% of the tendon cell population.[7]

Cells derived from tissues located elsewhere in the body, such as muscle and skin cells, have also been investigated. Muscle-derived cells including myocytes and fibroblasts have been used due to their role in the natural development of embryonic tendon tissue.[2,26] They share a similar morphology and secretome to tenocytes, being able to synthesise collagen types I and III, decorin and fibronectin.[7] Dermal fibroblasts from skin have also been previously tested.[12,50] These cells are available in abundance, are easily proliferated in culture and the harvesting process is not associated with donor site morbidity or invasive procedures. Although both these discussed cell lines are easier to harvest and expand *in vitro*, they come from differentiated tissue and therefore, there are concerns surrounding their specificity.[7,26]

Cell Type	Type of study	Results
BM-MSC	*In vitro / in vivo* Equine tendon	Improved tissue organisation. Formation of crimp structure. Histological improvement of tissue, including reduction in GAG, DNA and cell content, comparable to normal tendon.[21]
ADSC	*In vitro / in vivo* Rabbit Achilles tendon	Neo-tendon formed, with tensile strength comparable to 60% of normal tendon. Production of parallel collagen fibres and elongated cells aligned longitudinally with collagen fibres.[45]
ADSC	*In vitro / In vivo* Rabbit Achilles tendon	Increased tensile strength of tendon tissue. Partially regular and longitudinal alignment of collagen fibres. Increased collagen type I production.[31]
Tenocytes	Clinical trial level 4 Human extensor carpi radialis brevis tendon	Improvement of patients' pain score by 86% after 12 months. Improved grip strength. Reduction in clinical prevalence of tendinosis. Functional improvement and structural repair of tendon.[13]
Tenocytes	*In vivo* Rabbit Achilles tendon	Increased collagen type I expression, demonstrating enhanced alignment. Increased stiffness of tissue.[47]
Dermal Fibroblast	Randomised controlled trial level 1 Human patella refractory tendinopathy	Pain, severity and functionality scores improved from 44-75 after 6 months. Decrease in tendon thickness.[12]
Muscle derived stem cells	*In vivo* Mouse muscularis fascia of dorsum tendon	Formation of cord-like neo-tendon similar to native tissue in appearance. Increased maximum load capacity. Increased stiffness at 12 weeks. Increase tensile strength.[26]
Tendon stem cells	*In vivo/ in vitro* Rat patella tendon	Increased expression of collagens type I and III, and tenomodulin. Formation of tendon-like tissue after 8 weeks. Enhanced collagen fibre thickness.[46]
Fibroblast	*In vitro* Rabbit infraspinatus tendon	Increased type I collagen expression. Increased tensile strength of regenerated tissue.[48]
Periosteal progenitor cells	*In vivo* Rabbit infraspinatus tendon	Increased matrix deposition. Increased production of agrecan and collagen type I and II. Formation of fibrocartilage and bone at the tendon-bone insertion site.[47]

Table 1: Cell based therapies for the treatment of tendon injuries. Adapted from Walden et al. [49]

Stem cells, such as mesenchymal (MSCs), bone marrow derived (BMSCs) and adipose derived (ADSCs) have been investigated.[2,7,15,21,25,45,51–55] Their pluripotency, abundance and relative ease of harvesting make them attractive candidates for T.E.R.M therapies.[25,45] They have the ability, in the appropriate conditions, to differentiate down a number of lineages into specialised cells such as bone, ligament, muscle, cartilage and tendon.[4,25,36] These cells can be pre-differentiated before delivery or post-implantation within the environment of the tissue.[7] It has been shown that simply aligning stem cells in the orientation of collagen fibrils of native tendon tissue can result in cell differentiation and the production of tendon specific markers.[56] A set of criteria has been produced to classify differentiated cells as tendon cells. These include; positivity for collagen type I, III and V, expression of decorin, scleraxis, tenomodulin, and tenascin-C, and an elongated, spindle morphology. These cells must be negative for non-tendon markers such as collagen type II, osteocalcin, alkaline phosphatase and myogenetic markers.[7,25] The use of stem cells in tendon tissue repair can be problematic. The inherent pluripotency of these cells means that the specificity of the tissue produced is not guaranteed. Differentiation of these cells into osteoblastic and chondrogenic lineages, with the formation of ectopic bone and cartilage at the repair site has been reported.[7,13]

6.2. Protein Delivery-Based Therapies

Another potential target emerging for the regeneration of tendon is the sustained release of proteins and growth factors.[10,57] These have the potential to regenerate tendon tissue by stimulating the natural remodelling pathways.[28,58] The use of exogenous growth factors presents the possibility of accelerating cell proliferation, collagen synthesis and extracellular matrix synthesis, leading to quicker recovery and enhanced repair.[6,38,40] The desired outcome is one in which the complex temporal and spatial delivery of signalling molecules mimics the natural healing of tendon, resulting in the regeneration of functional tissue, comparable to its undamaged counterpart.[28,57] Several growth factors have been studied for this purpose which have been shown to be expressed in nearly every phase of healing progression (Table 2).[4,15,59]

Treatment	Tendon Model	Results
PDGF	Canine flexor	Increased cell density and proliferation. Increased expression of collagen type I. 30% increase in reducible crosslinks.[14]
PRP	Equine superficial digital flexor	Increased cellularity. Increase collagen and GAG content. Increased tensile ability. Increased collagen matrix integrity.[60]
VEGF-11	Rat achilles	Increase ultimate tensile strength of tendon. Increase in mechanical stress needed to rupture healed VEGF tendons compared to controls.[61]
IGF-1 and TGFβ	Rabbit patellar	Increased vessel formation. Production of fibrous repair tissue, with enhanced orientation. Increased force at failure, ultimate stress and stiffness at 2 weeks.[35]
BMP-12	Sprague-Dawley rats calcaneal	Increased expression of tenocyte lineage markers such as scleraxis and tenomodulin. Formation of tendon like tissue. Increased cell proliferation. Elongation and alignment of cells, and increased matrix deposition.[62]
BFGF	Rat rotator cuff	Increased production of GAG. Improved collagen organisation, stiffness, and ultimate load to failure 8 weeks postoperatively. Improved healing at enthesis.[63]

Table 2: Protein delivery strategies for the regeneration of tendon tissue.
Adapted from Walden et al.[49]

Platelet rich plasma (PRP) consists of a concentrate of autologous blood platelets. It offers the potential release of a cocktail of proteins for tendon healing.[27] Platelets when delivered to the site of injury are able, upon degranulation, to release stored growth factors which initiate the healing process.[27,34,61] PRP has been shown to increase proliferation of human tenocytes, and synthesis of collagen type I, as well as upregulate essential matrix components; decorin and tenascin-C.[27,60] However, the use of PRP is controversial, with some studies finding it ineffective.[64] Additionally there are concerns over the potential for PRP to secrete inflammatory mediators, that would have a negative impact on healing.[61] Complications also arise when

considering the reproducibility of results, as variability can occur between each batch of PRP.[7]

PDGF has been implicated in the increased production of collagen type I during healing of tendons and ligaments.[33,40] It has been proposed that the exogenous application of PDGF may facilitate the healing of tendon tissue, with both *in vitro* and *in vivo* studies showing an increase in collagen type I production after its application.[14,33,65] Currently there are some concerns surrounding the exact dosage, and the suitable period in which to deliver PDGF as a therapeutic molecule. Further studies, including the most appropriate carrier system, are required before this growth factor can be used commercially.[15]

VEGF is important in the early phases of tendon healing. It is well known to stimulate angiogenesis, and increases the vascularity of tissue, and the corresponding proliferation of endothelial cells.[34,58,61,66] Within the healing tendon approximately 67% of the cells present at the repair site express VEGF.[33,67] In acute tendinopathy of patellar tendons, patients exhibited a higher VEGF expression when compared with those suffering from the chronic condition. This has led to the suggestion that increase in VEGF expression may lead to an accelerated healing after acute injury, especially when mechanical load is kept to a minimum.[61] Conversely however, VEGF has also been found to have a negative effect on the healing tendon tissue.[68–70] Correspondingly, the current opinion on the benefit of VEGF as a therapeutic agent for the regeneration of tendon tissue is still inconclusive, requiring further investigation and evidence of improved clinical outcomes.[66]

BFGF plays an important role in the proliferation of cells in tendon tissue, and the initiation of angiogenesis.[33,71] It is secreted by inflammatory cells and fibroblasts present after tendon injury and mediates cellular proliferation, migration, angiogenesis and the synthesis of collagen.[33] It has been suggested that BFGF is most effective when delivered during the inflammatory process, immediately after tendon injury.[59] Unfortunately, there is no consensus in the literature as to whether BFGF is beneficial for the treatment of tendinopathy, with contradictory hypotheses prevalent.[40,71]

BMPs are low molecular weight signalling proteins included within the TGF-β superfamily, with the ability to induce the formation of bone, ligament, cartilage and tendon tissue.[20,27] These small signalling molecules are able to initiate the transcription and expression of a range of genes responsible for the remodelling of tissue, and differentiation of cells.[28,37,72] Several studies of BMP-12 as a deliverable growth factor for the treatment of tendon injuries have made promising advances, showing its potential to induce the formation of tenogenic tissue both *in vitro*, and *in vivo*.[25,32,62,73–77] One promising feature of BMP-12 is its ability to differentiate stem cells down a tenogenic lineage.[73,74,78] BMP-12 has also been implicated in the formation of tendon tissue *in vivo*, using animal lacerations as model defects.[32,62,77]

6.3. Current Delivery Systems for Tendon Regeneration

In order to successfully deliver cells or proteins to tendon and mimic the spatial and temporal signalling profile seen in the healing tissue, a suitable delivery system is necessary.[79,80] Biomaterials can be designed as a delivery system, incorporating cell adhesion moieties, as well as signalling molecules and cells that are able to co-ordinate the regeneration of the tissue.[11,23,48,81]

Hydrogels are crosslinked polymer networks capable of retaining large volumes of water within their 3D structure.[82] They can be functionalised to have desired properties such as easy injection, mechanical stiffness, controllable degradation rates and sensitivity to temperature and pH.[62] Hydrogels, encapsulating cells and proteins, have been investigated for their application in tendon regeneration.[44,63,83,84] Injectable hydrogels are advantageous for smaller tendon defects, offering a non-invasive alternative to surgical intervention.[85] They can act as ‘plugs’ at the repair site, forming a sealant and barrier to the formation of adhesion sites.[86,87] They offer a simple and convenient method for the prolonged and controlled delivery of regenerative factors.[86,88]

Currently implantable systems are more commonplace in tendon repair than injectable ones, preferred in larger defects where the structural and mechanical properties of the tissue are greatly diminished.[88] They are able to bridge the gap

created within larger midpoint ruptures, allowing surgeons the ability to remove the necrotic frayed end of the tissue, reconnect the tendon, and suture in place the regenerative device.[88] Implantable systems explored have been woven sutures, patches, electrospun fibres, and sponges.[26,48,89–93]

Decellularised tissue offers the advantage of exactly resembling the structure of tendon tissue, whilst being able to provide the appropriate adhesion and signalling cues to host cells.[94] As a scaffold, it allows the growth of cells along the aligned collagen fibrils present, leading to an improved healing response.[46,94,95]

Exogenous delivery of growth factors has also been explored but is hindered by the short half-life of proteins, and their quick clearance and degradation[6,34,96] One method to combat this has been their incorporation into the bulk of microparticles.[97–99] Similarly, cells can be delivered via autologous injections, and have seen some success in clinical trials.[12,13,50]

Although it is clear that much work is being carried out to determine possible therapeutic agents for the treatment of tendinopathy, the optimal technique and delivery method has yet to be discovered. Each deliverable factor, and method of delivery, although with advantages, is not without limitations. There is still an apparent need for an effective T.E.R.M therapy that can deliver, and retain, growth factors at the site of tendon injury, with continued controlled release and the opportunity for sequential administration of different factors.

7. Aims and Objectives

The aim of the work carried out in this thesis was to produce an effective delivery system of a therapeutic protein for the treatment of tendon disorders. The ideal system would be a template model that could easily be adapted and manipulated for a multitude of different therapeutics. A good delivery system would have the ability to incorporate protein for delivery and would allow for controlled, tuneable and sustained release at the repair site. The overall aim was to produce a delivery system that is non-toxic, non-immunogenic and bio-resorbable that would be bio-responsive for the regeneration of tendon tissue.

To achieve this aim, it was decided that a microparticle system would be used for the delivery of therapeutics. To this end, the key objectives carried out were; 1) Decide on an appropriate polymer candidate that could be used to produce microparticles via a double emulsion method. 2) Decide the most appropriate method of incorporation of protein. To achieve this aim, encapsulation methods, surface modification methods and conjugation via click chemistry were investigated. 3) Formulate microparticles with a specific size range and uniform dispersity. 4) Demonstrate microparticles ability to conjugate proteins of interest.

The work described in this thesis highlights the steps taken to formulate a polymeric, microparticle drug delivery system which would be able to conjugate to a relevant protein; TGF-β, and therefore be capable of stimulating the natural tendon healing response. Chapter 2 gives a review into the multitude of polymers available for the formulation of a drug delivery system and the available methods of both pre and post functionalisation to allow for protein conjugation. The initial aim of determining an appropriate method for incorporating protein into microparticles is discussed, with a focus on protein encapsulation within the bulk. Investigations then turned to surface modification and eventually functionalisation of a polycaprolactone polymer, to allow for protein conjugation via click chemistry. Proof of concept experiments were carried out to validate the polymers ability to attach to an alkyne containing click chemistry linker molecule.

Chapter 3 highlights the use of microparticles as a drug delivery system, with specific interest into control of their size and uniformity. A detailed description of the method of microparticle production is given using the polymer synthesised in chapter 2. Extensive optimisation was carried out to ensure microparticles could be produced over a large size range and monodispersity could be tightly controlled by altering process parameters. It was important to show that the microparticles had the ability to attach to a crosslinking molecule, and therefore the potential to conjugate to proteins in physiological conditions.

Chapter 4 gives insight into the available sites of conjugation present in proteins that can be targeted for their attachment to the microparticle drug delivery

system. Detailed are the numerous cross-linking molecules that can be used with the same conserved dibenzocyclooctyne core. With the aim of producing a template drug delivery system, 2 model proteins; human serum albumin and bovine serum albumin and 2 therapeutic proteins; TGF-β1 and TGF-β3 were investigated for their ability to conjugate to microparticles produced in chapter 3.

This project has an added Industrial Cooperative Awards in Science & Technology (CASE) studentship. In partnership with Neotherix Ltd, work was carried out to investigate the process behind the transition from academic research to industrial translation with the aim of understanding the production of a commercially available clinical product for the treatment of tendon injuries.

Chapter 6 gives concluding statements on the key findings of the project and addresses the success of the project in reaching the aims and objective set out above.

Chapter 2: Functionalised Polymer Synthesis

1. Introduction

1.1. Polymers for Tissue Engineering and Drug Delivery

A critical factor in the design of a successful drug delivery system for application in tissue engineering is the selection of an appropriate polymer candidate.[100] Polymers are large molecules formed of chains of repeating monomer units, and can be natural or synthetic. An ideal polymeric material for tissue engineering should be biocompatible, without any toxic, immunogenic or inflammatory side effects. The material should be resorbable and degrade into harmless products that can be cleared from the body via normal biochemical pathways. It should have the ability to promote cell proliferation, adhesion and migration and facilitate the development of *de novo* tissue.[101] Additionally, the polymer of choice should degrade at a rate that is comparable to the healing and re-establishment of new tissue.[11] Biodegradable polymers are preferred in tissue engineering applications because surgical intervention can be kept to a minimum. Drug release can often also be tailored to coincide with polymer degradation, allowing for controlled release rates.[100]

The appropriate polymer for a drug delivery system depends on the desired function of the material and its final application.[102] Polymers can be selected based on the properties required of the scaffold such as mechanical strength and elasticity, or those needed for formulation processes, such as viscosity and rigidity.[101] Another consideration when selecting polymers for drug delivery is their ability to interact with biomolecules. This may be dependent on the polymer containing biomimetic adhesion sites for the facile conjugation of bioactive agents.[103]

Biodegradable polymers can be classified into either synthetic or natural, depending on their source of origin.[104,105] Currently, research towards the synthesis of these types of delivery systems has been met with the challenge of choosing between natural polymers, abundant in biologically active interaction sites, or mechanically superior synthetic polymers, amenable to controlled manufacture, but lacking useful functional groups for conjugation.[106]

1.2. Natural Polymers

Natural polymers are an attractive candidate for drug delivery systems due to their similarity to the ECM of cells. The ECM is responsible for the facilitation of tissue formation and maintaining homeostasis, therefore, natural polymers such as collagen have been the target of investigation.[101] One advantage of natural polymers is their abundance within living organisms, meaning that they are both readily available and inexpensive.[100] Due to their organic nature they are inherently able to interact with the biological environment and contain recognition sites for bio-conjugation, as well as being biocompatible and biodegradable in physiological conditions.[101] Natural polymers also offer the advantage of being able to undergo biological remodelling processes.[104]

Collagen type I is the most abundant protein within the ECM, and as such has been one of the most extensively studied biomaterials for tissue engineering.[101,105] It is readily purified from animal tissue, including tendon, and can support the proliferation and adhesion of cells.[23,105] Collagen can also be easily formulated into different formats such as hydrogels, fascicle fibres and scaffolds, depending on the final target application.[107–110]

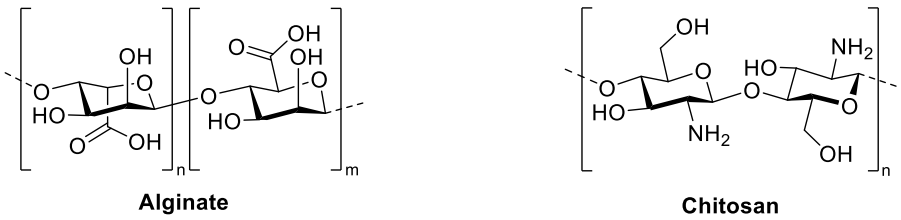

Figure 6: Examples of natural polymers used for tissue engineering and regenerative medicine

Alginate (Figure 6) is a natural polysaccharide that is readily extracted from brown algae. When in the presence of divalent cations, such as calcium, alginate can form a gel under mild conditions.[90,111,112] Therefore gelation can occur under physiological conditions, including pH and temperature, resulting in good cellular biocompatibility.[107] As a result of this, alginate has been investigated for the encapsulation of cells and proteins in tendon regeneration.[90,112–114]

Chitosan (Figure 6) is one of the most abundant polysaccharides in crustaceous marine animals, and can be readily cultivated from their exoskeleton.[78] It has great versatility due to its processability, being easily formulated into many structures such as hydrogels, fibres and sponges.[101,105,115–117] One advantage of chitosan is that it has been shown to reduce the formation of focal adhesions when implanted, improving the healing of regenerating tissue.[115,117] Additionally, chitosan displays good solubility in physiological conditions, allowing for maintenance of bioactivity when used in conjugation with proteins or peptides.[78] Table 3 gives a non-exhaustive overview of the different natural polymers and formulations used as drug delivery systems for the regeneration of tendon tissue. However, unfortunately, natural polymers also exhibit undesirable properties. Owing to the biological nature of the polymers, often degradation varies considerably between batches, which poses a problem when formulating a controlled delivery system with defined release rates.[104] Natural polymers also tend to exhibit poor mechanical strength in applications where load bearing is high, such as tendons. For these situations chemical crosslinking or modification is often needed to improve this.[100,109,118] Furthermore, when used in clinical applications, natural polymers can provoke adverse symptoms such as inflammation and immunogenicity, especially when derived from animal sources.[107,111] As a result of these shortcomings, synthetic polymers have been investigated as alternatives.

Formulation	Drug	Tendon	Results
Electrospun collagen fibre Implant	PRP	Rabbit Achilles	Promoted cell migration & proliferation. Increased number, diameter, & density of collagen fibrils, with improved alignment and maturation.[91]
Crosslinked alginate sponge	TGF-β1	Rabbit Supraspinatus	Enhanced cell proliferation. Increased collagen fibres bridging tendon-bone interface. Increased ultimate load failure.[90]
Fibrin heparin/peptide matrix	PDGF	Canine Flexor	Increased cell density and proliferation. Increased expression of collagen type I.[40]
Collagen sponge	BMP-12	Rat Calcaneal	Increased expression of tenocyte lineage markers. *De novo* tissue formation. Increased cell proliferation, elongation & alignment. Increased matrix deposition.[62]
Gelatin crosslinked gel	Ibuprofen	Chicken Flexor	Reduction in inflammation and adhesion formation compared to controls.[119]
Gelatin hydrogel	FGF-2	Rabbit supraspinatus	Improved mechanical strength, formation of dense well aligned collagen fibres compared to control groups.[120]

Table 3: Examples of in vitro drug delivery systems utilising natural polymers for tendon regeneration.

1.3. Synthetic Polymers

Synthetic polymers offer advantages over their naturally occurring analogues for applications in biomaterials and tissue engineering.[104] Synthetic polymers have demonstrated superior mechanical strength compared to their natural counterparts.[100,105] The synthesis of these polymers is also highly reproducible

and it is possible to precisely control polymer length, composition, and degradation rate, allowing tight control over batch to batch variability.[104] Among the polymers investigated to date, aliphatic polyesters have been the preferred biomaterials.[121] Their ability to degrade in physiological conditions via hydrolytic or enzymatic degradation into metabolisable products, have made them leading candidates.[121–123] Of these polyester polymers, poly(lactic-co-glycolic acid) (PLGA), poly(lactic acid) (PLA) and poly(caprolactone) (PCL), have been the preferred materials for delivery systems (Figure 7).[124,125]

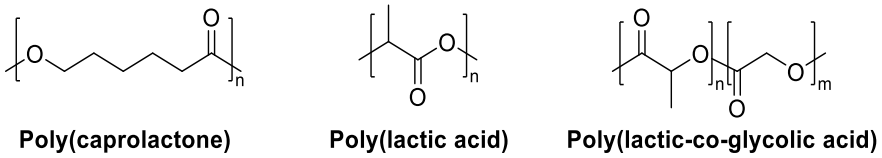

Figure 7: Examples of commonly used synthetic polymers for tissue engineering and regenerative medicine

PLA has been used as a biomaterial in tissue engineering due to its favourable mechanical properties, including tensile strength, as well as its low toxicity.[102] Moreover, its properties can be tailored to suit the application by copolymerisation. PLGA, a co-polymer of glycolic acid and lactic acid, is one such example.[100] Alterations in the ratio of glycolic acid to lactic acid results in precise control over both the degradation rate and mechanical properties of the subsequent polymer.[126,127] Furthermore, upon degradation, the polymer is hydrolysed to its monomeric acids, which are simply and efficiently removed from the body via the Krebs cycle and eliminated in urine.[100] PLGA has been used in many different formulations as a drug delivery system. Delivery of anti-inflammatory drugs, gene complexes, cells and proteins within PLGA scaffolds have all been applied to the regeneration of tendon tissue.[128–133] The degradation of these polymers has posed some concern, however, when encapsulating proteins, due to the acidic microenvironment created upon degradation of the monomeric acids.[102] At low pH the denaturation or aggregation of proteins can occur.[100]

PCL is one of the most extensively studied polymers for tissue engineering.[123,134] Table 4 gives some examples of clinical products for tissue

engineering and drug delivery utilising PCL. Within tendon regeneration specifically, PCL has been formulated into many structures, such as fibres, membranes and scaffolds.[135–139] PCL exhibits excellent properties such as mechanical strength, biocompatibility, and its degradation into easily eliminated metabolites.[102,140] It has been extensively studied as a drug delivery system by encapsulation within microparticles via a double emulsion process.[89,141,142] It is an excellent candidate biomaterial for application in tendon regeneration because its complete degradation takes between 2-3 years. This means it is able to match the long regeneration and remodelling periods seen in tendon repair.[104] PCL is easily synthesised via the ring opening polymerisation of ε-caprolactone. This technique requires the use of an initiator to open the first cyclic lactone, after which repeated reactions of monomers results in continual ring opening of subsequent monomers in chain growth polymerisation (Scheme 1).[104]

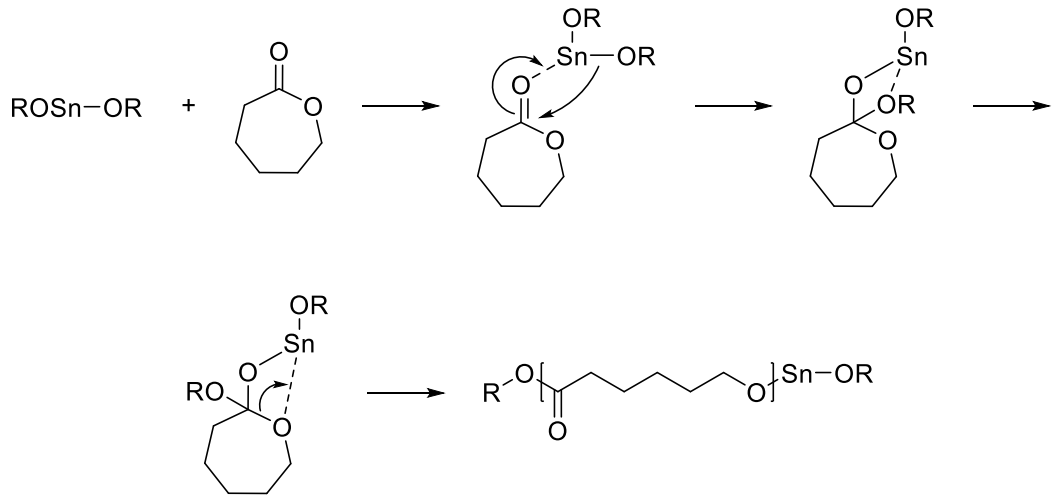

Scheme 1: Mechanism of ROP of PCL. Co-ordination insertion occurs using tin(II) 2-ethylhexanoate as a catalyst.[143]

A theoretical molecular weight can be predetermined based on the monomer/initiator ratio, resulting in predictable molecular weights and narrow polydispersity indices.[143] This is particularly advantageous in tissue engineering because good control over both molecular weight and polydispersity allows the degradation rate to be precisely tailored, as well as adding a high level of quality control and material reproducibility.[104] These polymers, however, lack the functional groups needed to allow easy conjugation to bioactive agents such as

peptides or proteins. This limits their interaction with cellular components and therefore their biological application.[106,121,134]

Product	Use	Description
Ellansé®	Collagen stimulator	Bioresorbable injectable dermal filler of PCL microspheres with results lasting 1-4 years.
Capronor®	Contraceptive	Sub dermal PCL capsule for the release of levonorgestrel for 12-18 months.
Monocryl®	Suture	Co-polymer suture made from glycolide and ε-caprolactone. Fully absorbed within 90-120 days.
Resilon™	Sealant	Root canal filling material comprised of PCL and inorganic fillers.
Osteoplug™	Implant	Bioresorbable porous implant for bone regrowth over burr holes in neurosurgery.
Artelon™	Implantable patch/strip	PCL and polyurethane copolymer fibres for tendon injury. Fully replaced by regenerated tendon tissue within 4-5 years.

Table 4: Clinical products utilising polycaprolactone for tissue engineering and drug delivery

1.4. Pre- and Post-Polymerisation Modification Strategies

In an attempt to synthesise polymers that are able to conjugate to biomolecules, their functionalisation and modification has been investigated.[144] Polymer functionalisation can involve the incorporation of functional groups throughout the backbone of the polymer or at specified regions.[145] Methods to functionalise PCL include; synthesis of new caprolactone monomers, co-polymerisation, post polymerisation modification, and chain end modifications prior to polymerisation through utilisation of the initiating species.[121,123,134,143,146–150] Surface modification is another method that can be used to alter the functional groups within polymers to allow for bio-conjugation.[151,152] Methods include passive surface coating, plasma etching, and chemical immobilisation of cell recognition ligands such as peptides.[118,153–156]

1.5. Aminolysis of Polycaprolactone

One of the most commonly employed techniques for polymer functionalisation is aminolysis, which has previously been applied to PCL.[151,157–159] Amine reactive groups are one of the most utilised functional groups in conjugation as they allow for reactivity with nearly all peptide or protein molecules.[145] Cross coupling reagents such as carbodiimides are necessary for the subsequent conjugation of biomolecules; they direct the conjugation of amines to carboxyl groups present within biomolecules, forming a stable amide bond.[145,159] The development of the water soluble carbodiimide cross coupling reagent (1-ethyl-3-(3-dimethylaminopropyl)carbodiimide hydrochloride) (EDC) has allowed for the occurrence of this reaction in aqueous solutions, ideal for the conjugation of proteins (Scheme 2).[145,160]

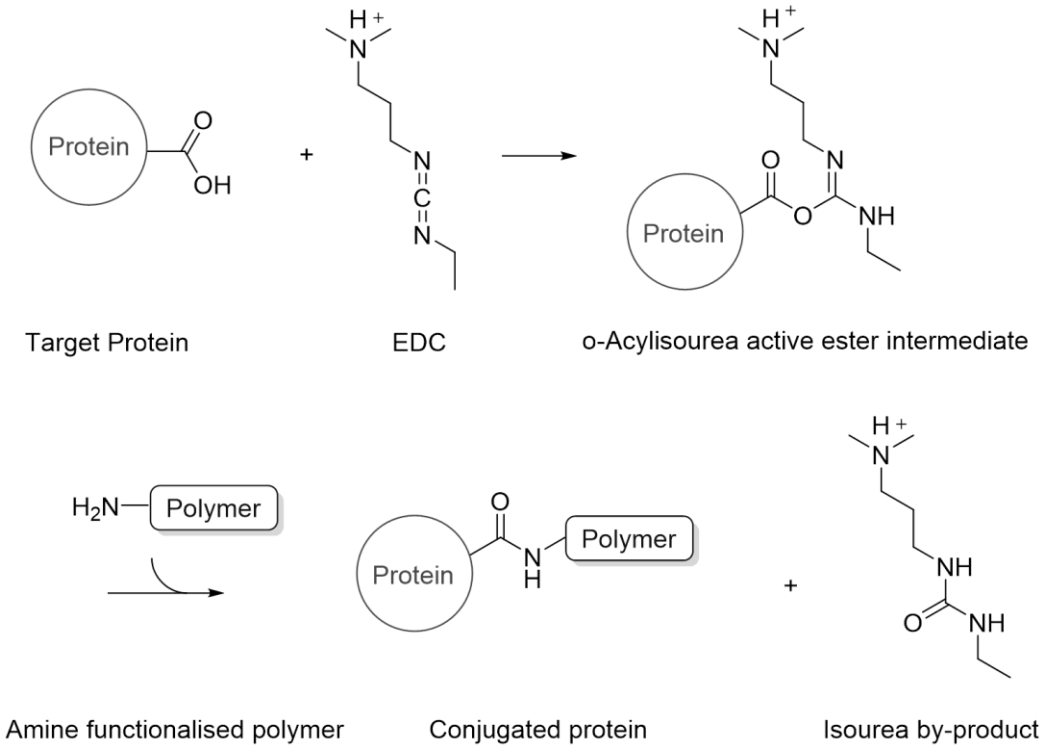

Scheme 2: EDC cross coupling reaction. Amine functionalised polymers can be conjugated to proteins via cross coupling chemistry.

One limitation of these reactions however, is that secondary side-reactions can occur if multiple reactive sites are present within the biomolecule. Moreover, common functional groups employed for the conjugation of proteins, such as N-

hydroxysuccinimide (NHS) esters, maleimides and activated carboxyl groups, are predisposed to hydrolysis and therefore not stable in aqueous solutions.[145,161]

1.6. Click Chemistry

One bio-conjugation method that is extremely selective, even within complex biological systems, is “click chemistry”, a term coined by Sharpless in 2001.[145,162] These reactions were described by Sharpless and his colleagues as possessing the following criteria;

“The reaction must give high yields, generate only inoffensive by-products. The required process characteristics include simple reaction conditions (ideally, the process should be insensitive to oxygen and water), readily available starting materials and reagents, the use of no solvent or a solvent that is benign (such as water) or easily removed, and simple product isolation”.[162]

These reactions are described as bio-orthogonal, meaning that there is little to no potential of cross-reactivity with other biological functional groups.[145,162] They are efficient and high yielding which is advantageous when designing a delivery system with the intention of clinical or industrial applications.[162] The most routinely employed click reactions include the Diels-Alder cycloaddition, the thiol-ene reaction, the Staudinger ligation and the copper(I) catalysed azide-alkyne cycloaddition (CuAAC).[163,164] Scheme 3 shows the potential for functionalisation of PCL to allow for the subsequent bio-conjugation of molecules using click chemistry.

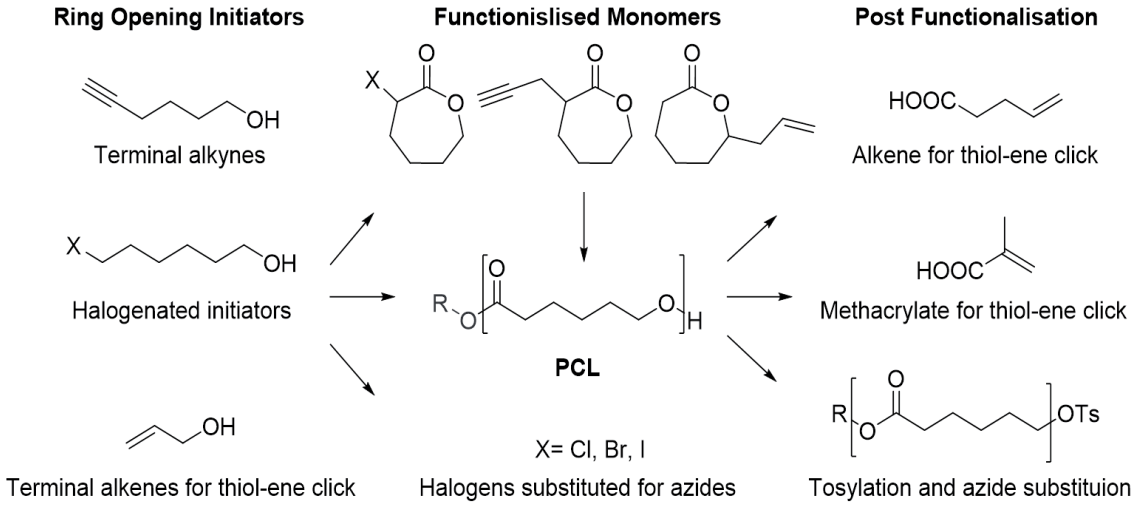

Scheme 3: Examples of functionalisation methods for PCL. Pre-and post-modification of polycaprolactone can allow for bio-conjugation using click chemistry techniques. Adapted from Chen et al and Hvilsted[134,261]

1.7. Copper Catalysed Azide-Alkyne Cycloadditions

Sharpless describes the "cream of the crop" of these reactions as being the 1,3-dipolar Huisgen cycloaddition between azides and alkynes, to form a stable triazole.[162] Huisgen developed this reaction in the early 1960s, however it requires elevated temperatures, long reaction times and gives no stereoselectivity.[165–167] The addition of a copper(I) catalyst allows the reaction to proceed in aqueous conditions at room temperature, yielding solely the 1,4-triazole, in a much shorter amount of time.[145,168] The copper catalysed azide-alkyne cycloaddition is deemed the click reaction and it is the archetypal reaction of click chemistry (Scheme 4).[122] CuAAC is highly applicable in the conjugation of biomolecules to polymers for drug delivery. The synthesis of azide or alkyne functionalised polymers, proteins and cells have all been reported.[149,167,169–172]

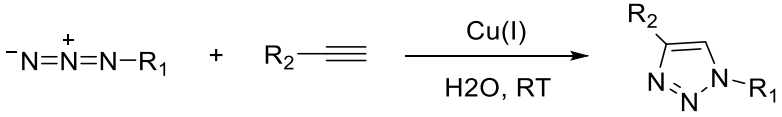

Scheme 4: CuAAC reaction. Reaction between azides and terminal alkynes result in the formation of 1,4-triazoles, referred to as the click reaction

One limitation to this reaction is the necessity of metal catalysts for it to proceed in aqueous solutions and at room temperature. These metal catalysts have been shown to display severe cytotoxic effects even in micromolar quantities.[167] Concerns around the toxicity of copper create the need for additional purification techniques, and has therefore restricted the use of these conjugations in biomedical applications where biocompatibility is paramount.[173]

1.8. Strain Promoted Azide-Alkyne Cycloadditions

An alternative cycloaddition reaction, which remains biorthogonal and follows the prerequisites of a click reaction but eliminates the need for a metal catalyst, is the strain-promoted azide-alkyne cycloaddition (SPAAC) (Scheme 5).[145,174] SPAAC relies on the highly reactive nature of an internal alkyne within a cyclooctyne ring, caused by ring strain.[175] The introduction of ring strain increases the ground state energies of the cyclooctynes and allows the reaction to occur without the need for a catalyst.[176]

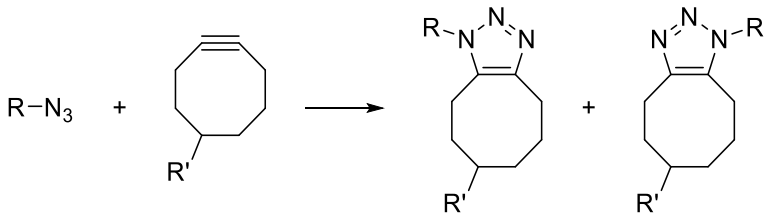

Scheme 5: SPAAC reaction

This method of click chemistry, utilising cyclooctynes, was first demonstrated in the literature by the Bertozzi group in 2004.[177,178] The reaction has similar reaction kinetics to copper-catalysed click reactions, whilst also being able to proceed in a living organism.[168,175] The reaction has been demonstrated *in vivo* within mouse models for live cell imaging.[167,168,175] The SPAAC reaction has drawn the attention of the tissue engineering and regenerative medicine communities, owing to its excellent biocompatibility, especially within physiological conditions.[171] The SPAAC reaction is a promising method for the conjugation of biomolecules for drug delivery.

1.9. Aims and Objectives

The main aim of the work carried out in this chapter was to determine an appropriate polymer candidate that could be used to produce microparticles. An appropriate polymer needed to be biocompatible, bioresorbable, have the ability to be formulated as microparticles and be able to incorporate proteins. A key aim was therefore to decide on an appropriate method for incorporation of protein with the polymer microparticles. To achieve this, it was necessary to carry out investigations into methods of incorporation including encapsulation, surface modification and polymer functionalisation. After deciding an appropriate polymer, and protein incorporation method, this polymer could then be used to produce microparticles.

After optimisation, protein conjugation via click chemistry to a functionalised polycaprolactone was decided as the appropriate protein incorporation method. Therefore, the overall hypothesis of the work carried out in this chapter is that functionalisation of a polycaprolactone polymer with azide groups could have potential as a microparticle based drug delivery system.

2. Results and Discussion

2.1. Selecting a Polymer Candidate and Protein Incorporation Technique

It was known from the beginning of the project that the main aim was to produce a drug delivery system, using microparticles, which could incorporate a therapeutic protein. Therefore, it was important for initial investigations to be carried out to identify a polymer candidate that could be used for the production of microparticles and an appropriate method of incorporating protein within or to them.

Polycaprolactone was initially chosen as the target polymer for the drug delivery system due to its commercial availability, slow biodegradation, good biocompatibility and ease with which its properties can be tailored to suit its function.[134] Polycaprolactone-triol (PCLT) was the first polymer candidate

investigated and was initially assessed for its ability to produce microparticles as it was paramount that the polymer candidate was able to do this.

Microparticles were produced via a membrane emulsification method in which polymer was dissolved in solvent and then injected into an aqueous phase containing poly(vinyl alcohol) (PVA) (Full detailed information regarding the manufacture process as well as optimisation and production of microparticles is given in chapter 3.) Table 5 details the reaction conditions used to attempt to make PCLT microparticles. It was found that PCLT alone was not able to produce solid microparticles, resulting in the production of an oil. To combat this, polymer concentration was increased, which resulted in a cream like substance. PCLT has a low melting point and is liquid at room temperature and thus it was hypothesised that PCLT on its own would not be able to form solid particles. PCLT was therefore blended with another commercially available polycaprolactone with a molecular weight of 10,000 g/mol (deemed PCL from herein). The addition of this secondary PCL resulted in the formation of particles; however, an oil was still present resulting in them being highly clumped and difficult to distinguished by microscopy. When PCL only was used at a concentration of 10% solid microparticles formed after solvent evaporation. These microparticles had a spherical morphology and were easily lyophilised. It was therefore decided that this PCL would be the chosen polymer candidate for further experiments and would be used to produce the microparticle drug delivery system. Full details of the manufacture and optimisation process of PCL microparticles is given in chapter 3 section 2.1.

Polymer	Solvent	Emulsifier	Solid Particles	Morphology
10% PCLT	DCM	1% PVA	No	Oil
20% PCLT	DCM	1% PVA	No	Oily Cream
PCLT: PCL 80:20 Blend	DCM	1% PVA	Yes	Multiphase powder/oil Clumped particles.
PCLT: PCL 50:50 Blend	DCM	1% PVA	Yes	Powdered highly clumped particles
10 % PCL	DCM	1% PVA	Yes	Solid particles with spherical morphology

Table 5: Reaction conditions tested to produce PCL-triol microparticles

The next aim to be fulfilled was deciding on an appropriate method of incorporation of therapeutic proteins into PCL microparticles. The most common method utilised to achieve this is through encapsulation within the bulk of microparticles via a double emulsion technique. Therapeutic proteins of interest are dissolved in an internal water phase within solid microparticles. For hydrophobic agents, encapsulation is within an internal oil phase instead. Therefore, tests were carried out to see if it was possible to produce solid microparticles, containing an internal water phase, using the PCL polymer through the creation of a water-in-oil-in-water (W/O/W) emulsion. An internal water phase which would have the potential to dissolve water soluble proteins, was emulsified into an oil phase containing PCL. This primary emulsion was further emulsified into an aqueous layer containing PVA to produce solid microparticles (Table 6). It was found that to be able to produce double emulsions it was necessary to use sonication, homogenisation or vigorous stirring. All of these techniques require high sheer stresses, which can cause protein aggregation or denaturation.[102] Additionally the resulting particles had a large size distribution, lacking uniformity. These issues were deemed to be incompatible with the final aim of a sustained release delivery system. Additionally, when looking further into the literature, it was found that one of the major limitations of proteins incorporated within microparticles via double emulsion is that they suffer burst release. Several studies using PCL to encapsulate drugs identified a bi-phasic release profile whereby there was an

initial burst release of the majority of the protein, followed by a sustained release until reaching a plateau phase.[89,141,179–181] There is evidence that the encapsulation efficiency of proteins in W/O/W emulsions is low, resulting in waste of expensive protein resources. With industrial scale up in mind, this was also a major limitation.[182] As a consequence of all of this, investigations into the encapsulation of proteins were ceased and potential conjugation methods were investigated instead.

W_1	O	W_2	Surfactant	Primary emulsion	Secondary Emulsion
0.1M PBS	10% PCL	1% PVA 13g/L NaCl	20% Span 80	Stirring	Membrane emulsification
0.1M PBS 2% PVA	25% PCL	1% PVA 13g/L NaCl	20% Span 80	Homogenisation 1min @ 24,000RPM	Membrane Emulsification
0.1M PBS 2% PVA	25% PCL	0.5% PVA	20% Span 80	Sonication 1 min	Dropwise addition stirring @ 1200RPM

Table 6: Conditions used to produce Water-in-Oil-in-Water (W_1/O/W_2) primary emulsions.

2.2. Functionalisation of Polycaprolactone by Aminolysis

A limitation of PCL as a drug delivery system is that it lacks the necessary functional groups required for the conjugation of biomolecules.[156] One method used to functionalise PCL is by introducing free amino groups into the polymer via aminolysis.[151,156,157] If PCL microparticles are modified to contain amino groups, bio-conjugation and immobilisation of proteins can then be carried out at the carboxylic acid present at the carboxyl-terminus (C-terminus) of amino acids using standard cross coupling techniques (Scheme 6).[156] Microparticles containing amino functional groups (**1**) were produced to investigate this as a potential bioconjugation method.

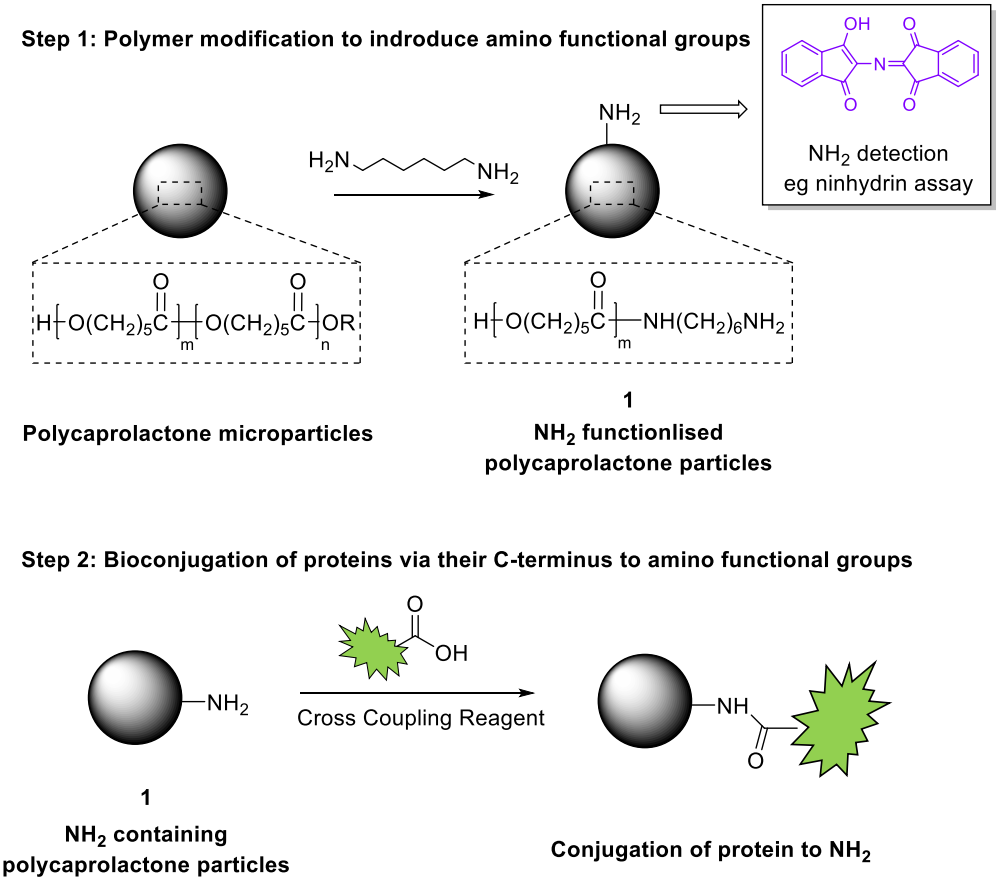

Scheme 6: Schematic representation of aminolysis technique. NH_2 groups can be incorporated into PCL which can be used for subsequent bio-conjugation to proteins (Step 2). Adapted from Zhu et al [151,157]

1,6-hexanediamine was used to introduce amino functional groups into microparticles formulated from commercial PCL (Scheme 6, Step **1**). The presence of amino groups was then confirmed using both trioxohydrindene monohydrate (Ninhydrin) and rhodamine B isothiocyanate. Ninhydrin works on the basis that nucleophilic attack from amino groups results in the formation of the chromophoric compound Ruhemann's purple (Scheme 6, insert), it is this compound that is measured using absorbance spectroscopy.[183] Rhodamine can be used for fluorescent labelling, where the isothiocyanate groups reacts with the amino groups present to form a stable thiourea.[161] This labelling can then be visualised using fluorescence imaging or quantified via absorbance spectroscopy. Standard calibration curves were created using known concentrations of rhodamine B isothiocyanate or known concentrations of 1,6-hexanediamine, reacted with Ninhydrin (Figure 8).

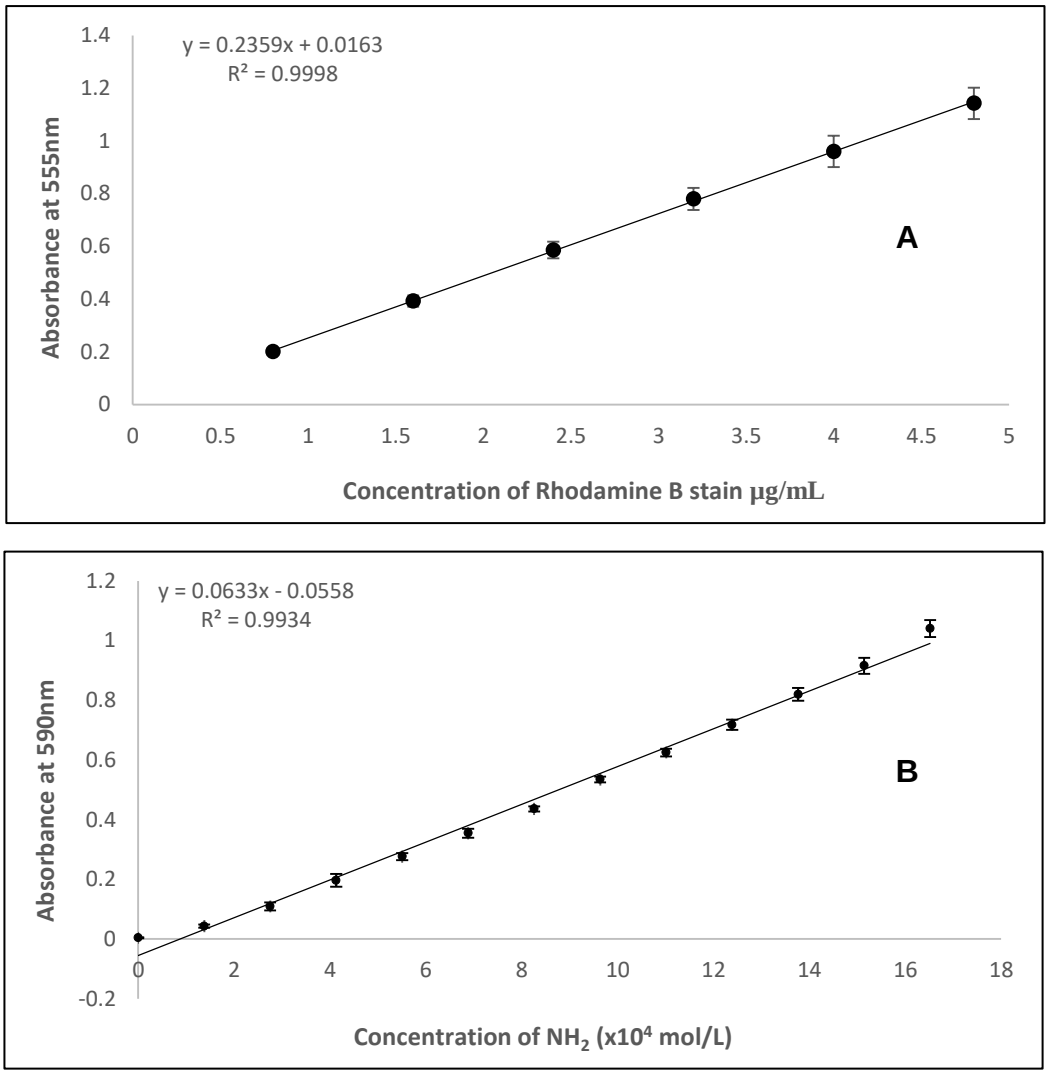

Figure 8: Standard calibration curves of rhodamine B or 1,6-hexanediamine for the detection of amino groups. Increasing concentrations of rhodamine B isothiocyanate (A) or 1,6-hexanediamine (B) were reacted with Ninhydrin. The concentration of 1,6-hexanediamine in µg/mL reacted with ninhydrin was converted to mol/L concentration of NH_2.

After microparticles were treated with 1-6 hexanediamide to introduce free amino groups (**1**) they were labelled with either rhodamine B isothiocyanate or ninhydrin and absorbance measurements taken. The absorbance readings of the microparticles treated with 1,6-hexanediamine increased at both 555 nm and 590 nm when stained with rhodamine B isothiocyanate and ninhydrin respectively (Figure 9). For both techniques the increase in absorbance for treated particles was statistically significant ($P > 0.05$) when compared to untreated particles, with $P=0.01$ when reacting with rhodamine and $P=0.02$ with

ninhydrin. This suggests that the microparticles have been successfully functionalised with amino groups to produce compound **1**.

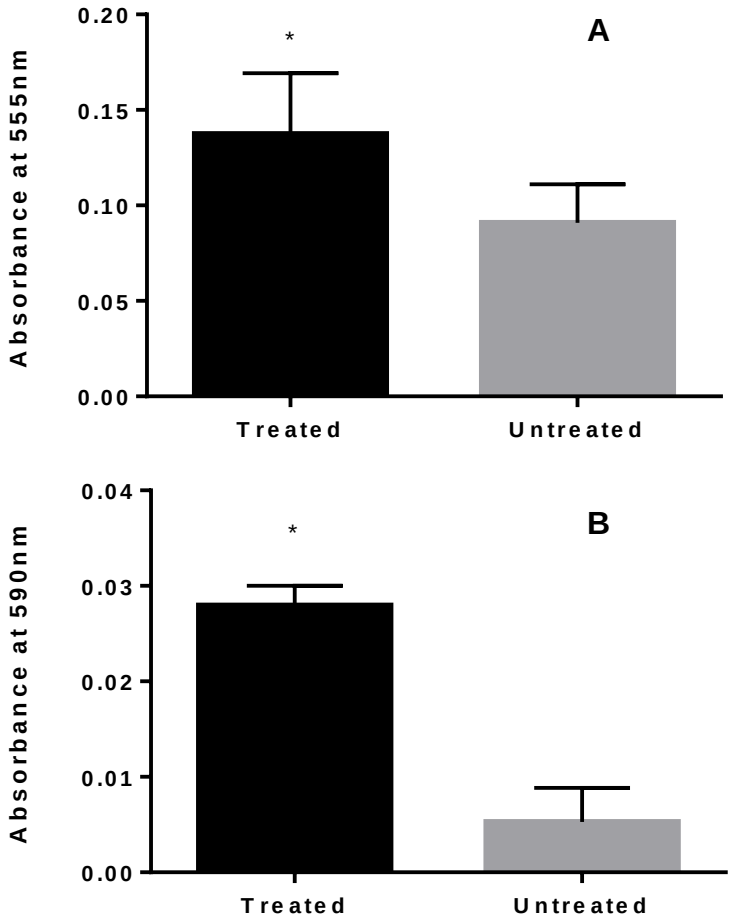

Figure 9: Absorbance of PCL particles treated with 1,6-hexanediamine. (A) shows absorbance after reaction with rhodamine B isothiocyanate and (B) with ninhydrin to detect the presence of NH_2 groups, with untreated PCL particles as a control.

There were concerns however, that this increase in absorbance could be due to physical absorption of unbound 1,6-hexanediamine on the surface of the microparticles. This would result in the detection of amino groups, even if the structure of PCL had not been altered, and therefore give rise to a false positive. To confirm if amino groups were from unbound 1,6-hexanediamine contaminating the sample, as opposed to being incorporated into the structure of PCL, thermogravimetric analysis (TGA) was performed. TGA gives information on the changes in mass of a sample over time when subjected to

heating.[184] It can be determined if a sample is a composite by analysing the weight loss curve and identifying changes to the onset of thermal degradation.[185,186] The thermal decomposition spectra of 1,6-hexanediamine, commercial PCL, PCL microparticles, and PCL microparticles treated with 1,6-hexanediamine (**1**) are shown in Figure 10**.**

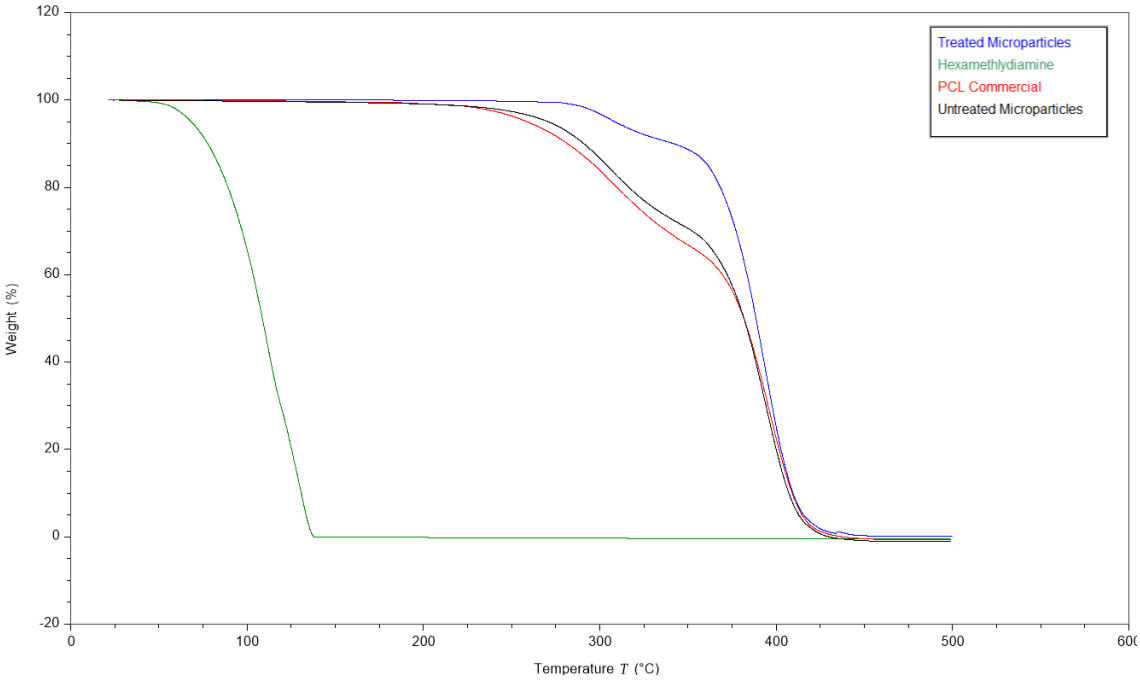

Figure 10: TGA of PCL microparticles treated with 6-hexanediamine (Blue). Untreated PCL particles (black) commercial PCL 10,000 mw from sigma (red) and 1,6-hexanediamine (green) were used as comparisons.

The thermal decomposition of 1,6-hexanediamine was rapid, with onset at 89^{o}C and 100% weight loss of the sample occurring by 133ºC. If the treated microparticle samples contained unbound 1,6-hexanediamine, that was physically absorbed to the surface, then two obvious thermal decomposition patterns would be expected, one comparable to the decomposition of 1,6-hexanediamine and the other comparable to PCL. However, there is no thermal decomposition in PCL samples treated with 1,6-hexanediamine (**1**) between 89ºC-133ºC. Onset of decomposition does not occur until 365ºC. This pattern of decomposition is more comparable to both commercial PCL and untreated PCL samples, where onset of decomposition does not occur until much higher temperatures, above 300ºC, in agreement with published literature.[185,187]

However, higher temperatures are required to reach 100% weight loss of PCL samples treated with 1,6-hexanediamine, when compared to commercial PCL, and untreated PCL samples. 100% weight loss was not achieved until 414ºC for treated particles compared to 411ºC for both untreated PCL particles and commercial PCL respectively. This slight difference in decomposition could be due to the addition of the amino groups throughout the carbon backbone of treated PCL particles. Additionally, all microparticles had a neutral pH of 7, suggesting there was no residual 1,6-hexanediamine. This suggests that aminolysis of PCL microparticles has been successful, resulting in a PCL polymer functionalised with amino groups (**1**).

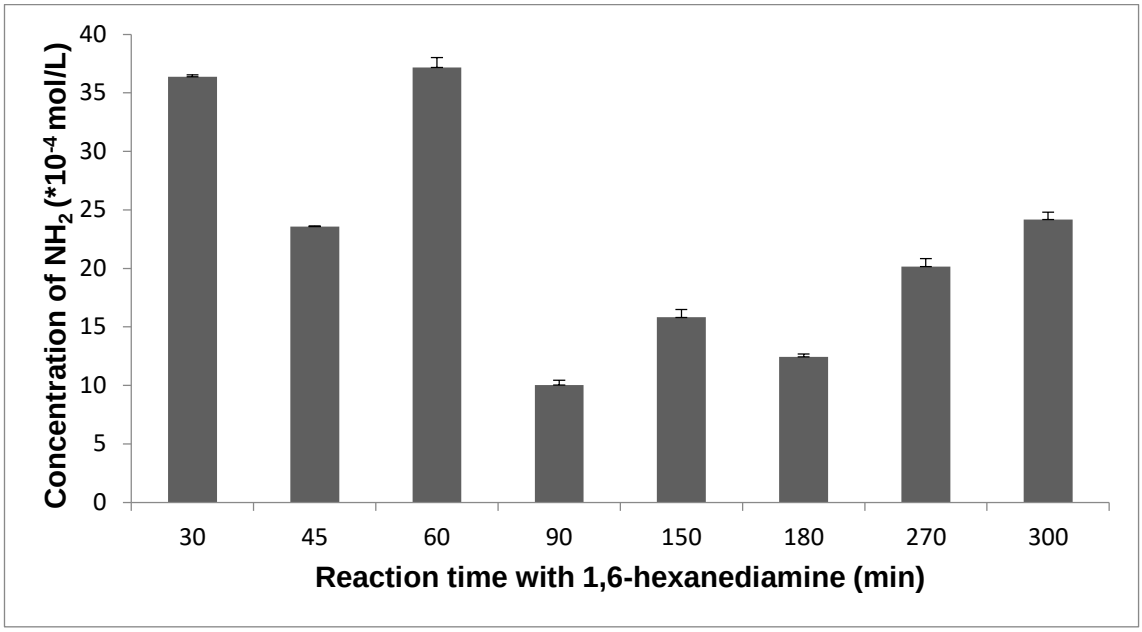

Figure 11: Effect of increasing reaction time of 1,6-hexanediamine on amine concentration within microparticles.

In an attempt to optimise the treatment time of PCL particles, the reaction of 1,6-hexanediamine was assessed at the following time points; 30 min, 45 min, 1, 1.30, 2.30, 3, 4.30 and 5 h, after which they were thoroughly washed and then reacted with ninhydrin to detect the presence of amino groups. However, it was found that there was no linearity between reaction time and NH_2 concentration (Figure 11). In addition to this, when using the calibration curve and equating increase in absorbance to 1,6-hexanediamine concentration, it was found that this increase was not significant. This meant that with each

treatment of 1,6-hexanediamine, there was no control over the number of NH_2 groups present, nor whether the aminolysis of PCL would be successful. With the final product and the aims of the project in mind, these anomalies could lead to inconsistencies when attempting to conjugate proteins of interest, especially when considering batch to batch variability. Therefore, other methods of bio-conjugation were investigated.

2.3. Synthesis of 2-[2-(2-azidoethoxy)ethoxy]ethanol Initiator for Ring Opening Polymerisation

The next conjugation method investigated was the click reaction. For this to be successful, either the polymer used to produce microparticles or the protein of interest would need to contain one of the reactive functional groups, an alkyne or an azide. Chain-end modifications of PCL can be carried out by incorporating target functional groups into the initiator used for the ring opening polymerisation (ROP) of ε-caprolactone.[123,134] For this reason, the modification of PCL was investigated via the use of an azide-containing initiator, which would result in the synthesis of an azide functionalised polycaprolactone (PCL-N_3) (**4**). This could subsequently be used for the bio-conjugation of proteins using click chemistry.

An azide-containing initiator for ROP was synthesised that included a small poly(ethylene glycol) (PEG) chain (**2**) (Scheme 7). PEG chains can be used to increase hydrophilicity and water solubility and the hypothesis was that incorporation of a small peg spacer would result in azides being present on the surface of the microparticles, as opposed to buried within the bulk.[145] To synthesise the initiator for ROP, commercially available 2-[2-(2-chloroethoxy)ethoxy]ethanol was reacted with sodium azide to substitute the chloride group (Scheme 7).

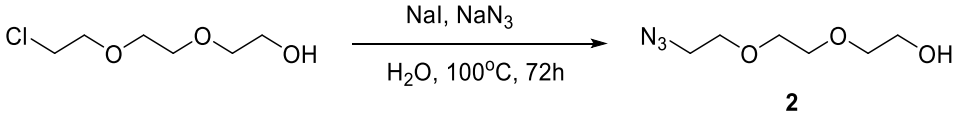

Scheme 7: Synthesis of 2-[2-(2-azidoethoxy)ethoxy]ethanol (**2**)

To confirm the success of the reaction (Scheme 7) and if the azide functionality was present in the initiator **2** Infrared spectroscopy (IR) and nuclear magnetic resonance (NMR) were carried out. ^{1}H NMR and ^{13}C NMR data showed a peak shift in the protons and carbons adjacent to the terminal azide (Appendix A, Figure 59 & Figure 60).[188] IR showed an obvious addition of a peak at 2095 cm^{-1}, corresponding to the newly introduced azide functionality (Figure 12).

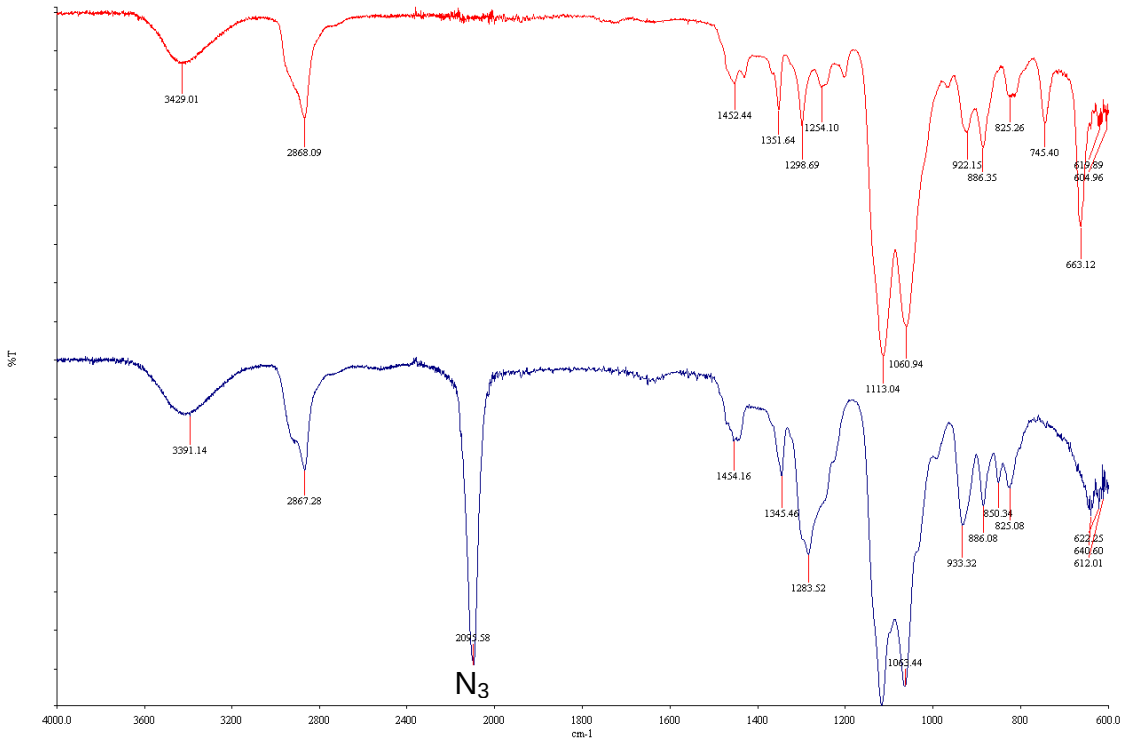

Figure 12: IR spectra of 2-[2-(2-azidoethoxy)ethoxy]ethanol 2 (blue). The starting material 2-[2-(2-Chloroethoxy)ethoxy]ethanol is used for comparison (red).

To confirm the azide group was reactive towards alkynes, a click reaction with phenyl acetylene was performed (Scheme 8). The 2-[2-(2-azidoethoxy)ethoxy]ethanol initiator (**2**) was successfully able to carry out the click reaction with the alkyne to form stable 1,4-triazole (**3**) (Scheme 8). This was confirmed with ^{1}H NMR analysis which showed a successful reaction with the presence of a triazole peak at 7.95 ppm (Figure 13, a).

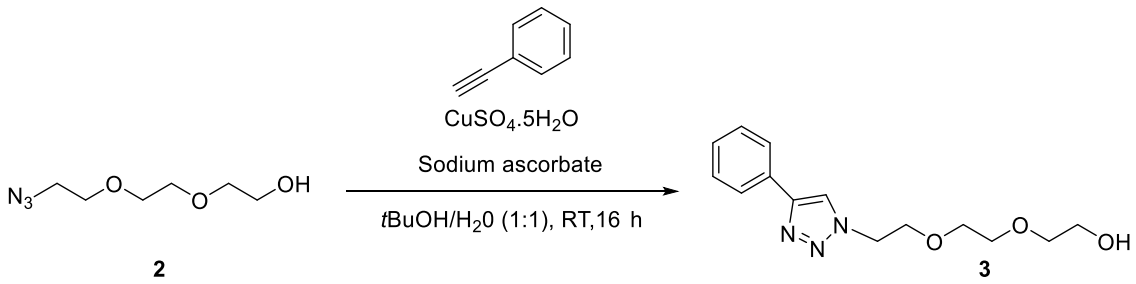

Scheme 8: CuAAC click reaction of 2-[2-(2-azidoethoxy)ethoxy]ethanol initiator with phenyl acetylene.

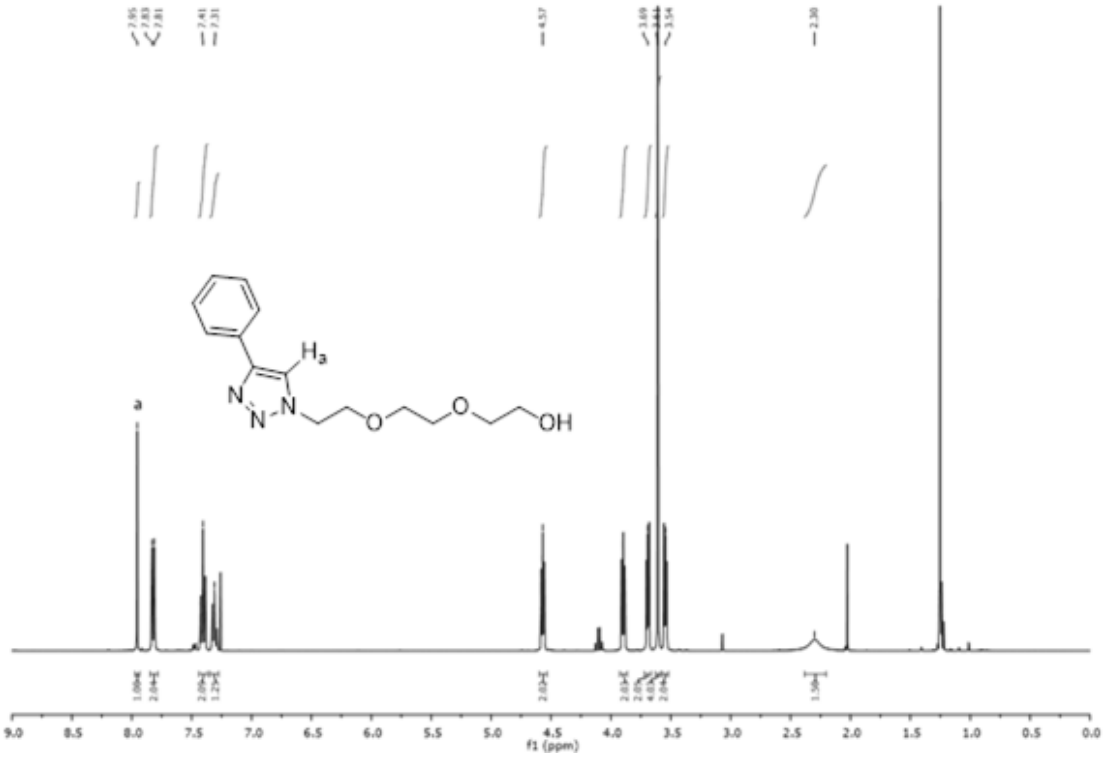

Figure 13: ^{1}H NMR analysis of copper click reaction. 2-[2-(2-azidoethoxy)ethoxy]ethanol reacted with phenyl acetylene results in a triazole peak (a) at 7.95 ppm.

2.4. Polymerisation of Polycaprolactone Using Azide-Containing Initiator

Once the successful synthesis of 2-[2-(2-azidoethoxy)ethoxy]ethanol initiator had been confirmed, ring opening polymerisation of ε-caprolactone was performed (Scheme 9). ROP facilitates the synthesis of well-defined polymers,

with an end group that can be altered depending on the initiator used to control the reaction.[134] Synthesis of an azide functionalised PCL (**4**) was attempted using 2-[2-(2-azidoethoxy)ethoxy]ethanol (**2**) as the initiator. Three batches of the resulting polymer were assessed by gel permeation chromatography (GPC) in filtered chloroform against polystyrene standards to assess the molecular weight (Figure 14). The number average molecular weight was confirmed as 19,502 Mn with a typical dispersity index (PDI) for ROP of 1.2. These results were indicative of a controlled polymerisation and a uniform polymer, in agreement with published work.[189,190] A PDI of 1.2 is very good for polymeric materials.[145,190]

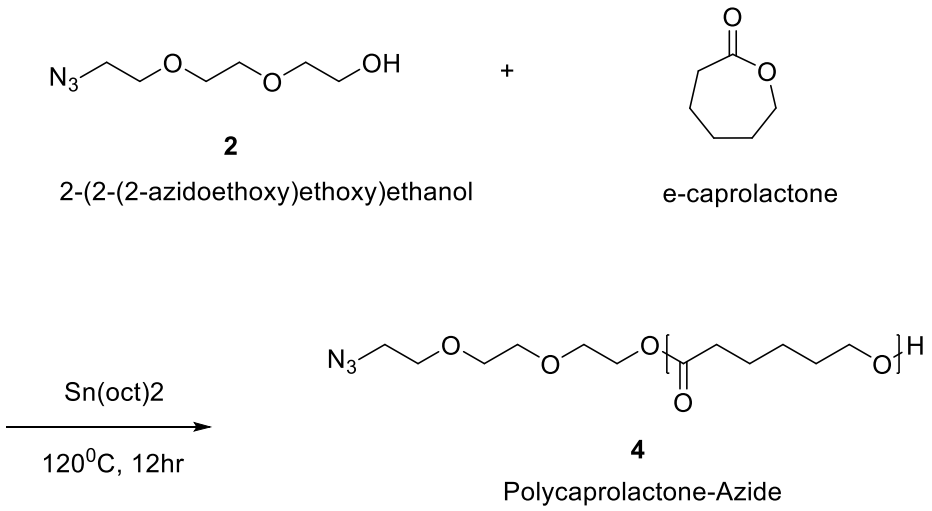

Scheme 9: ROP of ε-caprolactone. 2-[2-(2-azidoethoxy)ethoxy]ethanol (2). was used as an initiator, and Tin(II) 2-ethylhexanoate (Sn(Oct)2) as a catalyst, to synthesis azide functionalised PCL (PCL-N_3) (**4**).

PCL N_3	sample **1**	sample **2**	sample **3**	**Average**
Peak molecular weight	18920	18920	18626	**18822**
Number-average molecular weight	19007	20045	19456	**19502.67**
Weight-average molecular weight	22884	23067	22958	**22969.67**
Z-average molecular weight	27919	27223	27885	**27675.67**
Polydispersity Index	1.2029	1.1508	1.18	**1.1779**

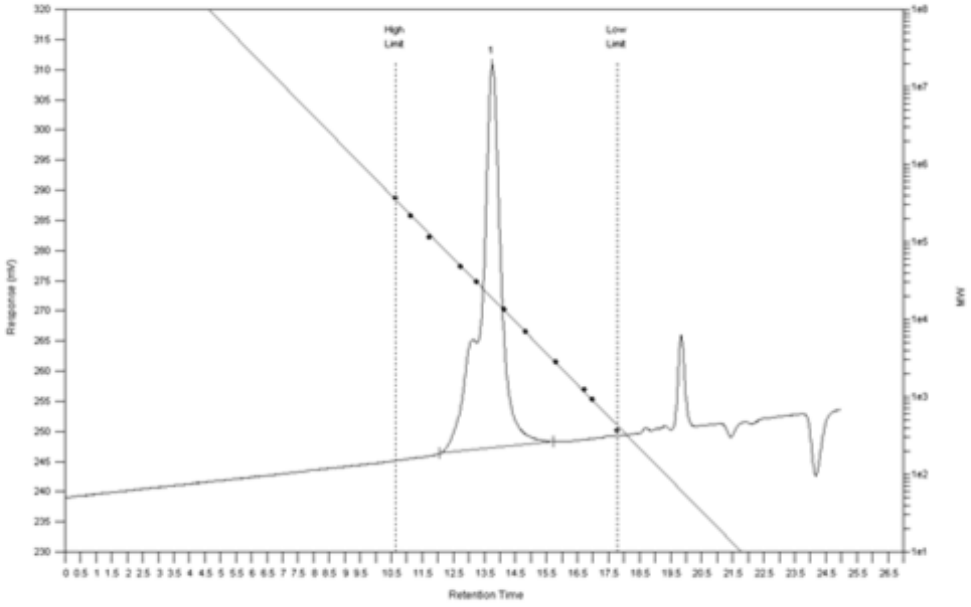

Figure 14: GPC analysis of PCL-N_3 polymer (**4**). Table above shows data for each batch tested and the average for the triplicate samples. Trace below shows sample 1 as an example

The resulting polymer (**4**) was characterised by ^{1}H NMR (Figure 15). The spectrum resembles a characteristic ^{1}H NMR for polycaprolactone with additional peaks present between 3.3-3.6 ppm in agreement with published literature.[149] These peaks correspond to the addition of CH_2 groups into the polymer, due to the incorporation of the initiating unit (**2**) during ring opening polymerisation. As the repeating units of the PCL are in much higher abundance when compared to the initiating unit, further proof of the addition of the azide into the polymer was sought. Thin film IR on sodium chloride crystal plates confirmed the addition of the azide by the appearance of a peak at 2100 cm^{-1}, suggesting the successful synthesis of PCL-N_3 (Appendix B, Figure 61).

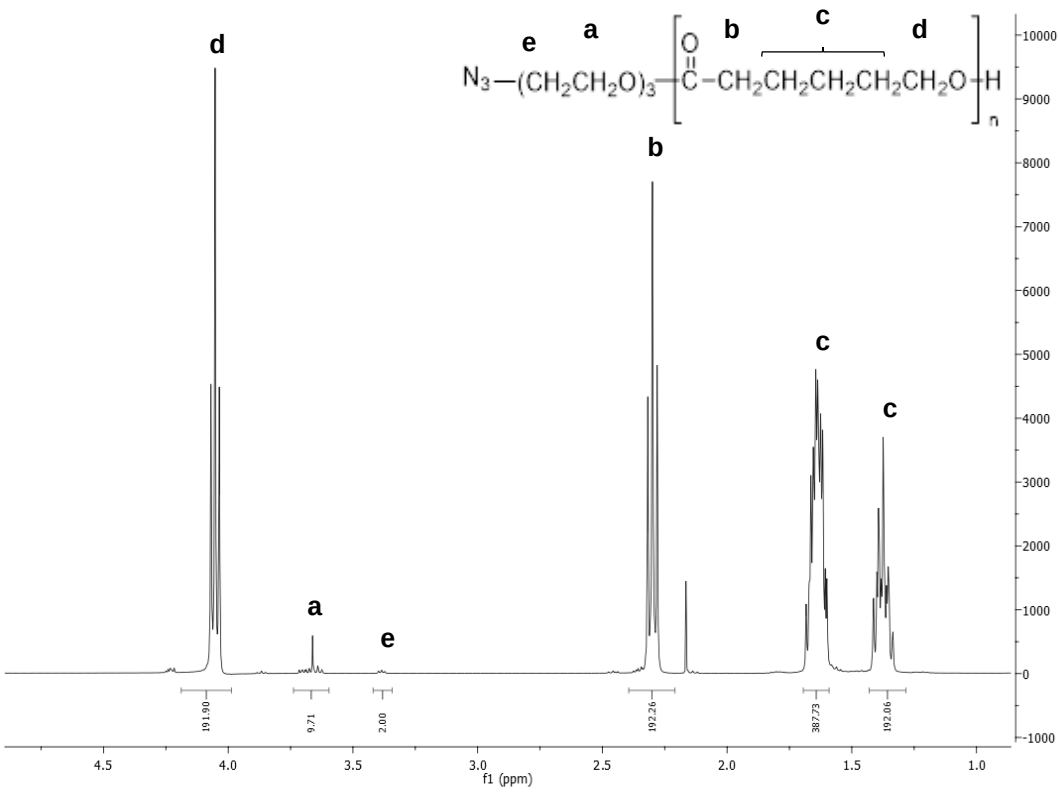

Figure 15: ^{1}H NMR of PCL-N_3 (4). Peaks a and e are representative of the CH_2 groups associated with the initiating unit.

Having successfully synthesised PCL-N_3, the ability of the polymer to undergo the click chemistry reaction was tested. With the application of the final product in mind, and biocompatibility being paramount, it was decided that the use of a copper catalyst for click reaction could pose potential problems.[173] Consequently, conjugation of PCL-N_3 was investigated utilising the strain promoted alkyne-azide cycloaddition (SPAAC) reaction to the internal alkyne situated within a dibenzocyclooctyne (DBCO) ring (**5**) (Scheme 10). Removal of copper for this reaction would allow for the direct conjugation of proteins or cells in physiological buffer with minimal purification.

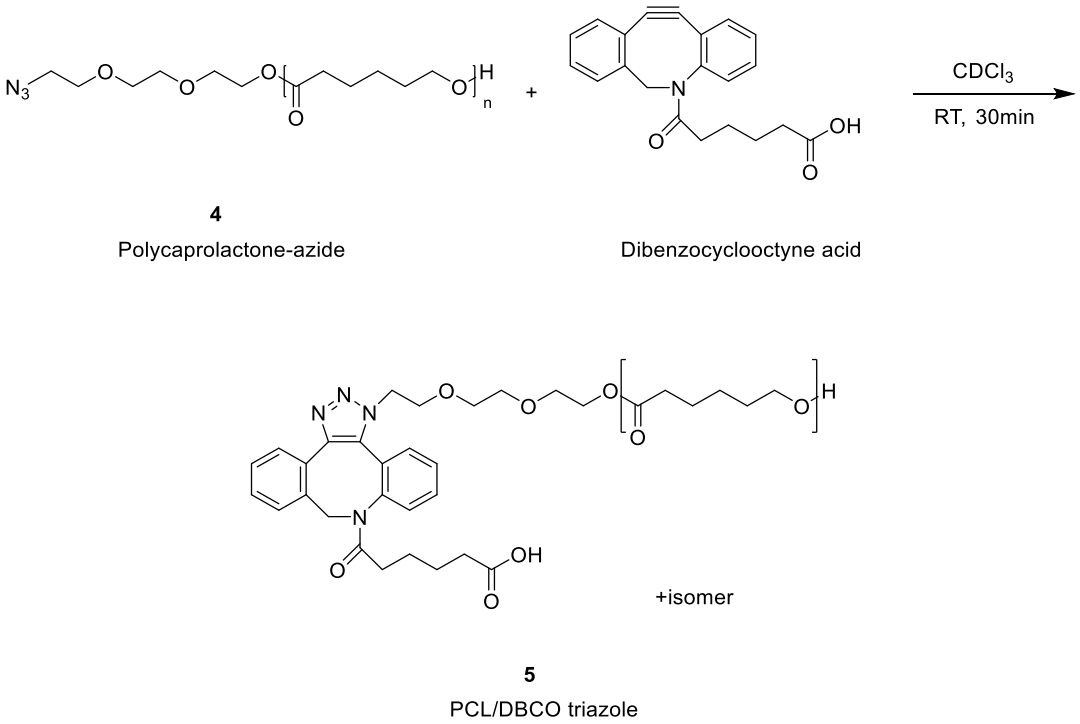

4
Polycaprolactone-azide

Dibenzocyclooctyne acid

5
PCL/DBCO triazole

Scheme 10: SPAAC reaction. Polycaprolactone-azide (PCL-N_3) attaches via the strained internal alkyne situated within a dibenzocyclooctyne (DBCO) ring.

The reaction shown in Scheme 10 was monitored using 2D diffusion ordered spectroscopy (DOSY). DOSY has been used for the identification of individual components within complex mixtures of small molecules.[191–193] Signals are separated according to their chemical shift along one axis, and their diffusion constant along the other.[191] Signals that originate from the same compound will appear in the same horizontal plane and share a diffusion constant. This means that it can be determined if the solution is a heterogenous or homogeneous mixture and individual compounds can easily be identified.[191,192] Therefore, it was possible to monitor the reaction between PCL-N_3 (**4**) and DBCO and determine if a successful SPAAC reaction had occurred. If PCL-N_3 conjugates to DBCO, and forms a stable triazole, only one species will be present, indicative of the formation of compound **5** (Scheme 10). If this does not occur, two separate species will be identifiable, one correlating to PCL-N_3 and the other to DBCO. Figure 16 shows the reaction between PCL-N_3 and DBCO-acid, using commercial PCL without azide as a control. The reaction between PCL-N_3 and DBCO-acid (**5**) results in the presence of only one diffusion pattern. The peaks between 2-4 ppm are indicative of the polyester backbone of PCL-N_3,

and 6-8 ppm are the aromatics within DBCO-acid. As these signals are grouped and share the same diffusion coefficient of 10.6 log(m_2/s), this strongly suggests that the SPAAC reaction has occurred between PCL-N_3 and DBCO-acid resulting in compound **5**. Additionally, it was found that this reaction occurred within just 30 minutes. When compared to the control reaction, two diffusion patterns can be seen, with one diffusion pattern being comparable to commercial PCL and the other to DBCO-acid. Due to the abundance of PCL backbone compared to DBCO unit, areas of the spectra needed to be magnified to clearly visualise the peaks identified.

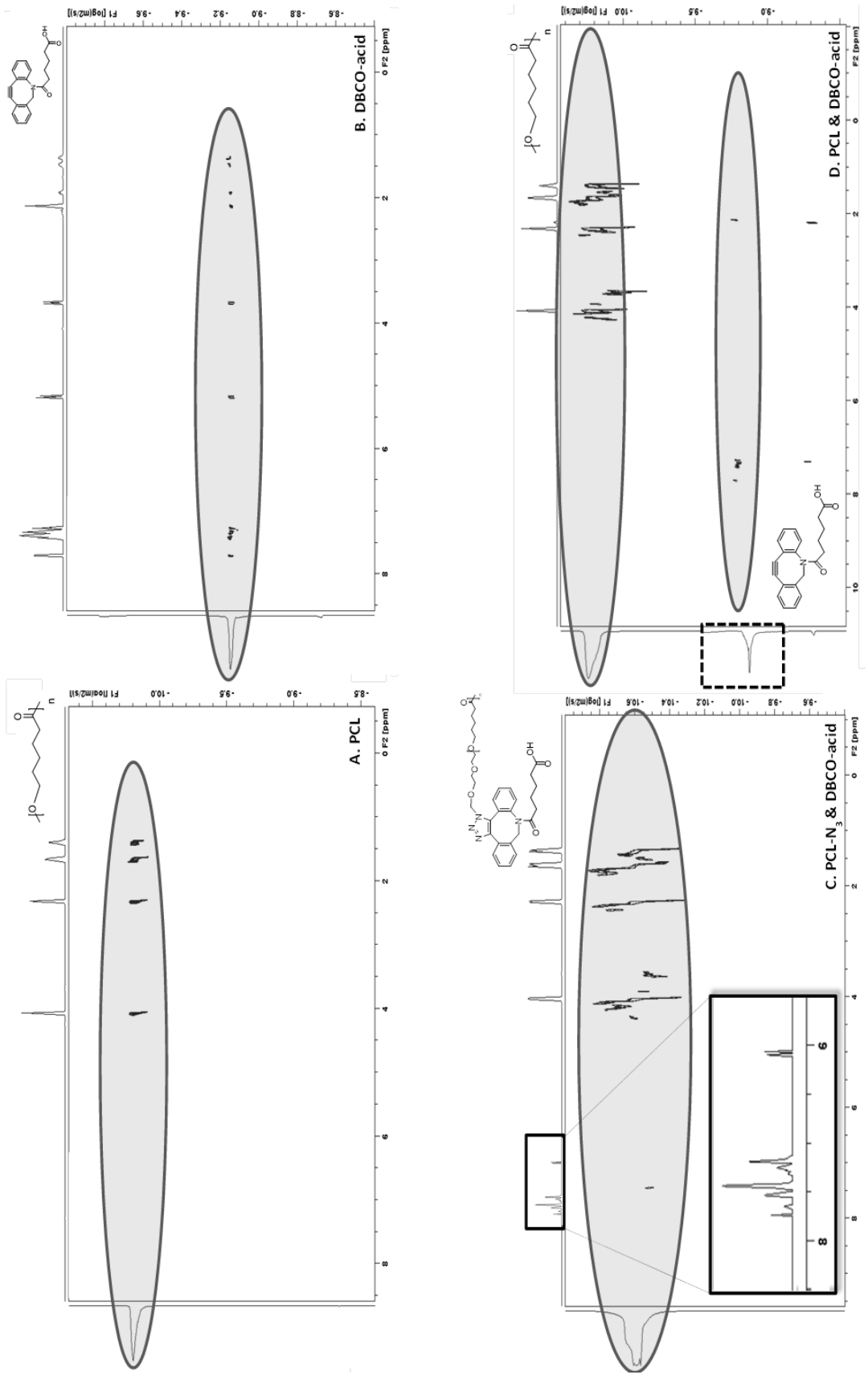

Figure 16: DOSY NMR monitoring of SPAAC reaction. Spectra show commercial PCL (A) DBCO-acid (B) and the reactions of DBCO-acid with either PCL-N_3 or PCL (C & D respectively).The boxes inserted in C & D have been magnified for visualisation of the peaks.

3. Conclusion

To summarise, polycaprolactone was chosen as the polymer candidate to be used to produce microparticles due to its excellent biocompatibility. Preliminary investigations showed that it was possible for polycaprolactone to produce microparticles. After optimisation, it was decided that the conjugation of biomolecules to microparticles would be investigated via the use of a bifunctional DBCO click chemistry linking unit. A polycaprolactone polymer containing an azide could be conjugated to a DBCO linking unit via the internal alkyne using click chemistry. This chapter detailed the successful synthesis of an azide functionalised polycaprolactone polymer that has the potential for bio-conjugation via the SPAAC reaction. The synthesis of the polymer is a one pot reaction, which is high yielding (>80%) and reproducible, demonstrating good control over the polydispersity index with an average PDI of 1.2. The presence of azide was confirmed by IR with the addition of a peak at 2100 cm^{-1} in both the initiating unit and the polymer after synthesis. The subsequent PCL-N_3 polymer was shown to be reactive toward internal alkynes present within a DBCO-acid unit. NMR DOSY showed that this reaction was efficient with conjugation occurring within just 30 minutes. As this polymer has shown the ability to conjugate to a click chemistry linking unit of DBCO-acid it can be taken forward and used in the formulation of microparticles to attempt to produce a drug delivery system for the conjugation of biomolecules.

4. Experimental Procedures

4.1. General Methods

Unless stated otherwise, all starting materials were commercially sourced and used without any further purification. Reactions were carried out under an atmosphere of nitrogen, using dried glassware and all solvents and liquid reagents were added via syringe injection through rubber septa.

4.2. Materials

All materials were purchased from Sigma Aldrich and used without any further purification unless stated otherwise. Hexamethylenediamine (98%), ninhydrin (95%), rhodamine B isothiocyanate (mixed isomers), ammonium chloride (99.5%), 2-[2-(2-chloroethoxy)ethoxy]ethanol (96%), ε-caprolactone (97%), polycaprolactone (MW ~14,000 average Mn ~10,000 by GPC), sodium azide (100%), sodium ascorbate (98%), copper sulfate pentahydrate (98%), phenylacetylene (98%), tin(II) 2-ethylhexanoate (92.5-100%), dibenzocyclooctyne-acid (Click Chemistry Tools, 95%).

4.3. Instrumentation

All ^{1}H and ^{13}C NMR spectra were recorded using a Bruker 400 spectrometer at 400 MHz and 101 MHz respectively. Deuterated chloroform ($CDCl_3$) was used as the solvent in all cases. All chemical shifts reported are in parts per million (ppm) and have been referenced to the residual protons (^{1}H) or carbons (^{13}C) of the deuterated solvent used. HNMR DOSY experiments were recorded using a Bruker Ascend™ 500 spectrometer at 500 MHz with $CDCl_3$ as the solvent. All IR spectra were recorded using a Perkin-Elmer Spectrum 100 FT-IR spectrophotometer in the range of 4000-400 cm^{-1} as thin films on NaCl plates. Polymer analysis of molecular weights and polydispersity index (PDI) were determined using Varian/Polymer Laboratories GPC 50 instrument. All samples were recorded in filtered chloroform as the solvent at a concentration of 1-5 mg/mL with a flow rate of 1 mL/min. All polymer samples were read in triplicate

and Mn and PDI values given as average. All molecular weights were calibrated to polystyrene standards. Thermal Analysis was carried out using a TGA Q5000 (TA instruments, Newcastle, USA) and analysed using Trios software v4.3.1.39215. Samples (2-10 mg) were analysed by applying a temperature programme of 10 °C/min to a final temperature of 500°C.

4.4. Aminolysis of Polycaprolactone Microparticles (1)

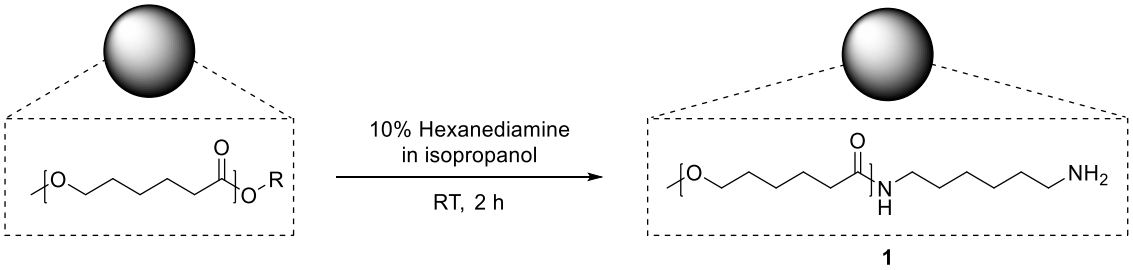

1

General Formula: $N_2H_{15}C_6(C_6H_{10}O_2)_n$

A calibration curve for 1,6-hexanediamine was constructed from a 25 mg/mL stock solution in isopropanol. Concentrations from 8 µg/mL to 96 µg/mL were reacted with a 1 M ninhydrin/ethanol solution (500 µL, 1:1) and heated with stirring at 75°C for 15 min. Absorbance was measured in triplicate at 590 nm.

PCL microparticles (0.5 g, 0.05 mmol) were immersed in a 10% 1,6-hexanediamine solution in isopropanol (20 mL) and stirred at room temperature for 2 h. Afterwards the particles were thoroughly washed with distilled water and lyophilized to yield compound **1**. Microparticles treated with 1,6-hexanediamine solution (**1**) were reacted with 1 M ninhydrin/ethanol solution (500 µL) and heated with stirring at 75°C for 15 min. Non-treated particles reacted with ninhydrin solution were used as a control. Absorbance of the particles was measured at 590 nm.

A calibration curve for rhodamine B isothiocyanate was constructed. Concentrations from 0.8 µg/mL to 4.8 µg/mL were dissolved in DMSO. Absorbance was measured in triplicate at 555 nm.

Microparticles treated with 1,6-hexanediamine solution (**1**) were suspended in PBS (5 mg/mL, 5 mL) and rhodamine B isothiocyanate was added in 5 µL aliquots to a total volume of 250 µL and left to react for 24 h at 4°C in the dark. Ammonium chloride was added to a final concentration of 50 mM and incubated for 2 h at 4°C to quench the reaction. The particles were washed with distilled water (10x1 mL), suspended in water (1 mL) and the absorbance read at 555 nm. Non-treated particles reacted with rhodamine b isothiocyanate were used as a control.

4.5. Synthesis of an Initiator for Ring Opening Polymerisation (2)[188]

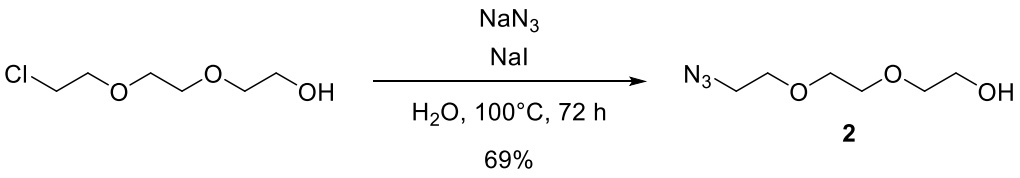

General Formula: $C_6H_{13}N_3O_3$

Molecular Weight: 175.19

2-[2-(2-Chloroethoxy)ethoxy]ethanol (9 g, 53 mmol), sodium azide (6.9 g, 106 mmol, 0.5eq) and sodium iodide (2 g, 13 mmol, 0.1eq) were dissolved in distilled water (25 mL) and heated at reflux for 72 h. The product was extracted using ethyl acetate (3x20 mL), the organic layers were combined, and solvents were removed under reduced pressure to yield compound **2** as a light pink liquid (6.406 g, 69%).

^{1}H NMR (400 MHz, $CDCl_3$) δ: 3.68 (m, 2H), 3.64 (m, 6H), 3.59 – 3.53 (t, 2H), 3.36 (t, 2H), 2.70 (s, 1H).

^{13}C NMR (101 MHz, $CDCl_3$) δ: 72.56, 70.64, 70.36, 70.02, 61.69, 50.65.

IR (NaCl, cm^{-1}) 3391, 2867, 2095, 1454, 1345, 1283, 1063.

4.6. 2-(2-(2-(4-phenyl-1H-1,2,3-triazol-1-yl)ethoxy)ethoxy)ethanol (3)

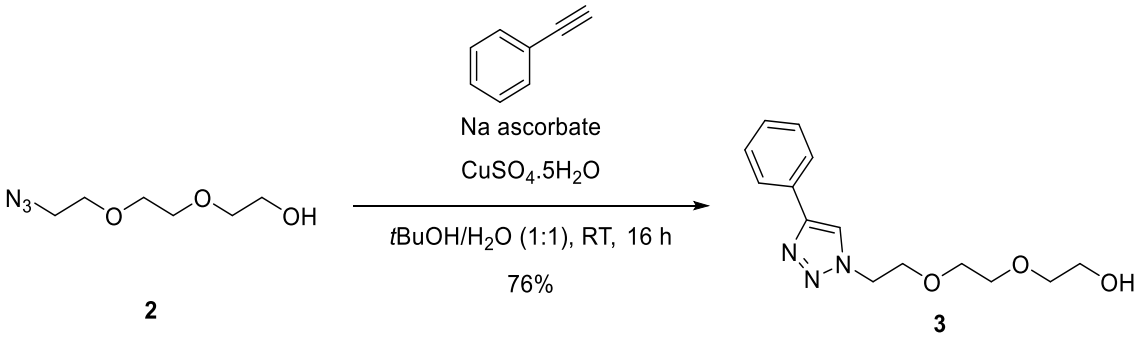

General Formula: $C_{14}H_{19}N_3O_3$

Molecular Weight: 227.32

Compound **2** (1.01 g, 5.76 mmol) sodium ascorbate (0.133 g, 0.67 mmol, 0.1eq), copper sulfate pentahydrate (0.149 g, 0.59 mmol, 0.1eq) and phenyl acetylene (0.7 mL, 6.37 mmol, 1.1eq) were dissolved in a *tert*-butyl alcohol/water (1:1, 40 mL) mix and stirred vigorously for 16 h. The solution was diluted with water and an extraction carried out using ethyl acetate (3x30 mL). The organic layers were combined and dried using magnesium sulfate. Impurities were removed using activated charcoal with filtration through cotton. Solvents were removed under reduced pressure to yield product **3** as a yellow oil (1.04 g, 76%).

^{1}H NMR (400 MHz, $CDCl_3$) δ: 7.95 (s, 1H), 7.85 – 7.79 (m, 2H), 7.44 – 7.36 (m, 2H), 7.34 – 7.27 (m, 1H), 4.64 – 4.46 (m, 2H), 3.97 – 3.81 (m, 2H), 3.77 – 3.66 (m, 2H), 3.64 – 3.57 (m, 4H), 3.57 – 3.45 (m, 2H), 2.30 (s, 1H).

IR (NaCl, cm^{-1}) 3404, 2869, 1441, 1372, 1242, 1114.

4.7. Polymerisation of Polycaprolactone (4)[149]

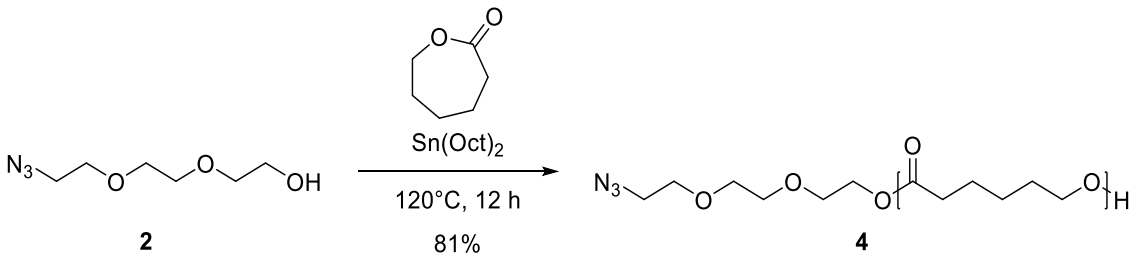

General Formula: $N_3C_6H_{12}O_3(C_6H_{10}O_2)_n$

Average Molecular Weight: ~23,000 (Confirmed by GPC)

ε-caprolactone (9.742 g, 85.35 mmol) was heated to 85°C under an atmosphere of nitrogen. Compound **2** (0.1 g, 0.57 mmol, 1eq) and catalytic tin(II) 2-ethylhexanoate (0.023 g, 0.05 mmol, 0.1eq) were added and the mixture was stirred for 12 h at 120°C. The solution was cooled to room temperature, and the solid mixture recrystallized from DCM using cold methanol to remove unreacted monomers. The precipitate was collected using a Buchner funnel to yield the desired compound **4** as a white solid (7.868 g, 81%). The polymer MW and polydispersity index were analysed using gel permeation chromatography with chloroform as an eluent.

^{1}H NMR (400 MHz, $CDCl_3$) δ 4.05 (t, 192H), 3.74 – 3.59 (m, 10H), 3.38 (s, 2H), 2.30 (t, 192H), 1.69 – 1.49 (m, 384H), 1.42 – 1.10 (m, 192H).

IR (NaCl, cm^{-1}) 3437, 2944, 2865, 2100, 1722.

(GPC) M_n 19502 (polydispersity Index) 1.17.

4.8. Polycaprolactone-Azide-Dibenzocyclooctyne Triazole (5)

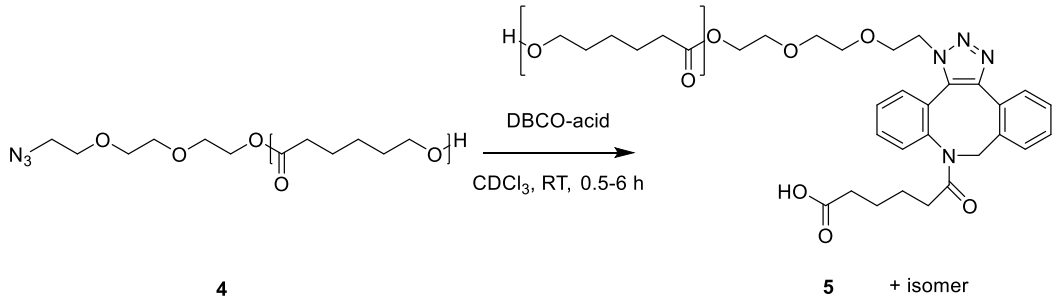

4 **5** + isomer

General Formula: $C_{27}H_{31}N_4O_6(C_6H_{10}O_2)_n$

Molecular Weight: ~23,376

Compound **4** (0.044 g, 0.0019 mmol 0.1eq) and DBCO-acid (0.005 g, 0.014 mmol, 1eq) were dissolved in $CDCl_3$ (250 µL) in an NMR tube and 2D ^{1}H NMR DOSY spectrum collected periodically every 30 min for 6 h to monitor the formation of compound **5**. Commercial PCL (0.0152 g, 0.00152 mmol, 0.1eq) and DBCO-acid (0.005 g, 0.014 mmol, 1eq) were treated the same and used as control.

Chapter 3: Microparticle Production and Optimisation

1. Introduction

1.1. Microparticles as a Drug Delivery System

From the beginning of the project, microparticles were the chosen method of drug delivery. Researchers need to consider several factors when formulating a drug delivery system; an appropriate receptacle for delivery, the duration and manner of release, and the method of formulation, which includes ensuring the therapeutic agent is not degraded during production.[100] A successful drug delivery system should be able to maintain a therapeutic dose of the delivered drug for a sustained period, corresponding to the healing time at the repair site.[126] Unfortunately, one of the major limitations to the delivery of proteins is their short half-lives and quick clearance by the body.[6,34,96,194] Concentrations can fall below the therapeutic dosage very quickly, making it necessary for either frequent administrations or high loading concentrations, which in turn can cause toxic side effects.[104,111,127,195] Frequent administrations of proteins are problematic, requiring high levels of patient compliance and close supervision from a medical professional. As a result, there has been limited industrial and commercial success of these types of products.[100,182] To negate these safety concerns, as well as improve the efficacy of the delivered protein, microparticles have been used as an improved delivery system.[100,126,127,12,13]

Microparticles are composed of highly crosslinked or entangled long chains of linear polymers with spherical morphology.[145] One of their advantages is that they can be formulated as injectable systems and localised to the site of repair.[101,194] Another advantage of microparticles is that they can also be formulated as dry powders, allowing for a long storage life.[127,194] When formulating microparticles as a delivery system it is important to consider the release profile; the timing of the protein's release is as equally important as its delivery.[194] The diffusion of proteins and the timing of their release can be tightly controlled depending on the method used to incorporate them into the microparticles. They can be encapsulated within the bulk, physically adsorbed, or conjugated to the surface.[179] Each method will alter the rate at which the protein is released. This can allow for controlled release of a singular protein, or

even cocktails of proteins, taking into account factors such as the degradation rate of the microparticles, which can be adjusted to closely match the rate of healing tissue.[79,89] The properties of the microparticles depend on the production and encapsulation method as well as the type and concentration of polymer used.[126,182] If a microparticle drug delivery system is to see commercial success, the encapsulation efficiency should be high to minimise wastage of expensive resources.[182]

1.2. Microparticle Encapsulation Techniques

Microparticles can be formulated via several techniques, with the technique used for production having an effect on both their size and entrapment efficiency.[101,126] These techniques include spray drying, dispersion polymerisation, the use of microfluidic devices, homogenisers and rotor-stator mixers.[81,100,101,182,196–199] These techniques rely on the production of either oil in water (O/W) or water in oil (W/O) emulsions.[200] The definition of emulsions is the dispersion of two immiscible liquids, usually water and oil, or organic solvent, where droplets from the dispersed phase form within the continuous phase.[196] Therapeutic proteins can be encapsulated within these droplets, and the type of emulsion used will be dependent on the solubility of the protein of interest.[126]

O/W emulsions are used for the encapsulation of hydrophobic or insoluble agents, but are not compatible with hydrophilic proteins, as they rapidly leach into the external water phase.[141,181,201] For these agents W/O emulsions are used.[141,182] However, these systems are not ideal because the external oil phase is either composed of large volumes of organic solvent, or oils such as mineral or vegetable oil, which are difficult to remove when washing and collecting the formed particles.[102] Therefore, the most common and extensively studied method for the encapsulation of proteins within microparticles is via double emulsions.[79,142,202,203] For this technique an emulsion is made within another emulsion.[200] Primary emulsions of either O/W or W/O are produced and then emulsified again into an appropriate secondary continuous phase producing either water in oil in water (W/O/W) or oil in water in oil (O/W/O)

emulsions.[124,204] In these emulsions the oil phase typically contains a biodegradable polymer, which upon solvent evaporation will form solid microparticles.[126,205]

The most common method for the entrapment of proteins within double emulsions is within the internal water phase of a W/O/W formulation (Figure 17). The internal oil phase separates the two water phases, and acts as a liquid membrane, therefore allowing for the controlled release of protein.[124,126] Using double emulsions, it is possible to deliver a cocktail of therapeutic agents, with water soluble drugs contained within the internal water phase, and lipophilic drugs within the oil phase.[102]

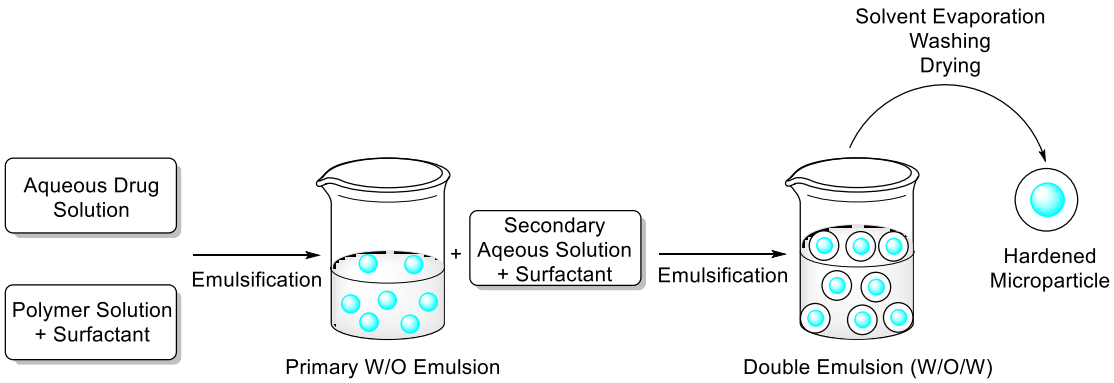

Figure 17: Representation of the double emulsion technique. Therapeutic proteins are encapsulated within the internal water phase of microparticles during production of a water-in-oil-in-water (W/O/W) emulsion.

The characteristics of the resulting microparticles are difficult to control with these conventional methods, and the population is rarely uniform.[182] The multi-step nature of double emulsions means that it is first necessary to produce a stable primary emulsion. Breakup of the primary emulsion during the secondary emulsification step can result in a broad size distribution in the resulting microparticles.[205] Successful production of double emulsions requires high shear forces to emulsify the primary emulsion into the secondary continuous phase. Typically, this is done via homogenisation, mechanical stirring, or sonication, which breaks down the larger droplets to disperse them in the external phase.[196,205] These forces need to be tightly controlled to prevent the rupture of the primary emulsion droplets.[124] These processes are not

homogenous throughout and as a result the particles produced often have broad size distributions, and highly variable average particle sizes between batches.[197] Additionally, as the mechanical energy required in these systems is so high, the microparticles are subjected to high temperatures during production and as such this method is not amenable to sensitive materials such as proteins and cells.[102,112,196] To combat this problem, milder systems have been employed to produce double emulsions that minimise the shear stress needed.

1.2.1. Membrane Emulsification

Membrane emulsification was first introduced by Nakashima and co-workers as a method to produce monodispersed microparticles with a tightly controlled size range.[206] This technique can be used to produce single or double emulsions, and reduces the high shear stresses, large surfactant volumes and high energy required to produce double emulsions.[196,198] For this, uniform microparticles are produced by forcing the primary emulsion through a membrane, into the secondary aqueous phase (Figure 18).[182,200] The membrane acts as the secondary emulsifying agent of the primary emulsion, with the reduced risk of rupture of the primary emulsion droplets[200,206] This process does not require the high energy levels or mixing techniques such as sonication or homogenisation because as the droplets are formed on the surface of the membrane, they detach upon reaching a critical size rather than needing to be broken up.[196,207] The membrane is made from materials with high mechanical strength such as Shirasu glass or metal, and has uniform pores throughout its surface, through which the dispersed phase is passed.[205,206] This technique offers advantages over the uniformity of the microparticles produced, resulting in smaller size distribution of the particle population.[208] This allows the particles to be reproducible, and possess the same characteristics between batches, meaning the process can be easily scaled for an industrial setting.[100]

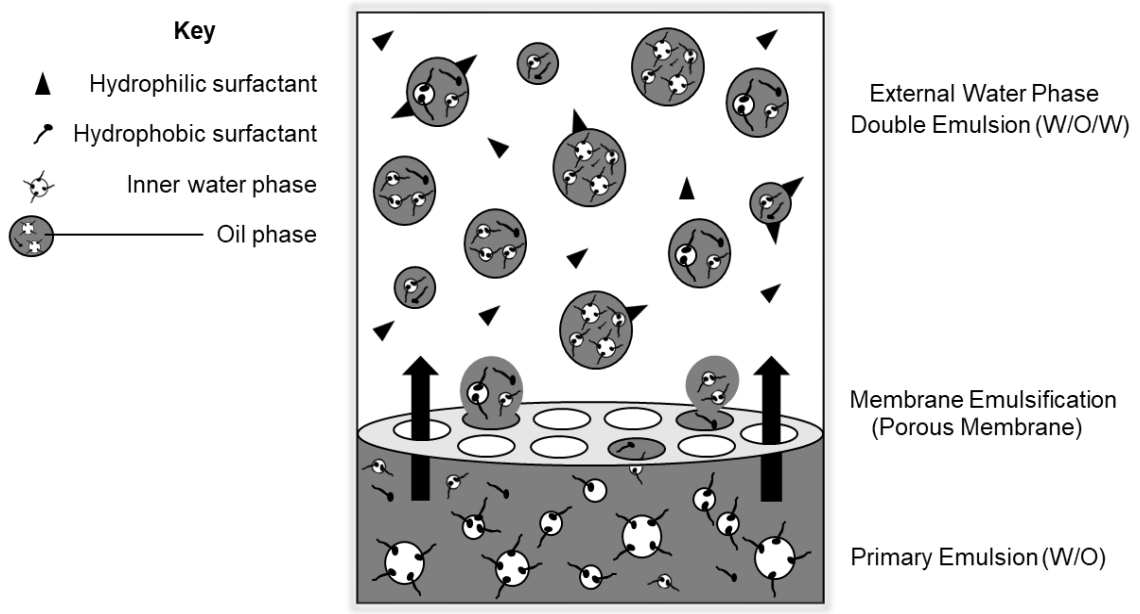

Figure 18: Representation of membrane emulsification. Water-in-oil-in-water (W/O/W) emulsions are produced by emulsifying the primary water-in-oil (W/O) emulsion through a membrane.

An advantage of membrane emulsification is that the particles produced are uniform in size. This is particularly advantageous when producing a drug delivery system as the release of the drug needs to be controlled and uniform.[200] Uniform particle size and distribution will mean that there is little batch to batch variability and that the delivery system has repeatable release characteristics.[78] Another advantage is that microparticle size can be tightly controlled by careful selection of the pore sizes present within the membrane.[182] It is possible to estimate the size of the microparticles produced before carrying out any experimental work as the relationship between pore size and microparticle size is linear.[206,207] As a rough guide, it is suggested that particles produced will be approximately three times larger than the size of the pores present in the membrane used, when following the manufacturers guidelines (Appendix C, Table 14). Reproducibility and energy efficiency of the systems means that the technique lends itself to industrial scale up. This can be achieved using industrial sized stirred cells or the addition of more membrane modules.[207]

1.3. Effect of Controlling Particle Size and Uniformity

If microparticles are to be used as a drug delivery system, it is extremely important to be able to control their size and uniformity.[78] Uniformity of microparticles is highly dependent on the uniformity of dispersed phase droplet size at creation during the membrane emulsification. If the microparticle population has a broad size distribution there will be variation in the amount of drug loaded within each batch, and the rate at which the drug is released.[78] Control of particle size is also important as it can affect their final application and method of delivery. Smaller particles with a size range below 10 μm can easily be phagocytosed by macrophages in the body, whereas larger particles would need to undergo degradation before this would occur. Therefore, particle size has a direct effect on the degradation rate and immune response times.[100] An advantage of larger particle sizes is the higher drug loading capacity they allow.[182] Particle size may also influence the route of administration that is needed. If the particles are to be injected, the smaller the particles are the smaller the needle needs to be.[209] The smaller the needle then the more cost effective the treatment, as these can be delivered either via ultrasound guided injections, or carried out under local anaesthetic. Particles around 150 – 200 μm offer the advantage of being large enough to remain at the repair site for longer periods of time before clearance by the body, but also small enough to allow for intravenous transfusion or subcutaneous injections.[182,209] Microparticle size can be tightly controlled by adjusting the process parameters used in their production.

1.4. Factors Affecting Particle Size and Uniformity

All the parameters used to produce the particles can be altered to affect their monodispersity and size. These parameters can be divided into three categories; membrane properties, processing conditions, and material properties.[198] These can include, but are not limited to, membrane pore size, the viscosity of the dispersed and the continuous phases, the rate at which the dispersed phase is injected, the rotation speed of the continuous phase, as well as the surfactant type and concentration. Optimisation of the production process

is usually necessary because small changes can result in varied and sometimes unpredictable outcomes within the microparticle population.[182,210] Different parameters also have varying levels of magnitude in terms of effect.[197]

Droplet size is controlled largely by the forces acting upon the droplet and the resulting detachment from the membrane. These forces each alter the droplet formation in a different manner and include those acting on the droplet, causing its adherence to the membrane surface, and those effecting its detachment. Droplets can detach from the membrane in two ways; spontaneously after reaching a critical size or involuntarily due to the presence of shear force.[197] These forces include the shear forces acting on the droplet from the rotation of the continuous phase, the interfacial tension, and the pressure of the injecting dispersed phase.[207] Shear stress is generated by the rotation of the continuous phase, this force acts upon the forming droplet to allow it to detach from the surface of the membrane.[196]

Surfactant type and concentration can also affect particle size and uniformity. The surfactant concentration must be sufficient to reduce the interfacial tension of the growing droplets, which is in part controlled by the rate at which the droplets grow from the membrane.[197,211] If surfactant concentration is too low it will result in the coalescence of particles with an increased size and polydispersity[124,198,207] Rotation speed of the continuous phase will also affect the resulting particle size. Higher rotation speeds will produce smaller droplets, whereas lower speeds can increase droplet size as well as size distribution. Viscosity of the materials used also affects the membrane size, lower viscosities decrease the critical pressure needed to pass the dispersed phase through the membrane pores, which results in more uniform microparticles.[78] Increasing viscosity increases the resulting particle size.[207]

1.5. Aims and Objectives

The hypothesis of the work detailed in this chapter is that previously synthesised PCL-N_3 polymer could be used to produce microparticles. It was necessary to assess if control over the parameters used at production could

result in particles with a tightly controlled size range that could easily be altered. It had to be confirmed that the azide of the PCL polymer was accessible and the particles could undergo the click chemistry reaction to deem the production of the microparticles a success and proceed to the next experimental steps.

2. Results and Discussion

2.1. Microparticle Production Optimisation

Microparticle production and optimisation was carried out in parallel to the experiments discussed in chapter 2. At the beginning of the project it was necessary to prove that microparticles could be produced and primarily it was necessary to decide on the most appropriate experimental conditions for their production. Particles should have a smooth spherical morphology, and a tightly controlled size distribution. Microparticles were produced using the dispersion cell, from Micropore Technologies Ltd. It is a mechanical membrane emulsification system used to produce emulsions containing uniform, monodisperse microparticles with a narrow size distribution. The system contains a 3-way injection valve, an electronic injection pump, an injection chamber, a glass cylinder and a motorised stirring unit (Figure 19). To produce microparticles via membrane emulsification, a dispersed phase is slowly and steadily injected into a continuous phase and passed through a membrane. The membrane is a circular sheet of metal with uniform pores spaced evenly on the surface. The pores can cover the entire surface or be confined to just a small area of the membrane in a ring formation, depending on if the membrane is standard or ringed (Figure 19, Insert).[209,212] The emulsification process is stirred cell emulsification. Droplets form on the surface of the membrane and the continuous phase is stirred by a paddle that sits above the membrane. This produces the required shear stress needed to detach the droplets. Hydrophilic membranes can be used to produce O/W emulsions and hydrophobic membranes for W/O emulsions[207].

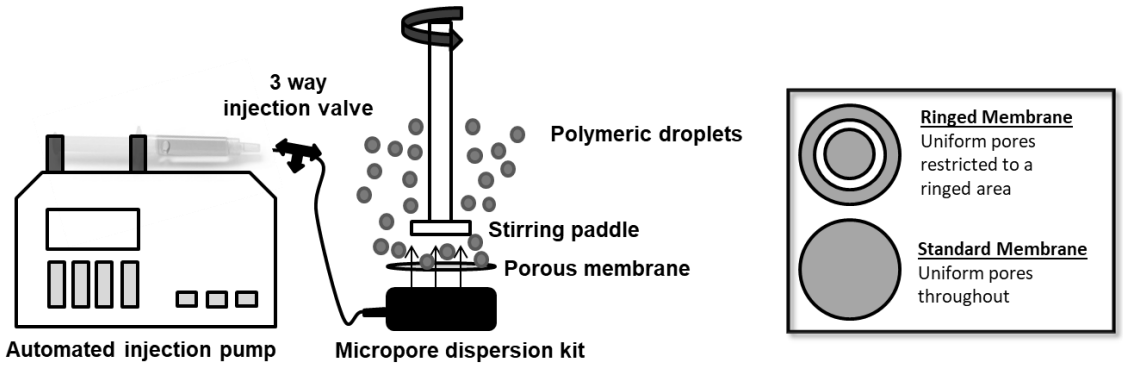

Figure 19: Representation of the process for microparticle production using a Micropore Dispersion Kit. Microparticles are produced via membrane emulsification by passing the dispersed phase through a membrane into a stirring unit. Insert shows the different membranes that can be used, either standard or ringed.

Microparticles were produced by injecting the PCL polymer as the oil phase into the aqueous phase through the membrane. After microparticle production, each batch of particles were measured using Image J analysis software to collect data relating to average particle size. Monodispersity was assessed based on the span of the particle population. The span of particles represents the size distribution, and can be calculated using the following equation;

$$Polydispersity\ (Span) = \frac{D90\% - D10\%}{D50\%}$$

Where D signifies the diameter at which that given percentage (10, 50 or 90) of the particle population is contained.[209,210,213,214] The more uniform a population of particles, the narrower the size distribution, the closer to zero the span value becomes.[215] A size distribution of less than 1 indicates a monodisperse population of particles.[212] Optimisation of the production of particles was carried out using commercial PCL to avoid wasting resources of PCL-N_3. Knowledge of the system and the production process of microparticles could then be applied when producing PCL-N_3 particles. Control over particle monodispersity and size was important because at the beginning of the project it was not known how proteins were going to be incorporated with microparticles. If protein was to be encapsulated within the internal phase of particles produced by double emulsion, then a broad size range would result in large batch to batch variability

of protein content within each microparticle. Additionally, it was undetermined at the beginning of the project if the bioactive agent would be proteins, or cells. The incorporation of cells with microparticles requires a larger particle size than protein, therefore it was important to be able to manipulate particle size. Table 7 shows the different parameters tested to try to produce monodisperse particles using commercial PCL and the resulting particle size distribution.

PARAMETER TESTED	OIL	WATER	RPM	RATE ML/MIN	AVERAGE (µM)	SPAN (µM)
PVA CONCENTRATION	10% PCL in DCM	0.3% PVA	779	0.5	61 ± 8.75	2.38
		1% PVA	779	0.5	35 ± 1.45	0.86
SALT ADDITION	10% PCL in DCM	1% PVA, 13 g/L NaCl	779	0.5	43 ± 0.69	0.43
		1% PVA 40 g/L NaCl	779	0.5	48 ± 1.06	0.22
STIR SPEED	10% PCL in DCM	1% PVA 13 g/L NaCl	1091	0.5	34 ± 0.84	0.42
INJECTION RATE	10% PCL in DCM	1% PVA 13 g/L NaCl	779	1	45 ± 1.23	0.52
			779	2.1	42 ± 0.62	0.63
PCL CONCENTRATION	15% PCL in DCM	1% PVA 13 g/L NaCl	779	0.5	54 ± 1.07	0.34
	20% PCL in DCM	1% PVA 13 g/L NaCl	779	0.5	55 ± 1.85	0.63

Table 7: Parameters tested to produce monodisperse microparticles.
Microparticle production was optimised using commercial PCL and standard membrane with 15 µm pore size. Poly(vinyl)alcohol (PVA).

Surfactant and salt concentration had the greatest effect on both average particle size and monodispersity of particles (Table 7). Initial investigations began by looking into the effect of altering the surfactant concentration. The addition of a surfactant in the aqueous phase is essential for the formation of

monodisperse particles. PVA is a popular stabiliser as it has low toxicity, is cost effective, is readily solubilised in water and is commercially available in a vast array of molecular weights.[205] PVA concentrations of 0.3% and 1% w/v in the aqueous phase were assessed. It was found that at 0.3% w/v PVA concentrations, the emulsion was not stable. The resulting droplets quickly coalesced producing very large particles, (>100 µm), as well as smaller particles (between 18-30 µm) (Figure 20). The resulting span was 2.38, proving that these particles were not monodisperse. This can be attributed to the low surfactant. concentration, resulting in increased interfacial tension and droplet coalescence.[198,205] Conversely, increasing the concentration of PVA to 1% w/v improved the droplet stability, decreased the risk of coalescence and reduced the presence of larger particles (>100 µm). Additionally, the span of the particles was 0.86, suggesting this concentration of PVA was sufficient to produce monodisperse particles. Increasing PVA concentrations beyond 1% w/v, although beneficial for size distribution and monodispersity, is unfavourable due to surfactant adherence to the surface of particles, which is difficult to remove.[205]

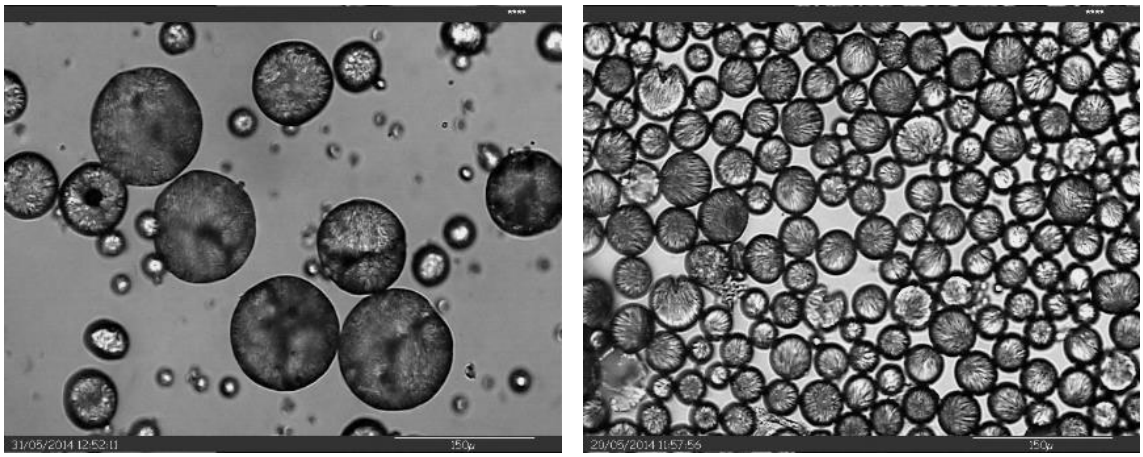

Figure 20: Improvement of particle dispersity and morphology. Particle dispersity and morphology was improved by altering process parameters. 0.3 %w/v PVA (left) increased to 1 %w/v PVA and addition of 13 g/L NaCl (right).

The addition of sodium chloride to the water phase was tested as this can also help to stabilise emulsions.[100,126] In an attempt to improve the span and monodispersity of particles further, concentrations of 13 and 40 g/L sodium

chloride were investigated. Overall the addition of salt had a positive effect on the morphology and monodispersity of the resulting particles (Table 7), at both concentrations. The span of microparticles was 0.22 and 0.43 for 40 and 13 g/L sodium chloride respectively. Monodispersity of particles was best at concentrations of 40 g/L. However, this resulted in the presence of salt crystals upon solidification and collection of microparticles, which were difficult to fully remove (Figure 21). For this reason, salt concentrations were kept at 13 g/L.

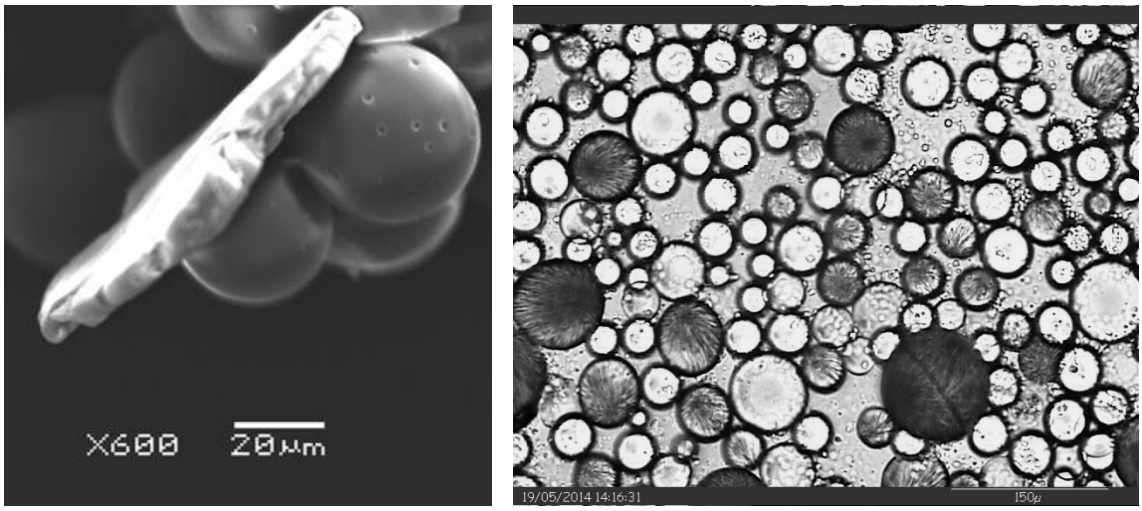

Figure 21: Microparticle images produced using 40 g/L sodium chloride. Microparticles contained a grainy like substance that was assumed to be salt that appeared as a solid in scanning electron microscopy (A) and a grainy appearance in optical microscopy (B).

Increasing stir speed resulted in a decrease in average particle size from 43±0.69 to 34±0.84 μm for speeds of 779 to 1091 RPM respectively. Although it was found that this had no effect on the span of the particles with these being comparable at both speeds. Increasing injection rates had an adverse effect on particle span, increasing from 0.43 at injection rate of 0.5 mL/min to 0.52 and 0.63 at speeds of 1 and 2.1 mL/min respectively. Also, it was found that increasing the injection speed, could result in damage to the membrane. This was assumed to be because of a pressure increase in the injection chamber of the dispersion kit. Increasing PCL concentration resulted in an increase in average particle size from to 54±1.07 and 55±1.85 μm for concentrations of 15 and 20% w/v respectively. Overall through multiple optimisations, it was found the best improvements in particle morphology and size were found when

particles were produced with 1% w/v PCL and 13 g/L sodium chloride (Figure 20)

As it was possible to produce monodisperse microparticles using the methods described above, investigations into the ability to alter the particle size were carried out. A recommended method for altering the size of microparticles is by changing the pore size of the membrane used for emulsification.[78] Droplet size is closely associated with membrane pore size in a linear relationship, in both O/W and W/O emulsions.[206,207] The use of ringed membranes results in the production of microparticles with better size distributions and tighter control over monodispersity when compared to particles produced using standard membranes.[216] Therefore ringed membranes with pore sizes of 10 and 5 µm were investigated.

Decreasing the pore size within the membrane resulted in a decrease in average particle size, changing from 24±0.4 µm to 16±0.2 µm for membranes with pore sizes 10 µm and 5 µm respectively. Additionally, decrease in the pore size resulted in a decrease in the size range, with smaller minimum and maximum particle sizes. The smallest particles measured were 11 µm and the largest 45 µm when using a membrane with 10 µm pore sizes. Whereas when a membrane with 5 µm pore size was used the smallest particles measured were 9 µm with the largest particles being only 26 µm (Figure 22). Both membranes resulted in the production of a monodisperse population of microparticles with span values of 0.8 and 0.4 for membranes with pore sizes of 10 and 5 µm respectively. This shows that it is possible to produce monodisperse microparticles by membrane emulsification and control particle size by altering the membrane used. This information could therefore be applied to the production of azide containing microparticles using PCL-N_3 as the polymer in the oil phase.

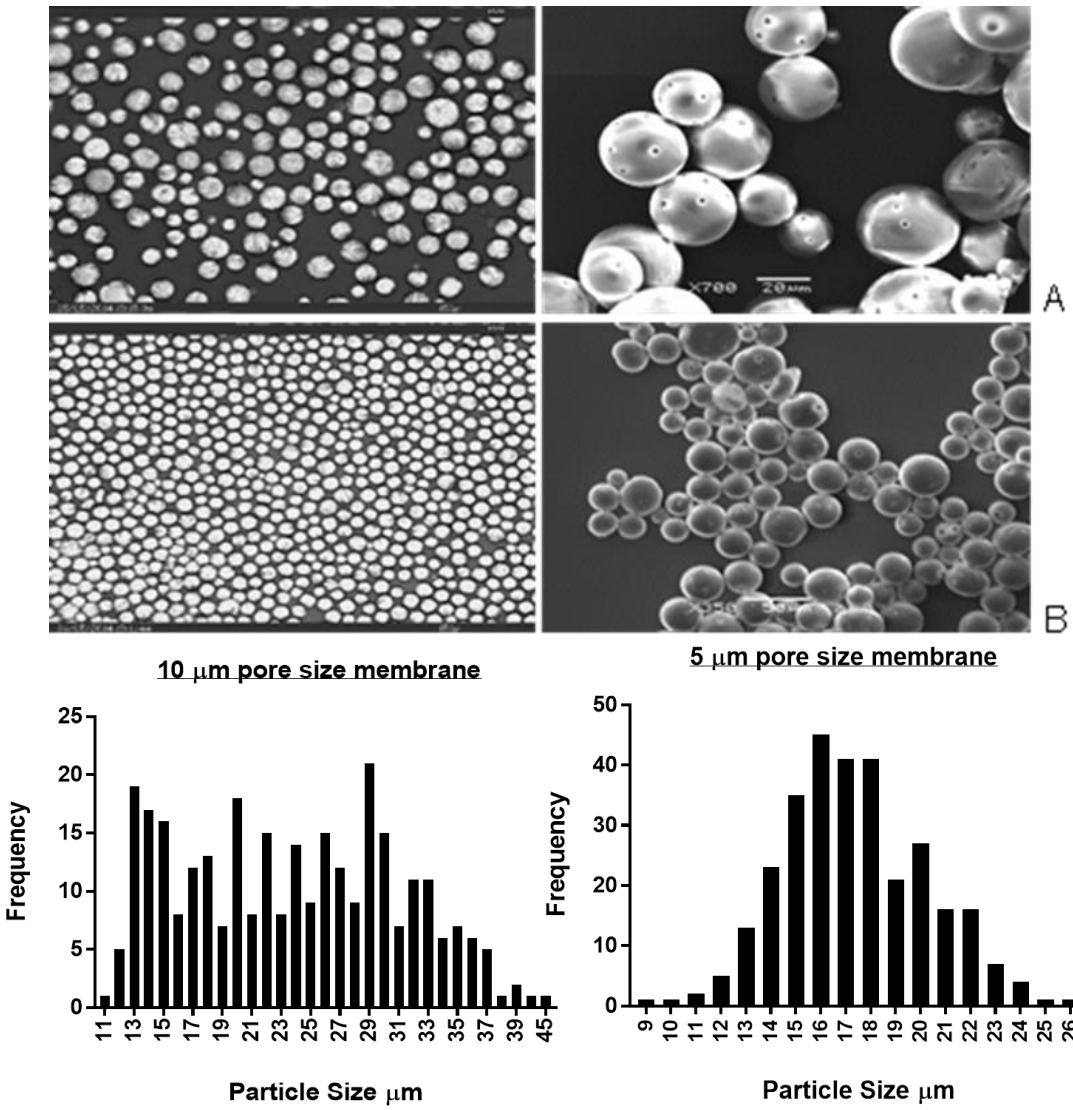

Figure 22: Effect of pore size on particle morphology and size distribution. Images show light microscope and scanning electron microscopy images of particles produced using membrane with pore sizes of 10 µm (A) and 5 µm (B) with corresponding histograms showing microparticle size (10 µm and 5 µm.)

2.2. Porous Microparticles

Another avenue that was investigated was the ability to produce porous microparticles. The presence of pores within microparticles allows for the formation of new tissue, neovascularisation, proliferation and migration of cells as well as free movement of nutrients and waste products.[217–219] Additionally porous surfaces, such as microparticles can allow for the *in vitro* culture of cells in a 3D environment. This more closely mimics the natural environment of

tissues.[220] This could have allowed for a microparticle system that was able to deliver cells to the repair site. The frequency of pores throughout the microparticles, as well as their diameter and interconnectivity are the most important factors for cell migration and proliferation as well as neovascularisation.[217] Pores can be introduced into microparticles by a process known as porogen leaching. During this process particulate substances, such as salts, are added to the polymeric material in which pores are to be introduced. Solvent is added to erode or dissolve the polymer allowing the salts to leave holes in the material. After this, the solvent is evaporated and the polymer hardens and the salt can be leached out with multiple washing steps leaving a porous microparticle (Figure 23).[220]

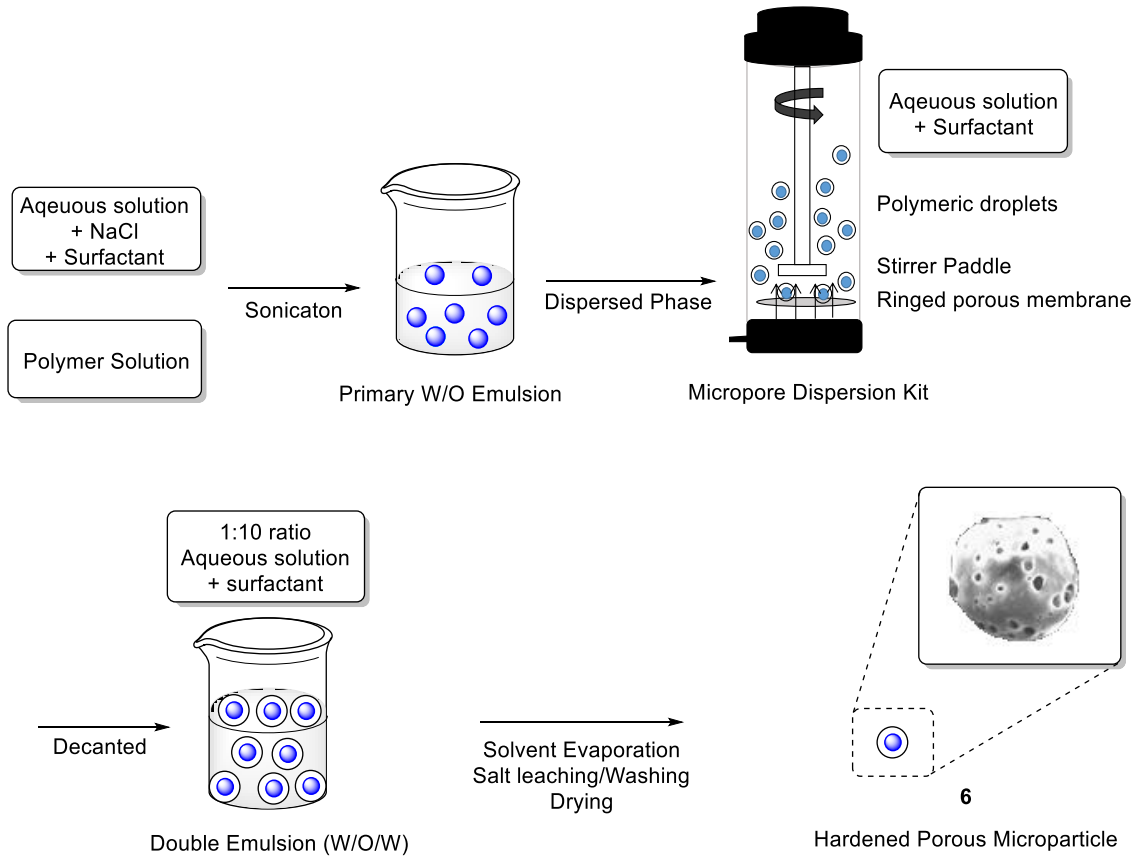

Figure 23: Production process for porous microparticles. A primary W/O emulsion containing salt as a porogen is used as the dispersed phase for membrane emulsification. The solvent is then allowed to evaporate, and the salt is leached from the particles with multiple washing steps, producing a hardened, porous particle.

Porous microparticles (**6**) were produced via double emulsion technique using commercially available PCL, incorporating sodium chloride as a porogen in the primary emulsion and using this as the dispersed phase for membrane emulsification. Pores were introduced after solvent evaporation and subsequent porogen leaching with aqueous washes. A membrane containing pore sizes of 40 µm was selected for membrane emulsification to produce larger microparticles to allow for the incorporation of pores on the surface without collapsing the particle. Table 8 details the experimental conditions attempted to produce porous particles with the resultant average particle size and pore diameter.

Primary Emulsion	W_2	Average (µm)	Span	Average Pore Size (µm)	Pore range (µm)
1% PVA 40g/L NaCl sonicated for 1 min with 15% PCL in DCM	1% PVA 40g/L NaCl	84 ± 0.91	0.27	7 ± 3.43	2-20
1% PVA 13g/L NaCl sonicated for 1 min with 15% PCL in DCM	1% PVA 13g/L NaCl	79 ± 1.20	0.43	5 ± 2.07	2-11
3% PVA 40g/L NaCl sonicated for 1 min with 15% PCL in DCM	3% PVA 40g/L NaCl	51 ± 1.39	0.72	4 ± 2.1	1-12
1 X PBS sonicated for 1 min with 20% PCL in DCM	0.3 % PVA	68 ± 0.92	0.37	5 ± 3.84	1-20

Table 8: Experimental conditions used to produce porous microparticles. Primary emulsions were used as the dispersed phase for membrane emulsification. W_2: External water phase.

It was possible to produce monodisperse microparticles >100 µm with pores throughout (**6**). Average particle size was 84 ± 0.91 µm and 79 ± 1.20 µm when using salt as a porogen at concentrations of 13 or 40 g/L respectively. The size range of particles was comparable with a range of particles from 60-110 µm for particles produced using 40 g/L sodium chloride and a range of 58-116 µm for particles produced with 13 g/L sodium chloride. Pores were present throughout for all particles produced using salt as a porogen. Pore sizes were largest when

using higher concentrations of salt, and lower concentrations of PVA (Table 8). Average pore diameter for particles produced using 40 g/L sodium chloride and 1% w/v PVA was 7 ± 3.43 µm with a pore size range of 2-20 µm. When salt concentrations were reduced to 13 g/L, pores were still present throughout the particles with an average diameter of 5 ± 2.06 µm and a pore size range of 2-11 µm. However, these pores were not present as uniformly across all particles as seen at higher salt concentrations (Figure 24). Increasing PVA concentrations to 3% w/v resulted in the presence of smaller particles with a size range of 23-81 µm. The decrease in particle size led to a decrease in pore size, and less uniformity between pore presence within microparticles. This meant that several microparticles appeared smooth in morphology when visualised by SEM (Figure 24). Additionally, higher concentrations of PVA decreased the average pore diameter to 4 ± 2.1 µm and a pore size range of 1-12 µm. Phosphate-buffered saline (PBS) was also investigated as a porogen in the same manner. It was found that particles contained pores throughout ranging from 1-20 µm, with an average pore 5 ± 3.83 µm. Highly porous particles have been reported in the literature with similar pore sizes of 8 ± 3 µm and a maximum pore diameter of 15 µm.[217]

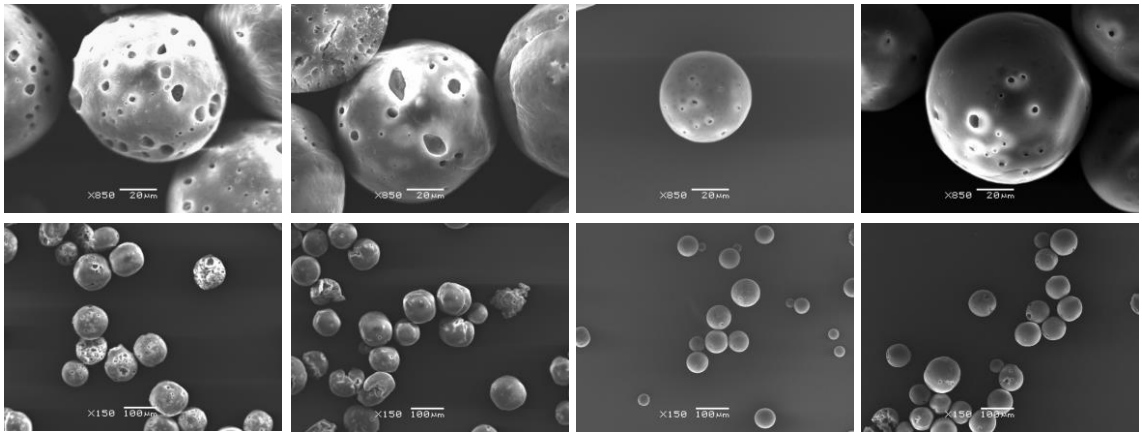

Figure 24: SEM images of porous microparticles. (Columns left to right); 40 g/L NaCl 1% w/v PVA; 13 g/L NaCl 1% w/v PVA; 40 g/L NaCl 3% w/v PVA; PBS 3% w/v PVA. Top row shows x850 magnification with scale bars representing 20 µm. Each image in the bottom row corresponds to the one above but shows x150 magnification with scale bars representing 100 µm.

Both micro and macro pores (20-100 µm) are necessary for successful dispersal of waste and nutrients.[217,218] It has been shown that cells were able to penetrate microparticles where pore diameters were 20 µm.[219] Pore diameters of 20 µm were seen in microparticles produced using 40 g/L sodium chloride concentrations with 1% w/v PVA and with PBS as a porogen. However, pore diameters of this size were rare and were not present in all microparticles. Therefore, an attempt was made to increase the pore diameter present on the microparticle surface. All particles (**6**) were treated with a sodium hydroxide and ethanol solution for the following time periods; 5, 10, 20 and 30 mins. However, it was found that the pore diameter did not increase (data not shown). It is possible that the pore diameter did not increase because the use of ethanol as a solvent was not sufficient to erode the particles, potentially this could be improved by using a solvent in which PCL has slight solubility, such as acetone.

2.3. Assessing Polymer Viscosity

Before attempts were made to produce microparticles with PCL-N_3, the viscosity of the polymer was assessed. There was a concern that due to the increase in molecular weight of the PCL-N_3 polymer (**4**) in comparison to commercial PCL (19,502 and 10,000 Mn respectively) PCL-N_3 would produce a more viscous solution when prepared for the disperse phase for particle production.[100,221] Alterations in the viscosity can influence the monodispersity of microparticles as at higher viscosities droplets collecting on the surface of the membrane are likely to adhere to the surface and remain there for longer than their less viscous counterparts. This can result in the coalescence of multiple droplets on the membrane surface, decreasing particle monodispersity and increasing particle size.[78,124] Additionally, an increase in viscosity can result in an increase in pressure when attempting to inject the polymer solution through the membrane.[196] This can lead to damage in which increased pressure forces the membrane to warp to allow the dispersed phase to flow through the pores. As well as being expensive to replace, damage to the membrane can result in the production of polydisperse microparticles. Therefore, the viscosity of PCL-N_3 polymer was investigated before attempting to produce microparticles to avoid any possible damage to the membranes. Successful production of

particles had already been achieved using 10% w/v commercial PCL (Section 2.1, above) and so the viscosity of PCL and PCL-N_3 at increasing polymer concentrations was tested. It was hypothesised that the concentration of PCL-N_3 with a viscosity most comparable to commercial PCL at 10% w/v would be appropriate for use in the production of microparticles, without risk to the membrane. Figure 25 shows the effect of increasing polymer concentration of both commercial PCL and PCL-N_3 on the viscosity.

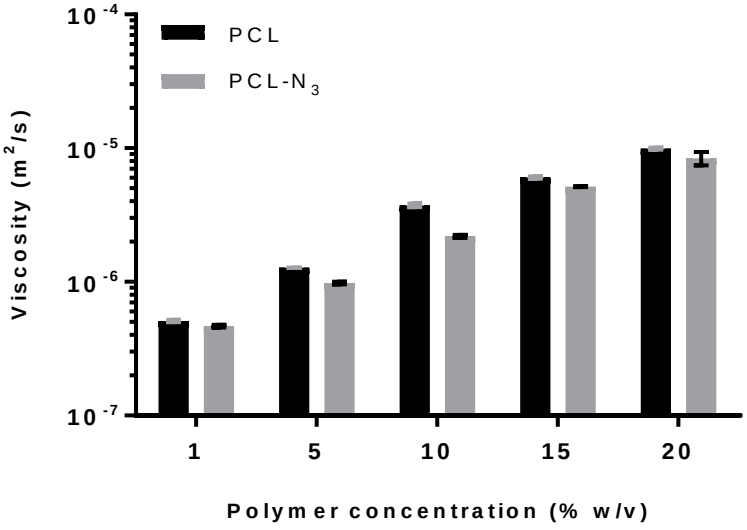

Figure 25: Effect of increasing polymer concentration on the liquid's viscosity.

As expected, for both commercial PCL and PCL-N_3 (**4**), as the concentration of the polymer increased so did the viscosity. It was found that commercial PCL and PCL-N_3 had comparable viscosities at all polymer concentrations. Commercial PCL increased from $5x10^{-7}$ m^2/s to $9.9x10^{-6}$ m^2/s from 1% w/v PCL in DCM to 20% w/v respectively. Similarly, PCL-N_3 increased from $4.66x10^{-7}$ m^2/s to $8.4x10^{-6}$ m^2/s at the same concentrations. This suggest that the increased molecular weight of the PCL-N_3 polymer did not affect its viscosity, with PCL and PCL-N_3 being comparable. This means that PCL-N_3 (**4**) can be used at a concentration of 10% w/v or higher to produce microparticles without the potential risk of damage to the membrane. Therefore the next step was to carry out the production of PCL-N_3 microparticles.

2.4. Producing Microparticles Using Polycaprolactone-Azide

PCL-N_3 microparticles (**7**) were produced using the same method of production as PCL microparticles but using PCL-N_3 (**4**) dissolved in DCM as the dispersed phase for membrane emulsification (Figure 26).

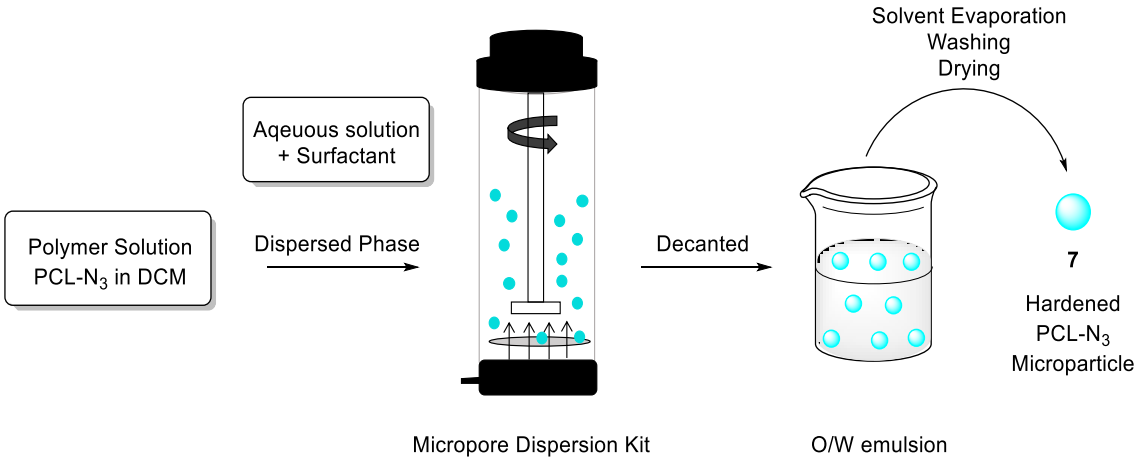

Figure 26: PCL-N_3 microparticle production process.

When optimising the microparticle production process, it was found that using ringed membranes resulted in better control over particle size and monodispersity. It was decided that to produce PCL-N_3 particles (7) the membrane would be kept constant and a ringed membrane with pore sizes of 15 µm was to be used. This membrane has the advantage of quicker production times, due to an increased injection rate correlating to larger pore size. Microparticle size was controlled by altering process parameters such as stir speed and polymer concentration. Table 9 and Figure 27 show the effect of changing these parameters on the resulting microparticle morphology and size distribution.

PCL-N_3 (W/V)	Stir Speed (RPM)	Size Range (μM)	Average (μM)	St Dev	Span	± (μM)
5 %	1140	16-34	24	3.46	0.42	0.21
10 %	1140	12-38	25	3.63	0.33	0.25
20 %	1140	18-41	30	4.23	0.33	0.31
30 %	1140	20-55	33	5.72	0.43	0.43
40 %	1140	24-50	34	4.80	0.35	0.39
10 %	400	22-153	71	23.08	0.74	2.18
10 %	590	16-64	40	9.84	0.61	0.70
10 %	770	23-58	36	4.84	0.28	0.36
10 %	950	17-39	29	4.20	0.38	0.32
10 %	1140	12-38	25	3.64	0.33	0.25
10 %	1500	10-33	22	3.67	0.40	0.23

Table 9: Effect of polymer concentration and stir speed on microparticle size distribution.

It was found that as the polymer concentration increased, so did the average particle size, resulting in particles of 24±0.21 μm and 34±0.39 μm in diameter for 5% and 40% w/v PCL-N_3 respectively (Table 9). The increase in particle size can be attributed to the increased viscosity, caused by the increased concentration of the polymer, which results in larger droplets forming on the surface of the membrane before detachment by the rotating stirrer paddle.[124] At all PCL-N_3 concentrations the size distribution of particles was low, with span values less than 0.5, indicating highly monodisperse populations. Particles at all PCL-N_3 concentrations exhibited a good spherical morphology and smooth particle surface (Figure 27).

When rotation speed was increased, the average particle size decreased, resulting in particles with a diameter of 71±2.18 μm and 22±0.24 μm at rotation speeds of 400 and 1500 respectively (Table 9). This inverse relationship is due to the decrease in droplet formation time caused by the increasingly rapid detachment of particle droplets from the surface of the membrane.[124,196] At the lowest RPM (400 and 590) it was found that the dispersity of the microparticles was poorest, with span values of 0.74 and 0.61 respectively. As rotation speed increased the polydispersity of particles improved with stir speeds of 770 RPM, resulting in the best span values (Table 9). At lower stir speeds droplets can remain attached to the surface of the membrane for longer periods before

detachment, resulting in droplet coalescence and therefore larger droplet size and increased polydispersity.[196,207] As stir speed increased, an improvement in the particle morphology can be seen. At the lowest stir speed of 400 RPM, small particles on the surface of larger particles are present, this is indicative of particle aggregation and coalescence, resulting in a polydisperse population (Figure 27). It was shown that highly monodispersed particles (**7**) with a uniform, spherical morphology could be produced using membrane emulsification. Precise control over the resulting particle size was possible by altering process parameters such as rotation speed of the continuous phase and polymer concentration.

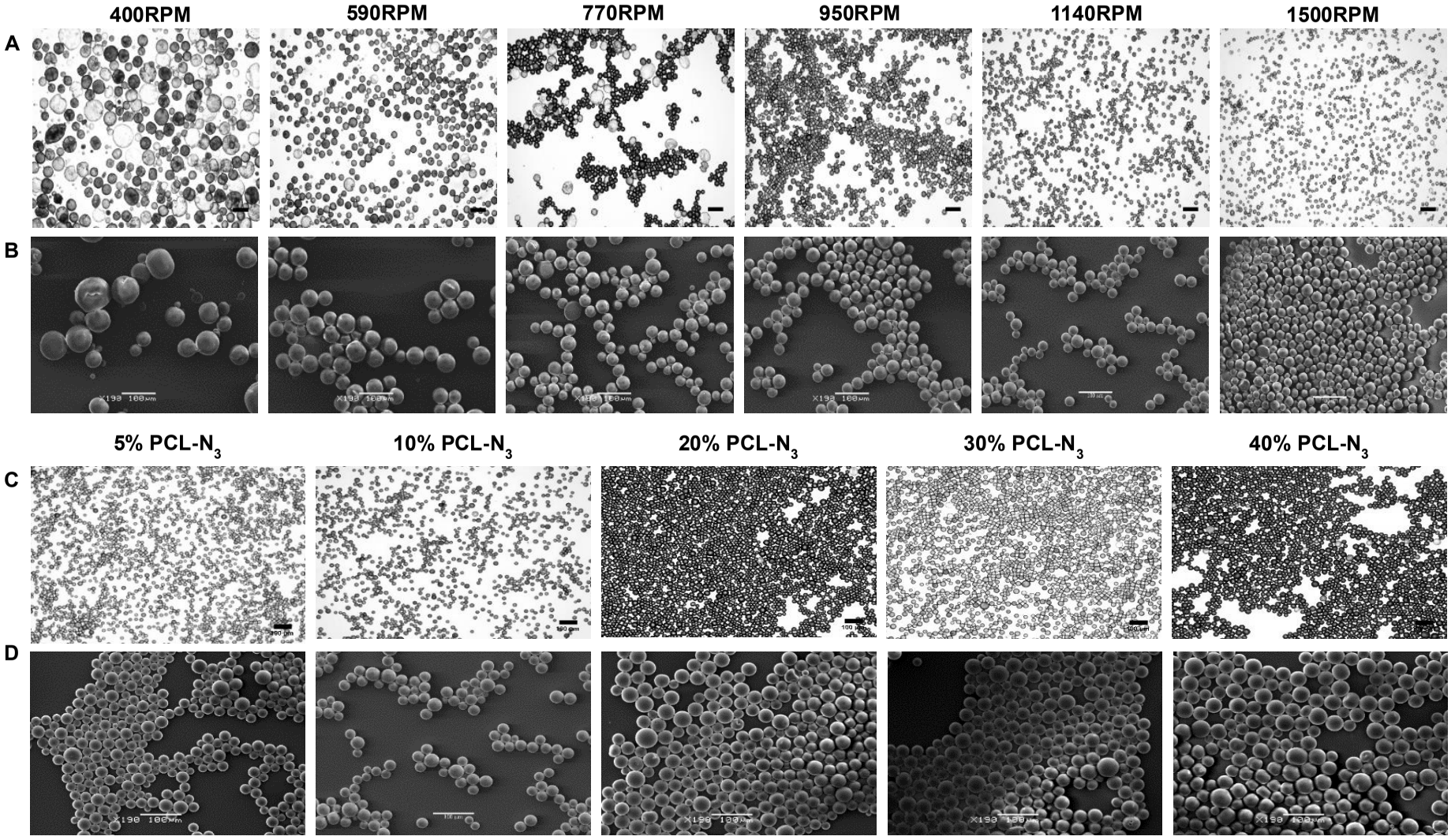

Figure 27: Effect of changing stir speed (A-B) and polymer concentration (C-D) on particle morphology. Images show solidified particles (A&C) and SEM (B&D). All optical images taken at 10 x objective. SEM shown at 190 x magnification. All scale bars represent 100 μm

2.5. Dibenzocyclooctyne Staining of Polycaprolactone-Azide Particles

The presence of an azide functional group was confirmed using IR for all batches of PCL-N_3 microparticles (**7**), with positive results showing a peak at 2100 cm^{-1} (Appendix D, Figure 62 & Figure 63). Although it was shown that the azide was present, it was not certain that it would be accessible for the click chemistry reaction. It has previously been shown that the polymer was able to carry out SPAAC click reaction (chapter 2, section 2.4). It was a possibility that after microparticle production, the azide may no longer be accessible on the surface, instead buried within the bulk of the particle. For protein conjugation to be successful in future experiments, it had to be confirmed at this stage that the microparticles were able to undergo the SPAAC reaction to an internal alkyne, forming a stable triazole. To test this, microparticles formulated using PCL-N_3 (**7**) were reacted with dibenzocyclooctyne-PEG4-Fluor 545. A control reaction was also performed using commercial PCL microparticles treated in the same way. Dibenzocyclooctyne-PEG4-Fluor 545 is a fluorescent reagent for labelling molecules containing an azide via SPAAC click chemistry. If the azide is present and accessible within microparticles then the internal alkyne present within the DBCO unit will readily conjugate, resulting in fluorescent particles that can be visualised using fluorescent imaging or quantified using fluorescent spectroscopy (**8**) (Scheme 11).

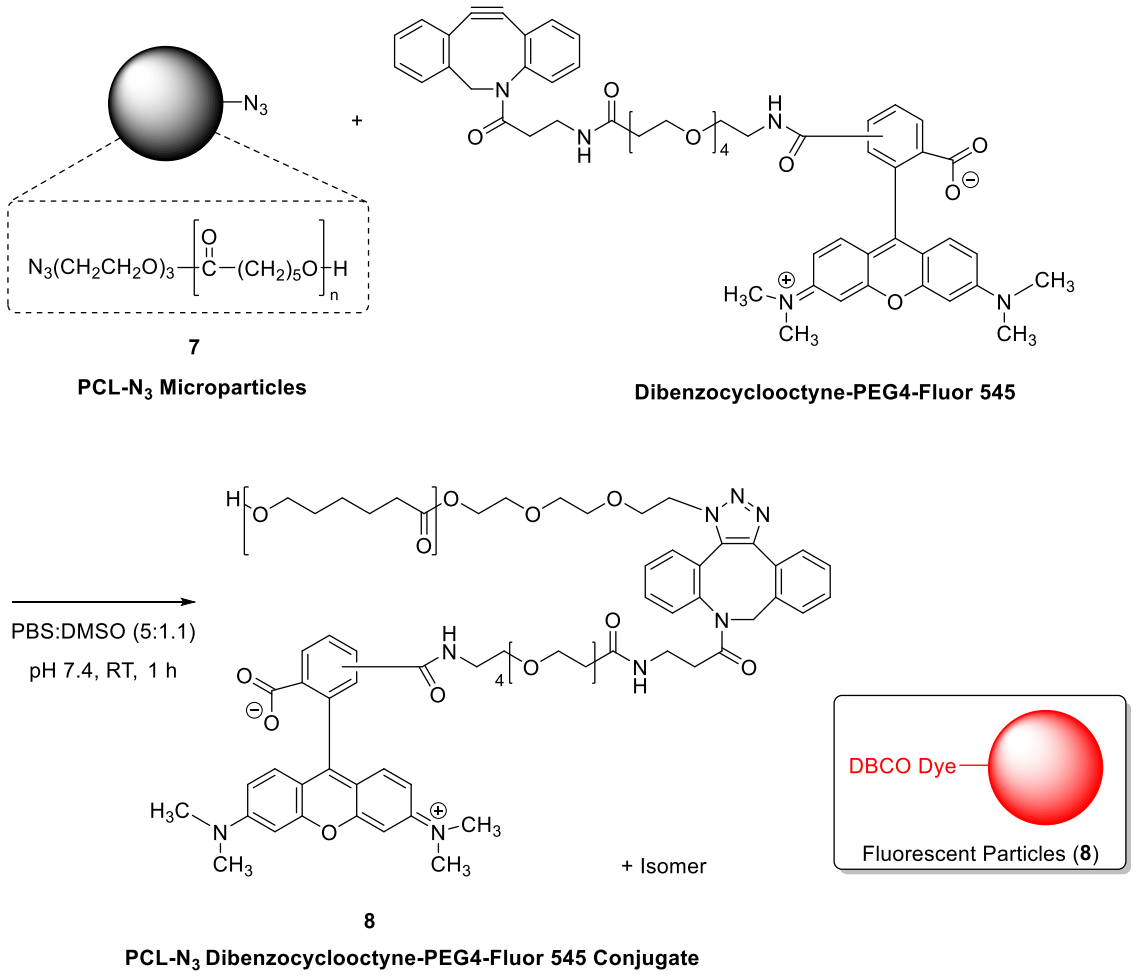

Scheme 11: Conjugation of PCL-N_3 microparticles to DBCO-PEG4-Fluor 545 fluorescent tag.

It was found that PCL-N_3 particles treated with dibenzocyclooctyne-PEG4-Fluor 545 (**8**) showed a statistically significant increase in fluorescence compared to particles produced using commercial PCL. Microparticles produced using commercial PCL had an average fluorescence reading, comparable to the water only control sample, which is negligible and can be considered as background. PCL-N_3 microparticles stained with dibenzocyclooctyne-PEG4-Fluor 545 (**8**) had an obvious colour change, resulting in pink particles that were visible to the naked eye (Figure 28, A) which was not present in commercial PCL control particles (Figure 28, B). PCL-N_3 fluorescence, following treatment with dibenzocyclooctyne-PEG4-Fluor 545, was visualised using a fluorescent microscope to clearly show the fluorescent particles (**8**) (Figure 28, insert).

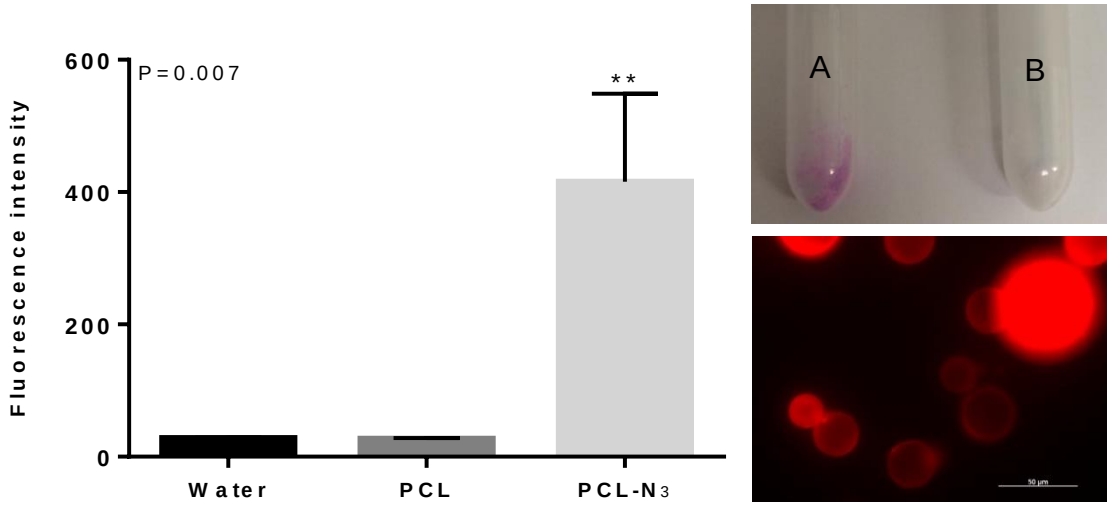

Figure 28: Fluorescence of PCL-N_3 and commercial PCL particles stained with DBCO-PEG4-Fluor 545. Water was used as a control. Inserts show visual effect of DBCO-PEG4-Fluor 545 on PCL-N_3 particles (A) and commercial PCL particles (B) and fluorescent imaging of PCL-N_3 DBCO dyed particles.

Next, optimisation of the reaction between dibenzocyclooctyne-PEG4-Fluor 545 and the PCL-N_3 microparticles was carried out. It was found that with increase in the mole ratio of dibenzocyclooctyne-PEG4-Fluor 545, in relation to the particles (**7**), a detectable increase in fluorescence intensity of compound **8** occurs (Figure 29). Increasing dibenzocyclooctyne-PEG4-Fluor 545 resulted in approximately a five-fold increase in fluorescence intensity at a mole ratio of 1.7:1 when compared to the lowest ratio (0.3:1). Similarly, an increase in the reaction time of dibenzocyclooctyne-PEG4-Fluor 545 with microparticles showed an increase in fluorescence intensity of compound **8** (Figure 29). It was found that when reaction times were increased to 2 hours, a 5-fold increase in fluorescence intensity occurred. This increased to a 10 and 20-fold increase when reaction times were 6 and 48 hours respectively.

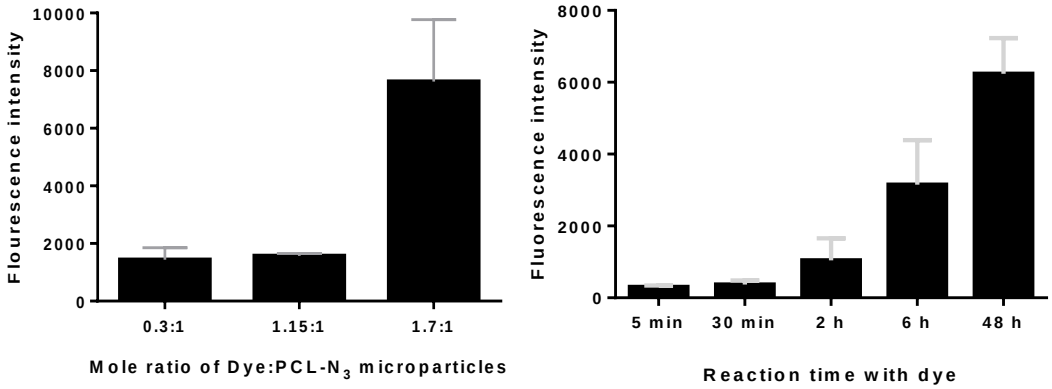

Figure 29: Effect of changing mole ratio of DBCO-PEG4-Fluor 545 (dye) to PCL-N_3 microparticles and reaction time.

2.6. Peptide Synthesis

After it had been shown that the microparticles could readily conjugate to a DBCO linking unit, it was hypothesised that this could be manipulated for the attachment of different bioactive agents. As the ideal microparticle delivery system would be a template for a multitude of therapeutics the synthesis of a cell adhesion peptide was investigated. A small 5 amino acid peptide; GRGDS (glycine-arginine-glycine-aspartic acid-serine) could be produced using solid phase synthesis and modified to contain a DBCO linking unit. The DBCO linking unit would then, in theory, be able to conjugate to the microparticles via the internal alkyne as previously demonstrated, and the peptide could help to facilitate cell adhesion.

In wound repair, adhesion molecules such as integrin and fibronectin are necessary to allow for cell migration and support cell adhesion to the site of repair. Fibronectin specifically can also act as a chemoattractant molecule for migrating cells.[222] The peptide sequence arginine-glycine-aspartic acid (RGD) identified in 1984 by Pierschbacher and Ruoslahti, is a conserved unit throughout many ECM proteins. It is an essential requirement for cell adhesion via integrin proteins, which act as cell surface receptors. Integrin binding to proteins containing the RGD sequence initiates a signalling cascade that can encourage the migration, proliferation and differentiation of cells.[223] The

pentapeptide; GRGDS specifically was chosen as it has previously been shown to promote and increase the adhesion, proliferation and differentiation of human tenocytes.[223]

Using a Wang resin containing an fluorenylmethyloxycarbonyl (FMOC) protected serine, solid phase synthesis was used to produce the GRGDS peptide. This was through the sequential cross coupling of amino acids between the carboxylic acid terminus of one and the amine terminus of the other using 1-[Bis(dimethylamino)methylene]-1H-1,2,3-triazolo[4,5-b]pyridinium 3-oxid hexafluorophosphate (HATU) as a cross-coupler to produce compound **9**. The terminal glycine was then modified to contain a DBCO-acid linking unit via standard cross-coupling techniques to produce compound **10** (Scheme 12). A kaiser test, a colorimetric assay used to determine the presence of free amines, was used between each addition of amino acid, and after the addition of DBCO linker to confirm completeness of the coupling reaction. If free amines are present and the coupling reaction has not gone to completion the Kaiser test solution will be a dark blue/brown colour. If there are no free amines present the solution will remain yellow.

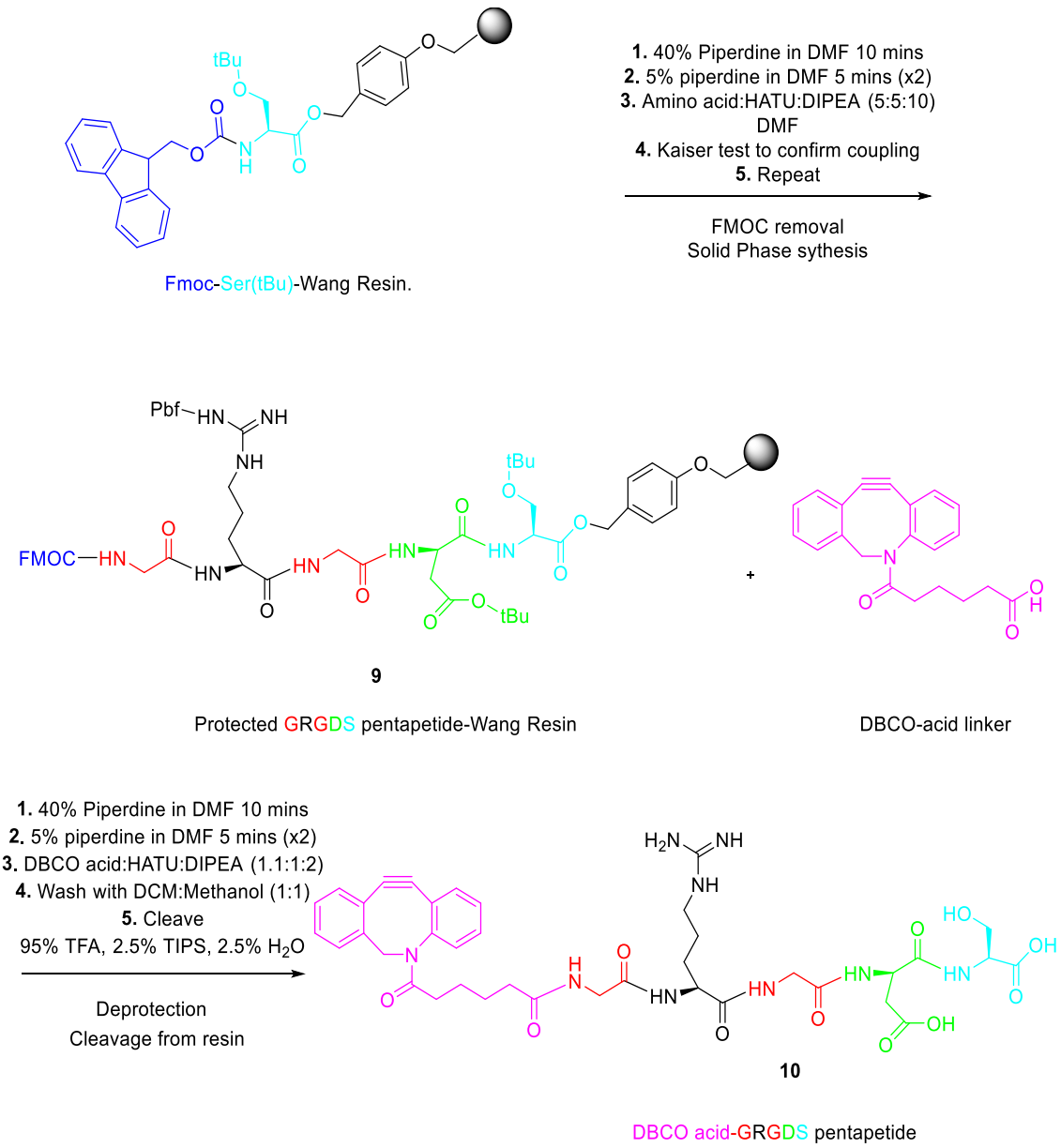

Scheme 12: DBCO acid-GRGDS peptide synthesis. Amino acids are added sequentially using solid phase peptide synthesis. DBCO acid is attached to the terminal glycine residue to produce a DBCO-acid-GRGDS pentapeptide. DIPEA: N,N-Diisopropylethylamine. TFA: Trifluoracetic acid. TIPS: Triisopropylsilane.

After synthesis and cleavage from the resin, the resulting products; compound **10** and control compound **11** were analysed by HPLC to ascertain their purity and to gauge the success of the synthesis. HPLC data showed a single peak for both DBCO-acid-GRGDS (**10**) and FMOC-GRGDS (**11**) at 11.42 minutes (Appendix E, Figure 64 & Figure 65). The percentage purity was estimated to

be 90% and 64% for each compound respectively. Both compounds were sent for mass spectrometry analysis and it was found that the exact mass (M+1) for both was correct with a mw of 806 for DBCO-acid-GRGDS (**10**) and 713 for FMOC-GRGDS (**11**) (Figure 30).

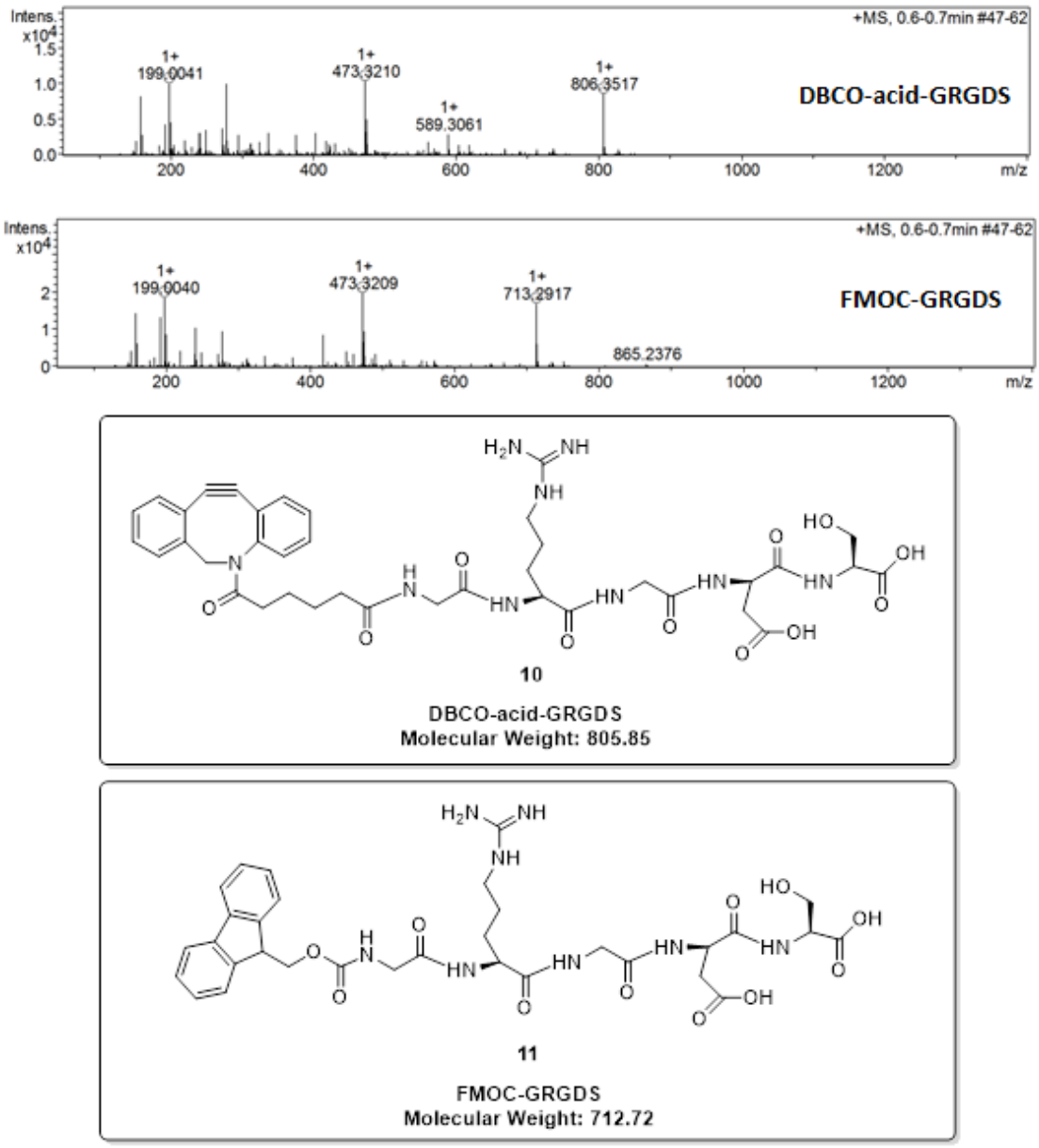

Figure 30: Mass spectrometry analysis of DBCO-GRGDS and FMOC-GRGDS peptide.

With the aim of ultimately using the peptide to carry out a cell adhesion assay, GRGDS peptide with no linker was also synthesised (**12**) (Figure 31). This would allow for a control when comparing adhesion to see if there was a

difference between cells treated with GRGDS peptide alone and cells with DBCO-GRGDS peptide attached to microparticles. Matrix assisted laser desorption/ionisation-time of flight (MALDI-TOF) analysis again showed the successful production of GRGDS peptide with a mw of 490 (Figure 31).

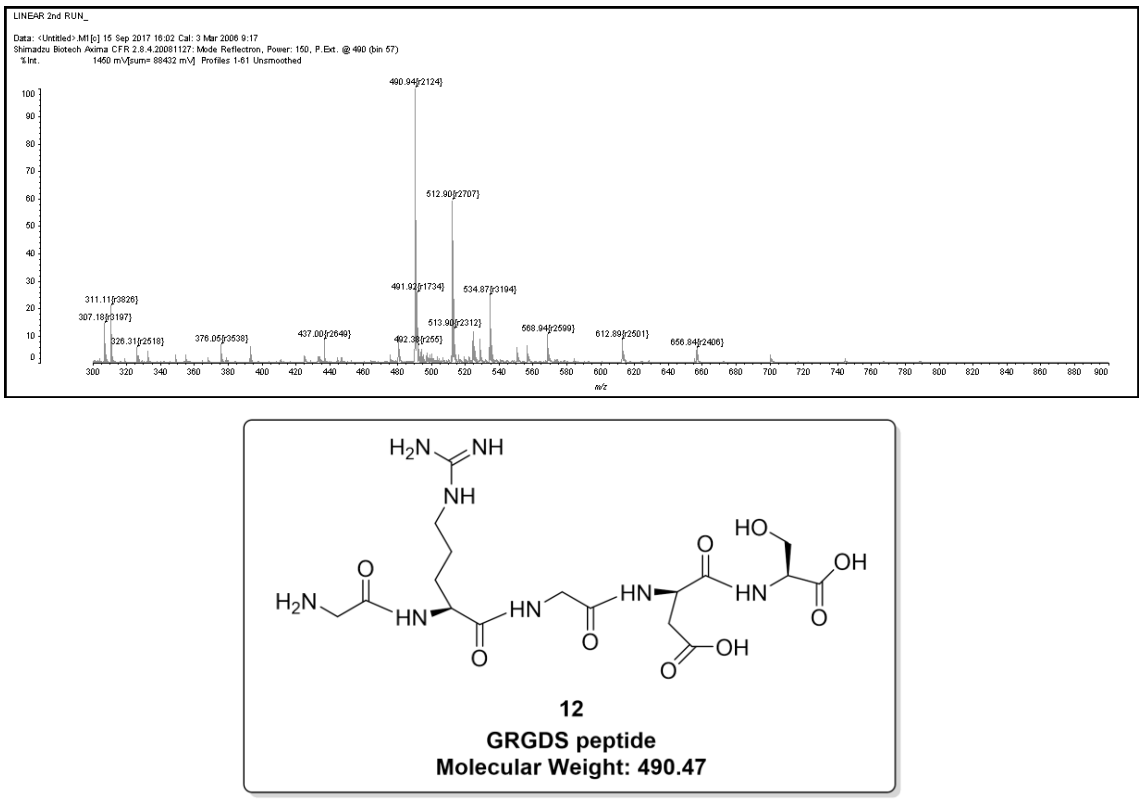

Figure 31: Mass spectrometry analysis of GRGDS peptide

After mass analysis showed all GRGDS peptides (**10, 11 and 12**) on a 100 mg scale had been synthesised successfully, attempts to scale this up to 300 mg were made. However, it was found when repeating the synthesis on a larger scale the results were unreproducible and production of the correct peptide was unsuccessful. Mass spec analysis of the DBCO-acid-GRGDS peptide (**10**) when scaled up, showed a molecular weight of 589 suggesting an unsuccessful synthesis of the compound. HPLC analysis corroborated this data with multiple peaks seen at 13, 17 and 18 min. (Appendix E, Figure 66 & Figure 67). As it was not possible to scale up the synthesis, attempts to purify compounds **10**, **11** and **12** were carried out using preparative HPLC. Fractions were collected at 3.4, 4.8, 14.3 and 16.5 minutes (Appendix E, Figure 68) and MALDI analysis carried out of all products. No peaks corresponding to the correct mw of 805 for

the DBCO-acid-GRGDS product (**10**) were found, and it was not possible to isolate a single product from the fractions (Appendix E, Figure 69-Figure 72). As it was not possible to purify the peptide no further experimentation was carried out to this end.

2.7. Microparticle cytotoxicity

With the final application of a drug delivery system for the regeneration of tendon tissue in mind, it was important that the formulated microparticles did not exhibit toxicity towards cells. In an effort to assess their cytotoxicity PCL-N_3 microparticles (**7**) were analysed using a 3-(4,5-dimethylthiazol-2-yl)-5-(3-carboxymethoxyphenyl)-2-(4-sulfophenyl)-2H-tetrazolium (MTS) assay and compared to microparticles formulated using commercial PCL. Live cells are able to convert the tetrazolium dye into a formazan, which has a strong absorbance at 490 nm and a deep purple colour. If the sample does not contain metabolically active cells, this formazan is not produced and the dye will remain yellow. The formation of formazan, and therefore the absorbance is directly proportional to the number of live cells present within the sample. The following concentrations of PCL and PCL-N_3 microparticles (**7**) were analysed; 30, 330, 630, 930, 1230, 1530, 1830, and 2000 μg/mL. Microparticles at increasing concentrations were incubated with 3T3 fibroblast cells for, 1, 3, 5 and 7 days (Figure 32). Control samples of cells only, treated with MTS was used.

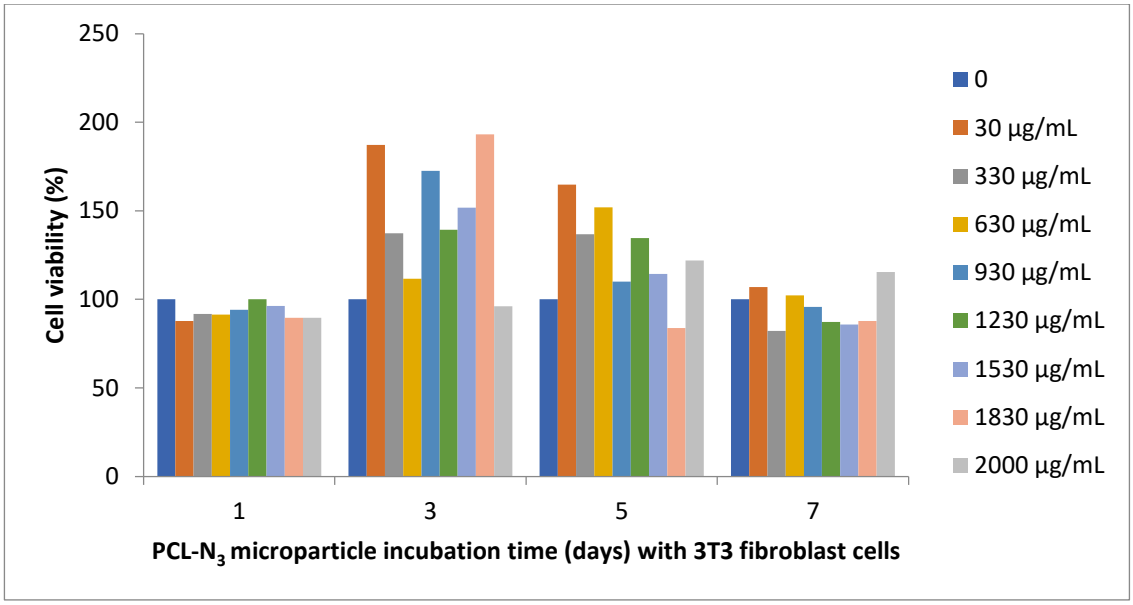

Figure 32: Cytotoxicity analysis of PCL-N_3 microparticles. N=3. Control wells of cells only reacted with MTS assay were taken to be 100% cell viability. All other wells were normalised against these controls.

It was found that PCL-N_3 microparticels (**7**) showed little cytotoxicity to 3T3 cells after 1 day with cell viability remaining >87% for all concentrations. After 3 days, viability of cells treated with PCL-N_3 microparticles was greater than that of untreated controls. This could suggest that PCL-N_3 microparticles results in cell proliferation. However, this trend was not seen consistently in all microparticle concentrations, with both a decrease and increase in cell viability seen across concentrations at days 5 and 7. If microparticles were increasing cell proliferation, linearity between microparticle concentration and increased cell viability would be expected. This trend was not seen however, and instead the results were concluded to be unreliable. Cells treated with PCL microparticles had comparable results (Appendix F, Figure 73). Samples were measured in a plate reader, in a 96 well plate. It was hypothesised that the presence of microparticles within the well plate resulted in interference with the assay and absorbance readings. To test this hypothesis, control samples containing microparticles only and no cells were treated with MTS assay. It was found that these control samples resulted in positive absorbance readings, although no colour change of the dye was observed. In an attempt to remove the potential interference of the microparticles from the assay the experiment was repeated.

After the necessary incubation time of cells with microparticles the media was removed, and the cells were washed multiple times with PBS. It was hypothesised that multiple washings of the cells would remove the particles before addition of the MTS and taking absorbance readings. However, it was found that this resulted in rounding of the cells and their detachment from the tissue culture plastic. Therefore, it was not possible to remove the interference of microparticles from the assay.

Investigations into a cytotoxicity assay that did not rely on absorbance therefore were carried out. Trypan blue is a cell viability staining assay. After cells undergo apoptosis, their membranes become permeable, which trypan blue is able to penetrate. Live cells however, are able to exclude the dye from their membranes. This means that dead cells treated with trypan blue will stain a vivid blue and can be counted using a haemocytometer. PCL-N_3 and PCL microparticles were incubated with adult horse tenocytes at increasing concentrations of 1, 10 and 20 mg/mL.

Trypan blue staining results indicated that PCL-N_3 microparticles (**7**) did not result in increased cell death (Figure 33). The total percentage of dead cells in the control sample was 11%. Percentage dead cells, in all populations treated with PCL-N_3 microparticles remained at or below 11%. Concentrations of 1, 10 and 20 mg/mL microparticle solution resulted in percentage dead cells of 9, 11 and 6% respectively. This suggests that PCL-N_3 microparticles (**7**) were not toxic to these cells.

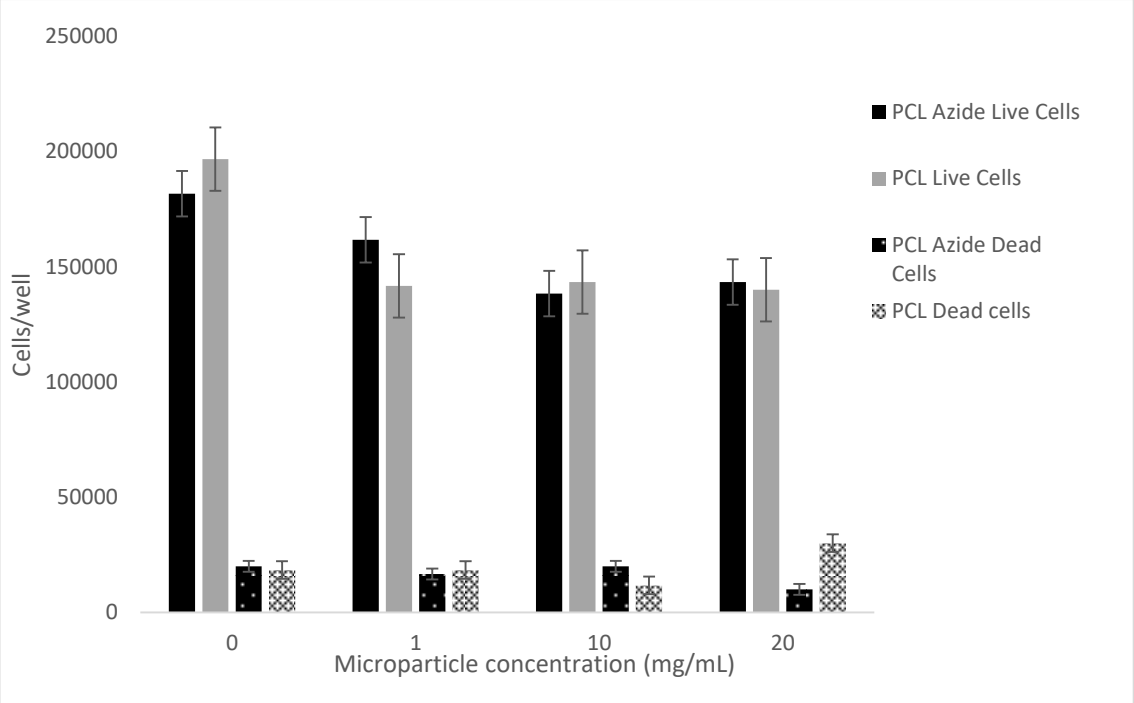

Figure 33: Trypan blue staining of tendon cells treated with PCL and PCL-N_3 microparticles.

3. Conclusion

To summarise, this chapter has shown the successful production of microparticles formulated using PCL-N_3 polymer. It has been shown that particle size can be tightly controlled by altering parameters during the production process such as stir speed and polymer concentration, resulting in particles that had monodispersed size ranges with good morphology. Microparticles contain accessible azide functionality and can undergo the SPAAC click reaction to conjugate to a fluorescent DBCO unit. The success of this model reaction is a promising indicator that these microparticles can be used for the conjugation of biomolecules. The production of these microparticles represents a template drug delivery system which can be taken forward and used for the conjugation of biomolecules to the particles surface using click chemistry and DBCO linkers.

4. Experimental Procedures

4.1. Instrumentation

LDC-1 dispersion cell (Micropore Technologies Ltd, UK) and Aladdin-1000 motorised injection pump (World Precision Instruments Inc, Uk) were used to produce microparticles. Injection rates were kept at the manufacturers recommended value unless otherwise stated (Appendix C, Table 14). RPM values were calculated using manufacturers guidelines. Hydrophilic nickel membranes were supplied from Micropore Technologies with pore sizes of 5, 10 or 15 µm orientated in either a ringed area or throughout the membrane (known as standard membranes). All microparticles were lyophilised and visualised using SEM analysis, mounted on aluminium stubs and coated with gold (Jeol Ltd, Japan). Light microscopy images were taken using Evos XL core microscope (Life Technologies, USA). Image J analysis was carried out to measure particles size. Fluorescent images were taken using an AxioPlan 2ie (Zeiss, Germany). Quantitative fluorescent data was gathered using a CLARIOstar® plate reader (BMG Labtech, UK). A Heraeus™ Megafuge™ 8 bencthop centrifuge (Thermo Fisher Scientific, USA) was used for centrifugation.

4.2. Materials

All materials were from Sigma Aldrich and used as received, unless otherwise stated. Tween® 20, polycaprolactone (Mw ~14,000 M_n, ~10,000 by GPC), sodium hydroxide (≥98%, anhydrous pellets), citric acid (≥99.5%), poly(vinyl alcohol) (89,000-98,000 M_w, 99+% hydrolysed), sodium chloride (≥99.5%), phosphate buffered saline (tablet), trypan blue, dibenzocyclooctyne-PEG4-Fluor 545 (dissolved in DMSO, 2.67 mM), N,N-diisopropylethylamine (≥99%), triisopropylsilane (98%), trifluoroacetic acid (99%), piperidine (99%, dissolved in DMF at a concentration of 40% or 5%), dibenzocylooctyne-acid (95%), potassium cyanide (≥98.0%), ninhydrin (dissolved in ethanol at final concentration of 5%), phenol (≥99.5%, dissolved in methanol to a final concentration of 80%), 2-(7-Aza-1H-benzotriazole-1-yl)-1,1,3,3-

tetramethyluronium hexafluorophosphate (98%, Fluorochem), FMOC-Ser(tBu)-Wang resin (100-200 mesh) (Serine resin, Novabiochem), Fmoc-Arg(Pbf)-OH (Arginine, Novabiochem), Fmoc-Gly-OH (Glycine, Novabiochem), Fmoc-Asp(OtBu)-OH (Aspartic acid, Novabiochem), fetal bovine serum (Filtered prior to use, Thermo Fisher Scientific), Dulbecco's modified eagle medium (DMEM, Thermo Fisher Scientific), penicillin and streptomycin (Pen Strep, 5000 units of penicillin and 5000 μg/mL of streptomycin in 0.85% saline), and L-Glutamine (Thermo Fisher Scientific).

4.3. Microparticle Production

General method

All membranes were calibrated prior to use using Micropore's dispersion cell calibration protocol. A 10% v/v oil in water emulsion of sunflower oil in 2% w/v Tween® 20 was produced and droplets analysed for signs of membrane damage. All membranes were cleaned as per the manufacturer's guidelines in 4 M NaOH and 2% w/v citric acid. All microparticles were produced using the same general procedure of membrane emulsification. Polymer was dissolved in DCM (10 mL) to produce the oil phase and injected using a syringe pump through a porous membrane into distilled water containing PVA as a surfactant (100 mL, filtered) under constant rotation. Once all the oil phase had been injected, particles were collected in a glass beaker and left stirring overnight at 120 rpm to solidify microparticles via solvent evaporation. Solidified particles were collected by centrifugation (5000 RPM, 3 min) and washed thoroughly with water (10 x 50 mL). Particles were lyophilised to yield white powder (typical yields ~50%).

4.3.1. Microparticle Optimisation

For microparticle optimisation tests, microparticles were produced using the general method detailed above with alterations made to one of the following; the oil phase, the water phase, the RPM of continuous phase rotation or the injection rate of the dispersed phase. Table 10 below details the experimental conditions tested for the optimisation of microparticles.

The effect of membrane pore size: Microparticles were produced using the general method detailed above, with 10% commercial PCL in DCM as the oil phase injected into 1% w/v PVA with 13 g/L NaCl, through a ringed membrane with either 10 or 5 µm pore sizes. All tests were carried out in triplicate to ensure reproducibility.

Membrane	Oil	Water	RPM	Rate mL/min
15 µm S	10% PCL	0.3% PVA	779	0.5
15 µm S	10% PCL	1% PVA	779	0.5
15 µm S	10% PCL	1% PVA, 13 g/L NaCl	779	0.5
15 µm S	10% PCL	1% PVA, 40 g/L NaCl	779	0.5
15 µm S	10% PCL	1% PVA, 13 g/L NaCl	1091	0.5
15 µm S	10% PCL	1% PVA, 13 g/L NaCl	779	1
15 µm S	10% PCL	1% PVA, 13 g/L NaCl	779	2.1
15 µm S	15% PCL	1% PVA, 13 g/L NaCl	779	0.5
15 µm S	20% PCL	1% PVA, 13 g/L NaCl	779	0.5
10 µm R	10% PCL	1% PVA, 13 g/L NaCl	779	0.26
5 µm R	10% PCL	1% PVA, 13 g/L NaCl	779	0.07
15 µm R	5% PCL	1% PVA, 13 g/L NaCl	1140	0.7
15 µm R	10% PCL	1% PVA, 13 g/L NaCl	1140	0.7
15 µm R	15% PCL	1% PVA, 13 g/L NaCl	1140	0.7
15 µm R	20% PCL	1% PVA, 13 g/L NaCl	1140	0.7
15 µm R	30% PCL	1% PVA, 13 g/L NaCl	1140	0.7
15 µm R	40% PCL	1% PVA, 13 g/L NaCl	1140	0.7
15 µm R	10% PCL	1% PVA, 13 g/L NaCl	400	0.7
15 µm R	10% PCL	1% PVA, 13 g/L NaCl	559	0.7
15 µm R	10% PCL	1% PVA, 13 g/L NaCl	770	0.7
15 µm R	10% PCL	1% PVA, 13 g/L NaCl	950	0.7
15 µm R	10% PCL	1% PVA, 13 g/L NaCl	1500	0.7

Table 10: Experimental conditions used for microparticle optimisation.

(S= standard membrane. R = ringed membrane.

The effect of stir speed and polymer concentration: Microparticles were produced using the general method detailed above with alterations made to either the concentration of PCL-N_3 (**4**) used as the oil phase, or the stir speed used at injection. For both experiments the oil phase was injected into 1% w/v PVA through a ringed membrane with pore sizes of 15 µm at an injection rate of 0.70 mL/min. For the effect of stir speed, 10% w/v PCL-N_3 (**4**) dissolved in DCM was used as the oil phase and stir speeds of 400, 590, 770, 950, 1140 and 1500 RPM were assessed. For polymer concentration, stir speeds were kept constant at 1140 RPM and PCL-N_3 (**4**) concentrations of 5, 10, 20, 30 and 40% w/v were used as the oil phase.

4.4. Porous Microparticles (6)

Porous microparticles were produced via double emulsion technique. First a primary emulsion of an internal water phase containing PVA (1 or 3% w/v) and NaCl (13 or 40 g/L) was emulsified by sonication with the oil phase containing 15% w/v commercial poly(caprolactone). The primary emulsion was then used as the dispersed phase for membrane emulsification. The emulsion was injected through a ringed membrane (40 μm) at an injection rate of 2.5 mL/min, stirring at 600 RPM into the external water phase (1% w/v PVA, 13 g/L NaCl). Once injection had been sufficient to produce a 10% v/v emulsion, droplets were collected and added to 1% w/v PVA solution at a ratio of 1:10 and left overnight stirring at 120 RPM to solidify microparticles via solvent evaporation. Solid particles were collected by centrifugation (3000 RPM, 3 min) and salt leaching was carried out via multiple aqueous washings (10 x 50 mL). Particles were lyophilised to yield compound **6** as a white powder (typical yields ~10%). Microparticle size, and pore diameter was evaluated using Image J software.

PBS was evaluated as a porogen. First a primary emulsion of 1x PBS (1 mL) was emulsified by homogenisation (9000 RPM, 2 min) with the oil phase containing 20% w/v commercial poly(caprolactone). The primary emulsion was then used as the dispersed phase for membrane emulsification. The emulsion was injected through a ringed membrane (40 μm) at an injection rate of 2.5 mL/min stirring at 779 RPM into the external water phase (0.3% w/v PVA). The solution was left overnight stirring at 120 RPM to solidify microparticles via solvent evaporation. Solid particles were collected by centrifugation (3000 RPM, 3 min) and washed (10 x 50 mL). Particles were lyophilised to yield a white powder.

4.5. Assessing Polymer Viscosity

The viscosity of commercial PCL and PCL-N_3 (**4**) was tested using a Rheotex U-tube viscometer. The viscosity of DCM, sunflower oil and water were used as controls. Concentrations of 1-20% w/v PCL or PCL-N_3 dissolved in DCM were produced. The amount of time taken for the liquid to flow through the viscometer was recorded and the following equation used to calculate viscosity.

$$Viscosity\ (m^2/s) = C\ x\ T$$

Where C = Constant for the specific viscometer used and T = Time in seconds.

The viscometer was cleaned thoroughly between each reading, and all concentrations were read in triplicate and an average time taken to record viscosity.

4.6. Fluorescence Staining of Polycaprolactone-Azide Particles (8)

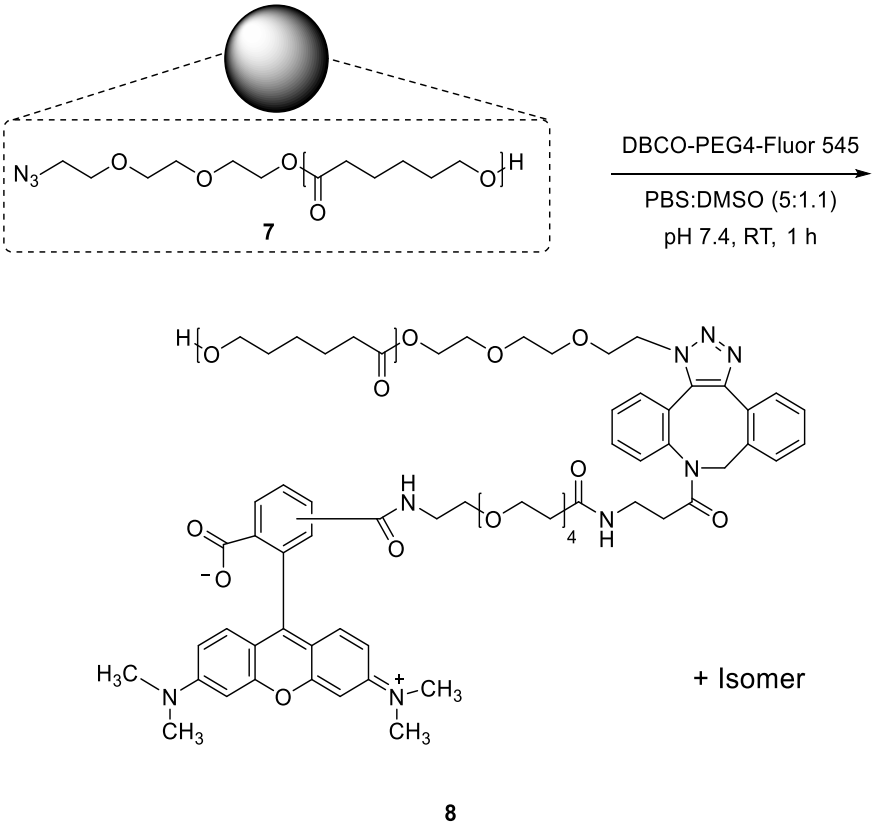

General formula: $N_8C_{63}H_{80}O_{13}(C_6H_{10}O_2)_n$

Molecular Weight: ~23,936.

PCL-N_3 microparticles (**7**) (10 mg, 0.51 nmol, 1eq) were suspended in PBS (1 mL, pH 7.4). 2.6 mM Dibenzocyclooctyne-PEG4-Fluor 545 (220 µL, 0.59 nmol, 1.15eq) was added and the solution was left to stir for 1 h at 200 rpm. The reaction was carried out in triplicate. The suspension was filtered via vacuum filtration through an organic membrane. The resulting particles (**8**) were washed thoroughly with water (10x50 mL) and lyophilised.

For fluorescence data, particles (**8**) were suspended in DMSO to a final concentration of 1 mg/mL and heated to fully dissolve. Particle solution (300 µL) was used for fluorescence spectroscopy (567 nm). Samples of water washes from particles were also taken and measured in triplicate to ensure no further dye leaching was evident. Samples of particles suspended in water were taken for fluorescence microscopy.

4.6.1. Optimisation

To optimise the conjugation of the dye, microparticles (**8**) were prepared using dibenzocyclooctyne-PEG4-Fluor 545 as previously described, stirring at 200 RPM and with reaction times altered to; 5, 30 min, 2, 6 or 48 h.

The effect of mole ratio of PCL-N_3 to dibenzocyclooctyne-PEG4-Fluor 545 was assessed. PCL-N_3 microparticles (**7**) (10 mg, 0.51 nmol) were suspended in PBS (1 mL, pH 7.4) and dibenzocyclooctyne-PEG4-Fluor 545 was added at either 55 μL (0.15 nmol, 0.3 eq), 220 μL (0.59 nmol, 1.15 eq) or 330 μL (0.88 nmol, 1.7 eq). The solution was left to stir for 1 h at 200 rpm.

4.7. Synthesis of GRGDS Peptide (9, 10, 11 & 12)

4.7.1. Protected GRGDS Peptide-Wang Resin (9)

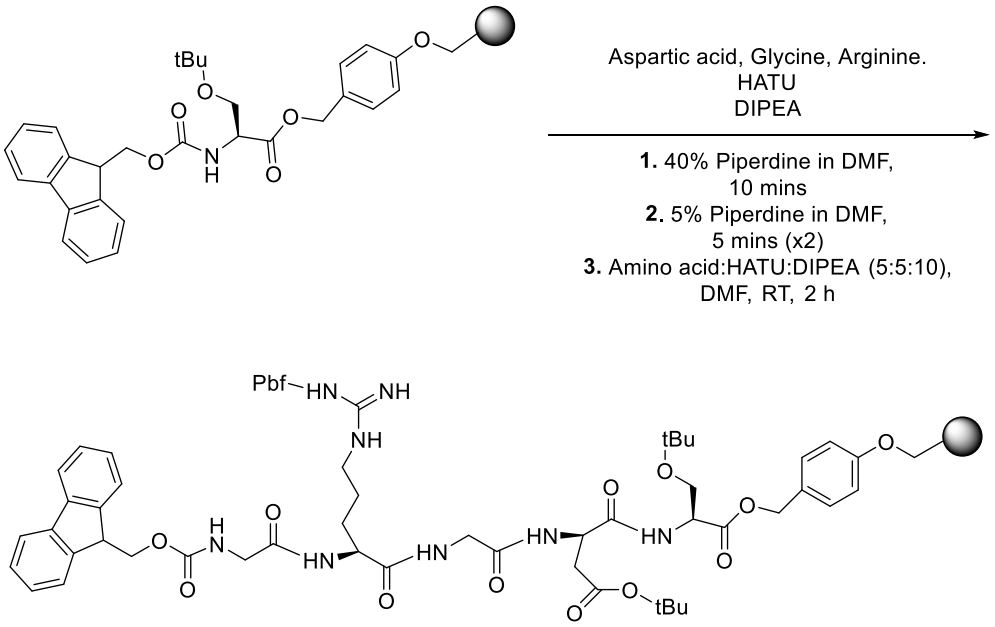

9

FMOC-Ser(tBu)-Wang resin (102.3 mg, 0.064 mmol, 1eq) was swelled whilst shaking with DCM (10 mL) for 30 min and then DMF (10 mL) for 30 min. Removal of FMOC protecting groups was with 40% piperidine in DMF (4 mL) for 10 min, 5% piperidine in DMF (2x4 mL) for 5 min whilst shaking, and then washed with DMF (6x10 mL). Aspartic acid (133.2 mg, 0.32 mol, 5eq) and HATU (122.2 mg, 0.32 mol, 5eq) were dissolved in DMF (2 mL) and left to activate for 2 min. DIPEA (111 µL, 0.64 mol, 10eq) was added and the amino acid and cross coupling solution was added to the peptide column to react whilst shaking for 2 h. The peptide was then washed with DMF (6x10 mL) and DCM (6x10 mL). A small sample of the peptide was taken and one drop of each solution of 0.001 M 2% potassium cyanide, 80% phenol in methanol, and 5% ninhydrin in ethanol was added and the solution boiled to carry out a Kaiser test, a brown colour confirmed the absence of primary amines. All steps were repeated for the sequential addition of the remaining amino acids; Glycine (95.1 mg, 0.32 mol, 5eq), Arginine (208.9 mg, 0.32 mol, 5eq) and Glycine (128 mg, 0.32 mol, 5eq) to produce compound **9** (93 mg, 55%)

4.7.2. GRGDS-Dibenzocyclooctyne Acid Pentapeptide (10)

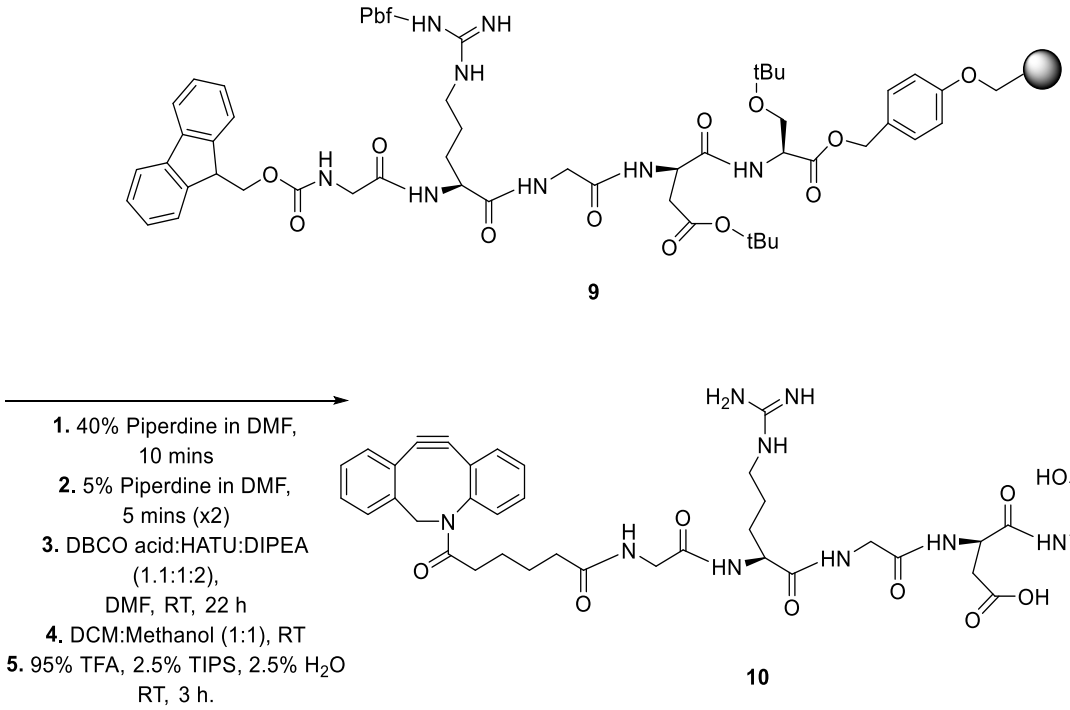

General Formula: $C_{38}H_{47}N_9O_{11}$

Molecular Weight: 805.35

A small portion of **9** (24.2 mg, 0.016 mmol, 1eq) was taken for the addition of DBCO acid. Removal of FMOC protecting groups was done with 40% piperidine in DMF (4 mL) for 10 min, 5% piperidine in DMF (2x4 mL) for 5 min whilst shaking, and then washed with DMF (6x10 mL). DBCO acid (5.9 mg, 0.0176 mmol, 1.1 eq) and HATU (6.8 mg, 0.0176 mmol, 1eq) were dissolved in DMF (500 µL) and left to activate for 2 min. DIPEA (7 µL, 0.032 mmol, 2eq) was added and the DBCO acid and cross coupling solution was added to the peptide column to react whilst shaking for 22 h. The peptide was then washed with DMF (6x10 mL) and DCM (6x10 mL) and a Kaiser test performed. The peptide was washed with methanol and DCM (1:1, 6x10 mL) and desiccated overnight. A cleavage cocktail (3 mL) of 95% TFA, 2.5% H_2O and 2.5% TIPS was added to the peptide column and left for 3 h whilst shaking. Peptide was washed with TFA (3x2 mL) the solvent was removed by rotatory evaporation and the peptide was precipitated with cold ether to yield compound **10**.

4.7.3. GRGDS- Fluorenylmethyloxycarbonyl Pentapeptide (11)

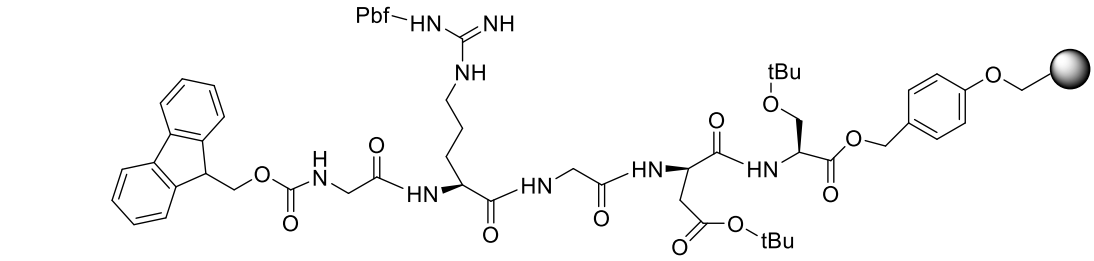

9

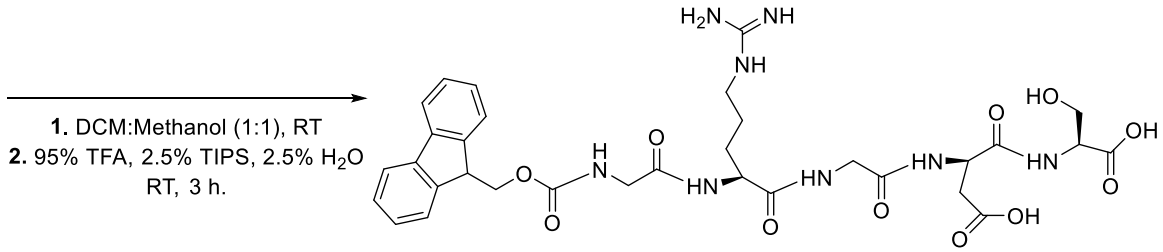

11

General Formula: $C_{32}H_{40}N_8O_{11}$

Molecular Weight: 712.29

A small portion of compound **9** was washed with methanol and DCM (1:1, 6x10 mL) and desiccated overnight. A cleavage cocktail (3 mL) of 95% TFA, 2.5% H_2O and 2.5% TIPS was added to the peptide column and left for 3 h whilst shaking. Peptide was washed with TFA (3x2 mL) the solvent was removed by rotatory evaporation and the peptide was precipitated with cold ether to yield compound **11**.

4.7.4. GRGDS Pentapeptide (12)

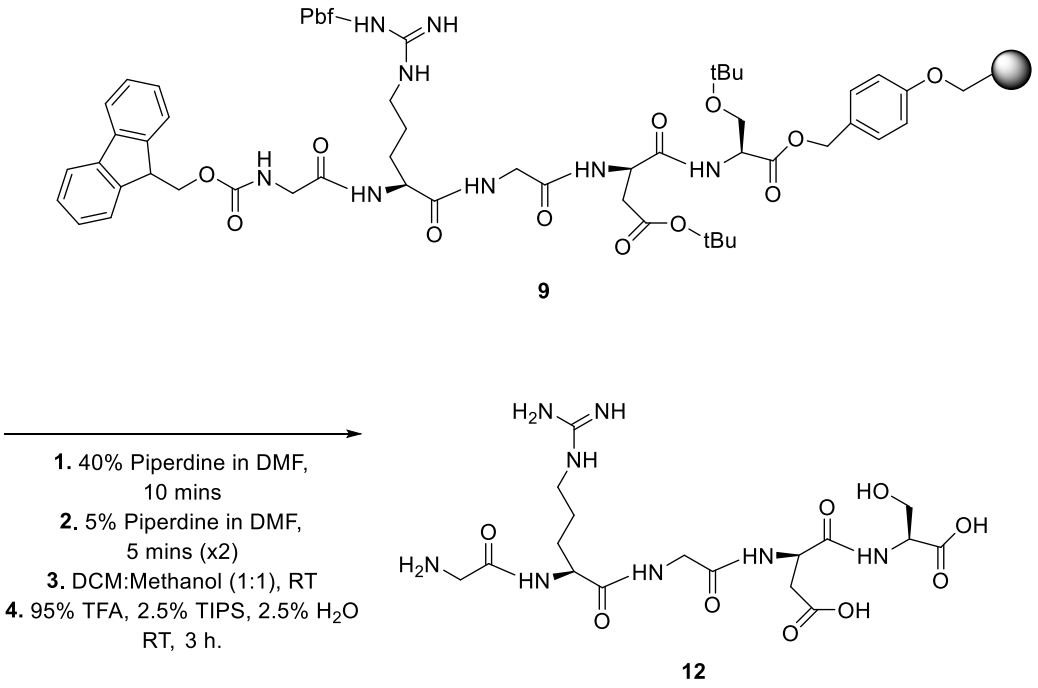

General Formula: $C_{17}H_{30}N_8O_9$

Molecular Weight: 490.47

Removal of FMOC protecting groups from a small portion of compound **9** was done with 40% piperidine in DMF (4 mL) for 10 min, 5% piperidine in DMF (2x4 mL) for 5 min whilst shaking, and then washed with DMF (6x10 mL). The peptide was washed with methanol and DCM (1:1, 6x10 mL) and desiccated overnight. A cleavage cocktail (3 mL) of 95% TFA, 2.5% H_2O and 2.5% TIPS was added to the peptide column and left for 3 h whilst shaking. Peptide was washed with TFA (3x2 mL) the solvent was removed by rotatory evaporation and the peptide was precipitated with cold ether to yield compound **12**.

4.7.5. Peptide Analysis

GRGDS peptide (**10**, **11** or **12**) were dissolved in HPLC grade methanol (400 μL) at a final concentration of 1 mg/mL and filtered through a 0.45 μM syringe filter. Analytical RP-HPLC was carried out on an Agilent 2000 (Agilent Technologies, USA) using an eclipse XDB-C18 column (Agilent Technologies, USA), 4.6x100 mm, 3.5 μM with a flow rate of 1 mL/min. Solvent A was; 95% H_2O with 0.05% TFA. Solvent B was 95% methanol with 0.05% TFA. Solvent B was increased to 95% over 15 minutes, then held at 95% for 5 minutes. Detection was carried out at 214 nm and 254 nm.

Mass analysis of compound was carried out either by Dr Nora Francini at the Boots science building in Nottingham in ESI positive mode or by MALDI-TOF analysis using an analytical Axima MALDI-TOF (Kratos analytical, Uk) in positive reflectron mode. Sinipinic acid in 50% ACN with 0.03% TFA was used as the matrix.

4.8. Cytotoxicity of Polycaprolactone-Azide Microparticles

Adult horse tenocytes (passage 18) were cultured in Dulbecco's modified eagle medium (DMEM) supplemented with foetal bovine serum, glutamine, penicillin and streptomycin (Penstrep). At 50% confluency, cells were seeded in a 96 well plate at a density of 15,000 cells per well and left for 12 h to adhere. Polycaprolactone azide particles (**7**) and polycaprolactone particles (1, 10 and 20 mg) were sterilised by ultra violet light for 12 h. After sterilisation, particles were suspended in media (1 mL) to final concentrations of 1, 10 and 20 mg/mL. After cells had adhered to the well plate, the media was removed, and replaced with 1 mL of particle solution to each well. Cells were incubated with the particle solution for 24 h at 37°C. After incubation, the media was aspirated from cells, and they were washed with PBS (6x1 mL). Cells were treated with a trypsin solution (200 μL) removed from the well plate and diluted in fresh media (800 μL). A sample from each well (10 μL) was taken and mixed at a ratio of 1:1 with trypan blue dye. 10 μL of this solution was taken for cell counting using a haemocytometer. All samples were carried out in triplicate. Three wells containing only cells and no particle solution treated in the same way were used as a control.

Chapter 4: Protein Conjugation

1. Introduction

As discussed previously, a multitude of proteins and growth factors are upregulated during the regeneration of tendon tissue. In order to validate microparticles as a drug delivery system it was important to choose a therapeutic protein of interest with which conjugation attempts could be investigated. Attentions were turned towards proteins from the superfamily; transforming growth factor-βeta (TGF-β). TGF-β has been shown to be upregulated in the inflammatory response and repair of tendon tissue.[20] Of particular interest was its critical role in the differentiation of tendon tissue in embryonic development.[2,22] The healing process in adult tendons is reparative, characterised by increased collagen III and disorganised matrix. Conversely, foetal tendon healing is regenerative, after which the healed tissue is identical to the original tissue.[35] Therefore, it was hypothesised that the incorporation of TGF-β proteins within the microparticle drug delivery system would result in regeneration of the targeted tissue.

1.1. Transforming Growth Factor-β for the Regeneration of Tendon Tissue

The TGF-β superfamily includes many growth and differentiation factors, including bone morphogenetic proteins, which regulate cell proliferation, differentiation, and overall homeostasis of tissues.[28,68] If TGF-β signalling is knocked out in mice, the resulting mutants are not able to form tendon tissue, highlighting its importance for tendon development.[2] After tendon injury, TGF-β is significantly increased and is active in the remodelling of the tissue.[28] In the inflammatory phase of healing, release of TGF-β stimulates the synthesis of collagen, inhibits the action of matrix metalloproteinase, aids the production of fibronectin and proteoglycans, and thus facilitates the remodelling of the extracellular matrix.[29,58,60,224] Currently three isoforms, TGF-β1, TGF-β2 and TGF-β3 have been identified in the repair process of tendon injury, each exerting a different regulatory role in tissue development and growth.[20] When cultured with tendon fibroblasts, all TGF-β isoforms were able to increase the production of collagen type I.[29]

TGF-β1 is highly upregulated during the healing process of adult tendon tissue, with it being expressed in the early stages of tendon healing, with a peak at fourteen days, which decreases after the first two months.[20,42] It is released from platelets and exogenous macrophages during the inflammatory phase of repair and it is necessary for a multitude of biological processes.[33,58,60] TGF-β1 has been implicated in cellular migration, proliferation and apoptosis, as well as being involved in the deposition of extracellular matrix.[20,68] It is able to regulate the action of matrix metalloproteinase and the production of matrix proteins, and collagens.[60,224] Application of TGF-β1 to regenerating patellar tendon resulted in an increase in the tissues tensile strength, improving its mechanical properties after damage.[225]

TGF-β3 is the predominant isoform upregulated during the embryonic development of tendon tissue.[33,42] When TGF-β3 was delivered to the repair site of tendon-to-bone insertions of rats, cell proliferation, vascularity and an accelerated healing process were observed.[35] TGF-β3 application in tendon repair has been shown to significantly increase biomechanical and structural properties of the tendon, leading to a better quality tissue when compared to controls.[35,224] When tested in a rat tendon healing model, TGF-β3 resulted in an increased expression of collagen types I and III, with evidence of matrix remodelling.[29]

Unfortunately, controversy still exists regarding the potential of TGF-β as a regenerative molecule. It has been shown that significant interaction occurs between the three isoforms, with TGF-β1 having the ability to inhibit the action of TGF-β2 and TGF-β3.[29] If all three isoforms are delivered simultaneously, the resulting tendon exhibits excessive scar formation and reduced mechanical strength.[29,42] Further investigations into each isoform as an individual entity still needs to be done before its potential in clinical settings will become more apparent[29,42]

1.2. Dibenzocyclooctyne Linkers for Protein Conjugation

As previously discussed (chapter 2) the chosen method of conjugation to the microparticles was using the strain-promoted azide-alkyne cycloaddition (SPAAC), utilising a dibenzocyclooctyne (DBCO) unit. DBCO molecules are a set of bifunctional cross-linkers that contain two different reactive groups, one of which is a strained internal alkyne. The second functional group can be specifically chosen to allow for conjugation to a protein from a vast array of commercially available products (Figure 34). Therefore, the protein can be directly conjugated to microparticles with the DBCO unit acting as a crosslinking spacer arm. Each linker molecule can be tailored to conjugate to a specific group within the protein by choosing a specific functional group on the linker. DBCO units can be purchased with or without a poly(ethylene) glycol (PEG) spacer arm depending on the desired level of hydrophilicity of the particles after conjugation. The more repeat units that are incorporated, the higher the degree of the hydrophilicity imparted and the increased likelihood of the conjugate to be located on the surface of the microparticle.[145]

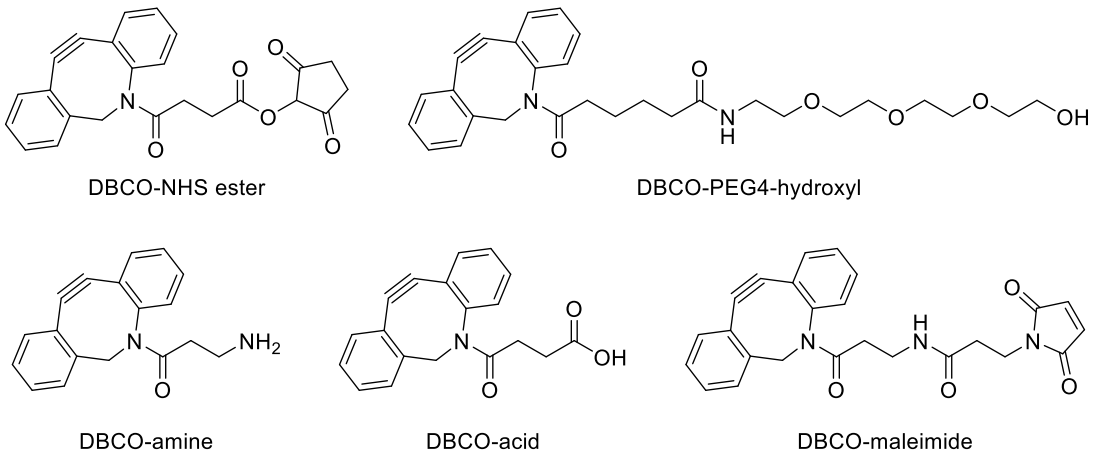

Figure 34: Examples of commercially available DBCO molecules.

To be able to successfully conjugate a protein of interest to PCL-N_3 microparticles it is important to understand the functional groups available within proteins. Identification of appropriate functional groups abundant on the surface of the protein, can allow for conjugation without the need to sacrifice the biological activity of the protein.[226]

1.3. Functional Groups Present in Proteins for DBCO Conjugation

Of the twenty natural amino acids used as the building blocks for proteins, only nine are chemically active for conjugation (Figure 35). These active amino acids are; arginine, histidine, methionine, tryptophan, cysteine, tyrosine, lysine, glutamic acid and aspartic acid.[226] The most commonly used of these for the conjugation to proteins are cysteine and lysine, with connections being made through reactions with the thiol and amino groups respectively.

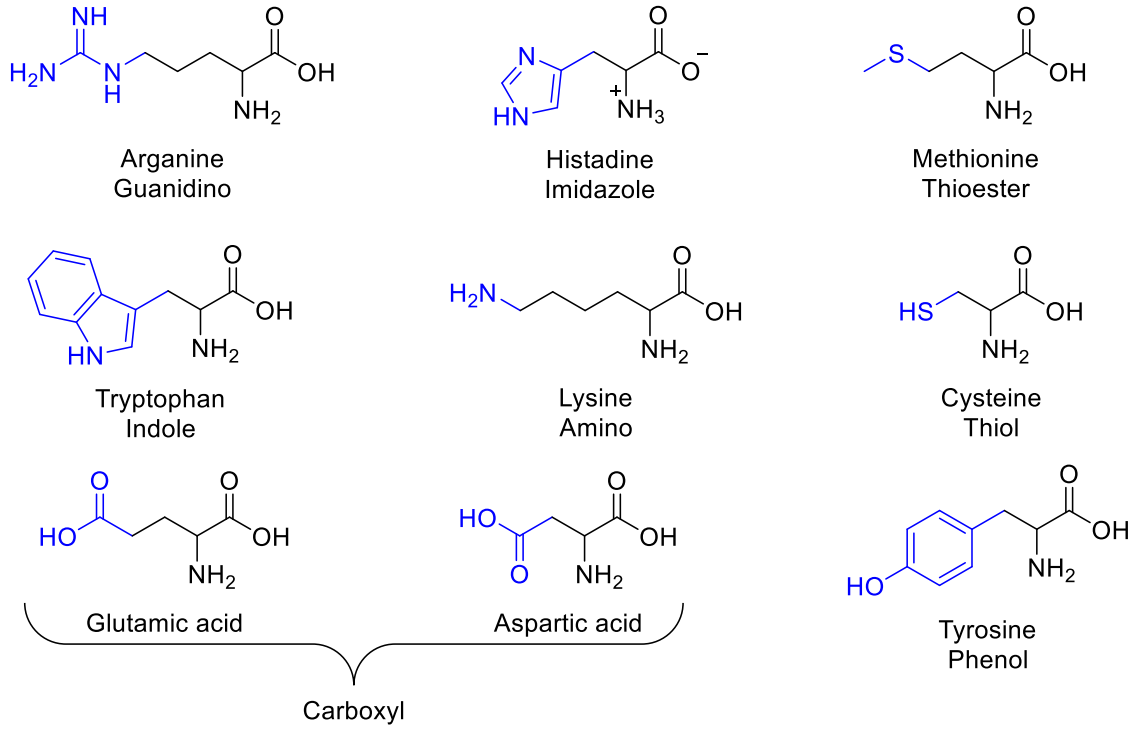

Figure 35: Functional groups available on common amino acids. The available functional group highlighted in blue for each amino acid can be target for the conjugation of proteins.

Primary amines are the most commonly used functional groups for protein conjugation.[161] They are abundant in proteins, found in the N-terminus and on amino acid side chains.[227] Primary amines are likely found on the surface of the protein and are therefore readily accessible.[145] As primary amines are predominately found on the proteins surface, conjugation to them does not tend to result In denaturation of the protein and conjugation via primary amines can be applied to nearly all proteins and peptides.[161] N-hydroxysuccinimide (NHS)

esters are commonly used for conjugation to primary amines, the reaction proceeds in alkaline conditions (pH 7-8) and results in the formation of a stable amide bond. Upon reaction with a primary amine, the NHS leaving group is released (**Scheme 13**), which is easily removed through dialysis.[145] Hydrolysis of the NHS ester can also occur, and this increases with pH of the reaction buffer. This is a competing reaction to the cross coupling with primary amines and therefore decreases the efficiency of protein conjugation.

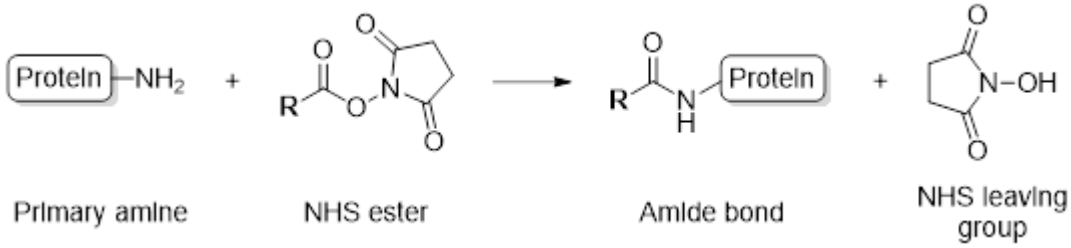

Scheme 13: Reaction scheme for the use of NHS esters for the conjugation of proteins. Primary amines present in the protein can conjugate with NHS resulting in a stable amide bond.

Free cysteines have a thiol functional group which can be used for conjugation. However, free cysteines are rare as they are necessary for disulphide bonding to maintain the quaternary structure of the protein, and join multiple polypeptide subunits.[104,228] Therefore to obtain a free thiol prior to conjugation cysteines must first be reduced, which can often have detrimental effects to the function of the protein. Another limitation to the conjugation of proteins via cysteines is the relatively hydrophobic nature of these amino acids means they predominate within the protein core and are therefore rarely accessible. However, if thiols are present, or can be reduced prior to conjugation, the reaction can be carried out in neutral conditions (pH 6-7.5) using water as the solvent.[145] Maleimide functional groups are reactive towards thiols and result in the formation of stable thioether linkages (Scheme 14).

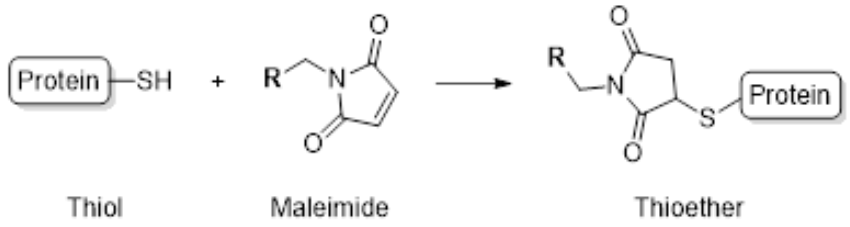

Scheme 14: Reaction scheme for the use of maleimide for the conjugation of proteins. Free thiol groups present in the protein can conjugate with maleimide functional group resulting in a stable thioether bond.

1.4. Aims and Objectives

The hypothesis of the work carried out in this chapter is that protein could be conjugated to previously formulated PCL-N_3 microparticles. The conjugation should be able to occur by utilising a bifunctional linker containing a DBCO unit. The best method of conjugation to the DBCO unit needed to be identified. It was necessary to assess if the conjugation reaction could occur between a model protein and the DBCO unit. If this reaction was successful endeavours to conjugate a therapeutic TGF-β protein could then be attempted.

2. Results and Discussion

2.1. Human Serum Albumin Conjugation to Polycaprolactone-Azide Microparticles

Whilst working on the DBCO conjugation to the azide polymer and microparticles (Chapter 2 section 2.3 and Chapter 3 section 2.5 respectively), parallel experiments were carried out to assess the feasibility of protein conjugation. Investigations began into the ‘proof of concept’ of conjugating a human serum albumin (HSA) protein to a DBCO-PEG4-maleimide (DBCO-mal) linker. HSA is an abundant protein that is commercially available at low cost. It is known to contain a free cysteine at residue 34 of its quaternary structure.[229] Therefore, this protein can be used as a model, to test the conjugation of DBCO-mal.[195,230] The first step in achieving this was to conjugate the HSA protein to a DBCO-mal linker, which could then in turn be attached to the azide

group of PCL-N_3 microparticles using click chemistry (**14**) (Scheme 15). Native HSA purchased from Sigma Aldrich was fully biochemically and biophysically characterised prior to conjugation using liquid chromatography mass spec (LC-MS), high performance liquid chromatography (HPLC), and matrix assisted laser desorption/ionisation-time of flight. (MALDI-TOF) (Appendix G, Figure 74-Figure 76).

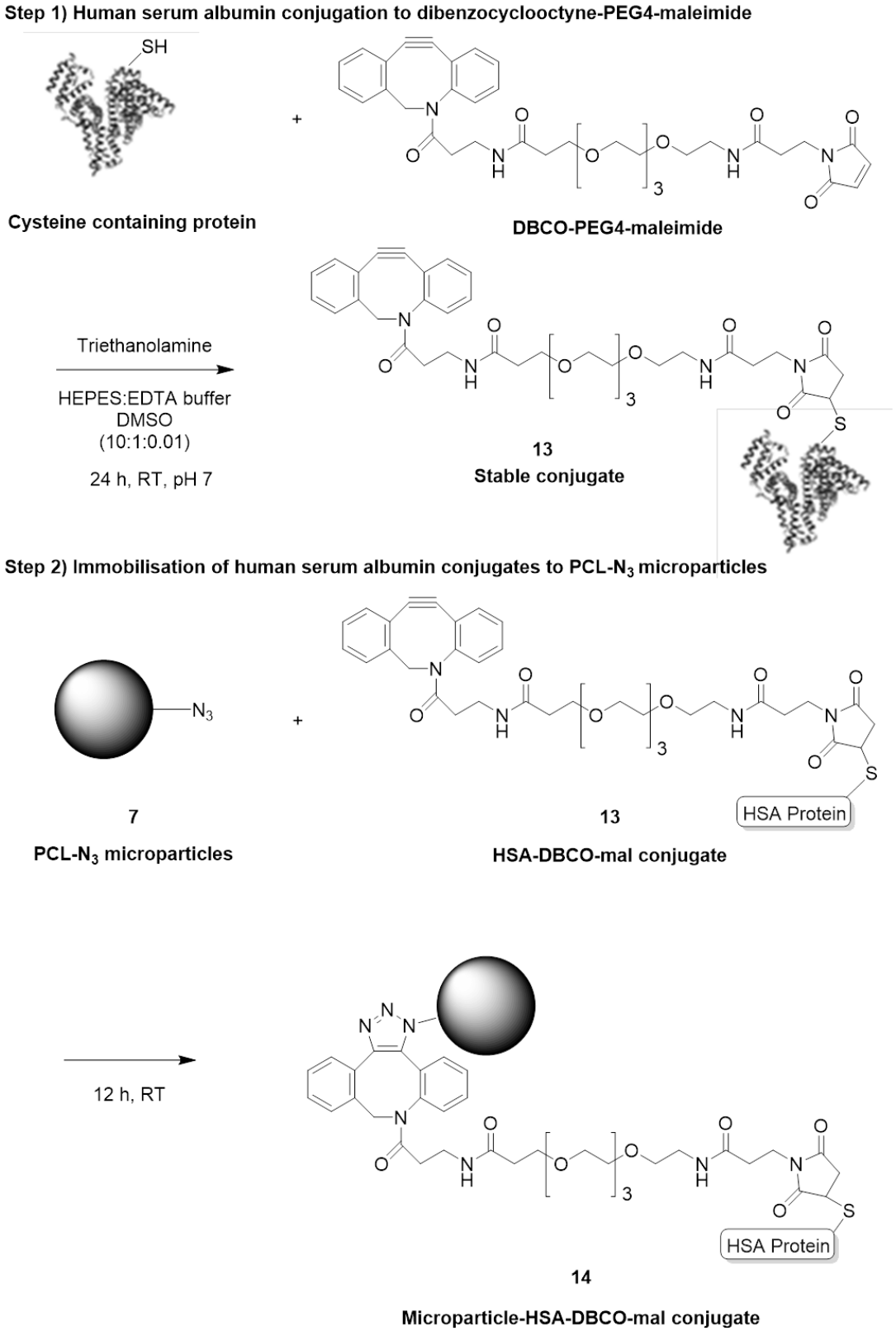

Scheme 15: Conjugation of HSA to PCL-N_3 microparticles. HSA (PDB ID:2BX8)[260] can be conjugated to dibenzoclyooctyne-PEG4-malemide via the free cysteine at residue 34 (Step 1) and subsequently to the azide group on the PCL-N_3 microparticles via click chemistry (Step 2)

2.1.1. Human Serum Albumin-Dibenzocyclooctyne-PEG4-Maleimide Conjugation

The first experiment to carry out was the conjugation of HSA to DBCO-mal (**13**), as detailed in reaction Scheme 15, Step 1. DBCO-mal was added to HSA samples with increasing concentrations of triethanolamine (TEOA, 40 and 400 mM). Initially, HPLC was the chosen method to assess the success of the conjugation reaction. Native HSA and DBCO-mal control samples showed clear, separate elution profiles, with HSA eluting at 11.5 minutes and DBCO-mal eluting at 10.9 minutes (Figure 36). In theory if the conjugation reaction is successful the new species (**13**) would ideally elute with its own unique retention time. However, it was found that retention of HSA conjugated to DBCO-mal (**13**) was comparable to native HSA with elution times of 11.7, 11.6 and 11.6 for 4, 400 and 0 mM TEOA respectively (Figure 36). Therefore, this technique was not suitable for determining if the reaction had been successful and as a result, other techniques for analysis were investigated.

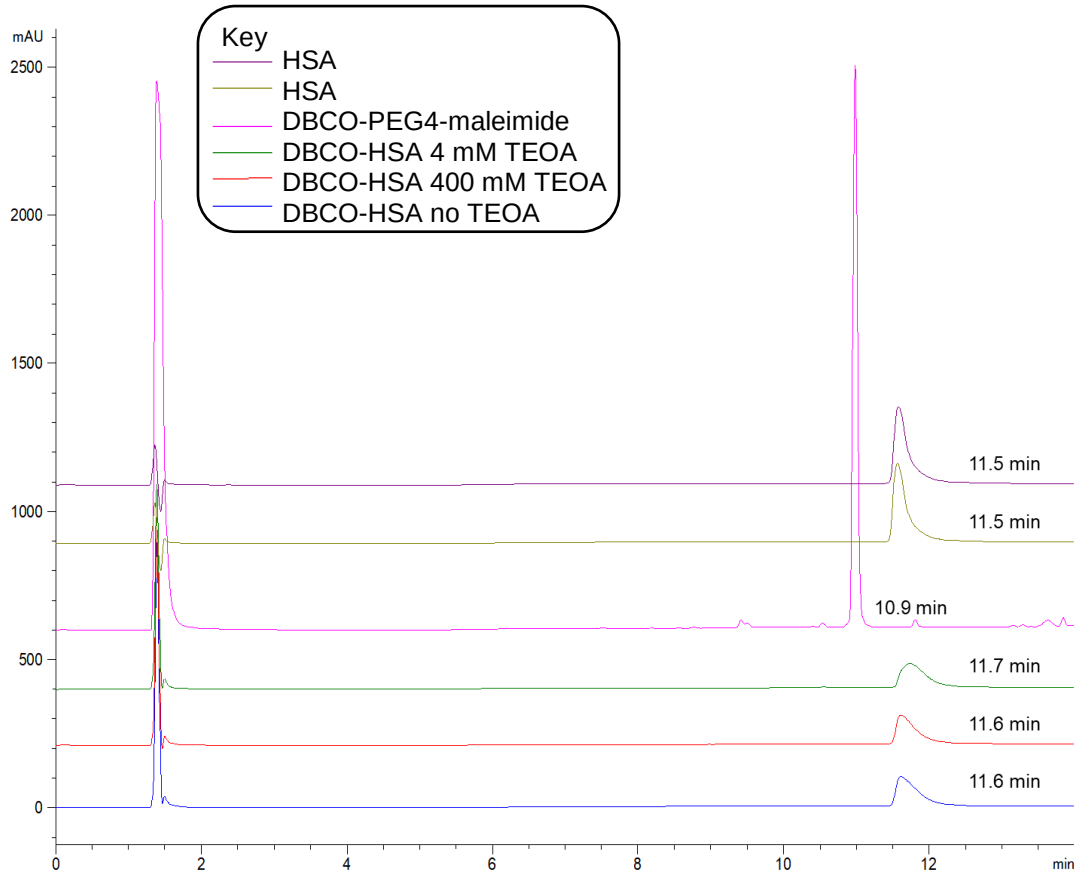

Figure 36: HPLC analysis of HSA conjugated to DBCO-PEG4-maleimide with and without triethanolamine. Elution times for each sample are indicated.

The conjugation of DBCO-mal to HSA relies on the thiol-maleimide chemistry between the free thiol present on residue 34 of the protein. It was therefore possible that an Ellman's assay could be used to determine the success of the conjugation reaction as Ellman's reagent can be used for the quantification of free thiol groups present within a sample. The main compound of the reagent, 5,5'-dithio-bis-(2-nitrobenzoic acid) (DTNB) contains a disulphide bond between the two 5-sulfido-2-nitrobenzoate (TNB) groups. Upon contact with a free thiol, one TNB group is released, resulting in a bright yellow colour which can be observed at 412 nm (Scheme 16).[145] Each thiol present within the sample will result in the release of just one molecule of TNB and so it is possible to quantify the concentration of free cysteines present within the protein sample with the use of a calibration curve (Appendix H, Figure 77).

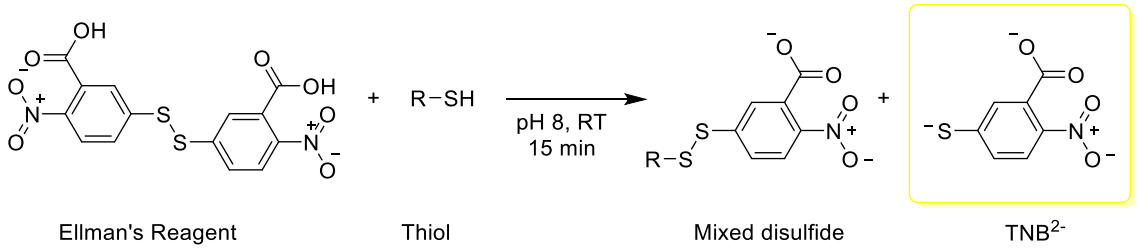

Scheme 16: Ellman's assay reaction scheme. On contact with the reagent, thiols result in the release of TNB which has a strong absorbance at 412 nm, and a yellow colour.

It was anticipated that native HSA would give a positive Ellman's assay as there is a free thiol present within the protein. Once reaction with DBCO-mal has occurred (**13**), this thiol would no longer be available and therefore a negative Ellman's result or significant reduction in absorbance was expected. This was reflected in the data, control samples of DBCO-mal and DBCO-acid gave absorbance readings similar to water only controls (data not shown). The native protein gave an average absorbance value equivalent to 0.93 mM of cysteine, and a bright yellow colour. The average absorbance for the conjugated sample (**13**) resulted in a significantly lower ($P < 0.05$) cysteine concentration at 0.17 mM (Figure 37). When taking into the account concentration of the protein solution this equates to a ratio of cysteine to protein of 1.24 mM:1 mM for the native unconjugated reaction and 0.23 mM:1 mM for the conjugated reaction suggesting that the conjugation of DBCO-mal (**13**) had been successful.

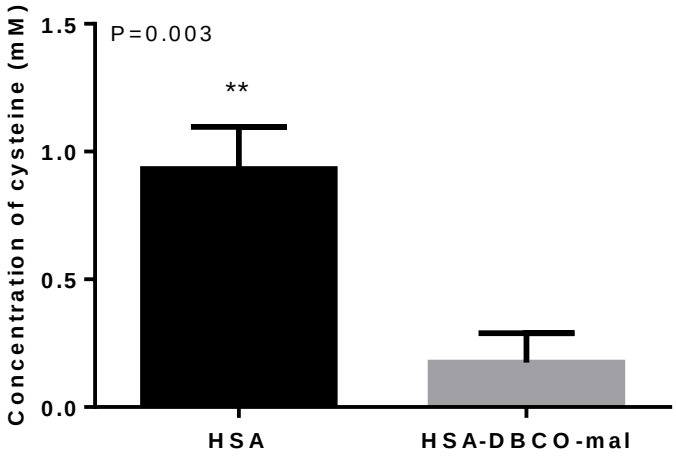

Figure 37: Effect of conjugation reaction on concentration of cysteine present within HSA sample. HSA is native unconjugated protein. HSA-DBCO-mal is the conjugated sample.

Although it could be inferred from the Ellman's data that the conjugation of HSA to DBCO-mal had been a success, more data was needed to prove this conclusively before attempting to conjugate the HSA to the PCL-N_3 microparticles. To this end LC-MS was used to analyse the success of the conjugation reaction (**13**). If conjugation is successful, a new peak will be identifiable with an increased molecular weight corresponding to the addition of the DBCO-mal linker in relation to the native protein. Unmodified native HSA protein shows multiple peaks when analysed using LC-MS, with the most abundant peak found at 66,560 Da. (Figure 38).[231]

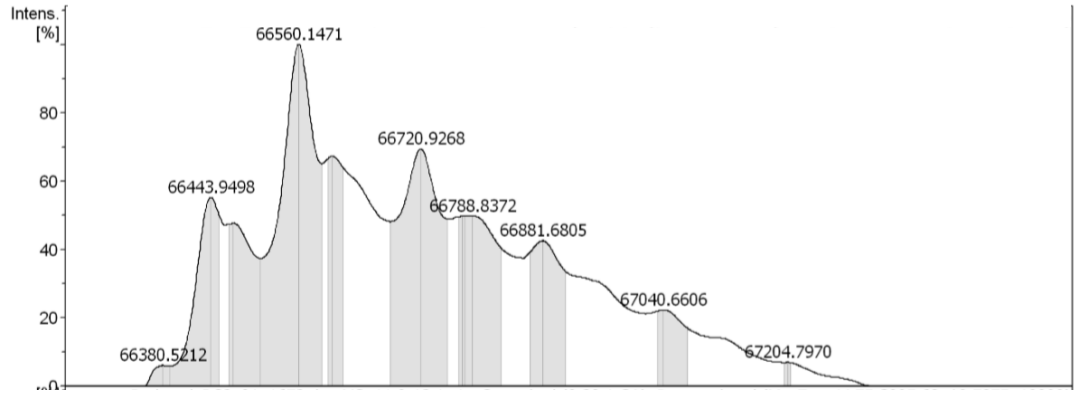

Figure 38: LC-MS analysis of native unconjugated HSA protein. The most abundant peak is present at 66,560 Da.

When HSA was reacted with DBCO-mal (13) LC-MS analysis showed an increase in the molecular weight in comparison to the unmodified protein. The spectrum (Figure 39) shows multiple peaks similar to those seen in native unconjugated protein. The peak at 66,559 is assumed to be an unlabelled, unconjugated native protein, with 23% relative abundance. The remaining peaks represent 73% relative abundance and suggest the successful conjugation reaction of DBCO-mal (**13**). This is evidenced by an increase in mw of 680 Da at each peak when compared to the previous. DBCO-mal has a MW of 674.74, therefore this suggests the possibility that the DBCO-mal is able to conjugate at multiple sites within the protein.

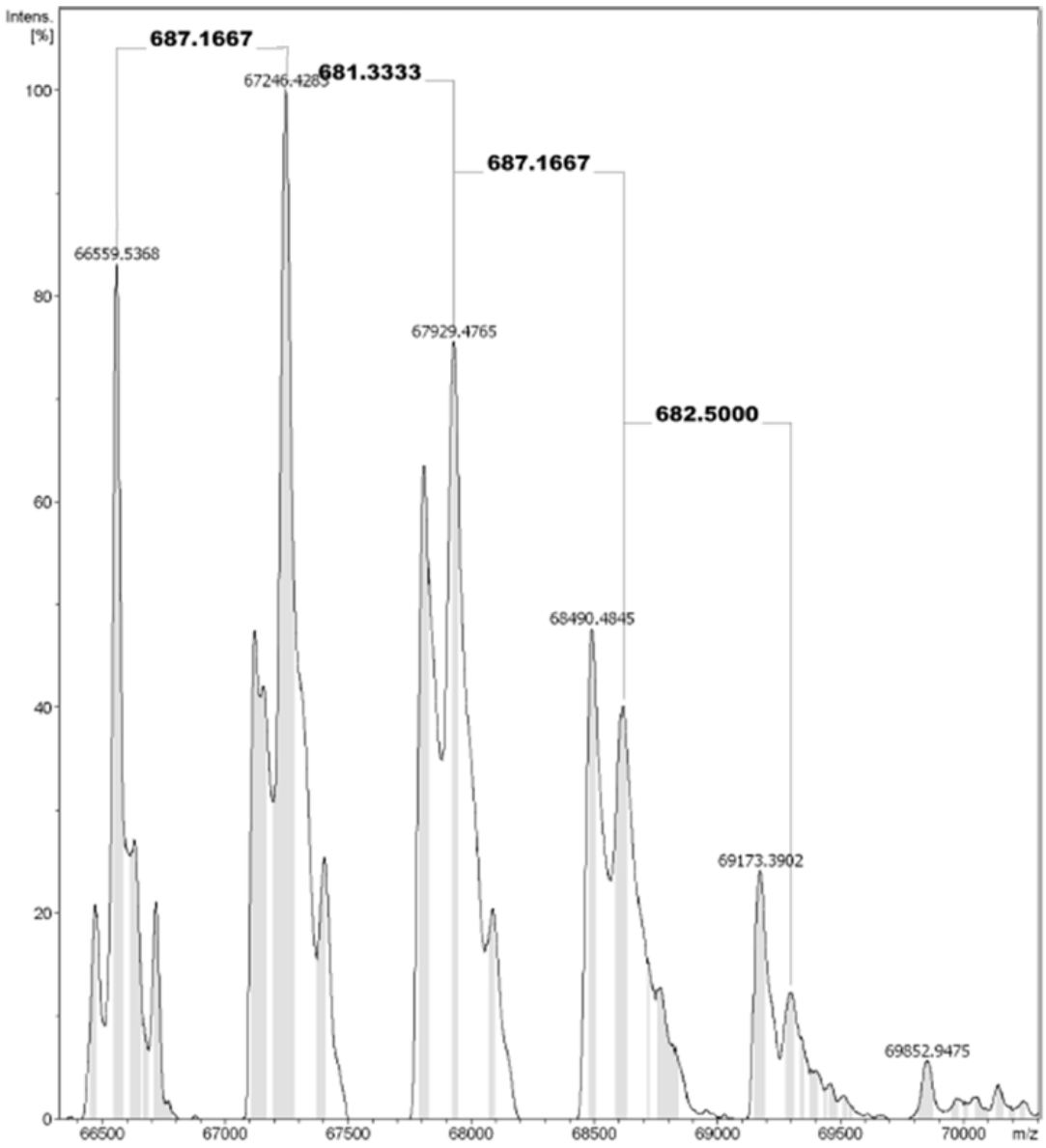

Figure 39: LC-MS analysis of HSA conjugated to DBCO-PEG4-maleimide. The addition of ~680 Da relative to unlabelled HSA (66,5 kDa) indicates a successful conjugation of the DBCO-PEG4-maleimide linker (674.74 MW).

2.2. Human Serum Albumin-Dibenzocyclooctyne-PEG4-Maleimide Conjugation to Polycaprolactone-Azide Microparticles

After showing that it was possible to conjugate the HSA protein to the maleimide on the bifunctional DBCO linker, the next step was to see if this conjugate could then attach to the PCL-N_3 particles via the internal alkyne (**14**) (Scheme 15, step 2). Qualitative confirmation of the success of this reaction was carried out using a Bradford assay. The Bradford assay utilises the colour

change observed from red to blue upon the binding of the dye Coomassie Brilliant Blue to proteins.[232] A resulting blue solution can therefore be used to indicate the presence of protein within a sample. PCL-N_3 microparticles (**7**) (synthesised in chapter 3, section 2.4) were reacted with HSA-DBCO-mal conjugates (**13**) and thoroughly washed to remove any unbound reactants to produce HSA-DBCO-mal-PCL-N_3 microparticle conjugates (**14**). Several controls were also carried out for this reaction; 1) PCL microparticles produced using commercially available PCL (containing no azide). 2) PCL-N_3 particles reacted with HSA containing no DBCO-mal and 4) PCL-N_3 particles reacted with DBCO-mal and no protein. All control experiments resulted in brown solutions, with no protein present. This suggest no conjugation of HSA to the particles. The PCL-N_3 microparticles reacted with HSA-DBCO-mal conjugates (**14**) gave a positive result and a strong blue coloured solution (Figure 40) suggesting successful conjugation.

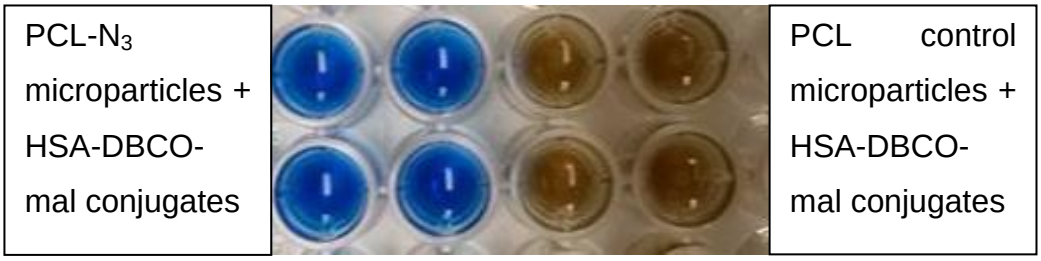

Figure 40: Visual identification of protein using the Bradford assay. PCL-N_3 microparticles reacted with HSA-DBCO-mal conjugates (left) gave a blue colour indicating the presence of protein when incubated with Bradford assay. PCL control particles reacted under the same conditions gave a negative result for the presence of protein (right).

From these results, it was possible to infer that the conjugation of the HSA-DBCO-mal to the PCL-N_3 microparticles reaction (**14**) had been a success. The Bradford assay can also be used to quantify the amount of protein present in a sample, when compared with standards. This would provide quantification of the success of the reaction, thereby increasing confidence in the result. At this point, therefore it would be important to discuss the amount of protein loaded onto the particles and quantify the protein content. However, the presence of microparticles within the sample made it difficult to achieve meaningful

quantitative data for this. Microparticle interreference in the assay meant that even if the solution colour suggested a negative result (brown) the absorbance reading was still very high. When comparing PCL-N_3-DBCO-mal-HSA conjugates (**14**) with commercial PCL control particles treated the same way, it was found that the average absorbance at 595 nm was 1.88 and 0.945 for both samples respectively. Visually however, samples showed a positive blue result for PCL-N_3-DBCO-mal-HSA conjugates (**14**) and brown for commercial PCL control particles (Figure 41). This absorbance value is high for a negative result, especially when considering that control wells containing reaction buffer only, and DBCO-mal only gave absorbance readings of 0.305 and 0.425 respectively.

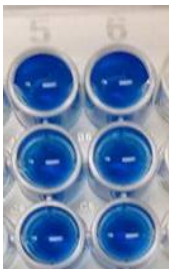

	5	6
Abs @ 595 nm	1.891	1.855
	1.89	1.897
	1.828	1.92
Average	1.880	

PCL-N_3-DBCO-mal-HSA conjugates

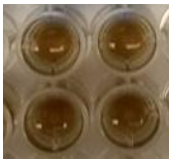

Abs @ 595 nm	0.931	0.982
	0.948	0.918
Average	0.945	

PCL control particles

Figure 41: Bradford assay absorbance readings of PCL-N_3 and PCL microparticles conjugated to HSA.

To try to remove the microparticles completely, after carrying out the Bradford assay the reaction solution from each well was removed and passed through a viva spin column. It was hoped that the particles would be retained at the top of the column and the solution would elute, allowing absorbance to be read with no particles present. However, it was found when this was carried out the solution that eluted from the column was no longer blue, but clear, suggesting that the Coomassie blue complex was retained at the top of the column (Figure 42). This therefore meant that absorbance values obtained were comparable to water only.

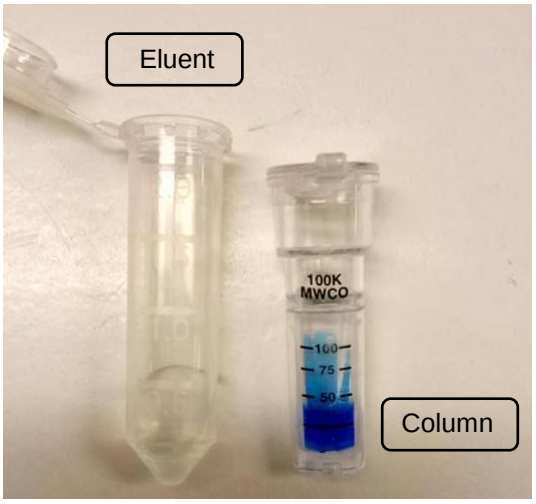

Figure 42: Attempted removal of particle interference from the Bradford assay.

Another attempt to remove particle interference was to dissolve them in DMSO before addition of the Bradford assay. Microparticles were mixed with DMSO and heated to fully dissolve them. However, again absorbance readings showed control sample of particles only, with no protein, had a similar absorbance reading (1.833) to HSA-DBCO-mal-PCL-N_3 microparticles (**14**) (1.706). The final attempt tried to remove particle interference was to take just the supernatant after the Bradford assay reaction. 200 µL of each sample was taken from the top of each well and absorbance read at 595 nm for HSA-DBCO-mal-PCL-N_3 microparticles and PCL control particles. It was found that the absorbance reading of HSA-DBCO-mal-PCL-N_3 microparticles (**14**) equated approximately 1.73 mg/mL of protein which was statistically significant (P= <0.0001) when compared to PCL control (Figure 43).

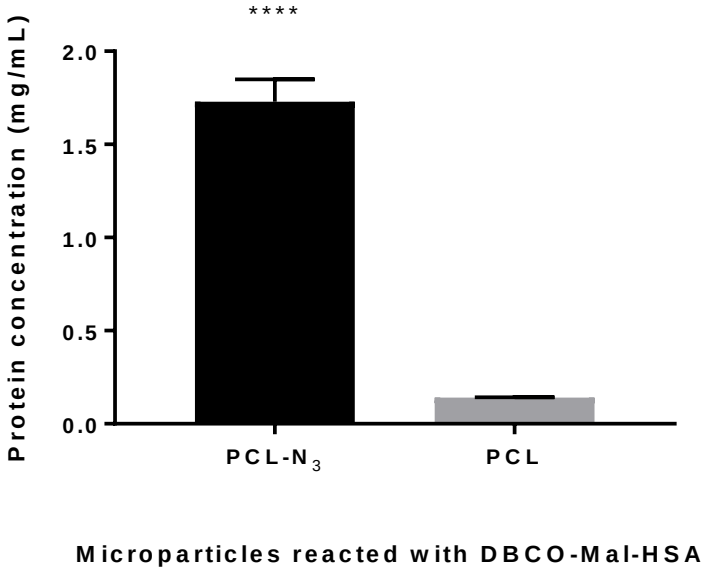

Figure 43: Protein concentration of microparticles reacted with DBCO-mal-HSA conjugates. PCL-N_3 and PCL microparticles were conjugated with HSA and DBCO-maleimide and absorbance was read at 595 nm after reacting with Bradford assay.

2.2.1. Fluorescein Isothiocyanate conjugation to Human Serum Albumin-Dibenzocyclooctyne-PEG4-Maleimide-Microparticles

Next visualisation of the conjugation reaction using Fluorescein isothiocyanate (FITC) was carried out. To achieve this, the HSA was fluorescently labelled before conjugating to microparticles. FITC is a popular fluorescent probe which will react with primary amines present within a protein sample resulting in the formation of a stable thiourea linkage.[145] HSA protein was labelled with FITC (**15**) and conjugated to DBCO-mal in a one-pot reaction resulting in FITC-HSA-DBCO-mal conjugates (**16**), which were then subsequently reacted with PCL-N_3 microparticles (**17**). Successful reactions would result in green microparticles when visualised under fluorescence microscopy (Ex 485 Em 520) (Scheme 17). A control of microparticles produced from commercially available PCL that contained no azide treated in the same way, was used.

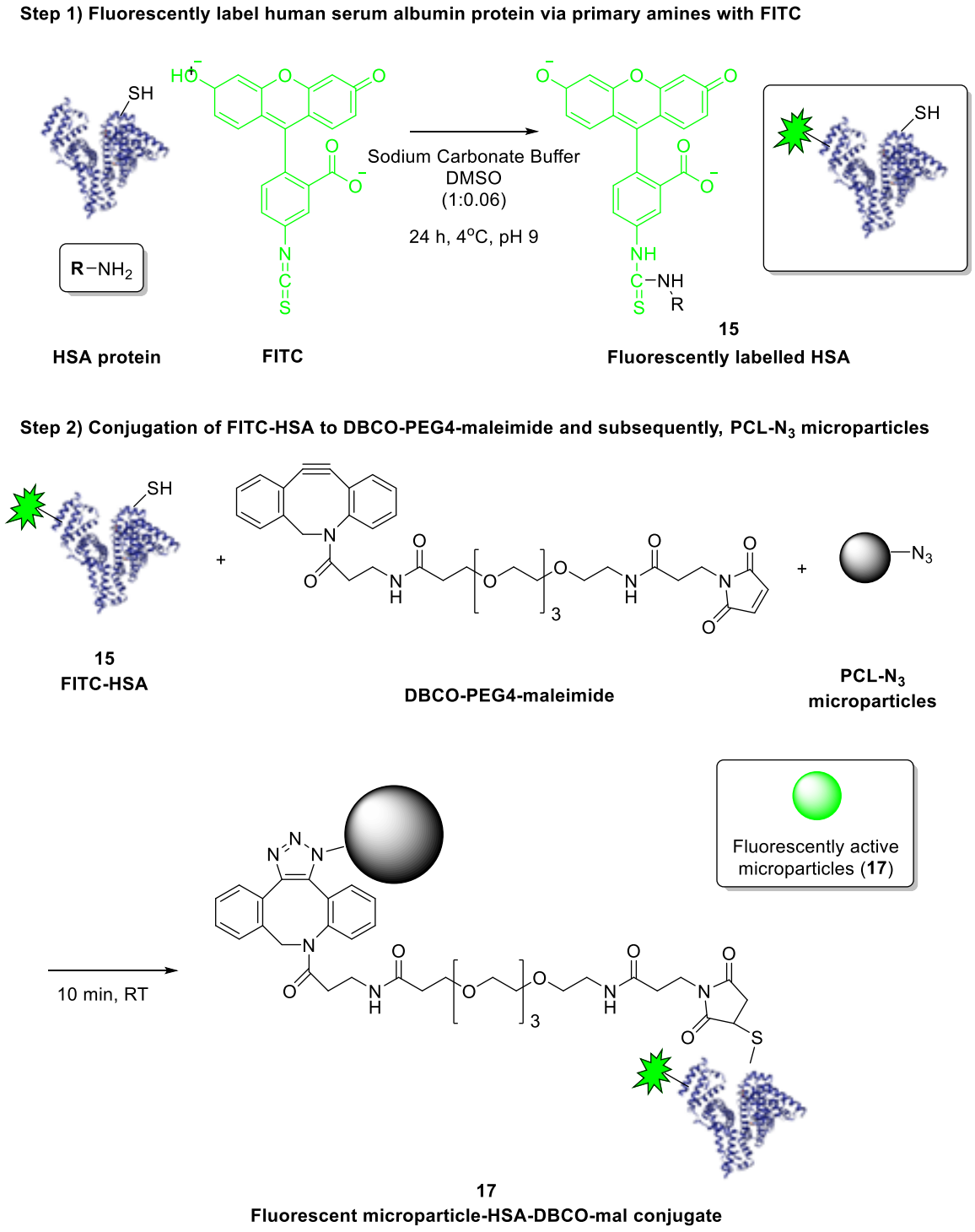

Scheme 17: Two step synthesis of fluorescently labelled microparticles.

FITC labelling of human serum albumin protein and subsequent conjugation to PCL-N_3 microparticles.

Time taken to produce fluorescent microparticles, was studied by looking at reaction times of 10 min, 1, 2 and 12 h (Figure 44). Fluorescent imagery of the resulting purified microparticles (**17**) showed that the reaction is highly efficient, occurring within just 10 minutes. Fluorescence was observed in all the samples containing PCL-N_3 microparticles (**17**) and no fluorescence was observed in control particles produced using commercially available PCL until after 12 hours, at which point low level fluorescence is observed. Physical adsorption of water and protein to the surface of the microparticles could have occurred at this time as opposed to a conjugation reaction occurring.

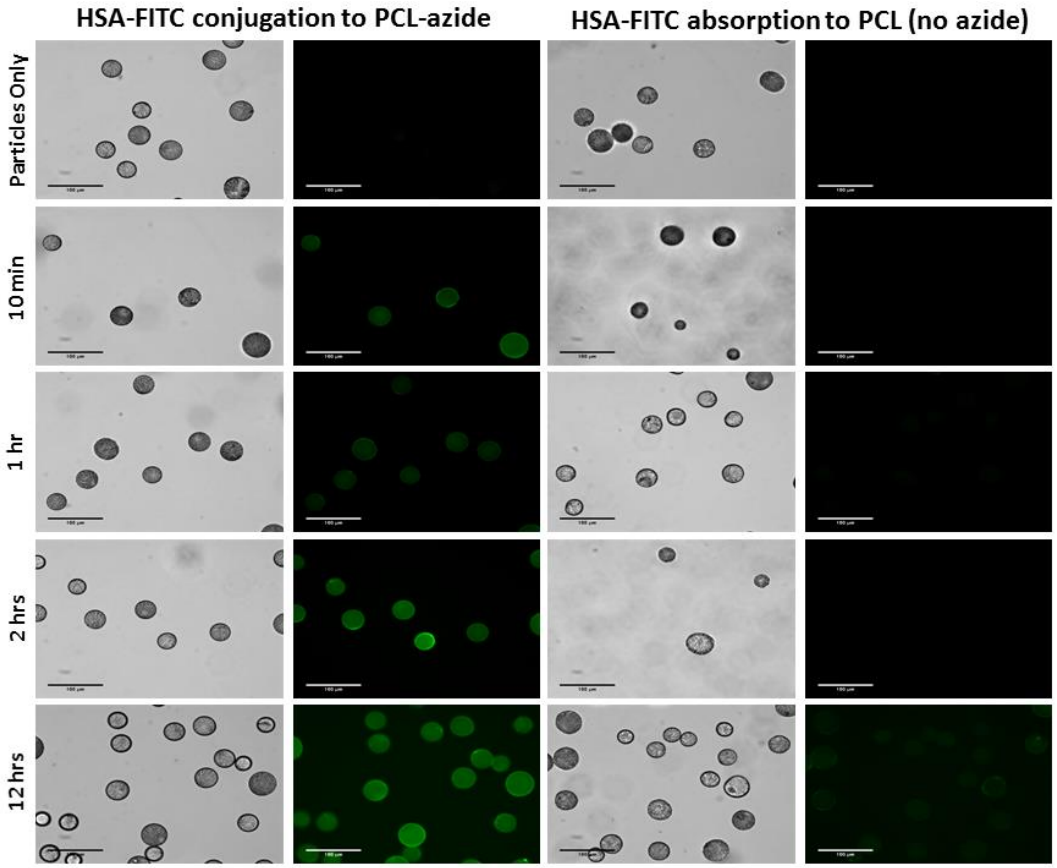

Figure 44: HSA tagged with FITC conjugated to PCL-N_3 microparticles via a DBCO-PEG4-maleimide linker. Commercial PCL microparticles were used as a control (right hand side). Scale bars show 100 μm.

Combined fluorescence and Bradford assay data show the successful conjugation of a model protein to PCL-N_3 microparticles using a bifunctional DBCO-linker. This success highlights that the microparticles can be used for conjugation to protein. This also has the potential to be adapted to other

proteins, if the native protein of interest has a free thiol, or can be modified to contain one, then in theory these conjugation techniques would be applicable also.

2.3. Transforming Growth Factor-β Conjugation to Polycaprolactone-Azide Microparticles

As it was possible to conjugate a model protein to the PCL-N_3 microparticles, efforts were made for the attachment of a relevant, therapeutic protein for the regeneration of tendon tissue. TGF-β1 and TGF-β3 were chosen due to their presence in embryonic development of the tendon tissue.[2] TGF-β3 is the predominant isoform during early foetal development, which is taken over by TGF-β1 in the later stages as development progresses.[42] Prior to experimentation, attempts were made to characterise the TGF-β1 and TGF-β3 to identify the best techniques for the analysis of the conjugation reaction. TGF-β has a molecular weight of 25 kDa. Structurally TGF-β proteins are a homo-dimer of two identical 112 amino acid polypeptide chains, with 9 conserved cysteines. The two subunits are held together by a disulphide bridge formed between cysteines 77 on each chain.[233,234]

2.3.1. Characterisation of Transforming Growth Factor-β1 and Transforming Growth Factor-β3

LC-MS analysis was used to characterise TGF-β1 and TGF-β3 native proteins purchased from PeproTech® at a concentration of 4 μM. Exact masses for each isoform were calculated using ExPASy ProtParam and were found to be 25,571 Da for TGF-β1 and 25,427 Da for TGF-β3, which was reflected in the LC-MS data (Figure 45). However, to achieve this data, a relatively large amount of sample of TGF-β was required. To conserve resources LC-MS analysis was carried out on solutions at a concentration of 0.4 μM as well. It was found that this concentration was too low to be able to achieve an identifiable peak in the spectra (data not shown.)

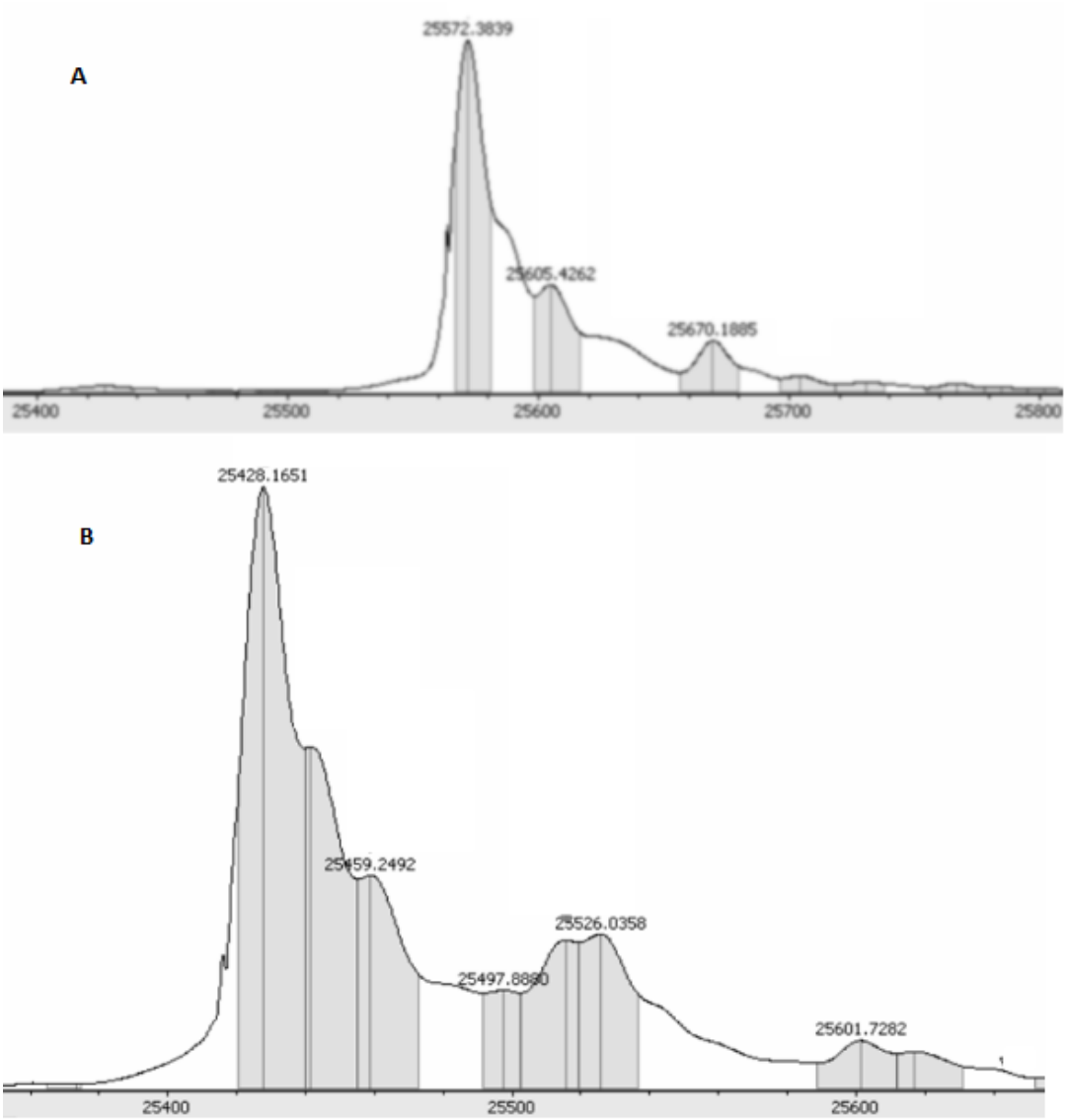

Figure 45: LC-MS analysis of TGF-β1 and TGF-β3 proteins at a concentration of 4 µM. TGF-β1 protein peak is seen at 25,572 Da (A) and TGF-β3 protein peak at 25,428 Da (B) as expected.

Characterisation by MALDI-TOF was then attempted with protein concentrations of 4 µM (Appendix J, Figure 80 & Figure 81) and 0.4 µM. MALDI-TOF offers the benefit of a reduced sample size in comparison to LC-MS (2 µL of sample compared to 30µL). Additionally, it was found that at the lower concentration of 0.4 µM it was possible to visualise the protein for both samples. Peaks were identifiable at 25,970 Da and 25,850 Da corresponding to the homo-dimer for TGF-β1 and TGF-β3 respectively. Smaller secondary peaks were present at 12,958 Da and 12,857 Da for TGF-β1 and 3 respectively, showing a small portion of the protein samples had been reduced to their

monomeric forms (Figure 46). Due to the quality of the spectra and the reduced sample size required, MALDI-TOF mass spec was used to analyse the success of the subsequent conjugation reactions.

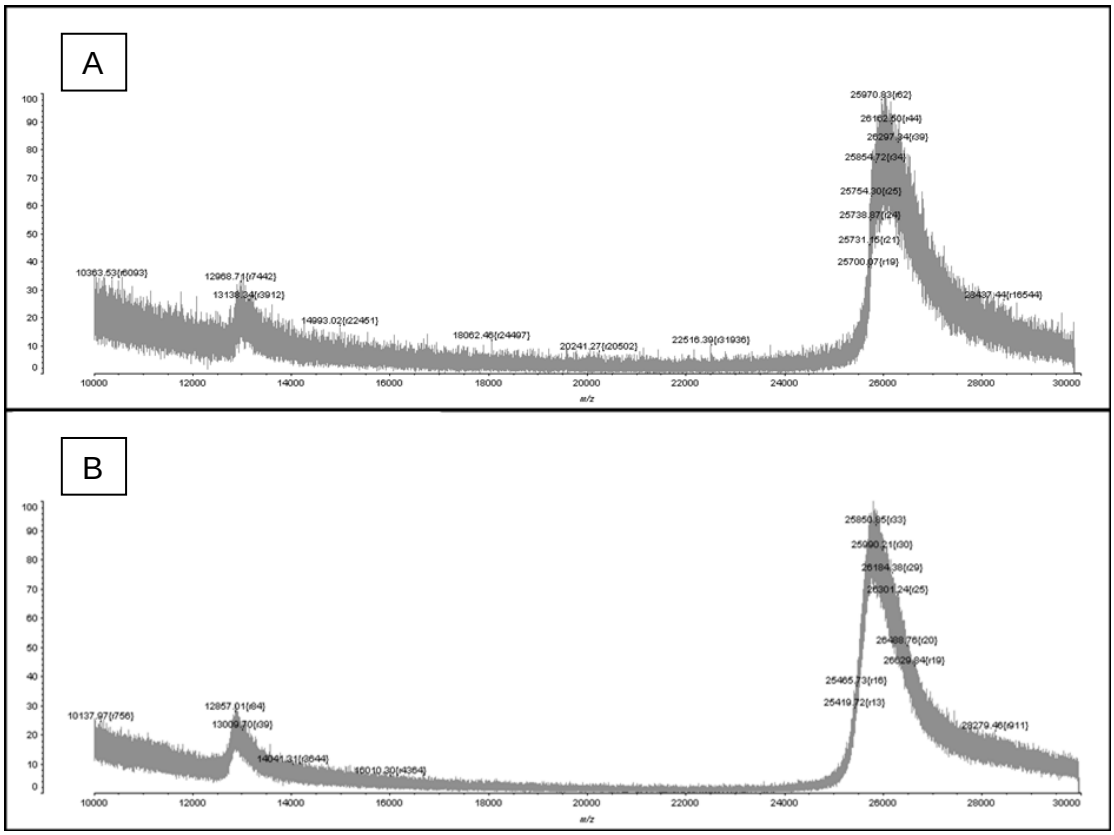

Figure 46: MALDI-TOF spectra for TGF-β proteins. TGF-β1 (A) and TGF-β3 (B) show peaks at ~25500 Da and ~13000 Da indicating the dimer and monomer respectively.

2.3.2. Transforming Growth Factor-β Conjugation using Thiol-Maleimide Chemistry

Investigations began into how to conjugate TGF-β to a DBCO linker. With HSA it was possible to conjugate to the free cysteine present within the protein. However, often cysteines are buried within proteins, or are involved in disulphide bridging necessary for the maintenance of the protein's structure. TGF-β specifically consists of a cysteine rich core which forms a knot-like structure held together by disulphide bonds.[233] Therefore, it is possible that there are no free thiols accessible within the protein for the direct conjugation of DBCO-mal. However, in 2015 kim et al reported the direct conjugation of TGF-

β1 protein to a methacrylated chitosan hydrogel via a free thiol and a succinimidyl-4-(N-maleimidomethyl)cyclohexane-1-carboxylate (SMCC) linker.[235] Therefore the conjugation of DBCO-mal directly to TGF-β was attempted.

2.3.2.1. Conjugating TGFβ to DBCO-PEG4-Maleimide

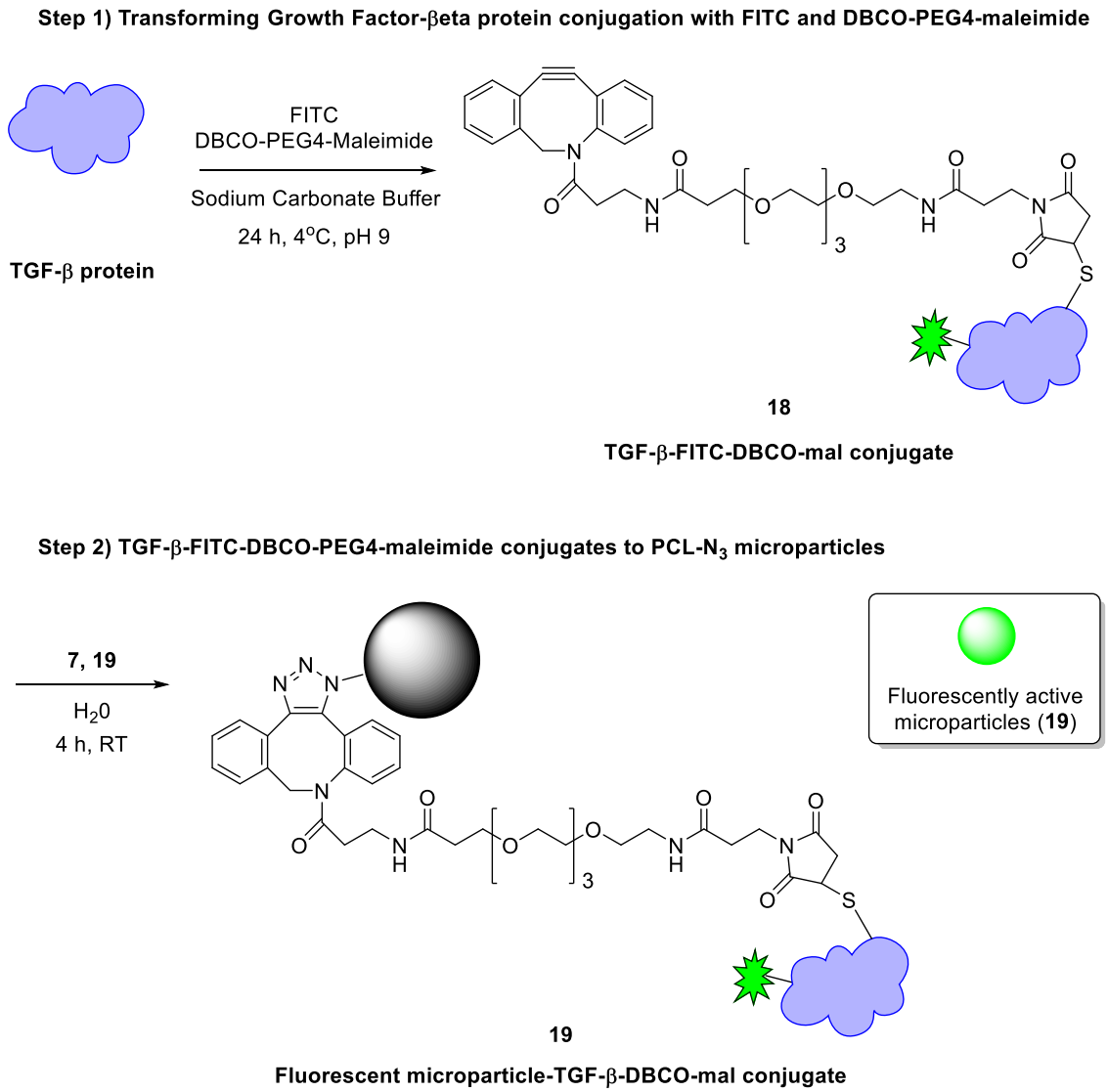

Scheme 18: Fluorescently labelled TGF-β conjugation to DBCO-PEG4-maleimide and PCL-N_3 microparticles.

TGF-β1 and TGF-β3 were reacted with DBCO-mal and FITC using the same methods as those described for the comparative reaction with HSA (Scheme 18). After reaction of TGF-β with FITC and DBCO-mal (**18**), the solution was

purified, and the resulting conjugate was then reacted with PCL-N_3 particles (**7**). Particles were thoroughly washed to remove all unbound FITC and DBCO-mal and produce FITC-TGF-β-DBCO-mal-PCL-N_3 microparticles (**19**). Table 11 details all the experimental conditions tested, and the controls used to generate TGF-β conjugated microparticles (**19**). Successful conjugation of microparticles would result in observable fluorescence at 520 nm. Fluorescence would only be observed in samples that contain protein, FITC, DBCO-mal and PCL-N_3 microparticles (reactions 1 and 3). All other control samples should have no observable fluorescence.

Reaction no.	Protein	DBCO-mal	FITC	Particles
1	TGF-β1	5 eq	20 μL	PCL-N_3
2	TGF-β1	5 eq	20 μL	PCL
3	TGF-β3	5 eq	20 μL	PCL-N_3
4	TGF-β3	5 eq	20 μL	PCL
5	TGF-B1	-	20 μL	PCL-N_3
6	TGF-B1	-	20 μL	PCL
7	TGF-β3	-	20 μL	PCL-N_3
8	TGF-β3	-	20 μL	PCL
9	-	2.6 μL	20 μL	PCL-N_3
10	-	2.6 μL	20 μL	PCL

Table 11: Experimental conditions used for the conjugation of TGF-β protein to FITC and DBCO-PEG4-maleimide

Unfortunately, no observable fluorescence was seen in any sample, suggesting that conjugation to TGF-β was unsuccessful. One explanation for this is that the cysteines present in the protein are not accessible or are involved in disulphide bonding. It is possible to reduce proteins by cleaving the disulphide bond to leave free thiols, reagents such as tris(2-carboxyethyl)phosphine hydrochloride (TCEP) are capable of this.[145] TGF-β is a dimer in which the quaternary

structure is maintained by a disulphide bond.[232] Therefore, in this case, reducing these cysteines could lead to further complications when attempting to assess the biological activity of the protein and its effectiveness as a regenerative agent. As a result, other conjugation methods were investigated.

2.3.2.2. TGF-β Conjugation to Fluorescein-5-maleimide

Traut's reagent (2-Iminothiolane) is a small molecule that is capable of reacting with primary amines present within a protein to introduce free thiol groups, which can then be used for subsequent maleimide conjugation (Scheme 19).[145]

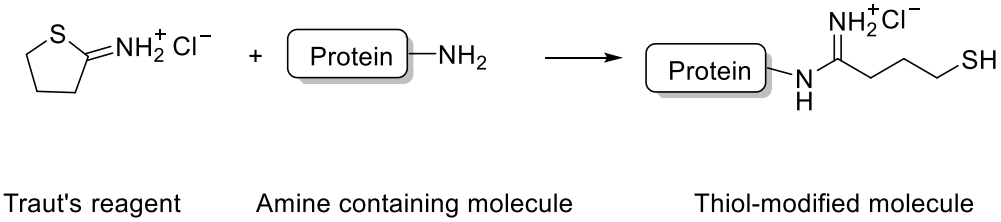

Scheme 19: Reaction scheme for 2-iminothiolane (Traut's reagent)

Fluorescine-5-maleimide is a fluorescent molecule, containing a maleimide functional group which can be used to test for the successfull conjugation of Traut's reagent to TGF-β. Fluorescence of conjugated protein can be monitored at 518 nm. TGF-β1 and TGF-β3 were reacted with Traut's reagent and then subsequently with flourescein-5-maleimide, before being purified. No observable fluorescence was seen for this reaction (data not shown). Multiple rounds of optimisation were attempted but to no avail and as a result different DBCO-units not containing a maleimide were investigated.

2.3.3. TGF-β conjugation to Dibenzocyclooctyne-PEG4-N-Hydroxysuccinimide

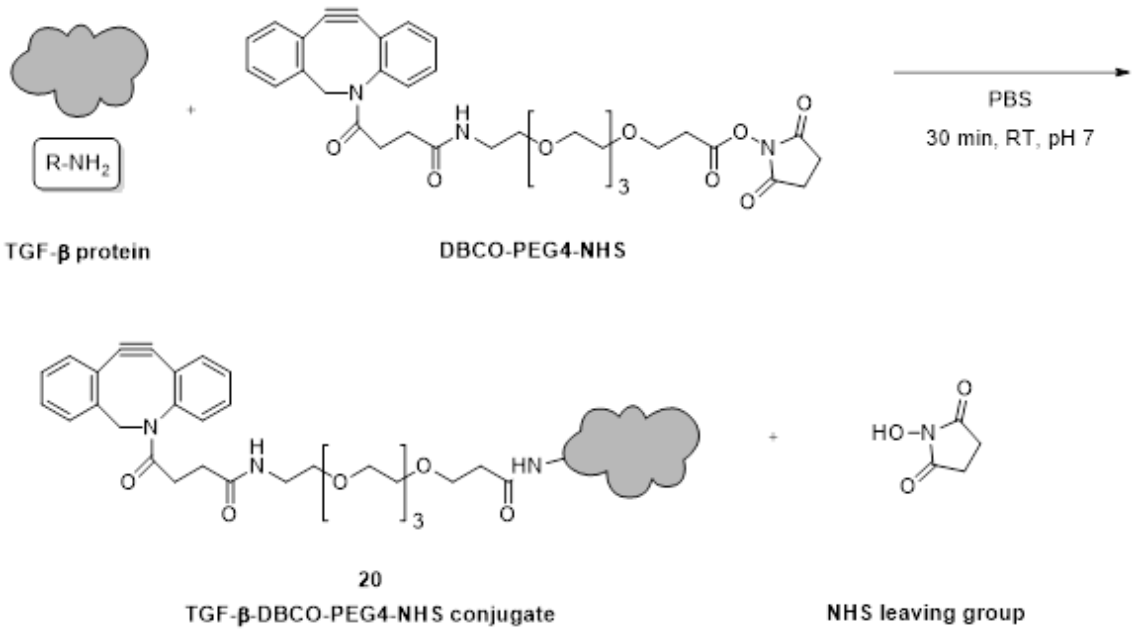

Scheme 20: TGF-β conjugation to DBCO-PEG4-NHS

Dibenzocyclooctyne-PEG4-NHS (DBCO-NHS) contains an N-hydroxysuccinimide (NHS) group that can be used for the conjugation of proteins through a reaction with primary amines. The reaction between the primary amines present in the protein results in the formation of a stable amide linkage between the protein and the DBCO unit (**20**), and the release of the NHS leaving group (Scheme 20).[145] TGF-β1 and TGF-β3 at a concentration of 0.4 µM were reacted with DBCO-NHS, and then purified using a desalting column. The resulting solution (**20**) was analysed using MALDI-TOF. No identifiable protein peak was present in the solution after the reaction (Figure 47).

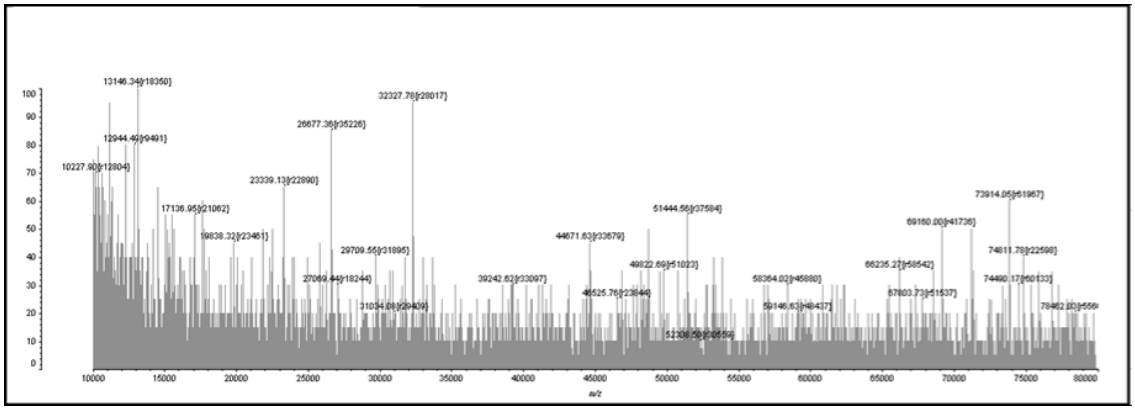

Figure 47: MALDI-TOF spectrum of TGF-β1 protein reacted with DBCO-PEG4-NHS. No protein was present, with no observable peaks, only background noise

The absence of a protein peak in the MALDI-TOF spectrum led to several optimisations of the reaction between TGF-β and the DBCO-NHS, detailed in Table 12. All these attempts resulted in no observable protein peaks, with data comparable to Figure 47. Due to the lack of protein peaks present in the MALDI-TOF spectra, the matrix used for analysis was investigated. Transferulic acid and sinipic acid were used as matricies. For both, peaks at around 25 kDa and 12 kDa were observed in the native protein, but again after DBCO-NHS conjugation reaction (**20**), these were no longer visible. Sodium dodecyl sulfate (SDS) can aid the solubilisation of proteins and has been used in the preparation of MALDI-TOF samples for both hydrophilic and hydrophobic molecules.[236] SDS was added to the matrix in increasing concentrations of 0.5, 1, 5, 10 and 50%. MALDI-TOF analysis was carried out on all samples, but again, no signal for protein was observable.

Reaction No.	TGF-β concentration (μM)	TGF-β (μL)	Temp	Time	DBCO Excess	Peak identifiable?
1	**0.4**	30	RT	30 min	50 eq. DBCO:Protein	No
2	**0.4**	**100**	RT	30 min	50 eq. DBCO:Protein	No
3	4	10	RT	30 min	50 eq. DBCO:Protein	No
4	**4**	**100**	RT	30 min	50 eq. DBCO:Protein	No
5	**0.4**	100	**37°C**	**12 h**	**50 eq DBCO:Lysine**	No
6	**0.4**	100	**0°C**	12h	**50 eq DBCO:Lysine**	No
7	**0.4**	100	**0°C**	**2 h**	**5 eq DBCO:Lysine**	No
8	**4**	100	0°C then RT	30 min then 90 min	**0.2 eq DBCO:Lysine**	No

Table 12: Experimental conditions tested for the conjugation of TGF-β to DBCO-NHS. All reactions were carried out independently for TGF-β1 and TGF-β3. The variable changed for each reaction is highlighted in bold.

In further attempts to troubleshoot the reasons as to why the protein was not observed in the MALDI-TOF, attention was turned to factors outside of the reaction conditions. Initial concerns were that the protein was not stable or had suffered multiple freeze-thaw cycles and as a result had lost its integrity, whether this be by degradation or aggregation. It was found that the MALDI-TOF analysis of the unconjugated stock protein was always consistently comparable to the data seen in Figure 46 for both TGF-β1 and TGF-β3. Degradation of the protein was therefore ruled out as a cause of signal loss.

In order to remove any unbound reactants, the reaction solution (**20**) was purified by being passed through a desalting column. It was hypothesised, that

the product (**20**) was remaining on the column and therefore there would be no protein present in the eluent sample being analysed. To test this, the reaction solution (**20**) was analysed by MALDI-TOF prior to any purification. This again yielded no peak present in the region of 10,000-80,000 Da for either TGF-β1 or TGF-β3 reaction samples where the protein would be expected. The DBCO-NHS starting material and hydrolysed DBCO were present in the region of 300-1000 Da (Appendix K, Figure 82).

To rule out the possibility of the loss of protein signal being due to an artefact of instrument or user error, a sample of the reaction carried out using TGF-β protein at a concentration of 4 μM (**20**) was sent to the National Institute for Mass Spectrometry in Swansea. The sample was analysed in positive-linear mode but only background noise was detected, a ZipTip clean up procedure was carried out and the sample was re-analysed, and again nothing was identified in the spectrum. The conclusion was that there was no protein present in either the TGF-β1 or TGF-β3 sample. Unfortunately, due to time and budget constraints it was not possible to send a sample of the native protein to be used as a control to verify if the concentration of the protein was detectable.

Previously it had been possible to analyse the success of the DBCO-mal conjugation reaction to HSA by LC-MS (Chapter 4, section 2.1.1). Native TGF-β, was only observable by LC-MS at a concentration of 4 μM (Figure 45). Therefore, conjugation of DBCO-NHS was carried out on TGF-β1 and TGF-β3 at a concentration of 4 μM (**20**). The purified reaction was analysed using LC-MS, however, the results of this also suggested that there was no protein present in the sample (data not shown) with small molecule peaks at 575 m/z being identified, indicative of hydrolysed DBCO-NHS ester (Figure 48).

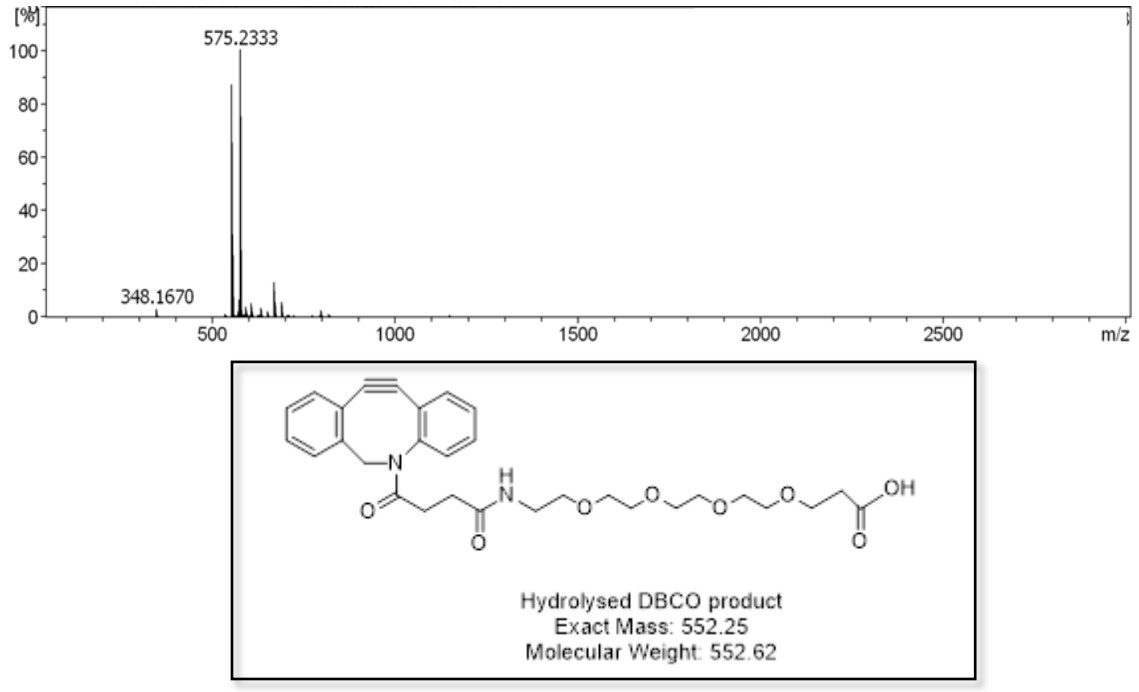

Figure 48: LC-MS Analysis of Conjugation Reaction Between TFG-β and DBCO-NHS. Peak present at 575 is indicative of hydrolysed DBCO-NHS plus a sodium ion ($M+Na^+$)

Since both LC-MS and mass spec data from Swansea concluded that there was no protein present in the sample (**20**), concerns that is was being lost, degraded or precipitated during the reaction arose. To test this, SDS-PAGE analysis was carried out. TGF-β1 and TGF-β3 at a concentration of 4 μM were reacted with DBCO-NHS in excess and the reaction purified (**20**). TGF-β1 and TGF-β3 native, unconjugated proteins at the same concentration were used as a control. The samples were then analysed by SDS gel electrophoresis and visualised using silver staining and Coomassie Blue (Figure 49, A and B respectively). After Coomassie staining, native unconjugated protein showed a clear band between 10-15 kDa corresponding to the protein monomers. Very faint bands were visible to the eye in the conjugated samples, but this did not translate when imaging. The visualisation was successfully achieved using silver staining, this is a more sensitive detection method and can be used to identify proteins with low abundance at just 0.1 ng/mm^2 within the gel.[237] After staining, TGF-β protein was visualised in all sample lanes, suggesting that protein is present in samples (**20**) after reaction and subsequent purification.

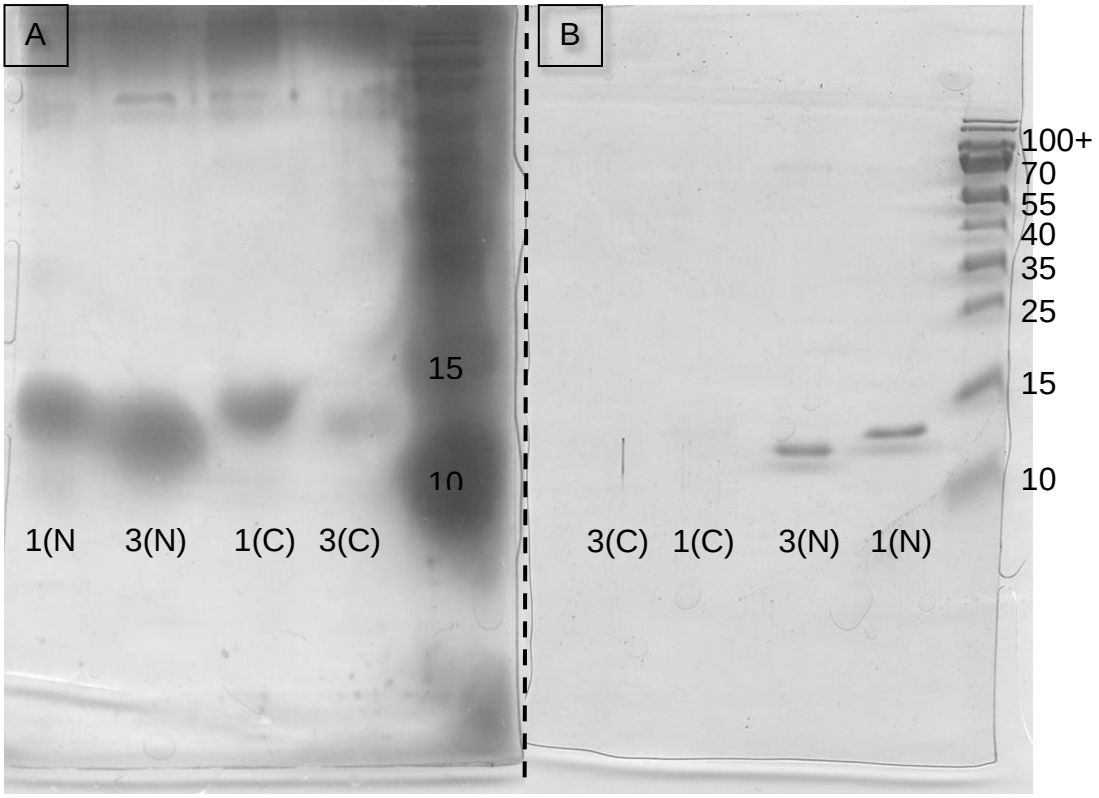

Figure 49: Gel electrophoresis of TGF-β proteins reacted with DBCO-NHS. (A) shows gel stained with silver staining and (B) with Coomassie Blue. In both gels TGF-β proteins are indicated as 1 and 3 in accordance to their isoform. N is native unconjugated protein control samples. C is conjugated protein with DBCO-NHS. The apparent molecular weights are displayed in kDa in the ladder on the right-hand side of the image and are identical for both gels.

After it was shown that the protein was still present in the sample after reaction (**20**), it was thought that the loss of its signal within the MALDI-TOF spectrum could be due to interference from the DBCO unit. To test this theory, DBCO-NHS which had been hydrolysed (confirmed by MALDI-TOF prior to reaction, appendix K, Figure 83) to no longer contain an active NHS ester was added to TGF-β. The working theory of this reaction was that with a hydrolysed DBCO it should no longer be able to conjugate to the protein. Therefore, if the protein signal was still missing from the spectrum, it could be that interactions between the DBCO linker unit and the protein are stopping the ionisation process from taking place. TGF-β1 and TGF-β3 proteins were mixed with hydrolysed DBCO-NHS (**20**) and spotted on the MALDI-TOF plate. As a control TG-β1 and TG-β3 were also reacted with non-hydrolysed DBCO-NHS. The reactants were mixed

directly on the surface of the MALDI-TOF plate and measured immediately. Interestingly, when the hydrolysed DBCO-NHS was added, the protein was present in both spectra at 25,978 Da for TGF-β1 and 25,942 Da for TGF-β3 (Figure 50, A and B respectively) similar to data described previously. For both proteins, a peak indicative of hydrolysed DBCO can be seen at ~555. (Figure 50, C) Conversely, for the reaction treated with non-hydrolysed DBCO, again the protein peak was missing in both spectra (Figure 50, D). This data suggests that the loss of the proteins signal is as a direct result of the NHS ester.

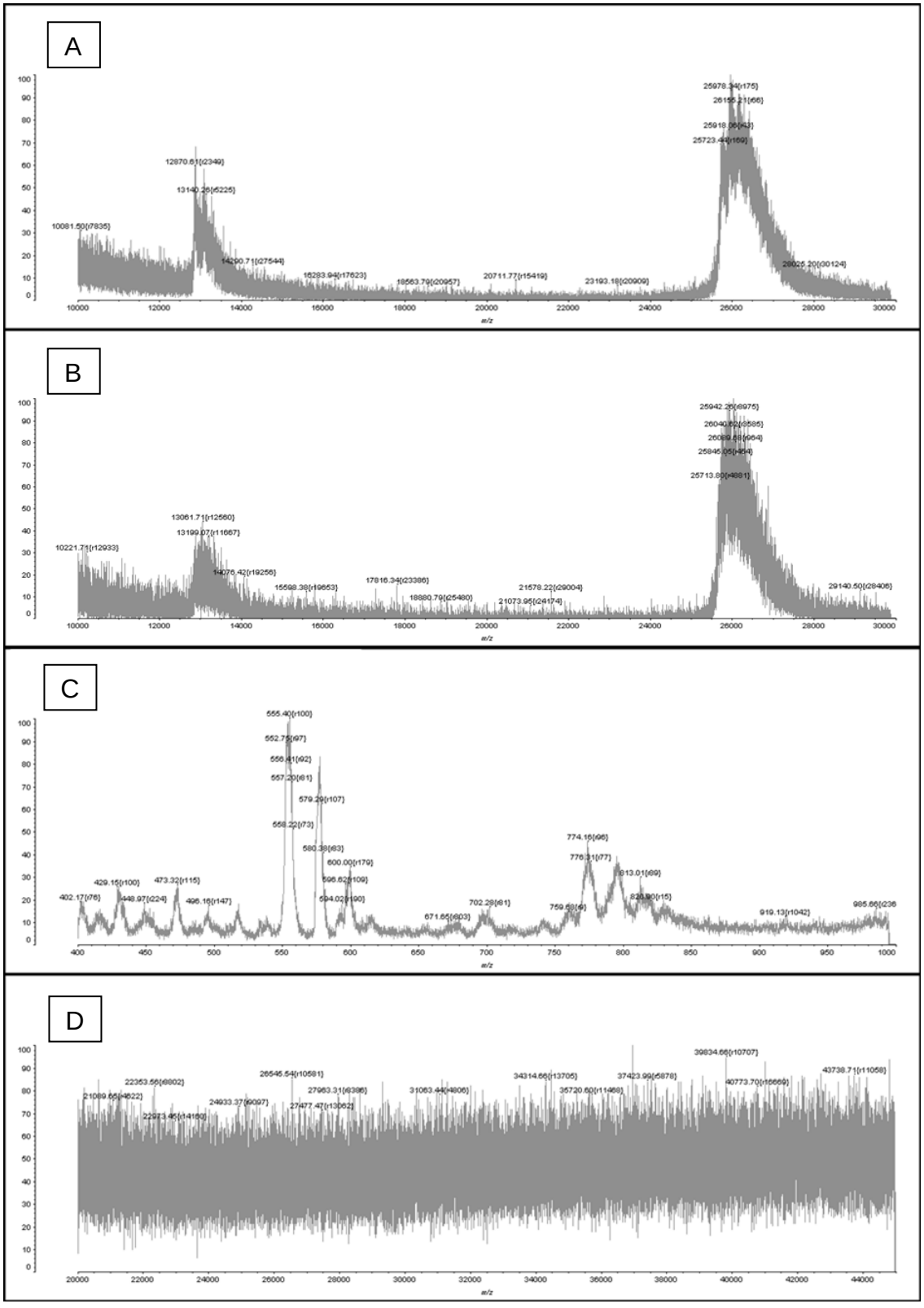

Figure 50: TGF-β reaction with hydrolysed and non-hydrolysed DBCO-NHS. TGF-β1 (A) and 3 (B) showed the presence of protein when reacted with hydrolysed DBCO (C, peak at 555). This disappears when reacted with a DBCO-NHS unit still containing an active ester (D).

The effect of changing the concentration of trifluoroacetic acid (TFA) present in the matrix used for MALDI-TOF analysis was then investigated. TGF-β1 and TGF-β3 samples reacted with DBCO-PEG4-NHS (**20**) were analysed by MALDI-TOF with increasing concentrations of TFA mixed with the sample. Table 13 shows all the experimental conditions tested.

No.	TFA concentration (%)	No of spots. Matrix:Protein:matrix	Matrix (µL)	Protein (µL)
1	0.3	3:2:3	12	4
2	0.3	3:2:3 + 1 spot 0.3%TFA	12	4
3	0.5	3:3:3	12	6
4	3	3:2:3	12	4
5	3	6:2:6	24	4
6	3	9:2:9	36	4
7	3	20:2:20	80	4
8	10	3:2:3	12	4

Table 13: Matrix conditions tested to increase the presence of TFA in Samples. All reactions were carried out on both TGF-β1 and TGF-β 3 as independent samples. All reactions were carried out using a sandwich method, where matrix was spotted and allowed to dry, followed by a protein spot which was also allowed to dry and finally a second matrix spot. Each 'spot' was a total volume of 2 µL.

All reactions, apart from reaction 4, resulted in no observable protein signals in the MALDI-TOF spectrum. Interestingly, reaction 4 did result in the presence of a protein signal at 25,820 Da for TGF-β1 and 27,303 Da for TGF-β3 (Figure 51). However, the spectra were of low quality and these peaks for the protein were only ever seen once, with the results being unreproducible. It is still unclear why the protein could not be detected after reaction with DBCO-NHS

(**20**) and therefore it has been impossible to prove the success of the reaction in this way.

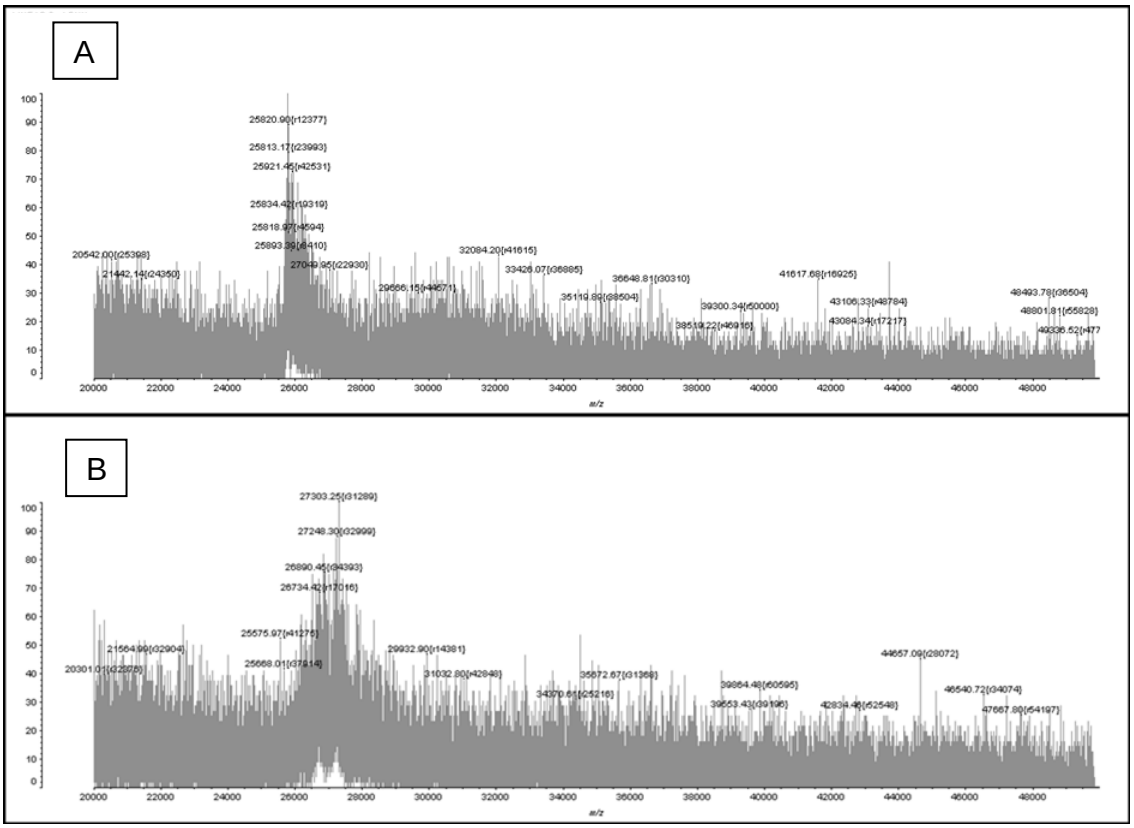

Figure 51: MALDI-TOF spectra of TGF-β1 and TGF-β3 conjugated with DBCO-PEG4-NHS. (A) shows TGF-β1 and (B) shows TGF-β3, samples were visualised by increasing TFA concentration present in the matrix to 3% (v/v).

2.4. Bovine Serum Albumin-Dibenzocyclooctyne-PEG4-N-Hydroxysuccinimide

After all attempts to show the successful conjugation of a TGF-β protein to a DBCO-NHS linking unit (**20**) had been unsuccessful, it was hypothesised that the NHS reaction was incompatible specifically with the TGF-β protein and MALDI-TOF analysis. In order to validate DBCO-NHS as a linker molecule and prove that this reaction could be used as a template for the conjugation of proteins to the PCL-N_3 microparticles, bovine serum albumin (BSA) conjugation was investigated. BSA has a MW of 66.5 kDa, with a broad peak at 67856 Da identified when analysing the native protein, as purchased from Sigma Aldrich, using MALDI-TOF (Figure 52, A). BSA was then reacted with DBCO-NHS (**21**)

using methods comparable to those used for TGF-β (Scheme 21). After reaction the protein was still present in the MALDI-TOF spectrum, and the entire peak broadened and shifted along the x-axis. The MW increased from 67856 Da to 70407 Da, which corresponds to the addition of roughly four DBCO-NHS units (MW 649.68) (Figure 52, B)

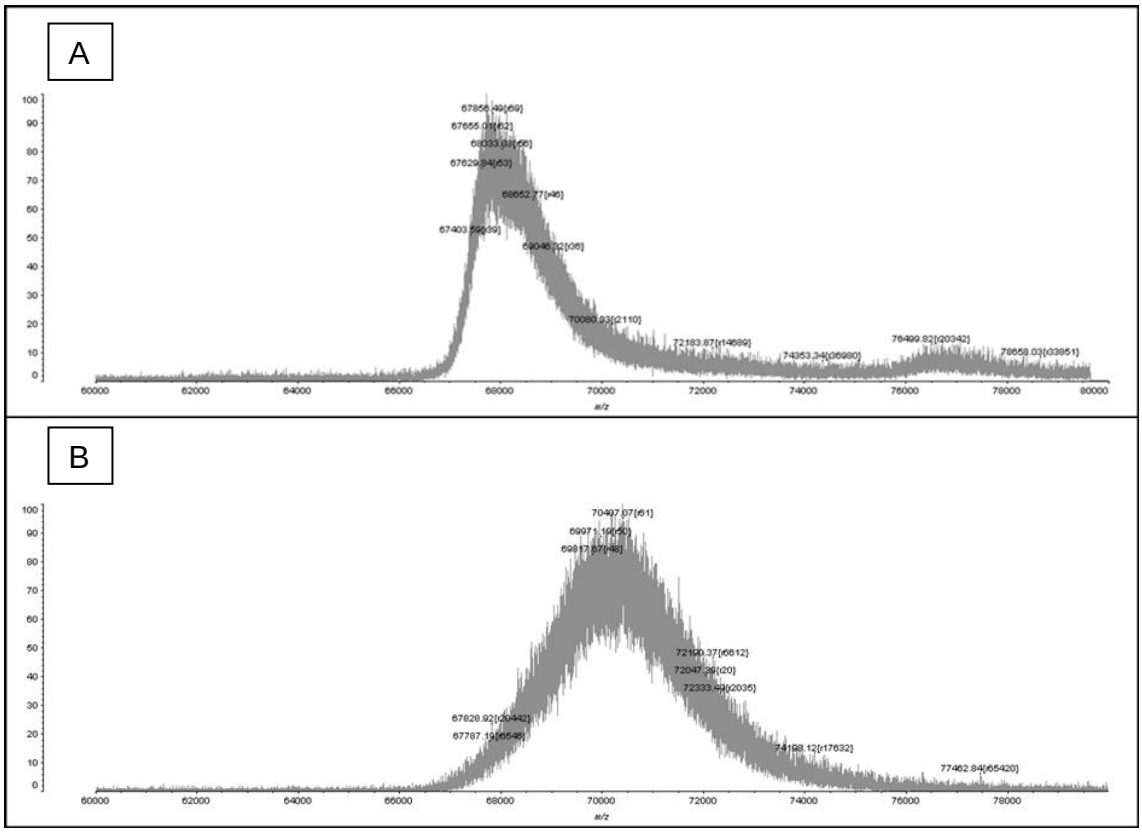

Figure 52: MALDI-TOF spectrum of native and DBCO-NHS conjugated BSA. A broad peak for the native protein is identified at 67855 Da (A). The whole peak is then shifted right and broadens further with a mw of 70407 Da, indicative of the addition of multiple DBCO-NHS linking units (B)

This data suggests that the issues seen with MALDI-TOF characterisation could be specifically as a result of attempting to conjugate with the TGF-β protein. It is believed that the conjugation reaction of DBCO-NHS to BSA (**21**) is successful and demonstrates that DBCO-NHS can be used as a linking molecule for the conjugation of proteins via their primary amines.

2.5. Transforming Growth Factor-β and Bovine Serum Albumin Conjugation to Polycaprolactone-Azide Microparticles

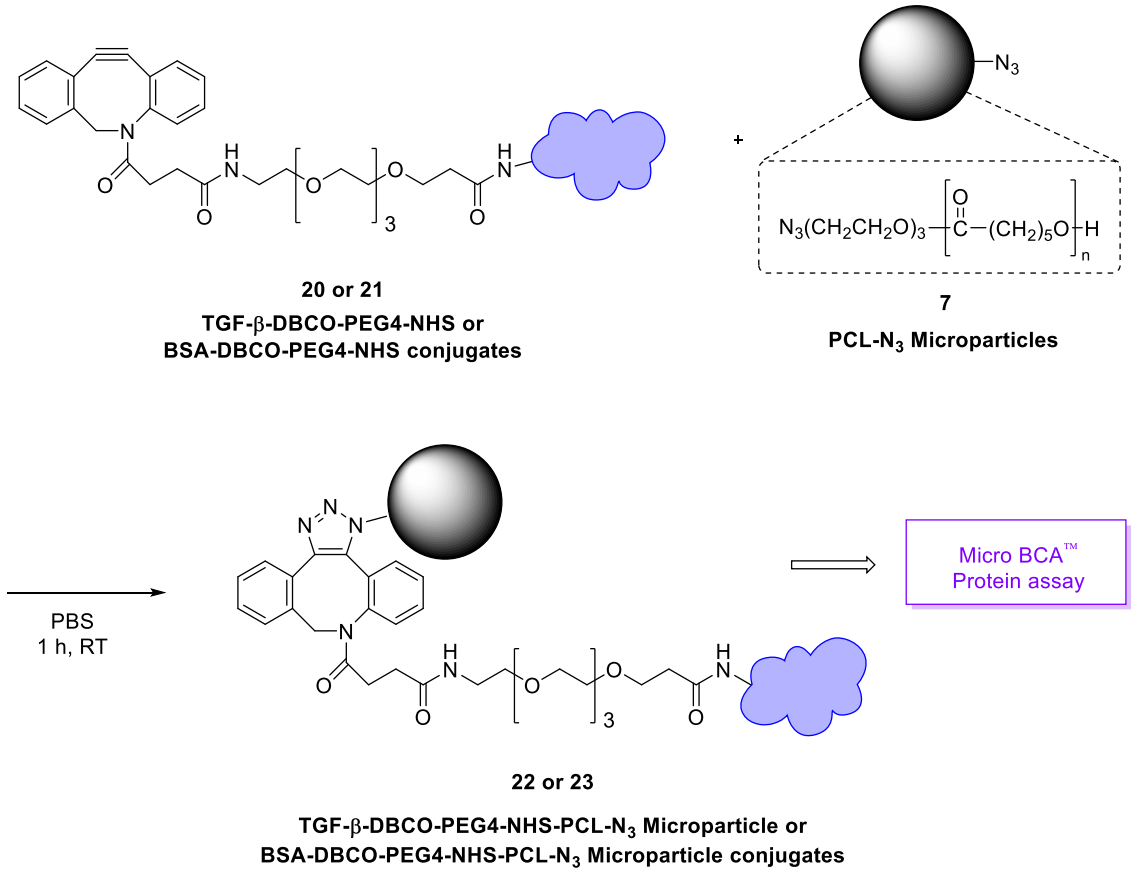

Scheme 21: Conjugation reaction of TGF-β or BSA to PCL-N_3 microparticles.

As it was possible to show the successful conjugation of model protein BSA to DBCO-NHS (**21**), it was assumed that the TGFβ reactions had also been successful despite the lack of convincing evidence for this. Therefore, the TGF-β methodology was resumed, taking forward the products of the DBCO-NHS conjugation reactions with TGF-β1 and TGF-β3 (**20**), as well as the BSA (**21**) (Scheme 21). TGF-β1 and TGF-β3 conjugates (**20**) produced during reaction **6** from Table 12, and the BSA-DBCO-NHS conjugate (**21**) were then independently reacted with PCL-N_3 microparticles to produce compounds (**22**) or (**23**) respectively. Microparticles formulated with commercially available PCL treated in the same way were used as a control. After the reaction, the microparticles (**22** or **23**) were thoroughly washed to remove all unbound reactants and the presence of protein determined qualitatively using a

bicinchoninic acid (Micro BCA) assay (Figure 53). Proteins are able to reduce copper(II) present in the assay reagents to copper(I) which can then complex to the BCA, yielding an intense purple compound.[238] This meant that a change in the solution from green to purple suggests the sample being analysed contains protein and that conjugation was successful.

Well location	Protein	Particle	Colour
5	BSA & DBCO-NHS	PCL	Green
6	BSA & DBCO-NHS	PCL-N_3	Purple
7	TGF-β3 & DBCO-NHS	PCL	Green
8	TGF-β3 & DBCO-NHS	PCL-N_3	Purple
9	TGF-β1 & DBCO-NHS	PCL	Green
10	TGF-β1 & DBCO-NHS	PCL-N_3	Purple

Figure 53: Colorimetric representation of protein present in PCL microparticles. Purple colour indicates the presence of protein, whereas green is a negative result.

All samples that contained microparticles formulated using commercial PCL gave a negative result for the presence of protein, producing a green solution (wells 5, 7 and 9, Figure 53). This is as expected because the PCL contains no azide, meaning it is not possible for the DBCO linking unit to attach, and so during the washing steps all protein would therefore be removed. All samples containing PCL-N_3 microparticles showed a positive result for the presence of protein, producing a purple solution (wells 6, 8 and 10, Figure 53). This suggests that all steps of the conjugation reaction were successful for both TGF-β (**22**) and BSA (**23**), with the DBCO-NHS being able to conjugate to the

primary amines present in the protein samples. This, in turn, is able to conjugate to the azide moiety of PCL-N_3 microparticles via click chemistry, utilising the internal alkyne of the DBCO unit. This data was interesting and strongly suggests that the conjugation of protein to PCL-N_3 microparticles is possible. Unfortunately, due to budget and resources, it was not possible to carry on any further with the investigations.

2.6. Conclusion

The work detailed in this chapter has shown that it is possible to conjugate protein to PCL-N_3 microparticles using two different conjugation techniques through the use of varying DBCO linking units. This highlights the potential for these methods to be used as a template for a successful drug delivery system. A model human serum albumin protein has been shown to successfully conjugate to PCL-N_3 microparticles using DBCO-mal as a linking molecule. The subsequent click reaction between HSA-DBCO conjugates and PCL-N_3 microparticles was shown to be efficient, occurring in just 10 minutes. The presence of protein on PCL-N_3 microparticles was visualised by fluorescence when tagged with a fluorescein isothiocyanate. Through several optimisations, it was eventually shown that it was possible to conjugate TGF-β to PCL-N_3 microparticles in a similar manner, using a DBCO-NHS linker. Similarly, model protein BSA was shown to be able to conjugate to the same DBCO linker with subsequent attachment to microparticles. The work in this chapter has shown that if the protein structure and accessible functional groups are known, conjugation to microparticles is possible and highlights their potential as a drug delivery system.

3. Experimental Procedures

3.1. Instrumentation

MALDI analysis was carried out using an analytical Axima MALDI-TOF (Kratos analytical, Uk) in positive reflectron mode. Sinipinic acid in 50% ACN with 0.03% TFA was used as the matrix unless stated otherwise. LCMS analysis was carried out using an LC-MS 2010EV (Shimadzu, Japan) using electrospray ionisation in positive mode (ES+). Absorbance and fluorescence values were obtained a CLARIOstar plate reader (BMG lab tech ltd, UK). Fluorescence microscopy was carried out using an axioplan 2ie microscope (Carl Zeiss Ag, Germany). Analytical RP-HPLC was carried out on an Agilent 2000 (Agilent Technologies, USA) using an eclipse XDB-C18 column (Agilent Technologies, USA), 4.6x100 mm, 3.5 μM with a flow rate of 1 mL/min. Solvent A was; ACN with 0.05% TFA. Solvent B was; H_2O with 0.05% TFA. 30% solvent A was increased to 50% over 20 minutes, then held at 75% for 5 minutes. Detection was carried out at 220 and 309 nm.

3.2. Materials

All materials were from Sigma Aldrich and used as received, unless otherwise stated. Dibenzocyclooctyne-PEG4-N-hydroxysuccinimidyl ester (95%, dissolved in DMSO prior to use to a final concentration of 10 mM), albumin from human serum (≥99%), 5,5′-dithiobis(2-nitrobenzoic acid) (≥98%), phosphate buffered saline (tablet), sodium phosphate (96%), sodium carbonate (≥99.0%), HEPES (≥99.5%), ethylenediaminetetraacetic acid (≥99.0%), triethanolamine (≥99.0%), fluorescein isothiocyanate isomer I (≥90%), acrylamide/Bis-acrylamide (30% solution, 37.5:1), Tris base, ammonium persulfate (≥98%), tetramethylethylenediamine (~99%), sodium dodecyl sulfate (≥98.5%), Dibenzocyclooctyne-PEG4-maleimide (dissolved in DMSO prior to use to a final concentration of 0.015 M), Sinapic acid (≥99.0%), bovine serum albumin (≥96%), coomasie plus bradford assay reagent (Thermo Fisher Scientific), micro BCA™ protein assay kit (Thermo Fisher Scientific), cysteine-HCL (Thermo Fisher Scientific), recombinant human TGF-β1 (≥98%, PeproTech, reconstituted

in water prior to use to a final concentration of 4 μM), recombinant human TGF-β3 (≥98%, PeproTech, reconstituted in 5 mM citric acid prior to use to a final concentration of 4 μM).

3.3. General Methods

Bradford Assay

The Bradford assay was used as qualitative analysis for the presence of protein in microparticle samples. The reaction was carried out using manufacturers protocols. 300 μL of Coomassie reagent was added to 10 μL of sample to be measured, and mixed well on a plate shaker for 30 s. The reaction was then incubated for 10 min at RT. The absorbance was read at 595 nm.

A calibration curve for the Bradford assay was carried out using Bovine Serum Albumin as per the manufacturer's protocol (Appendix I, Figure 78) . A stock solution of Bovine Serum Albumin (2 mg/mL) was prepared in 0.9% saline. Serial dilutions were carried out to produce concentrations of protein as follows; 2000, 1500, 1000, 750, 500, 250, 125 and 25 μg/mL. A sample containing buffer only was used as a control. 10 μL of each standard was mixed in a 96 well plate with coomasie blue reagent (300 μL) and mixed using a plate shaker for 30 s. The reaction was left to incubate at RT for 10 min after which absorbance was read on a CLARIOstar® plate reader (BMG labtech, UK) at 595 nm.

Ellman's Assay

The Ellman's assay was used for the quantitative and qualitative identification of free thiols present within protein samples. The reaction was carried out as per the manufactures protocol. Ellman's reagent solution was dissolved in 0.1 M sodium phosphate reaction buffer with 1 mM EDTA (pH 8.0) at a concentration of 4 mg/mL. 250 μL of sample to be measured was then mixed with 50 μL of Ellman's reagent solution and 250 μL of reaction buffer. The reaction was then allowed to incubate at RT for 15 minutes. Absorbance was read at 412 nm. A calibration curve was constructed following the manufactures guidelines, with

known concentrations of cysteine hydrochloride monohydrate. (Appendix H, Figure 77) The concentration of free thiol groups was calculated using the extinction coefficient for TNB (14,150 M cm^{-1}).

Micro BCA Assay

Micro BCA assay was used for qualitative analysis of protein content in samples. The reaction was carried out as per the manufactures protocol. Micro BCA Reagents were supplied from the manufacturer and were as follows; Micro BCA Reagent A (MA, 240 mL) Micro BCA Reagent B (MB, 240 mL) Micro BCA Reagent C (MC, 12 mL). Micro BCA working solution was made by mixing reagents at a ratio of 25:24:1, Reagent MA:MB:MC. Reaction sample to be measured (150 μL) was mixed thoroughly for 30 s with the working solution (150 μL) in a 96 well plate. The reaction was incubated for 2 h at 37°C. Absorbance was measured at 562 nm, after the plate had cooled to RT.

3.4. Human Serum Albumin Conjugation

Human serum albumin, as purchased from Sigma Aldrich, was characterised using MALDI-TOF, HPLC and LC-MS using the general methods described above. Samples at a concentration of 1 mg/mL were used for HPLC dissolved in H_2O and filtered.

3.4.1. Human Serum Albumin Conjugation to Dibenzocyclooctyne-PEG4-Maleimide (13)[230]

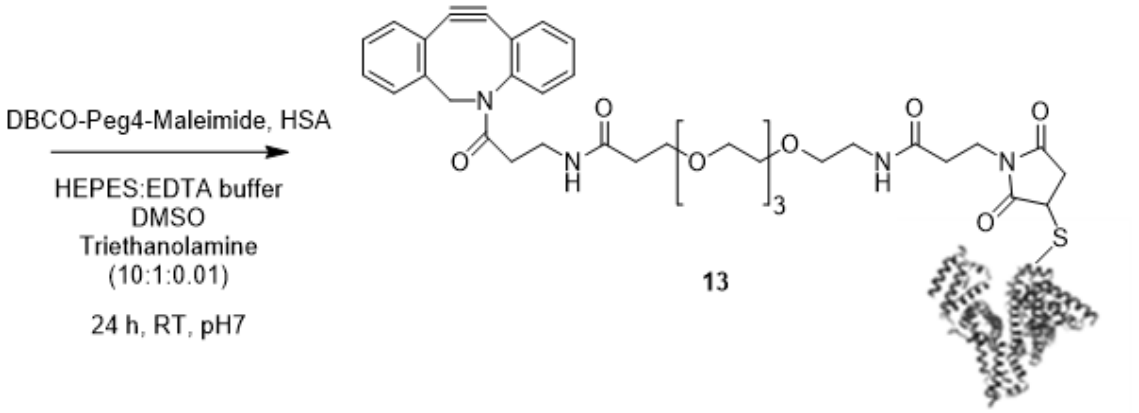

Human serum albumin (100 mg, 1.5 µmol, 1eq) was dissolved in 0.1 M HEPES and 5 mM EDTA buffer solution (2 mL, pH 7). 0.015 M DBCO-Maleimide dissolved in DMSO (200 µl, 2eq) and 4 mM Triethanolamine (2 µL) were added and allowed to react at RT for 24 h. The reaction was purified and analysed by LC-MS and Ellman's assay.

3.4.2. Human Serum Albumin-Dibenzolcycloctyne-Maleimide Conjugation to Polycaprolactone-Azide Microparticles (14)

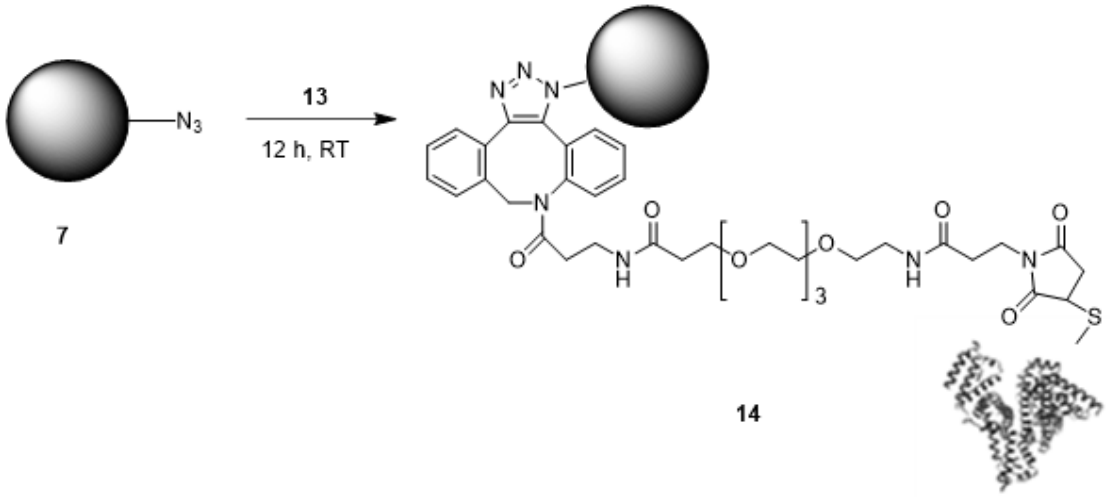

PCL-N_3 Microparticles (**7**) (15.3 mg, 665 nmol, 1eq) were mixed with HSA-DBCO-PEG4-malemide conjugate solution (**13**) (1 mL, 1eq) and allowed to react for 12 h with gentle agitation. Particles were washed with water (10x5 mL) and purified using a viva spin column (Sartorius, 100,000 MWCO, 500 µL). After purification particles were freeze dried to yield a fluffy white powder (**14**) (17.7 mg, 30%). PCL-N_3 Microparticles conjugated to DBCO-PEG4-maleimide with no HSA and PCL-N_3 Microparticles conjugated to HSA with no DBCO-PEG4-maleimide linker were used as controls. Bradford assay was used for qualitative identification of protein. The reaction was carried out in triplicate.

3.4.3. Fluorescein Isothiocyanate Labelling of Human Serum Albumin for Polycaprolactone-Azide Conjugation (17)

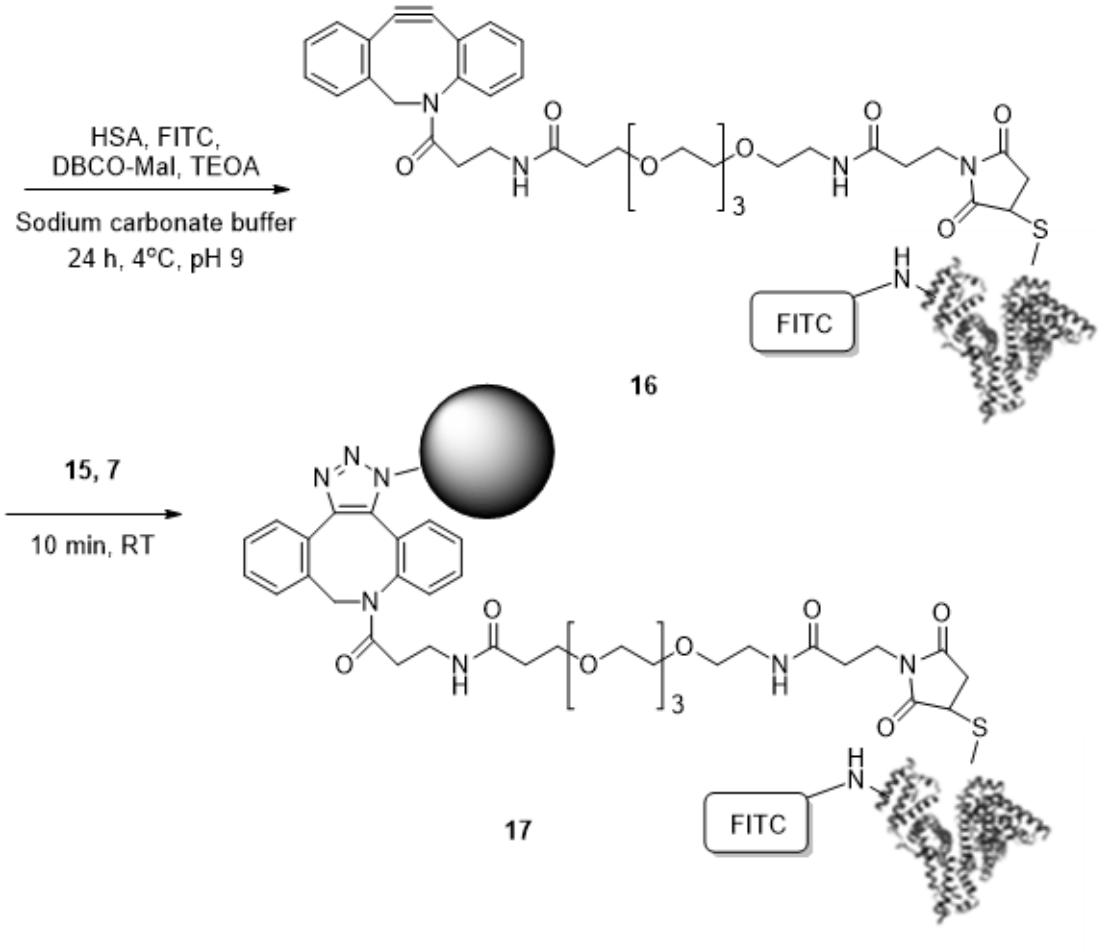

Human serum albumin (150 mg, 2.25 μmol, 1eq) was dissolved in 0.1 M sodium carbonate buffer (3 mL, pH 9). 0.015 M DBCO-maleimide dissolved in DMSO (300 µl, 2eq) and 4 mM triethanolamine (2 µL) were added. Fluorescein isothiocyanate isomer I (FITC) dissolved in DMSO at 1 mg/ml was added slowly with gentle agitation in 5 µL aliquots at a ratio of 50 µL per 1 mL of protein solution. The reaction was carried out for 24 hours at 4°C. Samples were purified using a PD10 desalting column (GE healthcare) with sodium carbonate buffer as eluent. Fractions collected were analysed using Bradford assay and fluorescent microscopy and relevant fractions combined to produce compound **16**.

PCL-N_3 (**7**) (10 mg, 410 nmol, 1eq) were mixed with **16** (700 µL, 410 nmol, 1eq) and left to react for 10 min, 1, 2, and 12 hours. Particles were washed (10x10 mL) to produce **17**. Washes were assessed for FITC leaching and particles were analysed qualitatively by fluorescence (Ex 485 Em 520) (Appendix I, Figure 79) and Bradford assay. Microparticles formulated using commercial PCL were used as a control.

3.5. Transforming Growth Factor-β Conjugation

3.5.1. Transforming Growth Factor-β1 and Transforming Growth Factor-β3 Characterisation

TGF-β1 and TGF-β3, as purchased from PeproTech, were characterised by LC-MS and MALDI using the methods described above. Expasay protparam was used to calculate exact protein mw. TGF-β1 and TGF-β3 (10 µg) were reconstituted as per manufacturers guidelines in water (100 µL, 4 µM) for TGF-β1 and 5 mM citric acid (100 µL, 4 µM) for TGF-β3. Aliquots of these solutions were taken to make individual samples diluted 1/10 at a final concentration of 0.4 µM. LC-MS and MALDI-TOF analysis were carried out on samples of the stock protein at concentrations of 4 µM for LC-MS and 0.4 and 4 µM for MALDI-TOF.

3.5.2. Sodium Dodecyl Sulfate–Polyacrylamide Gel Electrophoresis

0.1 mM dibenzocyclooctyne-PEG4-NHS in PBS (2 µL, 0.2 nmol, pH 7.4) was reacted with 0.4 µM TGF-β1 and TGF-β3 (10 µL, 0.04 nmol) for 2 h at 0°C. After reaction the sample was purified using a viva spin desalting column producing compound **20**. The resulting conjugate was analysed by SDS-PAGE gel electrophoresis. The resolving gel was 15% acrylamide (3.5 mL), 1 M tris buffer (2.8 mL, pH 8.8), milliq water (1 mL), 10% SDS (75 µL), 10% ammonium persulfate (50 µL) and TEMED (25 µL). The stacking gel was 15% acrylamide (1.7 mL), 1 M tris buffer (1.25 mL), milliq water (7 mL), 10% SDS (100 µL), 10% ammonium persulfate (75 µL), and TEMED (25 µL). The gel was run for 50 mins at 180 mV in running buffer (1 X SDS, 30 g tris, 144 g glycine). 10 µL of each sample was mixed with loading dye (1:1) and 10 µL of this was loaded into each well. The gel was stained with Coomassie blue stain (30 min) and destained overnight (methanol:acetic acid:H_2O, 2:1:7).

3.5.3. Transforming Growth Factor-β and Bovine Serum Albumin Conjugation to Polycaprolactone-Azide Microparticles (22 & 23)

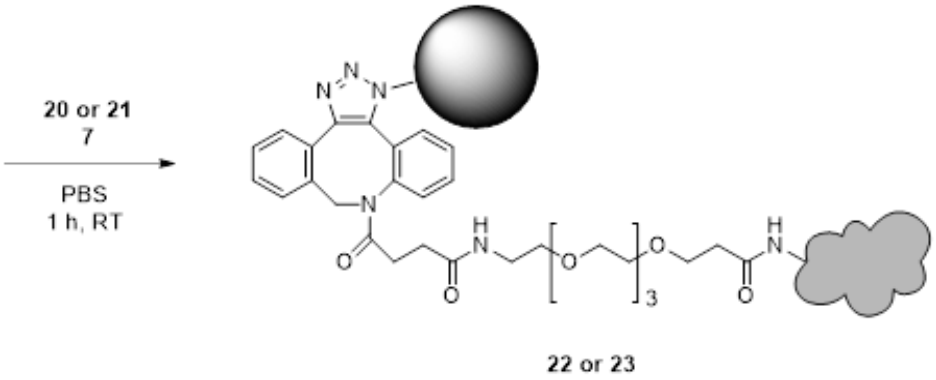

0.4 μM TGF-β1 and TGF-β3 (100 μL, 0.04 nmol) was reacted with 774 μM DBCO-PEG4-NHS (42 μL) and left to react overnight at 0°C. After reaction the solution was purified using a zebra spin column to produce compound **20**.

3 μM BSA (0.192 mg, 0.15 nmol) dissolved in PBS (1 mL) was reacted with 774 μM DBCO-PEG4-NHS (2.6 μL) and left to react overnight at 0°C. After reaction the solution was purified using a zebra spin column to produce compound **21**.

Aliquots of compound (**20**) or (**21**) (75 μL) were diluted in PBS (75 μL) to make working solutions (150 μL). PCL-N_3 microparticles (**7**) (5 mg, 0.22 nmol) were mixed with either BSA (150 μL) or TGF-β (150 μL) working solutions and left to react for 1 h, at RT whilst shaking. After reaction, microparticles (**22 or 23**) were washed with water (7x150 μL) and Micro BCA was carried out to determine presence of protein. Washes were collected and analysed using Micro BCA assay to ensure adequate washing steps.

Chapter 5: Industrial Translation

1. Introduction

This project was supported with an ICASE award to encourage collaboration and understanding between research academics and industrial partners. This award was in partnership with Neotherix Ltd a regenerative medicine company that specialises in tissue regeneration and bioresorbable scaffolds for repair. Dr Mike Raxworthy, was the industrial supervisor responsible for providing training and insight into the clinical translation of academic research. This was facilitated by a three-month placement at Leeds university undertaking a course in clinical translation; “Business and entrepreneurial skills training for medical technology” (MedTech Best). During this course, talks were given by industrial leaders, and informal interviews were held to gain insight into the process of clinical translation and the progression of academic research into a commercially available product. Industrial specialists included;

- A chief commercial officer
- An operations director
- A chief executive officer
- An investment director
- A programme manager in an enterprise hub team at the royal academy of engineering
- An independent non-executive director
- A director of the institute of medial and biological engineering
- A professor of biomedical engineering

Additionally, an informal interview was held with Professor Simon Donell, a consultant orthopaedic surgeon, to gain insight into the practical applications of a regenerative product for tendon injury. This interview was also used to gain insight into the opinions of a potential customer and user of a tendon regeneration product. Invaluable information was gathered regarding what the customer, a surgeon, would want and need from a product for tendon injury and how the product would best be implemented as a treatment.

This course allowed for the design of a hypothetical product that would be taken from academic research and translated into something that was commercially available. The concept should consider throughout the process what steps would be necessary to progress the product through each stage of translation. The work described throughout the thesis until this point to develop a template microparticle drug delivery system for tendon regeneration was used as the foundation for a concept product to this end. The information gathered during the course was used to identify weakness in the work already carried out, and to understand future work that would be necessary to solidify the template microparticle drug delivery system as a commercial product.

2. Aim and Objectives

The aim of this three-month placement period was to gain understanding of the process of translating academic research into clinical products. The information gathered throughout the course was used to produce a literature review of the translational process. A hypothetical concept product for tendon tissue engineering was designed and analysed to understand its level of development at each stage of translation.

3. Introduction to Translational Science

The UK has an exceptional reputation for scientific health research. One of the major contributing factors to this is that it has an extensive network of funders from charities, health organisations, and the public sector.[239] Funding comes from a variety of sources with charities such as Wellcome Trust, Cancer Research UK (CRUK) and the British Heart Foundation (BHF) investing millions annually. As well as research councils such as the engineering and physical sciences research council (EPSRC) and biotechnology and biological science research council (BBSRC). Private businesses also have a role to play, with the pharmaceutical industry estimated to provide 25% of the UK's Research and Development (R&D) income from industrial investments. On top of this, the two largest public-sector funders are the Medical Research Council (MRC) and the Health Departments of England, Wales and Scotland. The funding invested is to

not only encourage and support research, and to advance the knowledge base, but to also see a return, and to produce tangible products that can enter the UK market and increase public health benefits.[239] In order for this to be a reality, scientific laboratory research needs to be translated into the clinics, and applied once there.

However, currently the majority of projects that receive funding are those carrying out basic laboratory research. Basic research is considered to be driven by a quest for knowledge and doesn't necessarily have an agenda to address a pressing clinical need, but rather to better understand the biological workings of health and disease. This is the most common research undertaken within university institutes. However, in order to produce a tangible product, which can be incorporated into the UK healthcare system to provide substantial health benefits to the population, the scientific research carried out must be translational.[239] Translational science is seen as a from "bench to bedside and back" approach to research.[240] In order for research to be truly translational it needs to be collaborative, combining the skills from a range of experts. These include, but are not limited to, laboratory scientists, industrial experts, clinicians, manufacturers, and regulatory bodies. It must be able to address an unmet clinical need, whilst being practical for use in a clinical setting and be attractive to funders and financiers and therefore be cost effective.[240] It is rarely possible for translation to be achieved by individuals alone. It is much more likely to be successful when a team is involved. Physicians are in the strongest situation to best identify unmet clinical needs of patients. Engineers and academic researchers are able to design and develop ideas into therapies that could be used for public health benefits but often lack the insight into what is practical for use. By combining these two expertise and bringing in further help from industrial experts who are able to attract the funding necessary to take a product through development to launch, then an idea has a better chance of becoming a commercial product.[241]

Translational science is still very much in its infancy and there are considerable hurdles to overcome in order to truly translate basic research. The progression from idea to profit is a complicated, complex, arduous and risky process. The

process is also long, with an average progression time from initial idea to product launch being approximately 7 years on average.[241] The pathway from idea generation through to market penetration for new technologies is riddled with obstacles throughout, especially in the field of biomedicine and biomaterials where these obstacles present themselves at every step.[242] Several factors have been identified as inhibitors to translation. One major contributing factor is a lack of communication between laboratory researchers and clinicians. Unfortunately, the current climate of research means that entire projects can be funded and carried through with limited contact with healthcare professionals who have the most insight into patients' needs and the knowledge of how a product would work practically in a clinical setting.[239242] Impacting this problem is the fact that medical professionals undertaking academic research are often de-incentivised due to appraisals being carried out on either research productivity or clinical research but not often both, resulting in academic research partnerships being an unattractive prospect to the majority of medical professionals.[239] Similarly, within academic research, recognition is predominantly in the form of published articles in prestigious journals. Journals with excellent reputations and high impact factors such as Nature and Cell tend to be addressing a broad audience. Translational medicine, due to its very nature tends to serve a niche market and as such this research does not make it into aforementioned journals, therefore limiting its appeal to academic researchers.[239] Perhaps the biggest hurdle to translation science is finance. Basic science receives the biggest proportion of funding, taking over two thirds of government funding compared to translational projects. Additionally, in order to translate basic research, complex and lengthy clinical trials are necessary, funding is needed to secure intellectual property and high standards of efficacy and safety must be demonstrated in order to receive regulatory approval. This means that the whole process is exceedingly expensive.[239] Figure 54 shows the translational pathway for new technologies and highlights the two main areas where translation gaps occur, and where most projects fail.

Figure 54: Translation pathway from basic research to product delivery. The translational gaps that occur during the process are highlighted.[239]

Although this process is intimidating and the risk of failure is much higher than the chances of success, it is necessary for any individual aiming to commercialise their research to fully understand the necessary requirements essential for translation.[242] Herein this chapter aims to identify the key processes, stages and milestones that must be met to take academic research through the process of translation, and to become a commercial product that can be used from day to day in a clinical environment. Academic researchers, industrial specialists and medical professionals wanting to thrive in commercialisation need to understand these processes in depth, including how to source financial help, protect their intellectual property and analyse the market in which their product will be offered and is projected to penetrate. Specific examples will be given, in reference to the body of work carried out in the previous chapters of this thesis as a hypothetical product to be taken to market, to demonstrate and highlight the pathway to commercialisation from academic research.

3.1. A Hypothetical Injectable Delivery System for Tendon Regeneration

This thesis has described attempts to produce a microparticle delivery system for the regeneration of tendon tissue via the conjugation of proteins to polymeric microparticles. For the purpose of explaining the processes required to commercialise academic research an ideal product based on these initial findings has hypothetically been developed. The product detailed below will be used throughout this chapter to highlight the decisions that academics would need to make at each stage of the development pathway to translate their research.

The ideal product is a slow release injectable solution containing microparticles as the delivery vehicle and TGF-β protein as the payload. The protein is loaded onto the surface of the microparticles so that its release is controlled and consistent over time to allow for the gradual regeneration of tendon tissue. The ensuing healing process results in tissue that is comparable to pre-injured counterparts and identical to tissue formed in foetal development. Due to tissue remodelling the healing process results in a reduction of surgical re-ruptures and pain associated with tendinopathy and results in patients regaining mobility after injury. The product is predominantly aimed at achilles tendinopathy and rupture. The product has two uses: 1) It can be injected via ultrasound guided injections to patients presenting with pain and inflammation before rupture has occurred. 2) It can be applied after surgical intervention following a rupture.

Here on in this injectable delivery system for tendon repair will be referred to as “the product” when giving specific examples of the route to translation.

4. Development

Once initial conceptualisation has occurred the development process must begin. Translational science has a considerable amount of hurdles that the individuals interested in commercialisation must overcome.[239] Figure 55 shows the processes that the project must go through during design and development to ensure that commercialisation is always at the forefront. Design of a product should begin with the identification of a pressing unmet clinical need, and concurrently the identification of the user’s needs.[241] Once this is well established and understood the product can begin to be designed and take form. During the design process it is essential to continually review and analyse the project to ensure that it is still meeting the users’ needs and will remain practical once commercialised.[241]

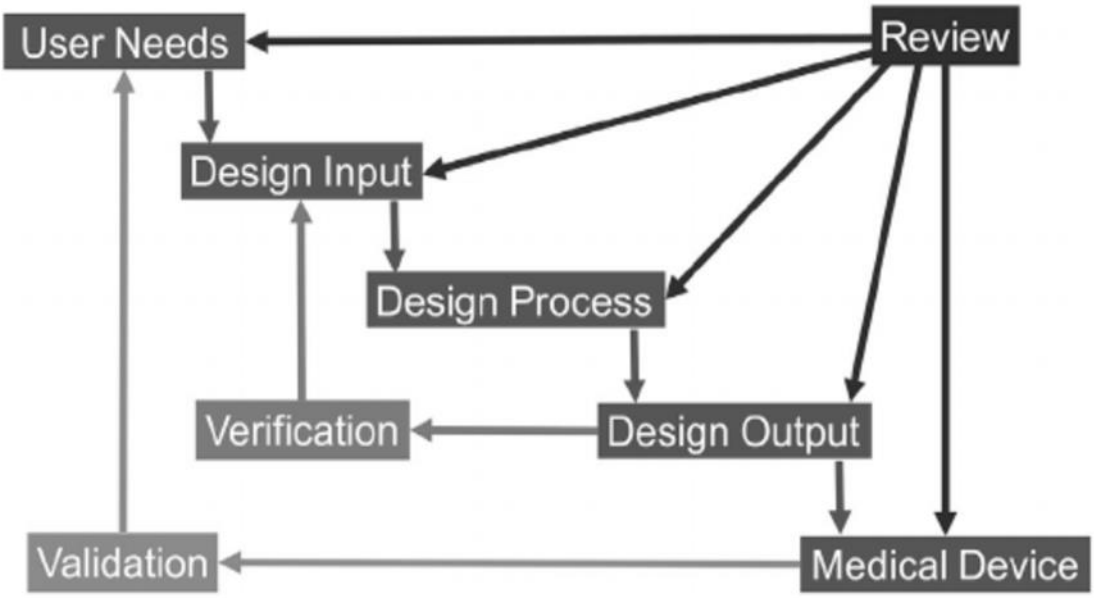

Figure 55: Illustrative representation of the cyclical process of development when designing a clinical device.[241]

The design and development processes are not linear; it is cyclical with continued assessments of project progress and evaluation of whether the projects criteria are being met. The best way to increase the chances of success is to continually evaluate if the project is performing well and meeting agreed objectives. The result of continual evaluation throughout the design process is a smoother route to market with fewer mistakes, and allows for the termination of projects likely to fail before large investments have been squandered.[243] There are several tools that can be used in order to do this, by utilising these systems the three major hurdles faced by new technology development: performance, schedule and budget will be well managed.[244]

4.1. Stage Gate Review

Stage Gate systems break down the entirety of the innovation process into smaller segments that are predetermined to allow for evaluation of the projects progress. At each Stage there are clearly defined outputs and criteria, agreed at the previous Gate review, that need to be met. It is a conceptual model that details the blueprints of a successful product launch. It allows for failure of the project at any Stage and a decision to terminate before resources are spent.

The pathway is separated into ‘Stages and Gates’. Stages act as the “doing” period where deliverables are met, and development is carried out, and the Gates act as Kill/Go/Hold checkpoints only allowing the product to progress to the next Stage if it is ready to do so. A typical Stage Gate system is comprised of between four and seven Stages. At the entrance to each Stage there is a Gate, at the Gate a review process and an evaluation of the previous Stage is implemented.

The Gate allows for the project managers and stakeholders to ensure that the project is on target to meet the defined outputs and that all milestones have been fulfilled. It also allows for transparency, with failures of the project progression clearly being highlighted at each Gate. This stops the project from progressing too far down the process before problems are identified. Each Stage is more expensive than the previous one, due to progressively increasing investment required with the increased complexity of the Stage. Therefore, by evaluating the project at the Gate before passing to the next Stage there is no wastage of funds on a project viewed to have a high risk of failure. This means that risk is managed and projects least likely to succeed are terminated early on when spending is minimal. In addition, the Stage Gate system allows for activities to be carried out in parallel. This means that the project is efficient with more being achieved in a shorter timeframe. Inherently this means that all members on the project need to be communicating effectively with one another. Additionally, by having Gates to each Stage, project managers can implement certain criteria that if met will instigate another review. Project managers can, for example, impose a maximum spend or a specified time allotment, if these are exceeded the project can undergo another formal review. Figure 56 shows a typical Stage Gate process from idea to post launch.[243]

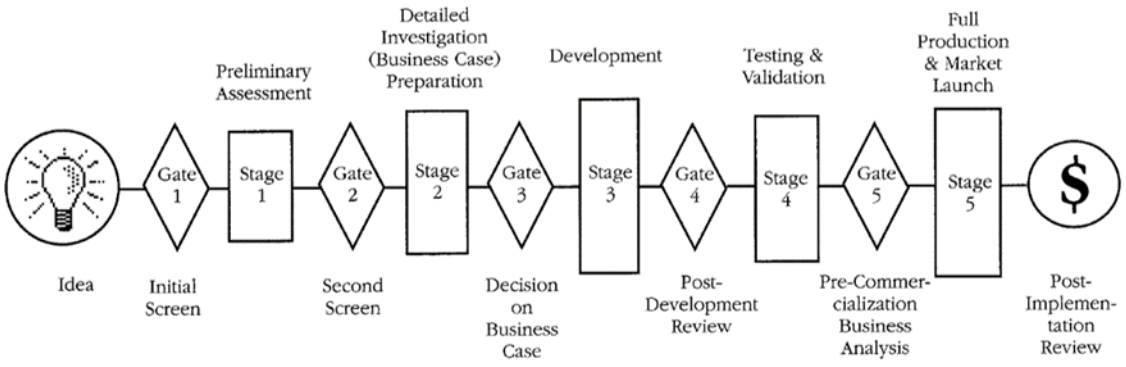

Figure 56: A typical Stage Gate process. A Gate at the entrance to each Stage from idea generation to full product launch must be past to continue development.[243]

The Stage Gate system is broken down into separate segments and it should be initiated upon idea generation. Initial screening can then be carried out to assess the feasibility of the project, and to establish the unmet clinical need that the project will be addressing. The second Stage is definition, this is the final Stage before product development begins, during this Stage the project managers should be convinced of the attractiveness of the project including market evaluation before funds are spent. At this Stage the design team should have an understanding of what the product needs to deliver and the desires that have been expressed from the customer research. Additionally, there should be an understanding of the competition within the market and if the product is likely to be able to compete. Gate 3 signifies the last point in the process where the project is still able to be terminated without suffering heavy loss of finances. Stage 4 is concerned with ensuring the product is viable, that it is able to perform and that any complications during development have been ironed out. Gate 5 is the last “kill” check point before full commercialisation of the product. The major driving factor for the project is the financial projections for the product and as such thorough market research and market testing is critical here. Post implementation review allows for the project managers to look back on the project progression and learn from any problems or successes that may have arisen during the process.[243]

4.1.1. Stage Gate Assessment for an Injectable Tendon Regeneration Product

The hypothetical concept product would be considered to have passed through to stage gate 2 and 3. An idea has been generated by the project manager and initial screening has been undertaken to assess the feasibility of the idea. This includes a literature research and preliminary data to highlight the presence of a niche in the market. Preliminary assessment has been carried out to ascertain the attractiveness of the product, funding has been obtained in the form of a grant to allow for academic research to begin. Investigations into the project and product development have begun through four years of academic research. Development of the product is however still very much in its infancy and the true feasibility of the product has not been realised. It is possible at this stage that the design and development of the product could prove impossible and therefore the project would be terminated and not pass through any more stages. More funding is still necessary to develop the project further, and the development is still focused within an academic setting.

4.2. Technology Readiness Levels

During the 1970s the National Aeronautics and Space Administration (NASA) introduced technology readiness levels, as a way of assessing the maturity of emerging technologies. In 1995 the technology readiness levels (TRL) was improved with definitions given at each Stage with accompanying examples. The original scale was proposed by Mr Stan Sadin and slowly over the course of a few decades the TRL scale developed and was redefined until it was accepted worldwide in 2005.[244] Companies can user the TRL scale in order to assess the development of a new technology and to ensure that the product is maturing at an acceptable rate. The original scale goes from 1-9 and explains the degree of maturation a technology should have gone through if it is to be a commercial product. The scale is highly adaptable and differs from subject to subject. The basic principles are the same, with TRL 1 being the least mature level and TRL 9 being product launch. Some systems also include a TRL 10 which considers evaluation of the product post launch. Figure 57 shows a typical TRL scale.[244]

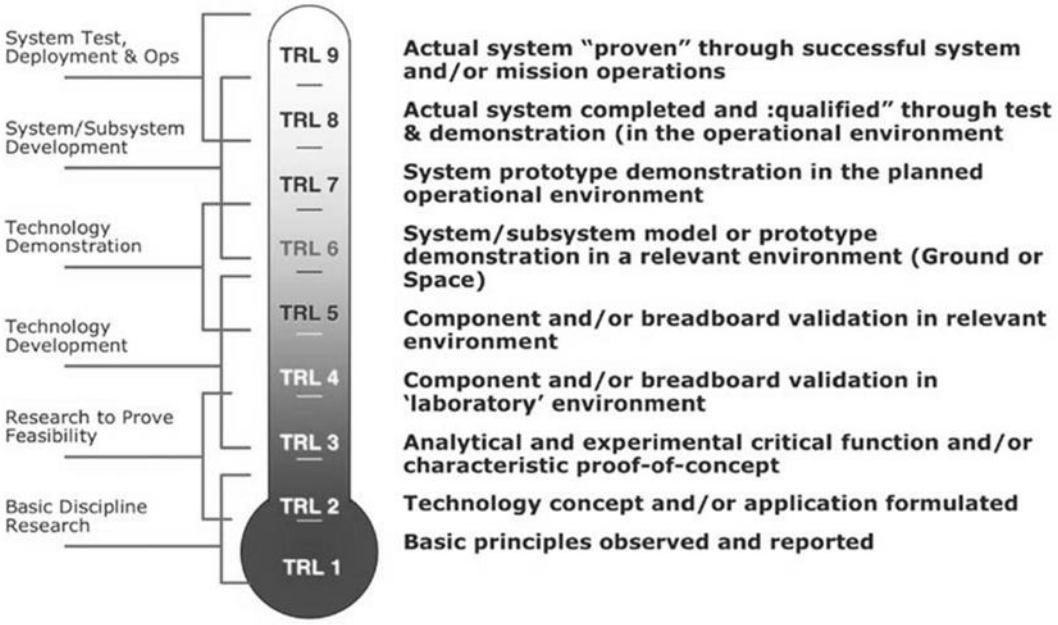

Figure 57: Technology readiness level scale.[244]

TRL 1 is the beginning point of the TRL scale, at this Stage the new technology is in its infancy, no experimental data is present to validate the hypothesis and the project is speculative. At TRL 2 again the project is still speculative, with potential applications for materials discussed. At this Stage it is likely that there are many avenues the project could potentially take, with lots of ideas being generated.[245] At TRL 3 active R&D is initiated to prove the hypothesis for material application. The work carried out between TRL 3 and 4 should be designed to establish proof of concept. At this Stage all work carried out comes with relatively low costs, unique to the project, and can easily be funded through basic scientific investments such as research councils.[244]

TRL 4 and onwards begins the Stages where collaborative research is likely. Funding from these Stages is likely to come from formal avenues such as industry specialists or venture capitalists. The work carried out at TRL 4 is focused around the validation of the project concept; it is to prove that the technology will work in the hypothesised applications. At this Stage it does not have to be demonstrated as an entire technology but could be considered as pieces that individually perform the desired function or exhibit preferred effects. The costs at this Stage are low in comparison to the overall cost of translation; however, they are significantly greater than the funding needed in previous Stages.

TRL 5 sees the product prototype tested within a similar environment to that in which it is intended to be used, and if successful proof of concept can be said to be successful. The technology or product needs to be highly reproducible and the applications of the product need to be tested in a realistic environment.[245245] By this Stage the research is most likely to be carried out in an industrial laboratory.[244]

TRL 6 is the last step of validation of the product before it enters clinical trials and the product is demonstrated to have successful applications in its intended environment. At this Stage a demonstration of a model prototype needs to be successful to truly be at TRL 6.

By TRL 7 clinical trials should have begun for biomedical technologies. The clinical trials need to achieve a positive result to progress beyond this Stage. TRL 7 incurs one of the largest costs before product launch, needing two times the amount of investment than it takes to reach all other previous Stages.[245]

TRL 8 marks the end of testing of the product and is the beginnings of the process of product launch. Assuming all other TRL levels have been surpassed the product should not fail at TRL 8. To achieve TRL 8 it is always necessary to acquire formal funding from industrial investments or venture capitalists. TRL 8 is the most expensive of all the Stages and is 10 times greater than all previous TRLs combined, this is due to the high manufacturing costs associated with this Stage.

TRL 9 represents the product launch and penetration of the market. At this Stage any problems that may have arisen post launch will be fixed and it marks the end of the development process.[245] Throughout the TRL process assessments should be carried out to confirm that TRL Stages have been met and that the technology is maturing at an acceptable rate. During TRL assessments the hurdles that the project needs to overcome to achieve the next TRL status should be clearly defined. During TRL assessments it is also important for project managers to fully evaluate the risks that the project may face at each TRL Stage.

4.2.1. Technology Readiness Levels Assessment for an Injectable Tendon Regeneration Product

If the product were to be assessed at the point in which the body of this thesis leaves the work, it would currently sit between TRL 2 and TRL 3. Basic R&D has been carried out and publications, as well as consultations with clinicians, have proven that there is an obvious unmet clinical need for the regeneration of tendon tissue. Some experimental proof has been generated for the feasibility of a particle system conjugated to protein, using model proteins. This could be considered the first prototype although its applications have not yet been validated.

To reach TRL 4 more of the elements of the final product would need to be introduced. The particle protein conjugation should be prepared into an injectable formulation and the fluid mechanisms of this tested. The product would need to undergo evaluation for protein release to ensure that the hypothesised affect is feasible. Once this has been achieved the particle system would then need to prove feasibility within a cellular environment to fully prove the concept. Additional tests such as the shelf life would need to be tested. The product would then need to be tested in a similar environment to that in which it is intended. This could be achieved by carrying out tests in small animal models, then moving to larger animals that have tendons most similar to humans, such as horse.

From this work the project managers would then be able to carry out formal assessments to determine if the project is still feasible and if the results are corroborating the hypothesis. This would allow for identification and risk management. Following this a detailed plan of action could then be implemented to prepare for safety, efficacy trials and clinical trials to achieve higher TRLs and eventually product launch.

5. Market Analysis

Market analysis is one of the most crucial Stages of new product development. Poor market research has regularly been documented as the largest

contributing factor of product failure.[243] Market analysis encompasses more than just where the product sells. It is the detailed research that needs to be undertaken into who the customers are going to be, what their wants and needs from the product are, what the market size and growth is like, what regulations apply, what and who the competition is and how the new product is superior. Understanding the customer is just as important as understanding the underpinning science behind the product and how it produces its effect. The product must be acceptable to the customers who are going to be using it. In the case of medical devices this could be physicians or any other health care professionals. The device ideally should fit in with standard practices already established within the environment to.[243]

5.1. Market Analysis for an Injectable Tendon Regeneration product

The market for tendon injury can come under orthopaedic soft tissue repair. Based on a report by Grand View Research, Inc. the soft tissue repair market is estimated to be worth over $9.39 billion by 2024. The progression of the market is focused around minimally invasive procedures that minimize the potential disturbance to muscles and tendons and result in a more natural healing response. The market of orthopaedic soft tissue repair is still quite broad and can be broken down into the specific sections including, but not limited to: cruciate ligament repair, knee surgeries, hip joint procedures and posterior soft tissue.[246] The soft tissue repair market includes muscles, ligaments, tendons, fibrous tissue, skin, synovial membrane, nerves and other tissue required to protect organs and enable movement by supporting bones and the body. This means that tendon injury is only a small section of this market and when looking at market value and trends for soft tissue injury this must be taken into consideration. Tendon injury can also fall within the market of sports medicine. It is estimated that this market will reach $8.24 billion by 2022 with a compound annual growth rate (CAGR) of 7.4%.[247]

Market size and value can also be determined by the occurrence of injury. Of the multitude of tendons present in the body, flexor and extensor tendons of the hand, Achilles tendon and rotator cuff tendons are the most frequently injured. These account for 4.83 and 18 per 100,000 injuries per year for flexor and

extensor tendons respectively, 18 per 100,000 per year for Achilles and 3.73 per 100,000 per year for rotator cuff.[248] Additionally, of the 32.8million reported musculoskeletal injuries in the US, 45% involve tendons and ligaments.[2] Tendon injury is the most frequent soft tissue injury in orthopaedic surgery.[6]

5.2. Drivers to the Market

When considering market analysis, it is also important to understand what drivers there are to the market. Tendinopathy results from a large number of contributory factors including age, occupation and physical training.[22] A change, or an increase in risk factors associated with tendinopathy will therefore inevitably become a driver for tendon injury, which will in turn drive innovation. Age is a risk factor for degenerative tendon tissue, this means that an ageing population would therefore infer an increase in tendinopathy patients.[249] Rotator cuff tendon tendinopathy predominance, as an example, increases with age to 40% in patients aged 70 or above.[33] Tendinopathy is currently estimated to affect 25% of the adult population, at some point in their lives, with this figure expected to rise with life expectancy. According to the Office for National Statistics (ONS) life expectancy for men and women is at an all-time high with expectancy from birth at 79.1 and 82.8 years for men and women respectively, in the UK.[250] Therefore an aging population can be considered as a major driver for innovation in orthopaedic surgery.

Education and awareness of health and obesity will result in an increase in physical activity and high load activities such as gym usage, which are expected to lead to an increase in tendinopathy, and thus innovation. A 2017 report on the state of the UK fitness industry revealed that the industry is continually growing, which is a further driver for innovation. With 9.7million fitness members in the UK, the use of gyms is at its greatest rate at 14.9%, with 1 in 7 people a member of a gym. This market is estimated to increase 4.6% in the number of facilities, 5.1% in the number of members and 6.3% in market value.[251]

Drivers of innovation and markets can also be affected by local policy, interest and trends in the area. In the US, a growth in the market can be attributed to an increase in the popularity in physical activity and an increase in awareness of

sports. In Canada the market growth can be attributed to support from government initiatives.[247] It is becoming better understood the impact tendon injury such as tendinitis has on an athlete's performance, coupled with a growing awareness of treatment options available will result in an increase in market growth.[252]

5.3. Competition in the Market

Another factor that must be extensively researched when carrying out market analysis is the competition. According to a study published by Grand View Research Inc, the largest and dominant companies in the market of orthopaedic surgery and soft tissue repair are Stryker, Zimmer Biomet, Smith & Nephew, Arthres inc, CONMED and DePuy Synthes, Inc.[246] There are several products on the market that range from sutures, reinforcement devices, allografts, autologous injections and many more. Stryker provides a soft tissue repair matrix called TissueMend; an acellular collagen membrane made from foetal bovine dermis. It serves as a scaffold for cellular ingrowth and is remodelled by the body's own tissue. It provides a biologic environment to help the tissue mend and fortify the tissue until the healing process is complete. It can be used for re-enforcement of rotator cuff, patella, Achilles, bicep, quadriceps and other tendons. The product combines physical strength and thickness with biological properties that encourage cell and blood vessel penetration. A second product offered by Stryker is the AlloWrap DS an amniotic membrane used for the protection of tendon. It is a dual layer graft that is processed so the epithelial layer is facing outwards on both sides of the graft.[253] Additionally Stryker is able to offer allografts of tendon tissue for single use. They are able to provide an individualised service for each customer and exclude donors with conditions or behaviours that may affect the tissue quality, such as age. They offer tendon allografts for Achilles tendon, semitendinosus, gracills tendon, anterior tibialis tendon, posterior tibialis tendon and poroneous longus tendon.

Zimmer Biomet is able to provide sutures of superior quality that eliminate suture fray and breakage. The Maxibraid suture has a high tensile strength and a smooth feel as well as outstanding flexibility and pliability.[254] Additionally, they

are able to supply surgical aids such as the Toggleloc which can be used for tendon repair at the tendon-bone-tendon interface. It is resistant to slippage, requires simple surgical techniques and minimal implementation.[255] Smith & Nephew provide surgical augmentation devices such as the Endobutton and the Biceptor, both for the repair of the biceps tendon. Neoligaments (xiros) focus on the production of suture tapes that can be used to augment repair and provide mechanical stability as well as holding the ruptured tendon in position. They manufacture Poly-tapes which are open weave mesh implants and Ortho-tapes which are exceptionally strong and narrow sterile tapes. They also provide implants that can provide mechanical strength to the tissue during repair. The Leeds-Kuff Patch is a permanent implant that can provide stability and encourage tissue ingrowth throughout the healing process.[256] OrthoCell is a company which offer personalised injections of autologous tenocytes that is used for damaged or degenerate tendons. This treatment directly addresses the root cause of the pathology and uses a process by which tendon cells are harvested from the patient and re-injected after expansion using ultrasound guided methods.[257]

5.4. Value Proposition

A value proposition is a method of understanding what potential customers want from a product on the market and what the product should have to meet, and then surpass, expectations. Value propositions aim to concisely and effectively communicate the advantage a product has over others in the market by specifically highlighting its unique value. It aims to put the value of the product in the context of the customer's viewpoint with an understanding of what they want to gain rather than the inventors telling the customers what they should want from the product. A good value proposition is one in which the needs, desires and pains of the customer are fully understood and addressed in a way that makes it obvious to the customer the huge benefits they stand to gain from the product. Additionally, a value proposition allows the customer base to be broken down and categorised so that several different customers can be identified. This allows the project managers to see what the product has to offer specifically for each individual subset of customer populations. This is important

particularly for medical devices because the wants and needs of the customer will be different depending on if the customer is a surgeon, a patient or manager responsible for purchase requisitions.

The value proposition is divided into features and benefits, and wants and needs. When analysing customer information a need is something the product must be able to do to actually solve the problem it is intending to address. A want is something that the patient is able to gain above simply solving the problem and therefore goes above and beyond the customer's expectation. Value propositions have only gained traction in the last 30 years and there is no set standard of the best way in which they should be carried out.[258]

5.5. Value Proposition for an Injectable Tendon Regeneration Product

When considering an injectable product for the regeneration of tendon injury several potential customers have been identified. The customer base can be divided into those who will directly receive the treatment and therefore receive the intended health benefits, and those who will use the product. The main beneficiaries of this product are patients who are suffering from degenerative tendinopathy of the tendon and those who have experienced ruptures undergoing surgical repair. The primary users would be surgeons and radiologists. Radiologists would be able to administer the treatment via ultrasound guided injections using common practice that is already in place within clinics. Secondary benefiters would be GP's, physiotherapists and the National Health Service (NHS). Surgeons will be able to provide better repair to tendon tissue and thus providing better care for their patients. Surgeons will be able to give the injection at the point of surgical repair and would not need to change any operating procedures to administer the product. Surgeons should see a decline in the number of repeat surgeries needed to treat the same condition in a patient due to the decrease in re-rupture rate. The number of prescriptions for pain management medication would also decrease as the patients are able to be treated quicker with ensuing shorter rehabilitation times. Specific value propositions were generated for the product for each potential customer considered. Figure 58 shows a detailed example with surgeons given as the assessed customer.

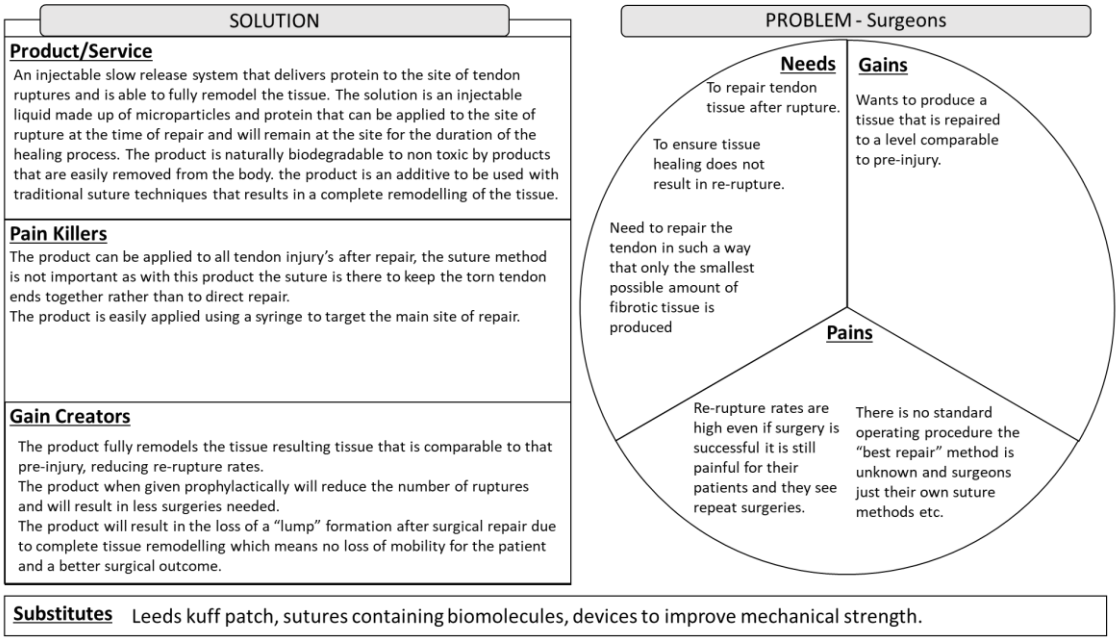

Figure 58: Value proposition for tendon injury. For this example, specific attention was paid to surgeons as customers and the gains and pains associated specifically with them.

6. Conclusion

In conclusion, the process of innovation and translation is a long and expensive process with many obstacles along the way. In order for academic researchers to take basic scientific research through to commercialisation they need to fully understand the necessary processes. Only through the development of an active hub between researchers, industrial experts and physicians will medical technologies stand the best chance of launch to market. Individuals involved need to be aware of the regulatory enforcements that devices must adhere to, as well as understanding how to protect their intellectual property rights. The best chance for innovation success is to intimately understand the unmet clinical need the product is addressing as well as the customer's needs at the very beginning of product development and to keep this at the forefront throughout the project. With the emergence of better access to technology resource centres in the universities and a collaborative culture of research more products will be able to make it from bench to bedside.

Overall Conclusions and Future Work

1. Overall Conclusions and Future Work

This thesis set out to identify a polymeric microparticle drug delivery system that could be used as a template for the delivery of proteins for the repair of tendon regeneration. From the beginning of the project a final application in a clinical setting was considered which helped to shape many of the choices and experiments tested.

Overall, this thesis has shown the successful synthesis of a PCL-N_3 polymer. This polymer has successfully been formulated into microparticles. Microparticle size and uniformity can be tightly controlled by altering the process parameters used at production. These microparticles have been shown to successfully conjugate to a DBCO linking unit through the use of azide/alkyne click chemistry. This reaction was shown to be quick occurring in as little as 10 minutes. Furthermore, the successful conjugation of model proteins HSA and BSA to PCL-N_3 microparticles through the use of DBCO-PEG_4-maleimde and DBCO-PEG_4-NHS linkers respectively has been shown. This proves that the delivery system is possible, and these methods can be followed as a template for other proteins. DBCO-PEG_4-maleimide chemistry can be successfully utilised for proteins containing a free thiol. Similarly, DBCO-PEG_4-NHS can be used for protein without a free cysteine, but abundant in primary amines, such as those found on lysine side chains. Conjugation of therapeutic protein TGF-β proved problematic requiring multiple optimisations. The results of the conjugation reaction of TGF-β to PCL-N_3 microparticles are promising, but more work is needed to prove this conclusively.

The three months spend working on the industrial CASE studentship allowed insight into the laborious and multistep process required to take academic research into a commercial setting. This has provided detailed information of the meticulous planning that is needed when considering academic research, with the ultimate aim of commercial application.

Overall the work described in these five chapters, shows promise as a template drug delivery system, future work could be carried out to build upon the

foundations described within the thesis. DBCO is available with a large range of functional groups present, and therefore additional work could be carried out to identify the most appropriate conjugation method for TGF-β. Additionally, the sheer number of growth factors relevant in the healing process of tendon injury allows for further identification of a different therapeutic protein for conjugation. If the structure of the protein is known, information about the available functional groups can be used when choosing a DBCO linker for conjugation. Once it is possible to conjugate a protein of interest to the microparticle delivery system, further tests can be carried out into its effect on stem cells or tenocytes for the full potential as a regenerative delivery system to be realised. Furthermore, experiments to prove that this delivery system is controlled, giving information of the release rates of the protein is needed. To meet the main aim of an injectable delivery system, work could be carried out on the microparticles to formulate a gel, or liquid solution that could fit small gauge needles for a minimally invasive treatment option.

References

1 A. Atala, D. J. Irvine, M. Moses and S. Shaunak, *MRS Bulletin*, 2010, **35**, 597–606.

2 C.-F. Liu, L. Aschbacher-Smith, N. J. Barthelery, N. Dyment, D. Butler and C. Wylie, *Tissue engineering. Part B, Reviews*, 2011, **17**, 165–76.

3 P.-O. Bagnaninchi, Y. Yang, A. J. El Haj, N. Maffulli and U. Bosch, *British Journal of Sports Medicine*, 2007, **41**, e10–e10.

4 S. I. Correia, H. Pereira, C. N. Van Dijk, J. M. Oliveira and R. L. Reis, *Journal of the royal society interface*, 2014, **11**, 2–20.

5 A. Jain and R. Bansal, *Journal of Pharmacy and Bioallied Sciences*, 2015, **7**, 188.

6 M. Rickert, H. Wang, P. Wieloch, H. Lorenz, E. Steck, D. Sabo and W. Richter, *Connective Tissue Research*, 2005, **46**, 175–183.

7 D. Gaspar, K. Spanoudes, C. Holladay, A. Pandit and D. Zeugolis, *Advanced Drug Delivery Reviews*, 2015, **84**, 240–256.

8 D. Docheva, S. a Müller, M. Majewski and C. H. Evans, *Advanced drug delivery reviews*, 2014, **84**, 222–239.

9 a. J. Lomas, C. N. M. Ryan, A. Sorushanova, N. Shologu, A. I. Sideri, V. Tsioli, G. C. Fthenakis, A. Tzora, I. Skoufos, L. R. Quinlan, G. O'Laighin, A. M. Mullen, J. L. Kelly, S. Kearns, M. Biggs, A. Pandit and D. I. Zeugolis, *Advanced Drug Delivery Reviews*, 2015, **84**, 257–277.

10 K. W.-H. Lo, T. Jiang, K. a Gagnon, C. Nelson and C. T. Laurencin, *Trends in biotechnology*, 2014, **32**, 74–81.

11 A. Moshiri, *Journal of Sports Medicine & Doping Studies*, 2013, **03**, 126.

12 A. W. Clarke, F. Alyas, T. Morris, C. J. Robertson, J. Bell and D. a Connell, *The American journal of sports medicine*, 2011, **39**, 614–23.

13 A. Wang, W. Breidahl, K. E. Mackie, Z. Lin, A. Qin, J. Chen and M. H. Zheng, *The American journal of sports medicine*, 2013, **41**, 2925–32.

14 S. Thomopoulos, M. Zaegel, R. Das, F. L. Harwood, M. J. Silva, D. Amiel, S. Sakiyama-

Elbert and R. H. Gelberman, *Journal of Orthopaedic Research*, 2007, **25**, 1358–1368.

15 U. G. Longo, A. Lamberti, N. Maffulli and V. Denaro, *British medical bulletin*, 2011, **98**, 31–59.

16 S. J. Warden, *British Journal of Sports Medicine*, 2007, **41**, 232–240.

17 A. Notarnicola and A. Notarnicola, 2012, **2**, 33–37.

18 P. Sharma and N. Maffulli, *Journal of Musculoskeletal Neuronal Interaction*, 2006, **6**, 181–190.

19 P. Kannus, *Scandinavian Journal of Medicine and Science in Sports*, 2000, **10**, 312–320.

20 J. H.-C. Wang, *Journal of biomechanics*, 2006, **39**, 1563–82.

21 R. K. W. Smith, N. J. Werling, S. G. Dakin, R. Alam, A. E. Goodship and J. Dudhia, *PloS one*, 2013, **8**, e75697.

22 A. Hoffmann and G. Gross, *International orthopaedics*, 2007, **31**, 791–7.

23 G. Yang, B. B. Rothrauff and R. S. Tuan, *Birth Defects Research Part C: Embryo Today: Reviews*, 2013, **99**, 203–222.

24 G. Riley, *Nature Clinical Practice Rheumatology*, 2008, **4**, 82–89.

25 S. Violini, P. Ramelli, L. F. Pisani, C. Gorni and P. Mariani, *BMC Cell Biology*, 2009, **10**, 29.

26 B. Chen, B. Wang, W. J. Zhang, G. Zhou, Y. Cao and W. Liu, *Biomaterials*, 2012, **33**, 6086–97.

27 C. H. Jo, J. E. Kim, K. S. Yoon and S. Shin, *The American Journal of Sports Medicine*, 2012, **40**, 1035–1045.

28 T. C. Keller, M. V Hogan, G. Kesturu, R. James, G. Balian and B. Chhabra, *Connective Tissue Research*, 2011, **52**, 353–364.

29 K.-M. Chan, S.-C. Fu, Y.-P. Wong, W.-C. Hui, Y.-C. Cheuk and M. W.-N. Wong, *Wound repair and regeneration : official publication of the Wound Healing Society [and] the European Tissue Repair Society*, 2008, **16**, 399–407.

30 M. D. Shoulders and R. T. Raines, *Annual Review of Biochemistry*, 2009, **78**, 929–958.

31 C. a Uysal, M. Tobita, H. Hyakusoku and H. Mizuno, *Journal of plastic, reconstructive & aesthetic surgery : JPRAS*, 2012, **65**, 1712–9.

32 S. Kuroda, N. Goto, M. Suzuki, K. Kaneda, K. Ohya, H. Shimokawa and S. Kasugai, *Journal of tissue engineering*, 2010, **2010**, 891049.

33 A. Bedi, T. Maak, C. Walsh, S. a Rodeo, D. Grande, D. M. Dines and J. S. Dines, *Journal of shoulder and elbow surgery / American Shoulder and Elbow Surgeons ... [et al.]*, 2012, **21**, 218–27.

34 A. Guevara-Alvarez and A. Schmitt, *Muscles Ligaments and Tendons Journal*, 2014, **4**, 378–385.

35 C. N. Manning, H. M. Kim, S. Sakiyama-Elbert, L. M. Galatz, N. Havlioglu and S. Thomopoulos, *Journal of orthopaedic research : official publication of the Orthopaedic Research Society*, 2011, **29**, 1099–105.

36 P. Sharma and N. Maffulli, *The Journal of bone and joint surgery. American volume*, 2005, **87**, 187–202.

37 P. P. Y. Lui, *Rheumatology*, 2013, **52**, 2116–2126.

38 R. J. de Vos, P. L. J. van Veldhoven, M. H. Moen, a Weir, J. L. Tol and N. Maffulli, *British medical bulletin*, 2010, **95**, 63–77.

39 G. Riley, *Rheumatology*, 2004, **43**, 131–142.

40 S. Thomopoulos, R. Das, S. Sakiyama-Elbert, M. J. Silva, N. Charlton and R. H. Gelberman, *Annals of Biomedical Engineering*, 2010, **38**, 225–234.

41 B. M. Andres and G. a C. Murrell, *Clinical orthopaedics and related research*, 2008, **466**, 1539–54.

42 H. M. Kim, L. M. Galatz, R. Das, N. Havlioglu, S. Y. Rothermich and S. Thomopoulos, *Connective tissue research*, 2011, **52**, 87–98.

43 S. Rawson, S. Cartmell and J. Wong, *Muscles, ligaments and tendons journal*, 2013, **3**, 220–8.

44 J. Chen, Q. Yu, B. Wu, Z. Lin, N. J. Pavlos, J. Xu, H. Ouyang, A. Wang and M. H. Zheng, *Tissue engineering. Part A*, 2011, **17**, 2037–48.

45 D. Deng, W. Wang, B. Wang, P. Zhang, G. Zhou, W. J. Zhang, Y. Cao and W. Liu,

Biomaterials, 2014, **35**, 8801–9.

46 J. Zhang, B. Li and J. H.-C. Wang, *Biomaterials*, 2011, **32**, 6972–81.

47 C.-H. Chen, C.-H. Chang, K.-C. Wang, C.-I. Su, H.-T. Liu, C.-M. Yu, C.-B. Wong, I.-C. Wang, S. W. Whu and H.-W. Liu, *Knee surgery, sports traumatology, arthroscopy : official journal of the ESSKA*, 2011, **19**, 1597–607.

48 T. Funakoshi, T. Majima, N. Iwasaki, N. Suenaga, N. Sawaguchi, K. Shimode, A. Minami, K. Harada and S. Nishimura, *The American journal of sports medicine*, 2005, **33**, 1193–201.

49 G. Walden, X. Liao, S. Donell, M. J. Raxworthy, G. P. Riley and A. Saeed, *Tissue Engineering Part B: Reviews*, 2017, **23**, 44–58.

50 D. Connell, a Datir, F. Alyas and M. Curtis, *British journal of sports medicine*, 2009, **43**, 293–8.

51 L. V Schnabel, M. E. Lynch, M. C. H. van der Meulen, A. E. Yeager, M. a Kornatowski and A. J. Nixon, *Journal of orthopaedic research*, 2009, **27**, 1392–8.

52 H. A. Awad, G. P. Boivin, M. R. Dressler, F. N. L. Smith, R. G. Young and D. L. Butler, *Journal of Orthopaedic Research*, 2003, **21**, 420–431.

53 E. E. Godwin, N. J. Young, J. Dudhia, I. C. Beamish and R. K. W. Smith, *Equine veterinary journal*, 2012, **44**, 25–32.

54 C. N. Manning, a. G. Schwartz, W. Liu, J. Xie, N. Havlioglu, S. E. Sakiyama-Elbert, M. J. Silva, Y. Xia, R. H. Gelberman and S. Thomopoulos, *Acta Biomaterialia*, 2013, **9**, 6905–6914.

55 A. Guercio, P. Di Marco, S. Casella, L. Russotto, F. Puglisi, C. Majolino, E. Giudice, S. Di Bella, G. Purpari, V. Cannella and G. Piccione, *Journal of Equine Veterinary Science*, 2015, **35**, 19–26.

56 V. Kishore, W. Bullock, X. Sun, W. S. Van Dyke and O. Akkus, *Biomaterials*, 2012, **33**, 2137–44.

57 S. Kobsa and W. M. Saltzman, *Pediatric research*, 2008, **63**, 513–9.

58 P. E. Heisterbach, A. Todorov, R. Flückiger, C. H. Evans and M. Majewski, *Knee surgery, sports traumatology, arthroscopy : official journal of the ESSKA*, 2012, **20**, 1907–14.

59 B. P. Chan, S. Fu, L. Qin, K. Lee, C. G. Rolf and K. Chan, *Acta orthopaedica Scandinavica*, 2000, **71**, 513–8.

60 G. Bosch, H. T. M. van Schie, M. W. de Groot, J. a Cadby, C. H. a van de Lest, A. Barneveld and P. R. van Weeren, *Journal of orthopaedic research : official publication of the Orthopaedic Research Society*, 2010, **28**, 211–7.

61 J. Kaux, L. Janssen and P. Drion, *Muscles Ligaments and Tendons Journal*, 2014, **111**, 24–28.

62 J. Y. Lee, Z. Zhou, P. J. Taub, M. Ramcharan, Y. Li, T. Akinbiyi, E. R. Maharam, D. J. Leong, D. M. Laudier, T. Ruike, P. J. Torina, M. Zaidi, R. J. Majeska, M. B. Schaffler, E. L. Flatow and H. B. Sun, *PLoS ONE*, 2011, **6**, e17531.

63 S. Zhao, J. Zhao, S. Dong, X. Huangfu, B. Li, H. Yang, J. Zhao and W. Cui, *International Journal of Nanomedicine*, 2014, **9**, 2373–2385.

64 S. Kesikburun, A. K. Tan, B. Yilmaz, E. Yaşar and K. Yazicioğlu, *The American journal of sports medicine*, 2013, **41**, 2609–16.

65 C. K. Hee, J. S. Dines, D. M. Dines, C. M. Roden, L. a Wisner-Lynch, a S. Turner, K. C. McGilvray, A. S. Lyons, C. M. Puttlitz and B. G. Santoni, *The American journal of sports medicine*, 2011, **39**, 1630–9.

66 M. a Zumstein, A. Rumian, V. Lesbats, M. Schaer and P. Boileau, *Journal of shoulder and elbow surgery / American Shoulder and Elbow Surgeons ... [et al.]*, 2014, **23**, 3–12.

67 M. Bidder, D. A. Towler, R. H. Gelberman and M. I. Boyer, *J Orthop Res*, 2000, **18**, 247–252.

68 Y. Hou, Z. Mao, X. Wei, L. Lin, L. Chen, H. Wang, X. Fu, J. Zhang and C. Yu, *Matrix biology : journal of the International Society for Matrix Biology*, 2009, **28**, 324–35.

69 H. Sahin, N. Tholema, W. Petersen, M. J. Raschke and R. Stange, *Journal of Orthopaedic Research*, 2012, **30**, 1952–1957.

70 K. Divani, O. Chan, N. Padhiar, R. Twycross-Lewis, N. Maffulli, T. Crisp and D. Morrissey, *Manual therapy*, 2010, **15**, 463–8.

71 S. Takahashi, M. Nakajima, M. Kobayashi, I. Wakabayashi, N. Miyakoshi, H. Minagawa and E. Itoi, *Tohoku journal of experimental medicine*, 2002, **198**, 207–214.

72 J. M. Granjeiro, R. C. Oliveira, J. C. Bustos-Valenzuela, M. C. Sogayar and R. Taga,

Brazilian journal of medical and biological research, 2005, **38**, 1463–73.

73 S. C. Fu, Y. P. Wong, B. P. Chan, H. M. Pau, Y. C. Cheuk, K. M. Lee and K.-M. Chan, *Life Sciences*, 2003, **72**, 2965–2974.

74 H. Shen, R. H. Gelberman, M. J. Silva, S. E. Sakiyama-Elbert and S. Thomopoulos, *PloS one*, 2013, **8**, e77613.

75 Q.-W. Wang, Z.-L. Chen and Y.-J. Piao, *Journal of bioscience and bioengineering*, 2005, **100**, 418–22.

76 J. Lou, Y. Tu, M. Burns, M. J. Silva and P. Manske, *Journal of Orthopaedic Research*, 2001, **19**, 1199–1202.

77 M. Majewski, O. Betz, P. E. Ochsner, F. Liu, R. M. Porter and C. H. Evans, *Gene therapy*, 2008, **15**, 1139–46.

78 L.-Y. Wang, G.-H. Ma and Z.-G. Su, *Journal of Controlled Release*, 2005, **106**, 62–75.

79 L. J. White, G. T. S. Kirby, H. C. Cox, R. Qodratnama, O. Qutachi, F. R. a J. Rose and K. M. Shakesheff, *Materials science & engineering. C, Materials for biological applications*, 2013, **33**, 2578–83.

80 C.-H. Chen, C.-H. Chang, K.-C. Wang, C.-I. Su, H.-T. Liu, C.-M. Yu, C.-B. Wong, I.-C. Wang, S. W. Whu and H.-W. Liu, *Knee surgery, sports traumatology, arthroscopy : official journal of the ESSKA*, 2011, **19**, 1597–607.

81 J.-M. Jeong, M. S. Oh, B. J. Kim, C.-H. Choi, B. Lee, C.-S. Lee and S. G. Im, *Langmuir*, 2013, **29**, 3474–3481.

82 E. M. Ahmed, *Journal of Advanced Research*, 2015, **6**, 105–121.

83 S. M. Kuo, S. J. Chang, H.-Y. Wang, S. C. Tang and S.-W. Yang, *Carbohydrate polymers*, 2014, **114**, 230–7.

84 M. Magra and N. Maffulli, *Journal of Science and Medicine in Sport*, 2008, **11**, 243–247.

85 G. P. Riley, *Scandinavian Journal of Medicine and Science in Sports*, 2005, **15**, 241–251.

86 X. Cai, M. Cai and L. Lou, *Molecular medicine reports*, 2015, **11**, 3047–54.

87 L. Khoury, M. Posthumus, M. Collins, W. van der Merwe, C. Handley, J. Cook and S.

Raleigh, *International Journal of Sports Medicine*, 2014, **36**, 333–337.

88 P. Lu, G. R. Zhang, X. H. Song, X. H. Zou, L. L. Wang and H. W. Ouyang, *PLoS ONE*, 2011, **6**, e21154.

89 M. Liu, L. Chen, Y. Zhao, L. Gan, D. Zhu, W. Xiong, Y. Lv, Z. Xu, Z. Hao and L. Chen., *Colloids and Surfaces A: Physicochemical and Engineering Aspects*, 2012, **395**, 131–136.

90 J. P. Yoon, C.-H. Lee, J. W. Jung, H.-J. Lee, Y.-S. Lee, J.-Y. Kim, G. Y. Park, J. H. Choi and S. W. Chung, *The American Journal of Sports Medicine*, 2018, **46**, 1441–1450.

91 A. Oryan, A. Moshiri, A. Meimandi-Parizi and N. Maffulli, *Experimental Biology and Medicine*, 2015, **240**, 194–210.

92 Y. Hou, Z. Mao, X. Wei, L. Lin, L. Chen, H. Wang, X. Fu, J. Zhang and C. Yu, *Biochemical and Biophysical Research Communications*, 2009, **383**, 235–239.

93 G. G. Mokone, M. P. Schwellnus, T. D. Noakes and M. Collins, *Scandinavian Journal of Medicine and Science in Sports*, 2006, **16**, 19–26.

94 A. Subramanian and T. F. Schilling, *Development*, 2015, **142**, 4191–4204.

95 J. Kohler, C. Popov, B. Klotz, P. Alberton, W. C. Prall, F. Haasters, S. Müller-Deubert, R. Ebert, L. Klein-Hitpass, F. Jakob, M. Schieker and D. Docheva, *Aging Cell*, 2013, **12**, 988–999.

96 J. B. Tang, Y. Cao, B. Zhu, K.-Q. Xin, X. T. Wang and P. Y. Liu, *The Journal of bone and joint surgery. American volume*, 2008, **90**, 1078–89.

97 S. A. Abbah, K. Spanoudes, T. O'Brien, A. Pandit and D. I. Zeugolis, *Stem cell research & therapy*, 2014, **5**, 38.

98 W. S. Toh and X. J. Loh, *Materials science & engineering. C, Materials for biological applications*, 2014, **45**, 690–7.

99 C. K. Kuo, J. E. Marturano and R. S. Tuan, *BMC Sports Science, Medicine and Rehabilitation*, 2010, **2**, 20.

100 V. R. Sinha and A. Trehan, *Journal of Controlled Release*, 2003, **90**, 261–280.

101 J. F. Mano, G. A. Silva, H. S. Azevedo, P. B. Malafaya, R. A. Sousa, S. S. Silva, L. F. Boesel, J. M. Oliveira, T. C. Santos, A. P. Marques, N. M. Neves and R. L. Reis, *Journal*

of The Royal Society Interface, 2007, **4**, 999–1030.

102 M. Iqbal, N. Zafar, H. Fessi and A. Elaissari, *International Journal of Pharmaceutics*, 2015, **496**, 173–190.

103 R. J. Mondschein, A. Kanitkar, C. B. Williams, S. S. Verbridge and T. E. Long, *Biomaterials*, 2017, **140**, 170–188.

104 K. Bansal, L. Sasso, H. Makwana, S. Awwad, S. Brocchini and C. Alexander, in *Pharmaceutical Nanotechnology: Innovation and Production*, Wiley-VCH Verlag GmbH & Co. KGaA, Weinheim, Germany, 2016, pp. 231–270.

105 E. Reverchon, L. Baldino, S. Cardea and I. De Marco, *Muscles, ligaments and tendons journal*, 2012, **2**, 181–6.

106 B. Dhandayuthapani, Y. Yoshida, T. Maekawa and D. S. Kumar, *International Journal of Polymer Science*, 2011, **2**, 1–19.

107 J. A. Hubbell, *Current Opinion in Biotechnology*, 2003, **14**, 551–558.

108 H. Yin, Z. Yan, R. J. Bauer, J. Peng, M. Schieker, M. Nerlich and D. Docheva, *Biomedical Materials*, 2018, **13**, 034107.

109 S. J. Kew, J. H. Gwynne, D. Enea, R. Brookes, N. Rushton, S. M. Best and R. E. Cameron, *Acta Biomaterialia*, 2012, **8**, 3723–3731.

110 A. Meimandi-Parizi, A. Oryan and A. Moshiri, *Journal of Biomedical Science*, 2013, **20**, 28.

111 J. J. Rice, M. M. Martino, L. De Laporte, F. Tortelli, P. S. Briquez and J. a Hubbell, *Advanced Healthcare Materials*, 2013, **2**, 57–71.

112 K. Möbus, J. Siepmann and R. Bodmeier, *European Journal of Pharmaceutics and Biopharmaceutics*, 2012, **81**, 121–130.

113 R. Costa-Almeida, R. M. A. Domingues, A. Fallahi, H. Avci, I. K. Yazdi, M. Akbari, R. L. Reis, A. Tamayol, M. E. Gomes and A. Khademhosseini, *Journal of Tissue Engineering and Regenerative Medicine*, 2018, **12**, 1039–1048.

114 A. Moshaverinia, X. Xu, C. Chen, S. Ansari, H. H. Zadeh, M. L. Snead and S. Shi, *Biomaterials*, 2014, **35**, 2642–2650.

115 L.-J. Ning, Y.-J. Zhang, Y. Zhang, Q. Qing, Y.-L. Jiang, J.-L. Yang, J.-C. Luo and T.-W.

Qin, *Biomaterials*, 2015, **52**, 539–50.

116 S. Deepthi, M. Nivedhitha Sundaram, J. Deepti Kadavan and R. Jayakumar, *Carbohydrate Polymers*, 2016, **153**, 492–500.

117 E. Chen, L. Yang, C. Ye, W. Zhang, J. Ran, D. Xue, Z. Wang, Z. Pan and Q. Hu, *Acta Biomaterialia*, 2018, **73**, 377–387.

118 Z. Cheng and S.-H. Teoh, *Biomaterials*, 2004, **25**, 1991–2001.

119 E.-H. Kim, J.-W. Kim, G.-D. Han, S.-H. Noh, J.-H. Choi, C. Choi, M.-K. Kim, J.-W. Nah, T.-Y. Kim, Y. Ito and T.-I. Son, *International Journal of Biological Macromolecules*, 2018, Doi:10.1016/j.ijbiomac.2018.07.180.

120 T. Tokunaga, T. Karasugi, H. Arimura, R. Yonemitsu, H. Sakamoto, J. Ide and H. Mizuta, *Journal of Shoulder and Elbow Surgery*, 2017, **26**, 1708–1717.

121 S. Lenoir, R. Riva, X. Lou, C. Detrembleur, R. Jérôme and P. Lecomte, *Macromolecules*, 2004, **37**, 4055–4061.

122 R.-J. Su, H.-W. Yang, Y.-L. Leu, M.-Y. Hua and R.-S. Lee, *Reactive and Functional Polymers*, 2012, **72**, 36–44.

123 G. G. Hedir, C. A. Bell, R. K. O'Reilly and A. P. Dove, *Biomacromolecules*, 2015, **16**, 2049–2058.

124 M. M. Dragosavac, R. G. Holdich, G. T. Vladisavljević and M. N. Sovilj, *Journal of Membrane Science*, 2012, **392**–**393**, 122–129.

125 A. O. Saeed, S. Dey, S. M. Howdle, K. J. Thurecht and C. Alexander, *Journal of Materials Chemistry*, 2009, **19**, 4529.

126 T. K. Giri, C. Choudhary, Ajazuddin, A. Alexander, H. Badwaik and D. K. Tripathi, *Saudi Pharmaceutical Journal*, 2013, **21**, 125–141.

127 G. Kirby, L. White, R. Steck, A. Berner, K. Bogoevski, O. Qutachi, B. Jones, S. Saifzadeh, D. Hutmacher, K. Shakesheff and M. Woodruff, *Materials*, 2016, **9**, 259.

128 S. E. Kim, Y.-P. Yun, K.-S. Shim, D. I. Jeon, K. Park and H.-J. Kim, *Journal of Industrial and Engineering Chemistry*, 2018, **58**, 123–130.

129 Q. Q. Yang, Y. X. Shao, L. Z. Zhang and Y. L. Zhou, *Colloids and Surfaces B: Biointerfaces*, 2018, **164**, 165–176.

130 Y. L. Zhou, Q. Q. Yang, Y. Y. Yan, C. Zhu, L. Zhang and J. B. Tang, *Acta Biomaterialia*, 2018, **70**, 237–248.

131 Y. Li, W. Zhang, X. Li, M. Comes Franchini, K. Xu, E. Locatelli, R. Martin, I. Monaco and S. Cui, *International Journal of Nanomedicine*, 2016, **11**, 2873.

132 C. N. Riggin, F. Qu, D. H. Kim, J. Huegel, D. R. Steinberg, A. F. Kuntz, L. J. Soslowsky, R. L. Mauck and J. Bernstein, *Annals of Biomedical Engineering*, 2017, **45**, 2348–2359.

133 R. H. Gelberman, H. Shen, I. Kormpakis, B. Rothrauff, G. Yang, R. S. Tuan, Y. Xia, S. Sakiyama-Elbert, M. J. Silva and S. Thomopoulos, *Journal of Orthopaedic Research*, 2016, **34**, 630–640.

134 T. Chen, T. Cai, Q. Jin and J. Ji, *E-polymers*, 2015, **15**, 3–13.

135 J. Huegel, D. H. Kim, J. M. Cirone, A. M. Pardes, T. R. Morris, C. A. Nuss, R. L. Mauck, L. J. Soslowsky and A. F. Kuntz, *Journal of Orthopaedic Research*, 2017, **35**, 1250–1257.

136 J.-Z. Hu, Y.-C. Zhou, L.-H. Huang and H.-B. Lu, *BMC Musculoskeletal Disorders*, 2013, **14**, 246.

137 E. Naghashzargar, S. Farè, V. Catto, S. Bertoldi, D. Semnani, S. Karbasi and M. C. Tanzi, *Journal of Applied Biomaterials & Functional Materials*, 2015, **13**, 156–168.

138 H. K. Min, O. S. Kwon, S. H. Oh and J. H. Lee, *Tissue Engineering and Regenerative Medicine*, 2016, **13**, 568–578.

139 C.-H. Chen, S.-H. Chen, K. T. Shalumon and J.-P. Chen, *Acta Biomaterialia*, 2015, **26**, 225–235.

140 C. A. Bell, G. G. Hedir, R. K. O. Reilly and A. P. Dove, 2015, 7447–7454.

141 M. Hombreiro Pérez, C. Zinutti, A. Lamprecht, N. Ubrich, A. Astier, M. Hoffman, R. Bodmeier and P. Maincent, *Journal of Controlled Release*, 2000, **65**, 429–438.

142 A. Mukerjee, V. R. Sinha and V. Pruthi, *Journal of Biomedical and Pharmaceutical Engineering*, 2007, **102**, 215–226.

143 A. P. Dove, *Chemical Communications*, 2008, **48**, 6446.

144 X. Lou, C. Detrembleur, P. Lecomte and R. Jérôme, *Journal of Polymer Science Part A: Polymer Chemistry*, 2002, **40**, 2286–2297.

145 G. T. Hermanson, *Bioconjugate techniques*, Academic Press, 2nd ed., 2008.

146 A. Lancuški, S. Fort and F. Bossard, *ACS Applied Materials & Interfaces*, 2012, **4**, 6499–6504.

147 A. L. Korich, A. R. Walker, C. Hincke, C. Stevens and P. M. Iovine, *Journal of Polymer Science Part A: Polymer Chemistry*, 2010, **48**, 5767–5774.

148 W. J. Jia, Y. C. Gu, M. L. Gou, M. Dai, X. Y. Li, B. Kan, J. L. Yang, Q. F. Song, Y. Q. Wei and Z. Y. Qian, *Drug Delivery*, 2008, **15**, 409–416.

149 J. Guo, G. Chen, X. Ning, M. A. Wolfert, X. Li, B. Xu and G.-J. Boons, *Chemistry - A European Journal*, 2010, **16**, 13360–13366.

150 H. Wang, C. V. Synatschke, A. Raup, V. Jérôme, R. Freitag and S. Agarwal, *Polymer Chemistry*, 2014, **5**, 2453.

151 Y. Zhu, Z. Mao, H. Shi and C. Gao, *Science China Chemistry*, 2012, **55**, 2419–2427.

152 S. P. Pilipchuk, A. Monje, Y. Jiao, J. Hao, L. Kruger, C. L. Flanagan, S. J. Hollister and W. V. Giannobile, *Advanced Healthcare Materials*, 2016, **5**, 676–687.

153 A. C. de Luca, A. Faroni, S. Downes and G. Terenghi, *Journal of Tissue Engineering and Regenerative Medicine*, 2016, **10**, 647–655.

154 C. Rodriguez, O. Ahumada, V. Cebrián, V. Torres Costa and M. Manso Silván, *Vacuum*, 2018, **150**, 232–238.

155 E. Punzón-Quijorna, V. Sánchez-Vaquero, A. Muñoz Noval, D. Gallach Pérez, A. Climent Font, G. Ceccone, R. Gago, J. P. García Ruiz and M. Manso Silván, *Vacuum*, 2011, **85**, 1071–1075.

156 H. Zhang, C.-Y. Lin and S. J. Hollister, *Biomaterials*, 2009, **30**, 4063–4069.

157 Y. Zhu, C. Gao, X. Liu and J. Shen, *Biomacromolecules*, 2002, **3**, 1312–1319.

158 R. Balmayor, E. Pashkuleva, I. Frias, A. Azevedo, H. Reis, *Journal of the royal society interface*, 2011, **8**, 896–908.

159 A. C. de Luca, G. Terenghi and S. Downes, *Journal of Tissue Engineering and Regenerative Medicine*, 2014, **8**, 153–163.

160 M. J. Poznansky and R. L. Juliano, *The American Society Pharmacology and*

Experimental Therapeutics, 1984, **36**, 277–336.

161 M. R. Mohammadi, A. Nojoomi, M. Mozafari, A. Dubnika, M. Inayathullah and J. Rajadas, *Journal of Materials Chemistry B*, 2017, **5**, 3995–4018.

162 H. C. Kolb, M. G. Finn and K. B. Sharpless, *Angewandte Chemie International Edition*, 2001, **40**, 2004–2021.

163 J. M. Palomo, *Organic & Biomolecular Chemistry*, 2012, **10**, 9297–9508.

164 H. Durmaz, A. Sanyal, G. Hizal and U. Tunca, *Polym. Chem.*, 2012, **3**, 825–835.

165 R. Huisgen, *The Journal of Organic Chemistry*, 1976, **41**, 403–419.

166 R. Huisgen, *Angewandte Chemie International Edition in English*, 1963, **2**, 565–598.

167 J. C. Jewett, E. M. Sletten and C. R. Bertozzi, *Journal of the American Chemical Society*, 2010, **132**, 3688–3690.

168 J. M. Baskin, J. A. Prescher, S. T. Laughlin, N. J. Agard, P. V. Chang, I. A. Miller, A. Lo, J. A. Codelli and C. R. Bertozzi, *Proceedings of the National Academy of Sciences*, 2007, **104**, 16793–16797.

169 A. Ikeda-Boku, K. Kondo, S. Ohno, E. Yoshida, T. Yokogawa, N. Hayashi and K. Nishikawa, *Journal of Biochemistry*, 2013, **154**, 159–165.

170 M. Li, P. De, S. R. Gondi and B. S. Sumerlin, *Macromolecular Rapid Communications*, 2008, **29**, 1172–1176.

171 J. Xu, T. M. Filion, F. Prifti and J. Song, *Chemistry - An Asian Journal*, 2011, **6**, 2730–2737.

172 K. Zhu, Y. Zhang, S. He, W. Chen, J. Shen, Z. Wang and X. Jiang, *Analytical Chemistry*, 2012, **84**, 4267–4270.

173 Q. V. Nguyen, D. P. Huynh, J. H. Park and D. S. Lee, *European Polymer Journal*, 2015, **72**, 602–619.

174 D. P. Y. Chan, S. C. Owen and M. S. Shoichet, *Bioconjugate Chemistry*, 2013, **24**, 105–113.

175 P. V Chang, J. a Prescher, E. M. Sletten, J. M. Baskin, I. a Miller, N. J. Agard, A. Lo and C. R. Bertozzi, *Proceedings of the National Academy of Sciences*, 2010, **107**, 1821–

1826.

176 J. M. Baskin and C. R. Bertozzi, *AldrichimiaACTA*, 2010, **43**, 15–23.

177 N. J. Agard, J. A. Prescher and C. R. Bertozzi, *Journal of the American Chemical Society*, 2004, **126**, 15046–15047.

178 R. Chadwick, S. Van Gyzen, S. Liogier and A. Adronov, *Synthesis*, 2014, **46**, 669–677.

179 X. Cheng, R. Liu and Y. He, *European journal of pharmaceutics and biopharmaceutics : official journal of Arbeitsgemeinschaft für Pharmazeutische Verfahrenstechnik e.V*, 2010, **76**, 336–41.

180 J. Yang, S.-B. Park, H.-G. Yoon, Y.-M. Huh and S. Haam, *International journal of pharmaceutics*, 2006, **324**, 185–90.

181 P. R. Ravi, R. Vats, V. Dalal, N. Gadekar and A. N, *Drug Development and Industrial Pharmacy*, 2015, **41**, 131–140.

182 M. Ye, S. Kim and K. Park, *Journal of Controlled Release*, 2010, **146**, 241–260.

183 C. B. Bottom, S. S. Hanna and D. J. Siehr, *Biochemical Education*, 1973, **6**, 4–5.

184 A. W. Coats and J. P. Redfern, *Analyst*, 1963, **88**, 906–924.

185 J.-P. Chen, S.-H. Chen, C.-H. Chen and K. T. Shalumon, *International Journal of Nanomedicine*, 2014, **9**, 4079.

186 J. Li, W. Xie, H. N. Cheng, R. G. Nickol and P. G. Wang, *Macromolecules*, 1999, **32**, 2789–2792.

187 J.-P. Chen and Y.-S. Chang, *Colloids and Surfaces B: Biointerfaces*, 2011, **86**, 169–175.

188 C. Salvagnini, S. Gharbi, T. Boxus and J. Marchand-Brynaert, *European Journal of Medicinal Chemistry*, 2007, **42**, 37–53.

189 T. Urbaniak and W. Musia, *Acta Poloniae Pharmaceutica - Drug Research*, 2016, **73**, 811–825.

190 M. Labet and W. Thielemans, *Chemical Society Reviews*, 2009, **38**, 3484.

191 H. Barjat, G. A. Morris, S. Smart, A. G. Swanson and S. C. R. Williams, *Journal of Magnetic Resonance, Series B*, 1995, **108**, 170–172.

192 S. Balayssac, S. Trefi, V. Gilard, M. Malet-Martino, R. Martino and M.-A. Delsuc, *Journal of Pharmaceutical and Biomedical Analysis*, 2009, **50**, 602–612.

193 S. Trefi, V. Gilard, S. Balayssac, M. Malet-Martino and R. Martino, *Journal of Pharmaceutical and Biomedical Analysis*, 2008, **46**, 707–722.

194 J. Rui, M. Dadsetan, M. B. Runge, R. J. Spinner, M. J. Yaszemski, A. J. Windebank and H. Wang, *Acta Biomaterialia*, 2012, **8**, 511–518.

195 S. I. Lim, Y. S. Hahn and I. Kwon, *Journal of Controlled Release*, 2015, **207**, 93–100.

196 D. M. Lloyd, I. T. Norton and F. Spyropoulos, *Journal of Membrane Science*, 2014, **466**, 8–17.

197 D.-X. Hao, F.-L. Gong, G.-H. Hu, Y.-J. Zhao, G.-P. Lian, G.-H. Ma and Z. Su, *Industrial & Engineering Chemistry Research*, 2008, **47**, 6418–6425.

198 S. van der Graaf, C. G. P. . Schroën, R. G. . van der Sman and R. . Boom, *Journal of Colloid and Interface Science*, 2004, **277**, 456–463.

199 W. Li, L. Zhang, X. Ge, B. Xu, W. Zhang, L. Qu, C.-H. Choi, J. Xu, A. Zhang, H. Lee and D. A. Weitz, *Chemical Society Reviews*, 2018, **47**, 5646–5683.

200 S. Van Der Graaf, C. Schroen and R. Boom, *Journal of Membrane Science*, 2005, **251**, 7–15.

201 D. Hernán Pérez de la Ossa, a Ligresti, M. E. Gil-Alegre, M. R. Aberturas, J. Molpeceres, V. Di Marzo and a I. Torres Suárez, *Journal of controlled release : official journal of the Controlled Release Society*, 2012, **161**, 927–32.

202 L. Chen, L. Mei, D. Feng, D. Huang, X. Tong, X. Pan, C. Zhu and C. Wu, *Colloids and Surfaces B: Biointerfaces*, 2018, **163**, 146–154.

203 P. Ghosh, S. M. S. Gruber, C. Y. Lin and P. W. Whitlock, *Biofabrication*, , DOI:10.1088/1758-5090/aaa637.

204 H. Okochi and M. Nakano, *Advanced Drug Delivery Reviews*, 2000, **45**, 5–26.

205 R. Liu, G.-H. Ma, Y.-H. Wan and Z.-G. Su, *Colloids and Surfaces B: Biointerfaces*, 2005, **45**, 144–153.

206 T. Nakashima, M. Shimizu and M. Kukizaki, *Advanced Drug Delivery Reviews*, 2000, **45**, 47–56.

207 S. M. Joscelyne and G. Trägårdh, *Journal of Membrane Science*, 2000, **169**, 107–117.

208 B. G. Nikolovski, J. D. Bajac, F. L. Martinovic and N. Bogunović, *Chemical Papers*, 2018, **72**, 533–542.

209 G. Gasparini, R. G. Holdich and S. R. Kosvintsev, *Colloids and surfaces. B, Biointerfaces*, 2010, **75**, 557–64.

210 G. T. Vladisavljević and H. Schubert, *Journal of Dispersion Science and Technology*, 2003, **24**, 811–819.

211 J. Jiao, D. G. Rhodes and D. J. Burgess, *Journal of Colloid and Interface Science*, 2002, **250**, 444–450.

212 G. Gasparini, S. R. Kosvintsev, M. T. Stillwell and R. G. Holdich, *Colloids and surfaces. B, Biointerfaces*, 2008, **61**, 199–207.

213 A. Cambronero-Rojas, P. Torres-Vergara, R. Godoy, C. Von Plessing, J. Sepúlveda and C. Gómez-Gaete, *Journal of Controlled Release*, 2015, **209**, 229–237.

214 N. S. Barakat, G. a Shazly and A. H. Almedany, *Drug Development and Industrial Pharmacy*, 2013, **39**, 352–362.

215 F. Ito, H. Fujimori and K. Makino, *Colloids and Surfaces B: Biointerfaces*, 2007, **54**, 173–178.

216 I. W. Stillwell, M T. Holdich, G. Kosvintsev, S R. Gasparini, G. Cumming, *Industrial and Engineering chemistry research*, 2007, 965–972.

217 O. Qutachi, J. R. Vetsch, D. Gill, H. Cox, D. J. Scurr, S. Hofmann, R. Müller, R. A. Quirk, K. M. Shakesheff and C. V Rahman, *Acta Biomaterialia*, 2014, **10**, 5090–5098.

218 S. Bose, M. Roy and A. Bandyopadhyay, *Trends in Biotechnology*, 2012, **30**, 546–554.

219 T.-K. Ryu, M.-J. Oh, S.-K. Moon, D.-H. Paik, S.-E. Kim, J.-H. Park and S.-W. Choi, *Colloids and Surfaces B: Biointerfaces*, 2013, **112**, 368–373.

220 R. T. Tran, E. Naseri, A. Kolasnikov, X. Bai and J. Yang, *Biotechnology and Applied Biochemistry*, 2011, **58**, 335–344.

221 T. G. Fox and P. J. Flory, *Journal of the American Chemical Society*, 1948, **70**, 2384–2395.

222 K. M. Yamada, *The Journal of clinical investigation*, 2000, **105**, 1507–9.

223 T. Kardestuncer, M. B. McCarthy, V. Karageorgiou, D. Kaplan and G. Gronowicz, *Clinical orthopaedics and related research*, 2006, **448**, 234–9.

224 D. Lyras and K. Kazakos, *Acta orthopaedica …*, 2010, 380–386.

225 Y. Anaguchi, K. Yasuda, T. Majima, H. Tohyama, A. Minami and K. Hayashi, *Clinical biomechanics (Bristol, Avon)*, 2005, **20**, 959–65.

226 S. Wong, *Chemistry of Protein Conjugation and Crosslinking*, CRC Press, Boca Raton, 1991.

227 Q. Y. Hu, F. Berti and R. Adamo, *Chemical Society Reviews*, 2016, **45**, 1691–1719.

228 H. Tan, L. Zhao, W. Liu, L. Ren, S. Xu, L. Chen and W. Li, *RSC Advances*, 2014, **4**, 60413–60420.

229 M. E. B. Smith, M. B. Caspersen, E. Robinson, M. Morais, A. Maruani, J. P. M. Nunes, K. Nicholls, M. J. Saxton, S. Caddick, J. R. Baker and V. Chudasama, *Organic and Biomolecular Chemistry*, 2015, **13**, 7946–7949.

230 M. Simon, R. Frey, U. Zangemeister-Wittke and A. Plückthun, *Bioconjugate Chemistry*, 2013, **24**, 1955–1966.

231 J. Anguizola, R. Matsuda, O. S. Barnaby, K. S. Hoy, C. Wa, E. DeBolt, M. Koke and D. S. Hage, *Clinica Chimica Acta*, 2013, **425**, 64–76.

232 M. Bradford, *Analytical Biochemistry*, 1976, **72**, 248–254.

233 P. R. E. Mittl, J. P. Priestle, D. A. Cox, G. Mcmaster, N. Cerletti and M. G. Grütter, *Protein Science*, 1996, **5**, 1261–1271.

234 A. P. Hinck, S. J. Archer, S. W. Qian, A. B. Roberts, M. B. Sporn, J. A. Weatherbee, M. L. S. Tsang, R. Lucas, B. L. Zhang, J. Wenker and D. A. Torchia, *Biochemistry*, 1996, **35**, 8517–8534.

235 J. Kim, B. Lin, S. Kim, B. Choi, D. Evseenko and M. Lee, *Journal of biological engineering*, 2015, **9**, 1.

236 G. A. Breaux, K. B. Green-Church, A. France and P. A. Limbach, *Analytical Chemistry*, 2000, **72**, 1169–1174.

237 F. Gharahdaghi, C. R. Weinberg, D. A. Meagher, B. S. Imai and S. M. Mische, *Electrophoresis*, 1999, **20**, 601–605.

238 P. K. Smith, R. I. Krohn, G. T. Hermanson, A. K. Mallia, F. H. Gartner, M. D. Provenzano, E. K. Fujimoto, N. M. Goeke, B. J. Olson and D. C. Klenk, *Analytical Biochemistry*, 1985, **150**, 76–85.

239 D. Cooksey, *A review of UK health research funding A review of UK health research funding*, 2006.

240 F. Chen, Y. Zhao, Y. Jin and S. Shi, *Biotechnology Advances*, 2012, **30**, 658–672.

241 J. DiMaio, J, Michael. Potz, A, Brittany. Thatcher, E, Jeffrey. Squiers, J, *JACC: BASIC TO TRANSLATIONAL SCIENCE*, 2017, **2**, 328–334.

242 J. J. Harris, S. Lu and P. Gabriele, *polymer international*, , DOI:DOI10.1002/pi.5590.

243 R. G. Cooper, *Business Horizons*.

244 J. C. Mankins, *Acta Astronautica*, 2009, **65**, 1216–1223.

245 J. C. Mankins, *A White Paper*.

246 Orthopedic Soft Tissue Repair Market Worth $9.4 Billion By 2024, https://www.grandviewresearch.com/press-release/global-orthopedic-soft-tissue-repair-market, (accessed 9 March 2018).

247 Sports Medicine Market worth 8.24 Billion USD by 2022, https://www.marketsandmarkets.com/PressReleases/sports-medicine-devices.asp, (accessed 9 March 2018).

248 J. T. Shearn, K. R. C. Kinneberg, N. A. Dyment, M. T. Galloway, K. Kenter, C. Wylie and D. L. Butler, *Journal of Musculoskeletal Neuronal Interactions*, 2011, **11**, 163–173.

249 arc Hochberg Alan J. Silman Josef Smolen Michael Weinblatt Michael Weisman, *Rheumatology*, Elsevier, 5th edn., 2014.

250 National Life Tables, United Kingdom - Office for National Statistics, https://www.ons.gov.uk/peoplepopulationandcommunity/birthsdeathsandmarriages/lifeexpectancies/bulletins/nationallifetablesunitedkingdom/2015-09-23, (accessed 9 March 2018).

251 2017 STATE OF THE UK FITNESS INDUSTRY REPORT - OUT TODAY — The Leisure

Database Company, http://www.leisuredb.com/blog/2017/5/5/2017-state-of-the-uk-fitness-industry-report-out-now, (accessed 9 March 2018).

252 Soft Tissue Repair Market Worth $10.73 Billion By 2025 | CAGR: 7.3%, https://www.grandviewresearch.com/press-release/global-soft-tissue-repair-market, (accessed 9 March 2018).

253 AlloWrap DS | Stryker, https://www.stryker.com/us/en/trauma-and-extremities/products/allowrap-ds-amniotic-membrane.html, (accessed 9 March 2018).

254 MaxBraid Suture, http://www.zimmerbiomet.com/medical-professionals/sports-medicine/product/maxbraid-suture.html, (accessed 9 March 2018).

255 Sports Medicine | ToggleLoc™ Device with ZipLoop™ Technology | Zimmer Biomet, http://www.zimmerbiomet.com/medical-professionals/sports-medicine/product/toggleloc-device-with-ziploop-technology.html, (accessed 9 March 2018).

256 Artificial Ligaments & Tendons | Neoligaments products, https://www.neoligaments.com/products/, (accessed 9 March 2018).

257 Tendon Regeneration — Orthocell, https://www.orthocell.com.au/new-page/, (accessed 9 March 2018).

258 V. Camlek, 2010, **30**, 119–123.

259 A. Scott, E. Huisman and K. Khan, *Canadian Medical Assosication Journal*, 2011, **183**, 1159–1165.

260 J. Ghuman, P. A. Zunszain, I. Petitpas, A. A. Bhattacharya, M. Otagiri and S. Curry, *Journal of Molecular Biology*, 2005, **353**, 38–52.

261 S. Hvilsted, *Polymer International*, 2012, **61**, 485–494.

Appendix

Appendix

Appendix A: Characterisation of 2-[2-(2-azidoethoxy)ethoxy]ethanol Initiator (2).

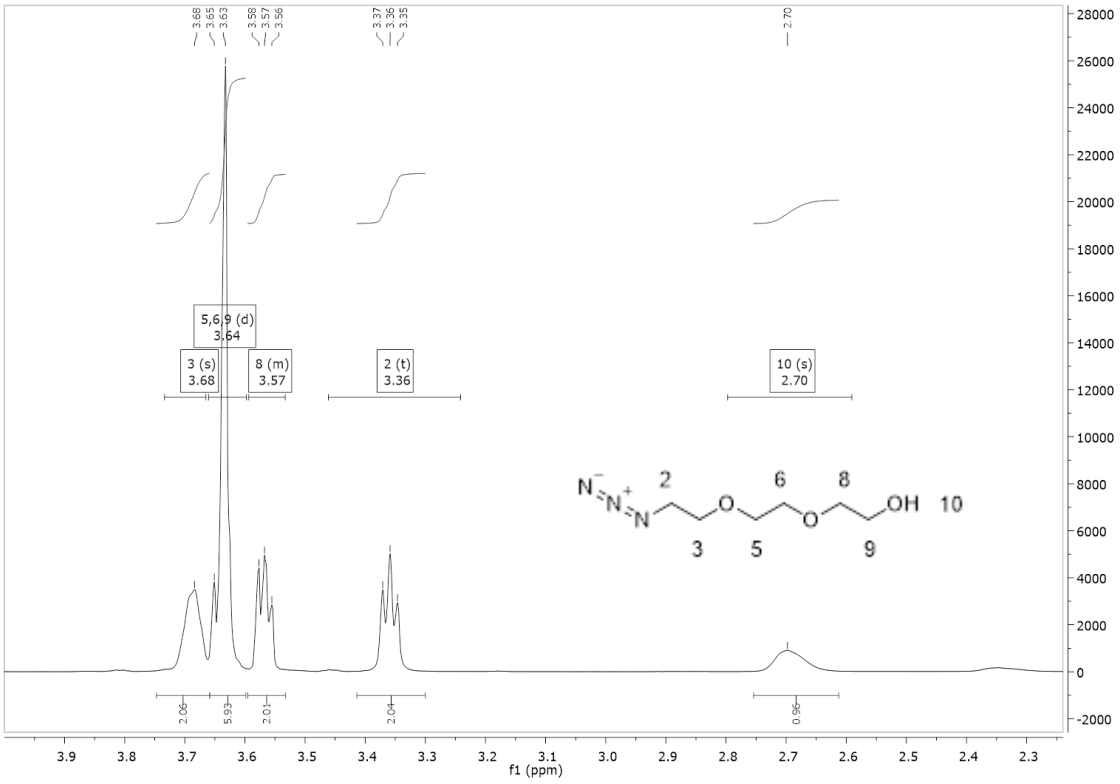

Figure 59: ^{1}H MNR of 2-[2-(2-azidoethoxy)ethoxy]ethanol Initiator (2). Peak at 3.36 is indicative of the proton next to the terminal azide.

2-[2-(2-azidoethoxy)ethoxy]ethanol: ^{1}HNMR 3.68 (m, 2H), 3.64 (m, 6H), 3.59 – 3.53 (t, 2H), 3.36 (t, 2H), 2.70 (s, 1H).

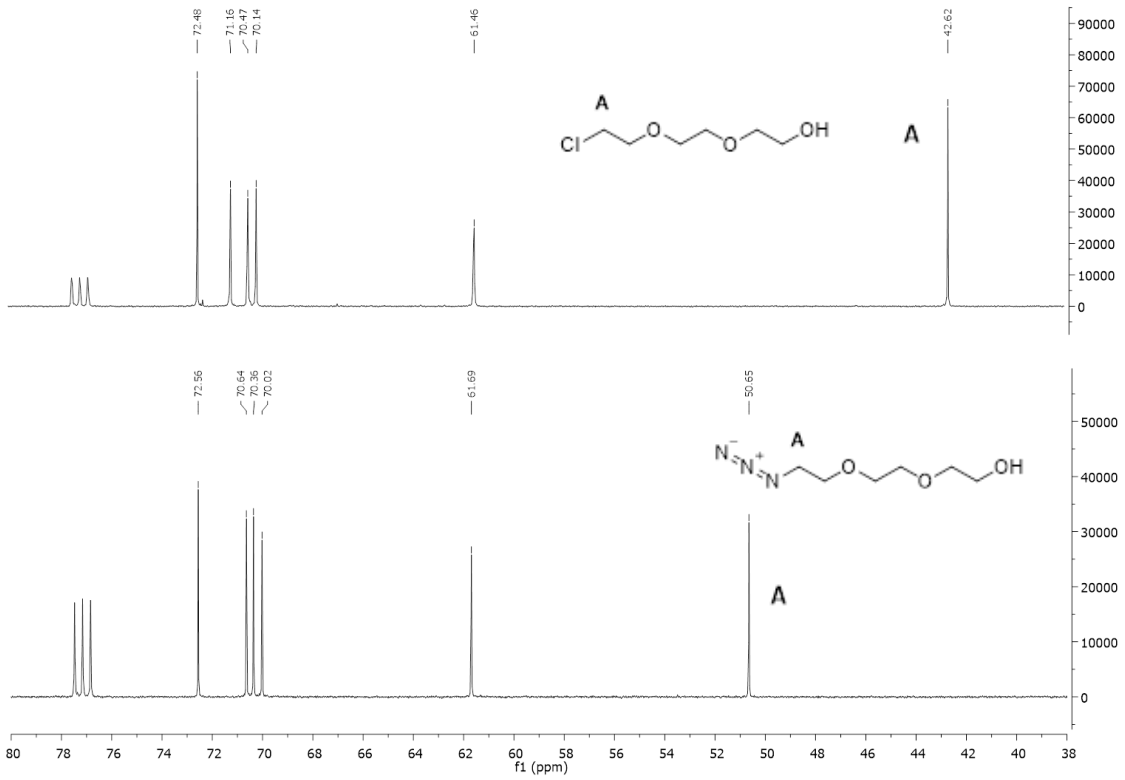

Figure 60: ^{13}C NMR of 2-[2-(2-azidoethoxy)ethoxy]ethanol Initiator 2. Top spectra shows 2-[2-(2-Chloroethoxy)ethoxy]ethanol starting material and bottom shows 2-[2-(2-azidoethoxy)ethoxy]ethanol Initiator. The carbon peak next to the azide or chloride (A) clearly shifts from 42.62 to 50.65 ppm after azide substation.

2-[2-(2-Chloroethoxy)ethoxy]ethanol: ^{13}C NMR (101 MHz, $CDCl_3$) δ 72.48, 71.16, 70.47, 70.14, 61.46, 42.62.

2-[2-(2-azidoethoxy)ethoxy]ethanol Initiator 2: ^{13}C NMR (101 MHz, $CDCl_3$) δ 72.56, 70.64, 70.36, 70.02, 61.69, 50.65.

Appendix B: Characterisation of Polycaprolactone-Azide (4).

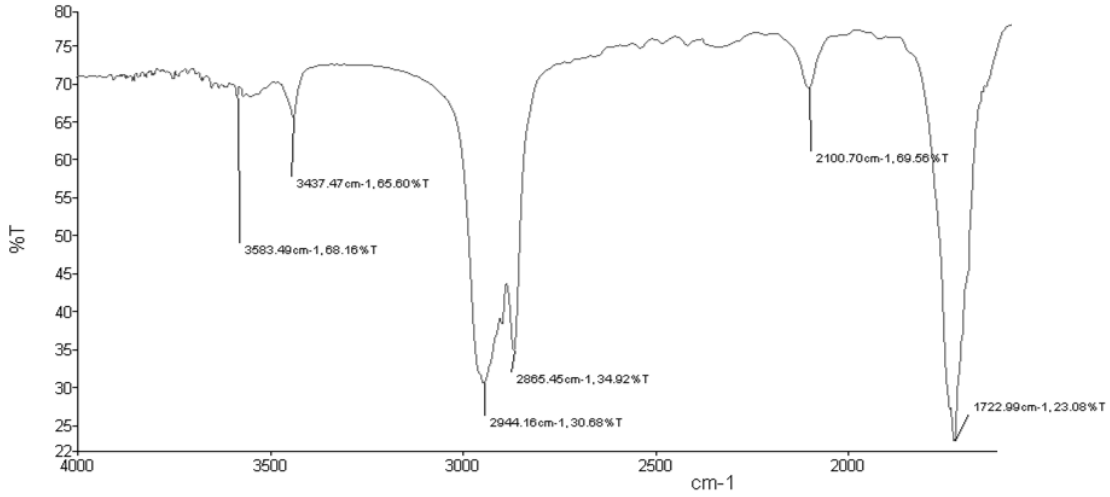

Figure 61: IR of PCL-N_3 (4). Peak at 2100 indicates the presence of the azide.

IR (NaCl, cm^{-1}) 3391, 2867, 2095, 1454, 1345, 1283, 1063

Appendix C: Manufacturer's Injection Rates

Type	Material	Pore Size Microns	Total area cm^2	Porosity %	Injection rate ml/min	Drop size Microns
Standard	Nickel	5	8	0.06	0.2	≥15
Standard	Nickel	10	8	0.23	0.9	≥30
Standard	Nickel	15	8	0.51	2.1	≥45
Standard	Nickel	20	8	0.91	3.7	≥60
Standard	Nickel	40	2.8	3.63	14.5	≥120
Ring	Nickel	5	2.8	0.06	0.08	≥15
Ring	Nickel	10	2.8	0.23	0.31	≥30
Ring	Nickel	15	2.8	0.51	0.7	≥45
Ring	Nickel	20	2.8	0.91	1.25	≥60
Ring	Nickel	40	2.8	3.63	5	≥120
Ring	Stainless	5	2.8	0.05	0.07	≥15
Ring	Stainless	10	2.8	0.19	0.26	≥30

Table 14: Micropore Ltd manufacturer's guidelines for injection rates of dispersed phase through the membrane, and the resulting expected particle size depending on a ringed or standard membrane.

Appendix D: Infrared Analysis of Polycaprolactone-Azide Microparticles Produced with Increasing Stir Speeds and Polymer Concentrations (7).

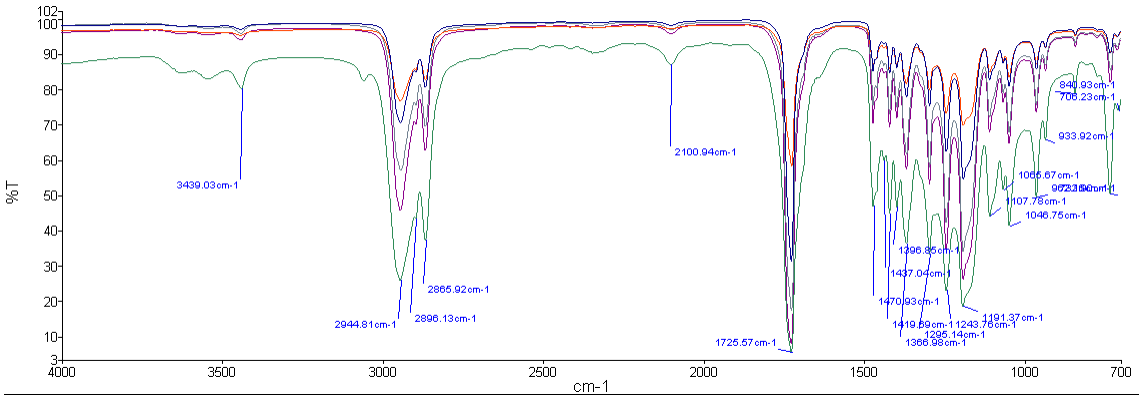

Figure 62: IR of PCL-N_3 particles produced by altering stir volts applied at production. Key; 1500 RPM, 1140 RPM, 950 RPM, 770 RPM, 590 RPM and 400 RPM. Azide peak can be seen at 2100 cm^{-1} for all samples.

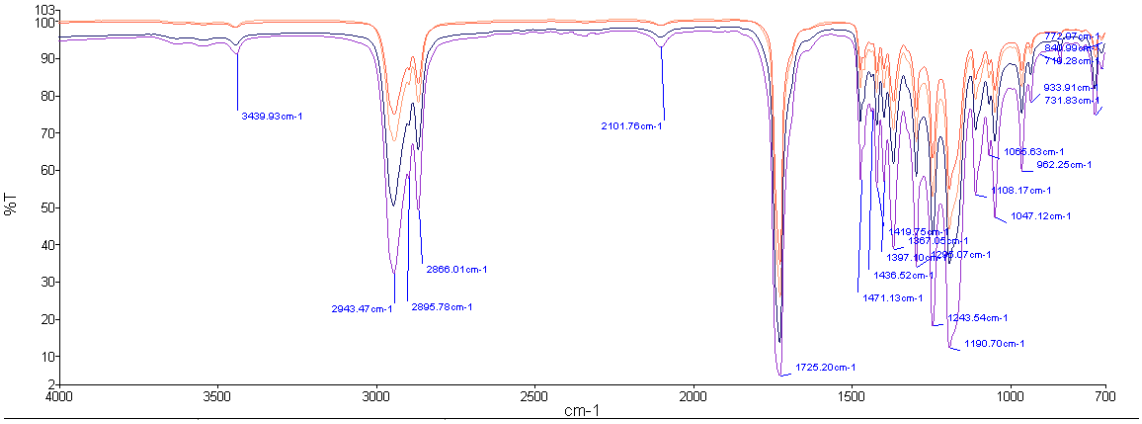

Figure 63: IR of PCL-N_3 particles produced by altering the polymer concentration. Key; 5%, 20%, 30%, and 40% PCL-N_3. Azide peak can be seen at 2100 cm^{-1} for all samples.

Appendix E: Analysis of GRGDS-Pentapeptide (10, 11 & 12)

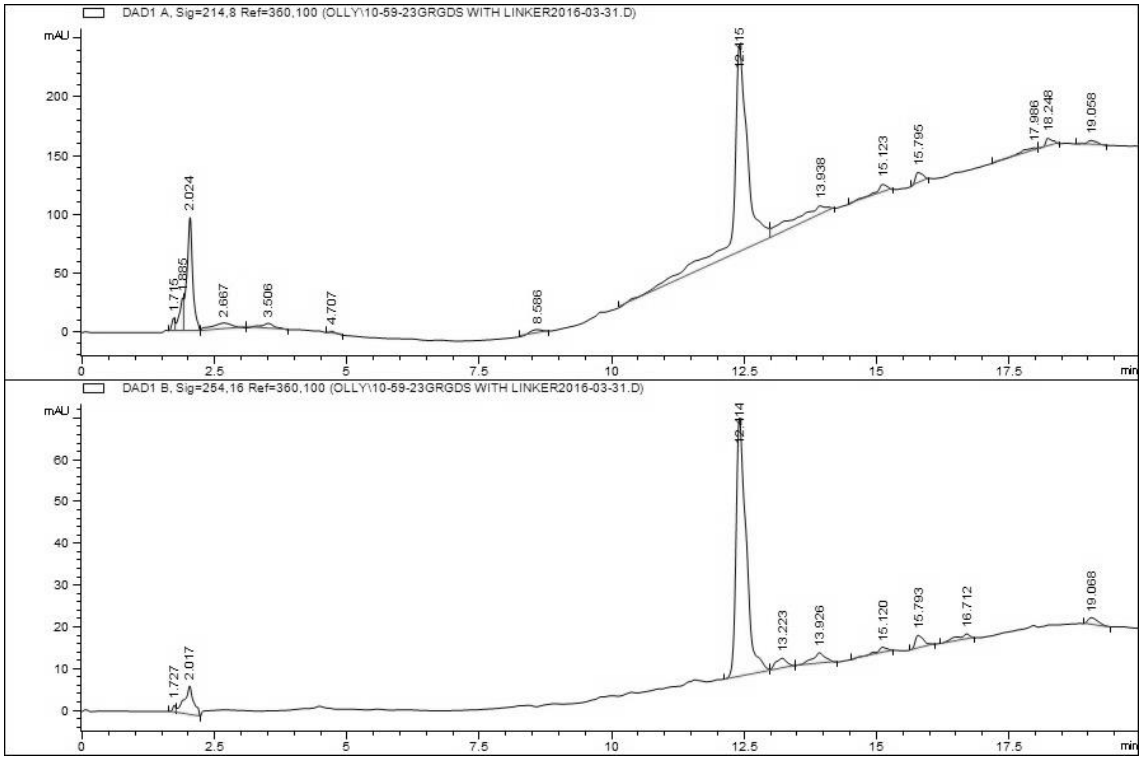

Figure 64: HPLC analysis of DBCO acid-GRGDS peptide on 100 mg scale (10).

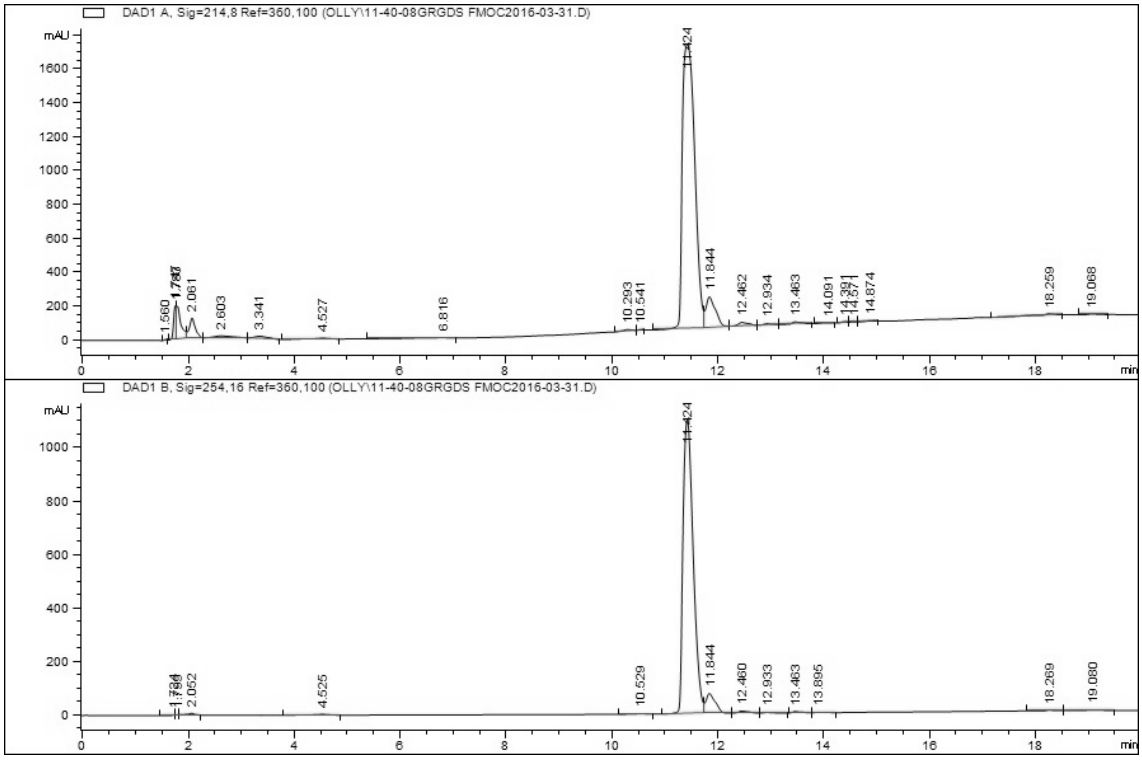

Figure 65: HPLC analysis of FMOC-GRGDS peptide on 100 mg scale (11).

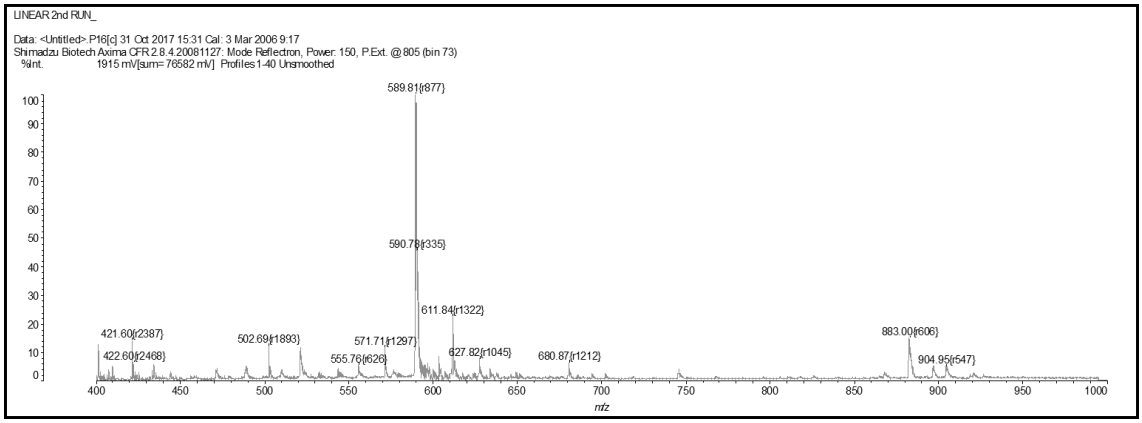

Figure 66: MALDI analysis of GRGDS peptide on 300 mg scale (12)

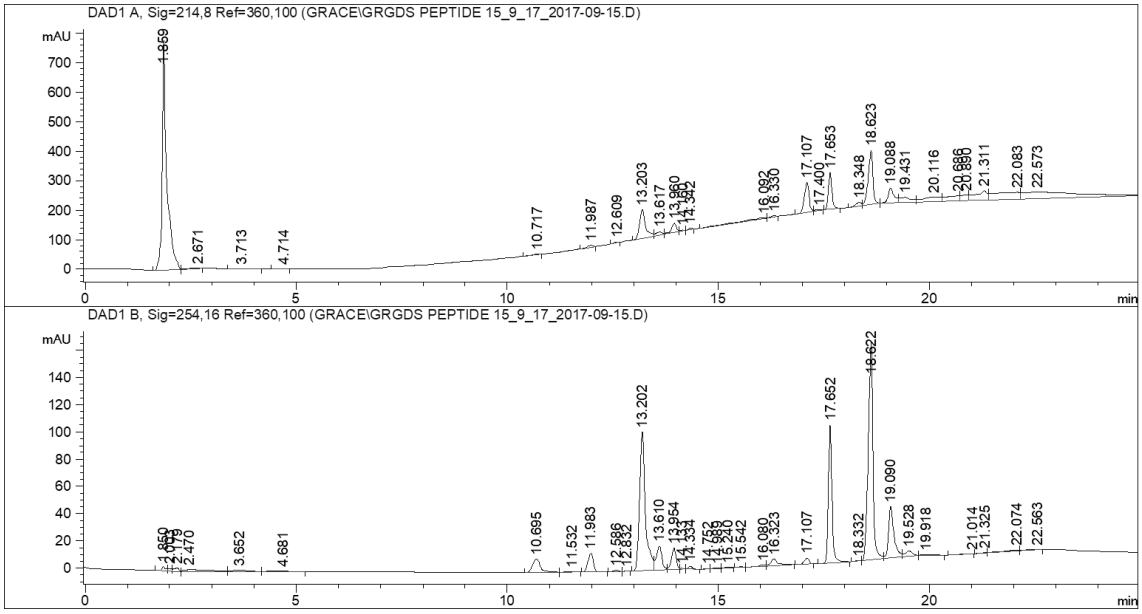

Figure 67: HPLC analysis of GRGDS peptide on 300 mg scale (12)

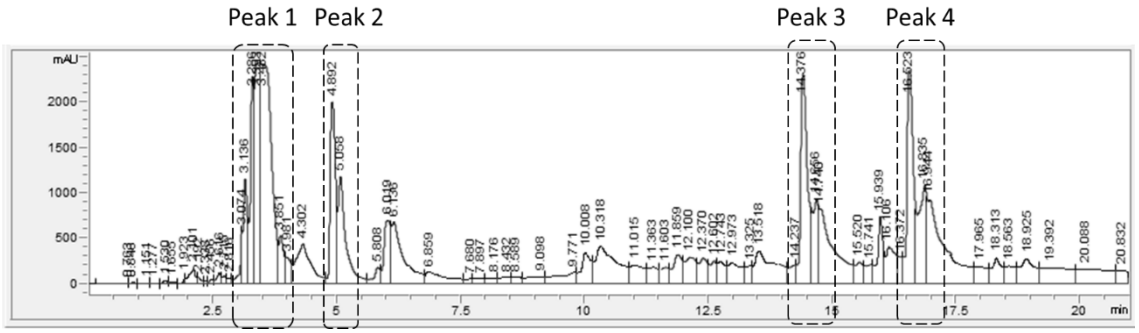

Figure 68: HPLC purification of DBCO acid-GRGDS peptide (12). Fractions were collected at 3.4 mins (peak 1) 4.8 mins (peak 2) 14.3 minutes (peak 3) and 16.5 minutes (peak 4).

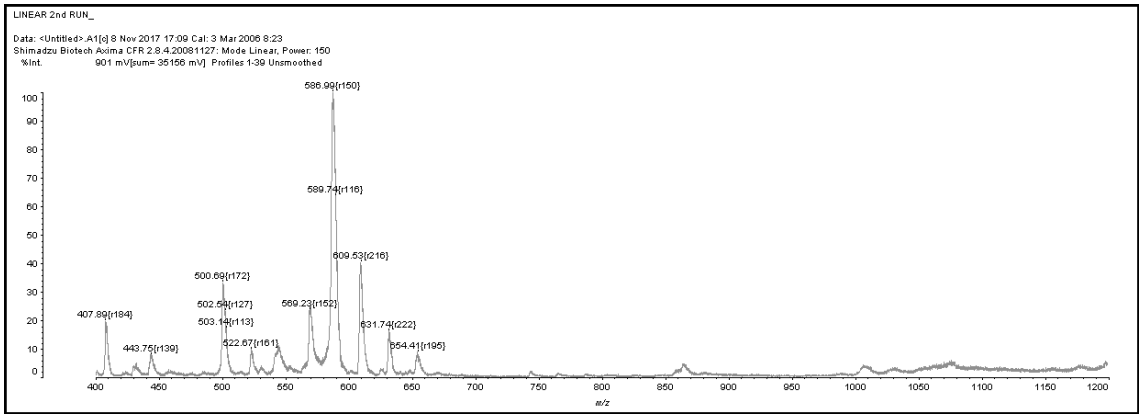

Figure 69: MALDI of HPLC peak 1 at 3.4 mins for DBCO acid-GRGDS peptide (12).

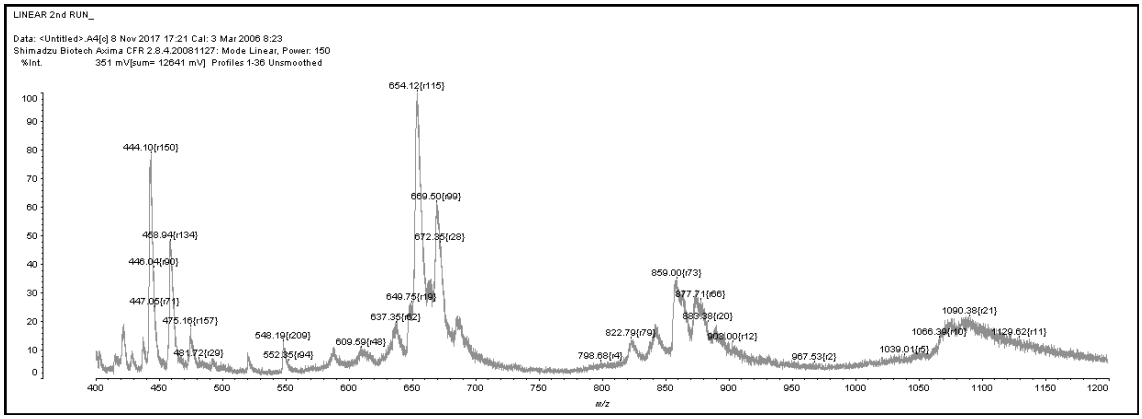

Figure 70: MALDI of HPLC peak 2 at 4.8 mins for DBCO acid-GRGDS peptide (12).

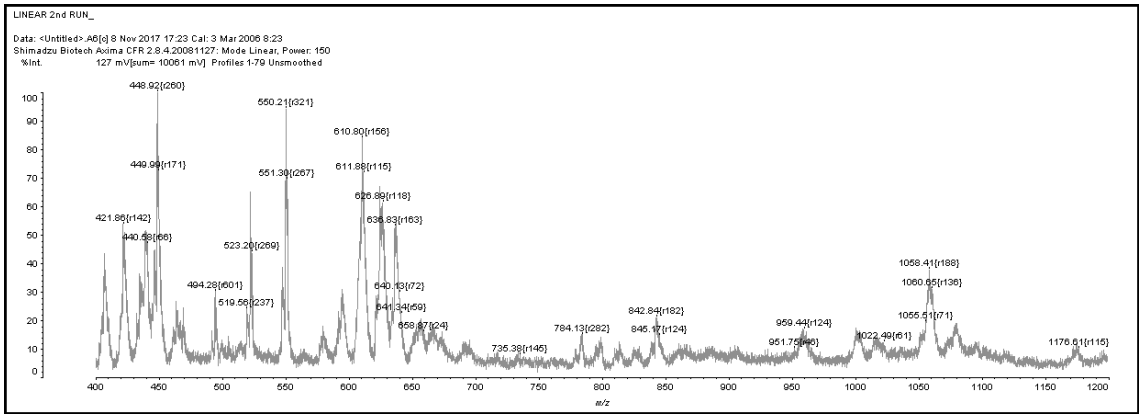

Figure 71: MALDI of HPLC peak 3 at 14.3 mins for DBCO acid-GRGDS peptide (12).

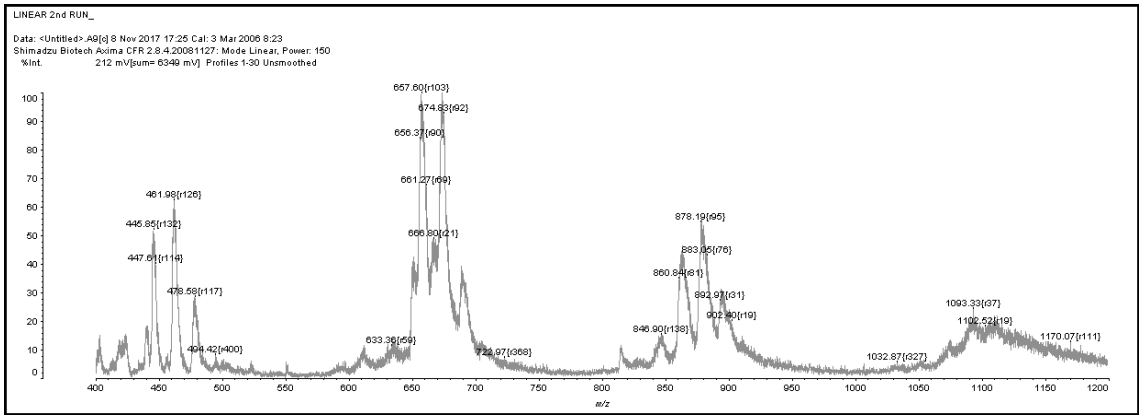

Figure 72: MALDI of HPLC peak 4 at 16.5 mins for DBCO acid-GRGDS peptide (12).

Appendix F: Cytotoxicity Testing of Polycaprolactone-Azide Microparticles (7)

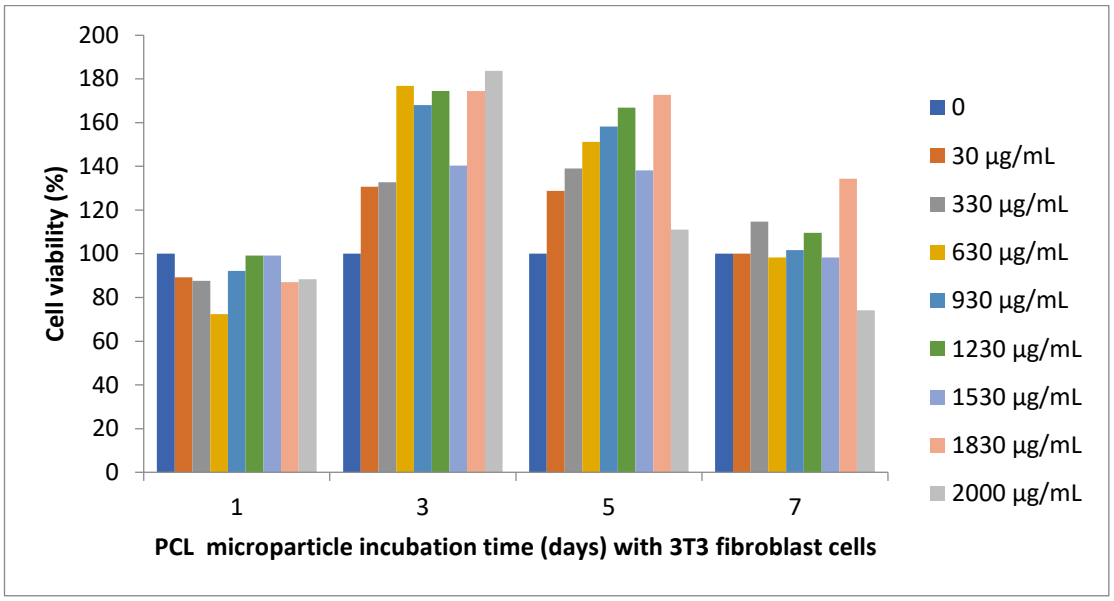

Figure 73: Cytotoxicity analysis of PCL microparticles. N=3.Control wells of cells only reacted with MTS assay were taken to be 100% cell viability. All other wells were normalised against these controls.

Appendix G: Characterisation of Native Human Serum Albumin

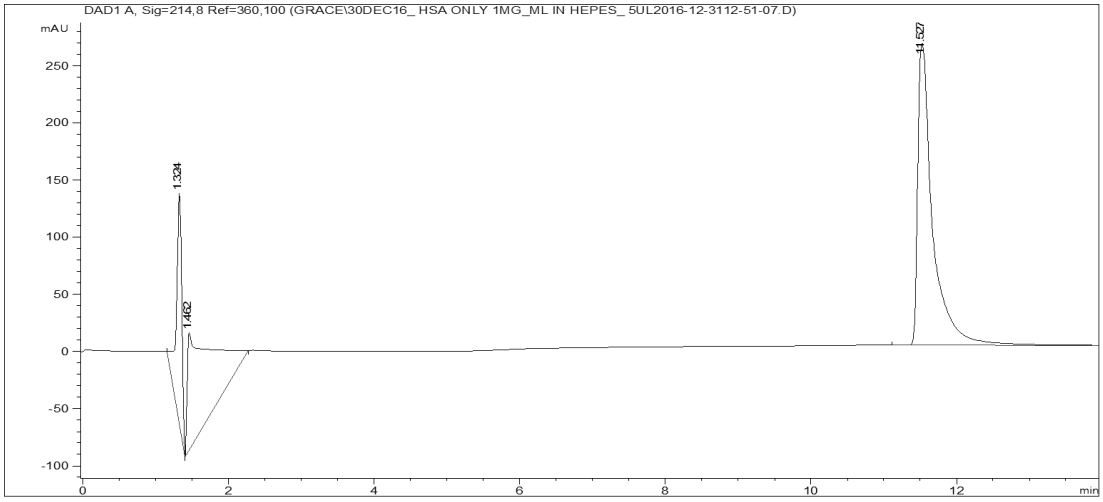

Figure 74: HPLC analysis of native HSA protein.

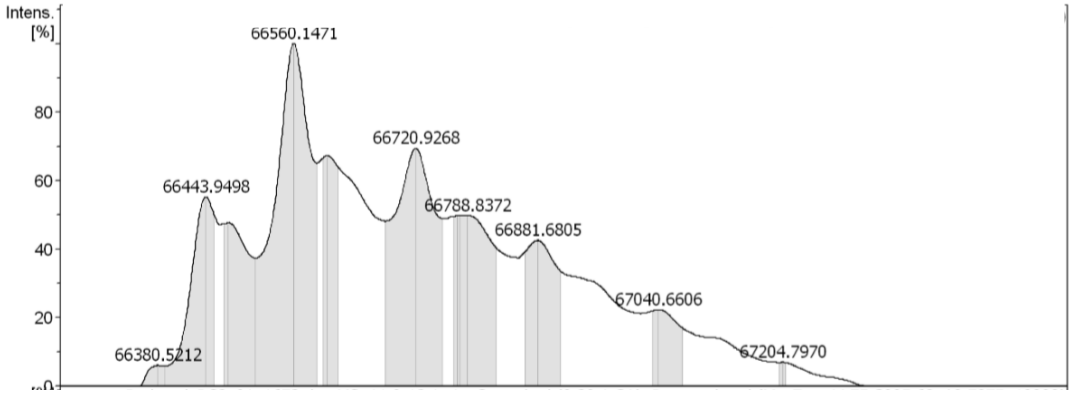

Figure 75: LC-MS analysis of native HSA showing a Mw of 66,560 Da.

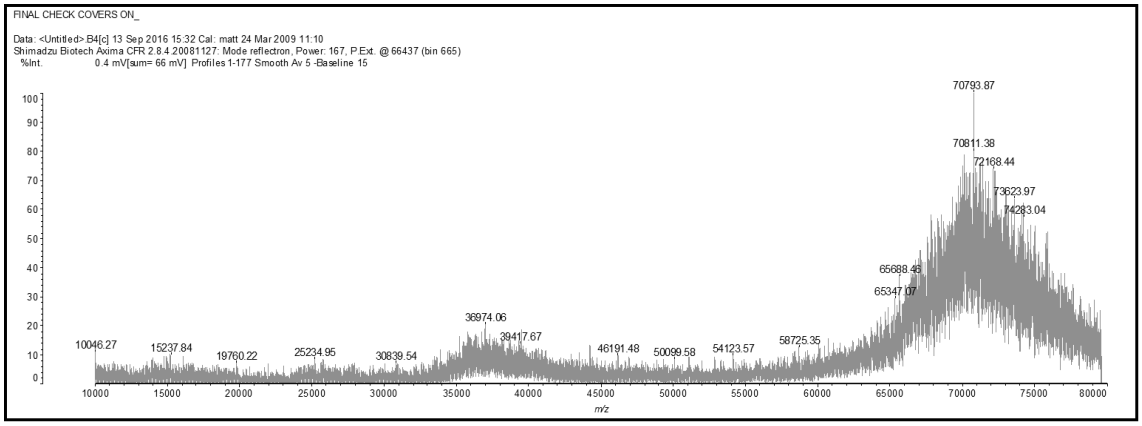

Figure 76: MALDI-TOF analysis of HSA.

Appendix H: Calibration Curve of Ellman's Assay

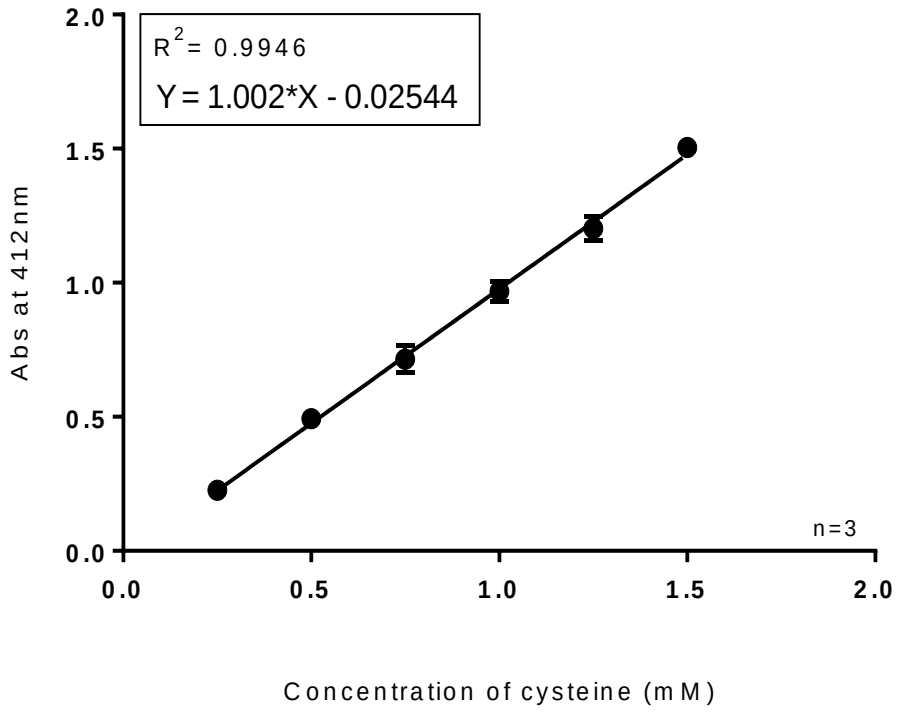

Figure 77: Ellman's assay calibration curve.

Appendix I: Human Serum Albumin-Fluorescein Isothiocyanate-Dibenzocylooctyne-Maleimide Conjugation to Polycaprolactone-Azide Particles (17)

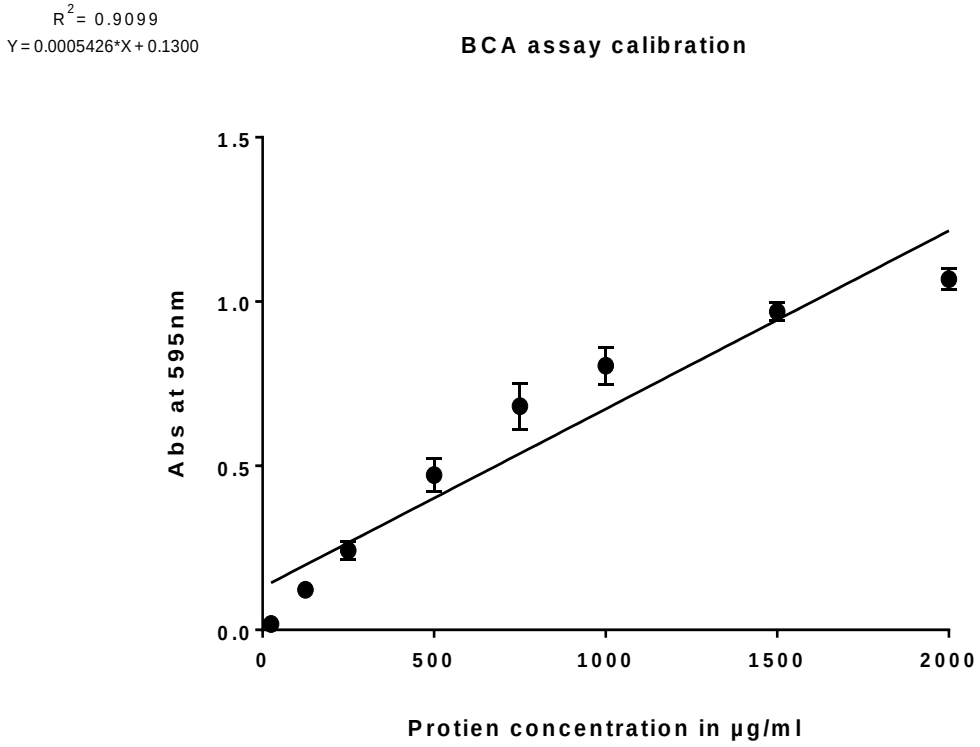

Figure 78: Bradford assay calibration curve. Constructed using a protocol from thermo fisher scientific with a stock solution of Bovine Serum Albumin.

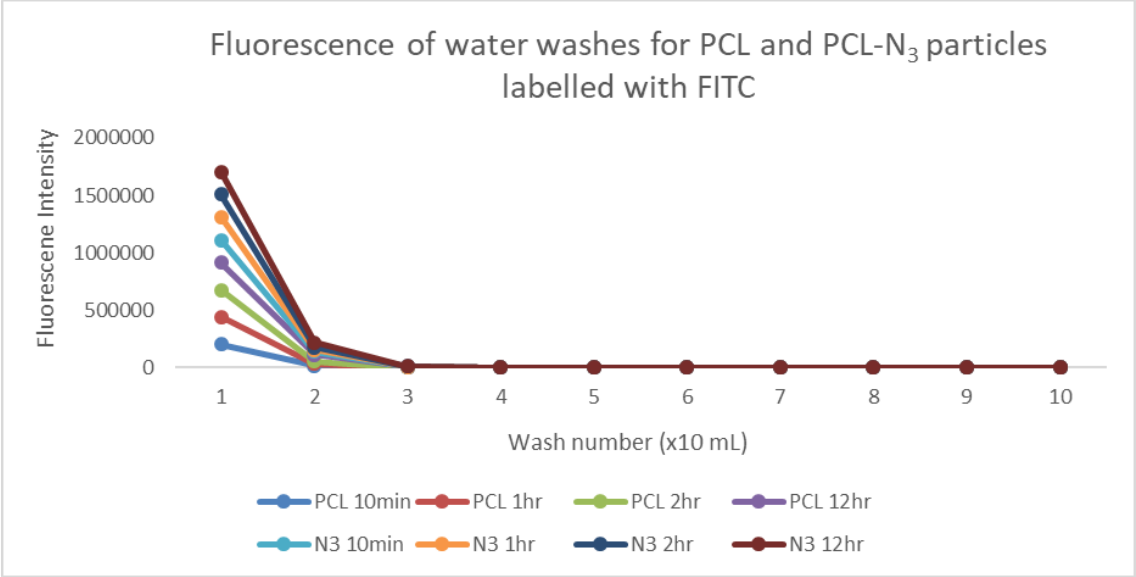

Figure 79: Water washes of microparticles after FITC labelling. PCL is microparticles produced using commercial PCL and N3 is PCL N_3 microparticles (7) The corresponding time is length of incubation of particles with FITC labelled HSA. After 3 washes of distilled water (3x10 mL) fluorescence intensity was comparable to water only sample suggesting that no more unbound FITC was leaching from the particles for all samples.

Appendix J: Analysis of Transforming Growth Factor- β1 and Transforming Growth Factor-β1

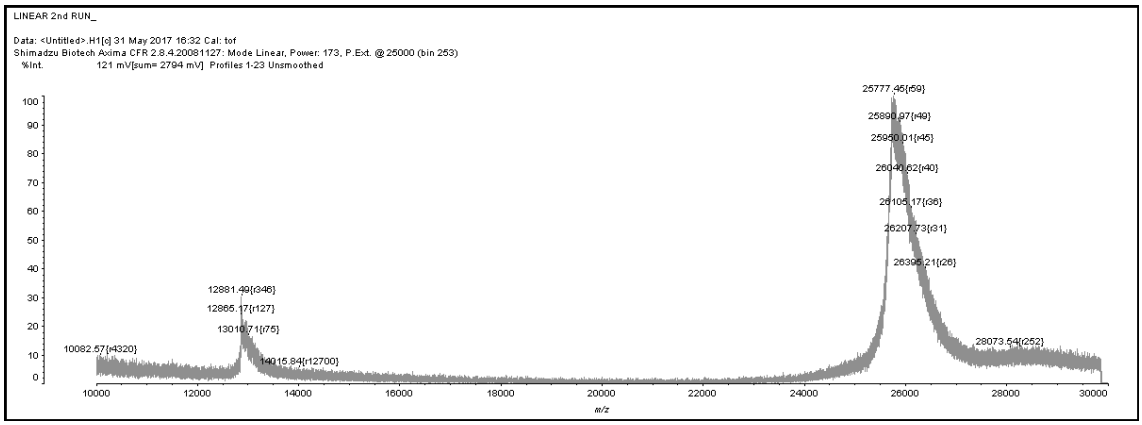

Figure 80: MALDI spectra of TGFβ1 protein at a concentration of 4 μM.

Peak observed at 25777 is as expected for the size of the protein (25 kDa) and the smaller peak at 12881 is indicative of one monomer of the protein.

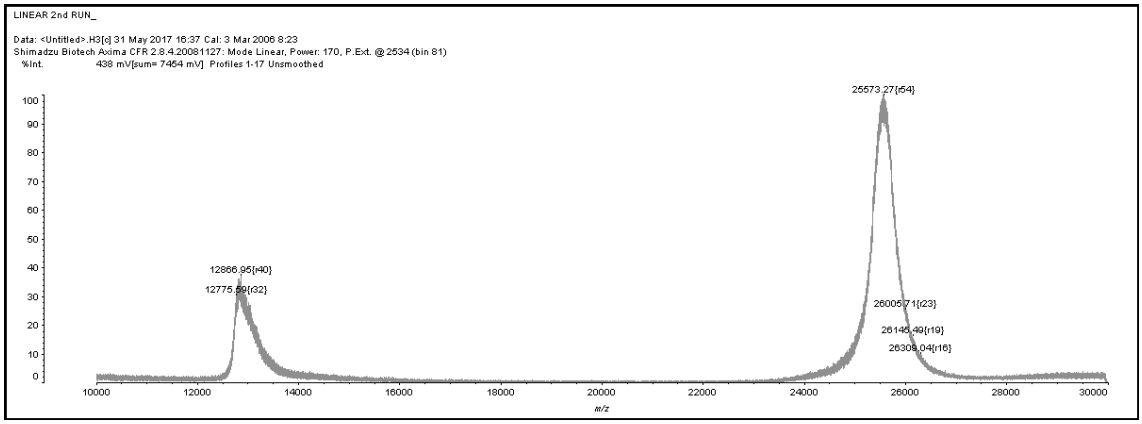

Figure 81: MALDI spectra of TGF-β3 protein at a concentration of 4 μM.

Peak observed at 25573 is as expected for the size of the protein (25 kDa) and the smaller peak at 12866 is indicative of one monomer of the protein.

Appendix K: Analysis of Hydrolysed Dibenzocylooctyne-N-Hydroxysuccinimide.

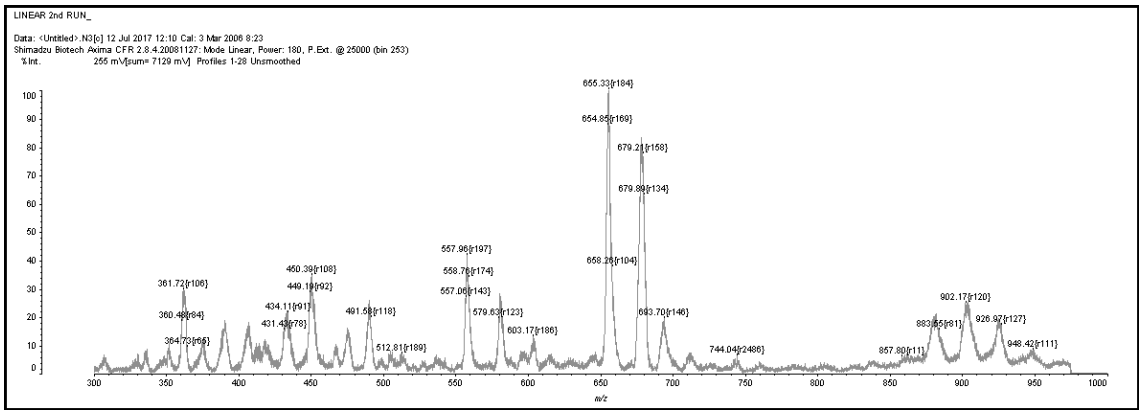

Figure 82: MALDI-TOF of DBCO-PEG4-NHS reacted with TGF-β protein. Peak at 655 is the most abundant peak which corresponds to the molecular weight of the compound (649.69), the peak at 557 corresponds to hydrolysed DBCO-NHS (mw 552.25)

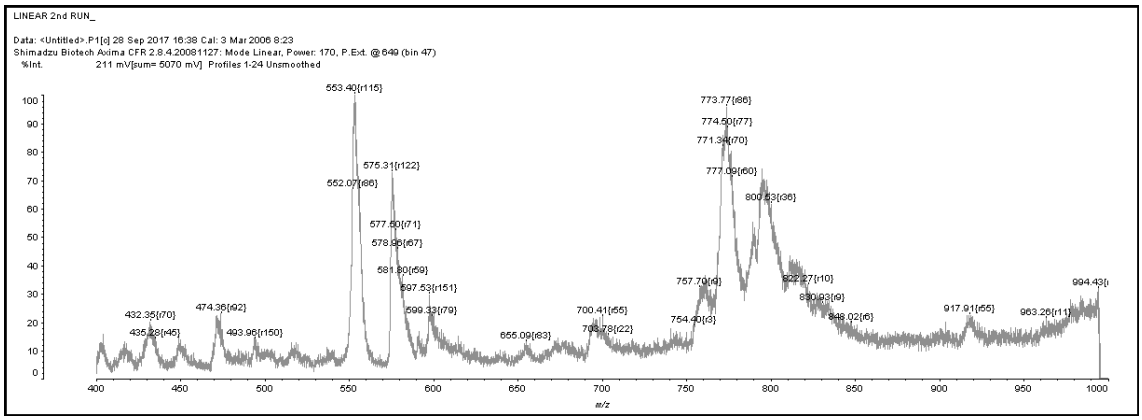

Figure 83: MALDI spectrum of hydrolysed DBCO-NHS. Peak at 553 is indicative of the hydrolysed DBCO unit (552.25)